Dissertation

submitted to the

Combined Faculties of the Natural Sciences and Mathematics

of the Ruperto-Carola-University of Heidelberg. Germany

for the degree of

Doctor of Natural Sciences

Put forward by

Clio Bertelli Motta

born in: Genova, Italy

Oral examination: 6 February 2018

THE FOOTPRINTS OF STELLAR EVOLUTION ON THE CHEMICAL COMPOSITION OF THE GALACTIC OLD OPEN CLUSTER M67

Referees: Prof. Dr. Eva K. Grebel

PD Dr. Sabine Reffert

ZUSAMMENFASSUNG

In dieser Arbeit untersuchen wir die Auswirkungen der Sternentwicklung auf die chemische Oberflächenzusammensetzung von Sternen. Wir benutzen als Beispiel den alten offenen Sternhaufen M67, für dessen Sterne Spektren mit höherer Auflösung in verschiedenen Entwicklungsphasen – von der Hauptreihe bis zum "Red Clump" – zur Verfügung stehen. Insbesondere verwenden wir Daten aus den Archiven von großen spektroskopischen Durchmusterungen wie APOGEE und Gaia-ESO. Zuerst untersuchen wir die Auswirkung des sogenannten "First Dredge-Up" auf die Häufigkeit von [C/N] auf der Sternenoberfläche. Wir analysieren dann Veränderungen in den Elementenhäufigkeiten von Sternen von der Hauptreihenphase bis zu der roten Riesenphase von M67 und diskutieren, wie diese mit atomarer Diffusion erklärt werden können. Wir präsentieren die Ergebnisse dieser Untersuchungen auch in dem Kontext von Studien der galaktische archäologie. Darüber hinaus erforschen wir die chemische Oberflächenzusammensetzung von drei blauen Nachzüglersternen und zwei entwickelten blauen Nachzüglersternem in M67, um Hinweise auf deren Entstehungsprozess zu finden und diskutieren dann die Ergebnisse auch aus der Sicht der Sternentwicklung. Schließlich präsentieren wir ein Experiment basierend auf Daten aus dem TGAS-Katalog für die Untersuchung der dynamischen Entwicklung von OB-Assoziationen.

ABSTRACT

In this work we investigate how stellar evolutionary processes change the surface chemical composition of stars. As a test-bench, we use the old open cluster M67, for whose stars high-resolution spectroscopic data are available in many different evolutionary stages, from the main sequence to the red clump. In particular, we use data retrieved from the archives of large spectroscopic surveys such as APOGEE and Gaia-ESO. First we investigate the effects of the so-called first dredge-up on the surface [C/N] abundance of M67 stars. We then analyse variations in the surface abundances of several elements from the main-sequence to the red-giant phase of M67 stars and discuss how these can be explained by atomic diffusion effects. We also present the results of these investigations in the broader context of Galactic archaeology studies. Furthermore, we investigate the chemical composition of three blue straggler stars and two evolved blue straggler stars in M67 in order to find hints for their formation scenario and discuss the results from the point of view of stellar evolution. Finally, we present an experiment based on TGAS data for the study of the dynamical evolution of OB associations.

Ai miei maestri

CONTENTS

ACRONYMS

SDSS Sloan Digital Sky Survey

APOGEE Apache Point Observatory Galactic Evolution Experiment

ASPCAP APOGEE Stellar Parameters and Chemical Abundances Pipeline

GES Gaia-ESO Survey

TGAS Tycho-Gaia astrometric solution

DR data release

OC open cluster

GC globular cluster

CMD colour-magnitude diagram

HRD Herzsprung–Russell diagram

PMS pre-main sequence

ZAMS zero age main sequence

MS main sequence

TO turn-off

SGB subgiant branch

RGB red giant branch

RC red clump

ZAHB zero age horizontal branch

AGB asymptotic giant branch

TPAGB thermally pulsating asymptotic giant branch

BSS blue straggler star

YSS yellow straggler star

PM proper motion

RV radial velocity

FDU first dredge-up

Part I

INTRODUCTION

OPEN CLUSTERS AND THEIR STELLAR CONTENT

Star clusters are fundamental components of the Milky Way. They are known to be the birth place of stars and, as such, they play a key role in many fields of astrophysical research: from stellar formation to stellar evolution, from the Galactic disc's structure to its chemical evolution in time. Open clusters (OCs) present very different characteristics with respect to globular clusters (GCs). The latter are much more massive and compact and have ages of more than 9 billion years, while the initial mass of OCs is usually of the order of $\sim 10^3 M_\odot$ and most of them do not survive for more than few hundred million years. In fact, due to their smaller mass and lower density with respect to GCs, OCs eventually get disrupted by internal and external gravitational interactions and release their stars into the field, contributing to the population of the Galactic disc. Thus, the distribution in age, Galactocentric distance and height above the Galactic plane of the OC population, together with the information about their chemical composition can help us understanding the recent star formation history and the evolution of our Galaxy.

In addition, since stars in a given OC are born from the same molecular cloud and within a very short time, they are perfect examples of single stellar populations. The relatively low total mass and density of these objects is probably the reason why, contrarily to globular clusters, they do not present multiple populations. Therefore, OCs are ideal laboratories in which to test theories of stellar evolution, as it has been done in the past, e.g. for models of core overshooting (Friel, 1995, and references therein) and as we do in this work for the effects of stellar evolution on the surface chemical composition of stars. While young OCs offer the possibility to study the evolution of very massive stars, that evolve quickly into supernovae and stellar remnants and are observable only for a short time, old OCs are very well populated in all evolutionary stages, from the main sequence, to the subgiant and giant branch, and the red clump (core helium burning phase). In particular the latter, given its high luminosity, is often used for studies of the chemical composition of clusters, as we will see later.

The catalogue of Galactic star clusters published in Kharchenko et al. (2013) contains $\sim$ 3000 objects, $\sim$ 2270 of which are open clusters. The catalogue contains detailed information e.g. about the clusters' distance from the sun, estimated age, number of members, radii, as well as 2MASS photometry and membership probability of individual stars. This list has been updated with 139 further cluster candidates by Schmeja et al. (2014) and 63 by Scholz et al. (2015). In particular, the objects from Schmeja et al. (2014) have the common property of lying close to the Sun at high Galactic latitudes (b > 20 deg). Furthermore, they all reached relatively old ages, ranging from $2 \cdot 10^8$ yr to $4 \cdot 10^9$ yr.

Old OCs (> 1 Gyr) are of particular interest due to their capability to survive disruption for such long times. In this context it is important to note the existence
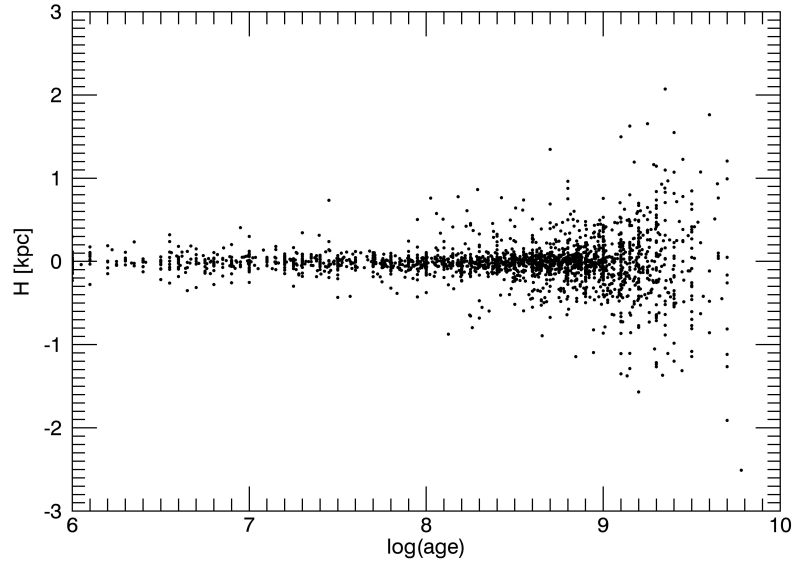
Figure 1: Distance from the Galactic plane as a function of age for the OCs in the catalogue of Kharchenko et al. (2013).

of a correlation between the age of open clusters and their height above the Galactic plane, with old clusters being distributed over much larger distances above and below the plane compared to young clusters (as pointed out in several works, e.g., Friel, 1995; Froebrich et al., 2010; Janes and Phelps, 1994), although the nature of this effect is not fully understood yet. In Figure 1, we plot the height above and below the plane calculated as

$$H = D \sin b, \tag{1}$$

where D is the distance of the cluster from the Sun and b is its Galactic latitude, as a function of age for the OCs in the catalogue of Kharchenko et al. (2013). It is clearly visible how young clusters populate the disc of the Galaxy, while clusters with age > 1 Gyr present a very large spread in height above and below the plane.

The large vertical velocity component of most old clusters is probably the reason for their comparatively long survival, since the probability to interact with large molecular clouds and other Galactic structures capable of disrupting a stellar cluster is smaller for them than for clusters embedded in the thin disc. Still, a question remains open, which is why these clusters happen to be located on such orbits. Were they born with this characteristic or did they form embedded in the disc and "migrated" to their present location as the result on their interactions with disc structures?

While a trend of the distance from the plane with age is clearly visible (see Fig. 1) this does not seem to be the case for the distances of the clusters from the Galactic
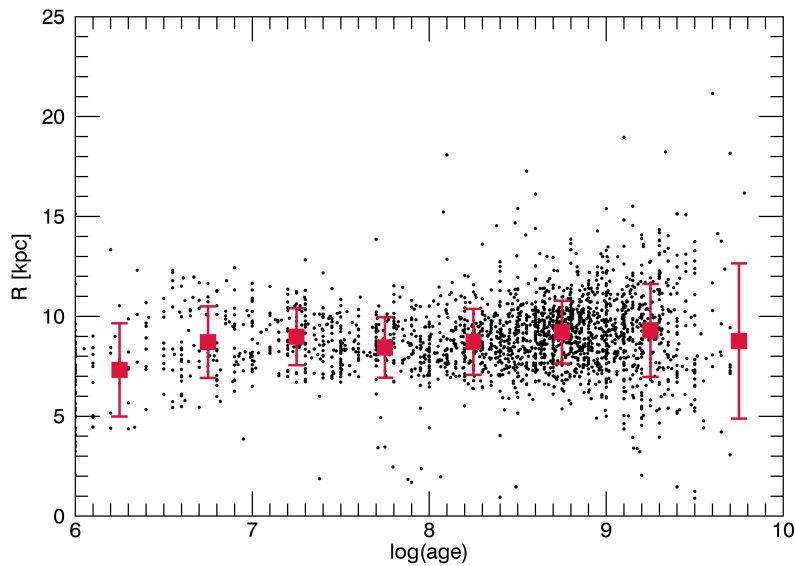
Figure 2: Distance from the Galactic centre as a function of age for the OCs in the catalogue of Kharchenko et al. (2013). We overplot as red squares the running mean of the distribution in bins of 0.5 in logarithmic age with the respective standard deviation.

centre. We calculated the Galactocentric distance R for the sample of open clusters of Kharchenko et al. (2013) as follows:

$$r = D \cos b \tag{2}$$

$$R = \sqrt{r^2 \sin l^2 + (R_0 - r \cos l)^2} \tag{3}$$

where D is the distance of the OCs from the Sun, l and b are their Galactic coordinates and R_0 is 8.5 kpc, the distance of the Sun from the Galactic centre. The results are shown in Fig. 2 together with the running mean of the distribution (red squares) calculated for bins of 0.5 in logarithmic age: no clear trend is visible and the bulk of the OCs is located at the Galactocentric distance of the Sun. This is not surprising since the catalogue of the Galactic OCs is complete only within a radius of 1.8 kpc from the Sun (with the exception of old clusters at high latitude) due to the decreasing brightness of more distant sources (Kharchenko et al., 2013). Fig. 3 shows the position of the OCs in the Galactic plane, with the Sun plotted as a red dot and the Galactic centre marked as a big black dot. Although no clear trend with age is visible, we note that the only clusters with R > 15 kpc are older than 10^8 yr.

In Fig. 4 we logarithmically plot the number of probable cluster members as a function of age for the sample of Kharchenko et al. (2013) together with the running mean of the distribution (we choose not to use the weighted running mean because most of the parameters analysed do not have errors in the catalogue of Kharchenko et al. 2013). Although we do not observe a trend in number of cluster members with age, we know that old OCs already lost part of their mass through dissolution and possible interactions with the disc. Since they also do not
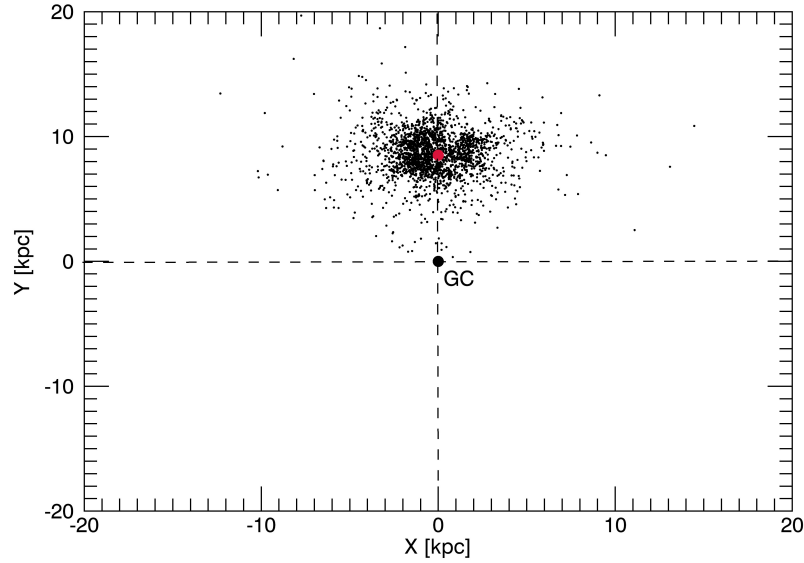
Figure 3: Position on the Galactic plane for the OCs in the catalogue of Kharchenko et al. (2013). The red dot represents the position of the Sun, the big black dot the Galactic centre.

seem to be less massive than their younger counterparts, this indicates that they must have been born with a mass larger than that of OCs born more recently (see also Friel 1995).

Also corroborating this theory is the trend in age visible for the King's tidal radii derived by Kharchenko et al. (2013). Fig. 5 shows how the running mean of the tidal radius increases with age. The core radii, on the other hand, do not seem to increase significantly with age (see Fig. 6). It is thus probable that old OCs survived to such ages not only because of their peculiar orbits, but also because they were more massive at birth, with masses up to $\sim 10^4 M_\odot$ (see, e.g., Friel, 1995, and references therein).

One of the key aspects of the study of OCs is their chemical composition. Since OCs are tracers of the properties of the disc, their chemical composition, which is supposed to be homogeneous at least in the luminous stars of the red clump, is used to derive chemical gradients in the disc (see, e.g., Chen, Hou, and Wang, 2003; Frinchaboy et al., 2013; Magrini et al., 2017). In Fig. 7 we use the metallicities from the literature listed for some of the clusters in Kharchenko et al. (2013), as well as their running mean, to show a possible trend in age. As pointed out e.g. in Friel (1995) there is no evidence of a trend of [Fe/H] as a function of age (also considering that the number of OCs with ages below 10^7 yr with metallicity estimates in the catalogue of Kharchenko et al. 2013 is too low to draw statistical conclusions). Instead, looking at Fig. 8 it is evident how the metallicity decreases with the Galactocentric distances of the OCs. Fig. 9 shows the metallicity from the Kharchenko et al. (2013) catalogue as a function of the height on the Galactic plane. The bulk of the stars embedded in the disc has solar metallicity, although a large spread is present towards lower [Fe/H]. The few OCs at large distances from the Galactic disc with an entry for [Fe/H] have metallicity on average lower than solar,
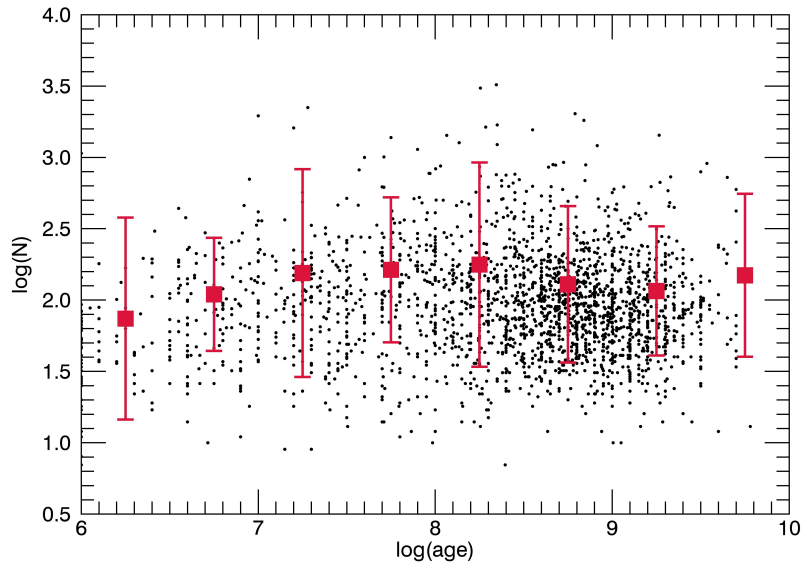
Figure 4: Number of probable cluster members as a function of age for the OCs in the catalogue of Kharchenko et al. (2013). The red squares represent the running mean with its respective standard deviation.
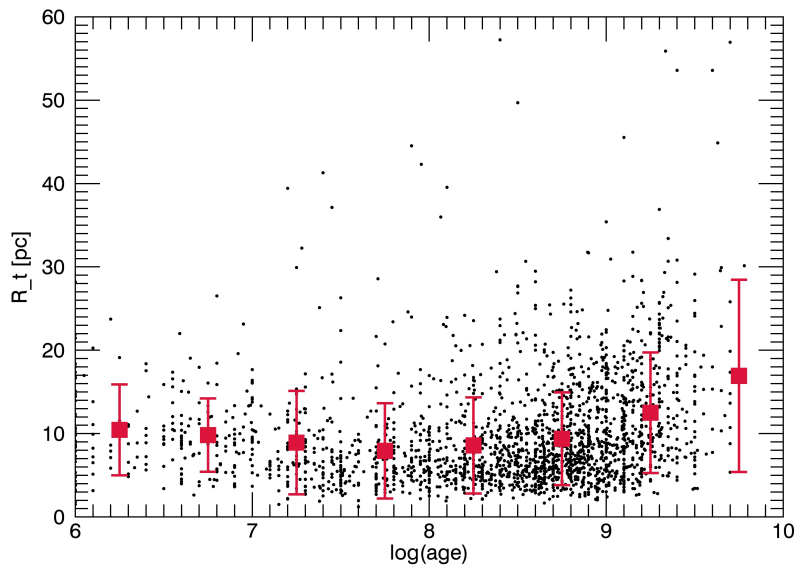
Figure 5: King's tidal radius as a function of age for the OCs in the catalogue of Kharchenko et al. (2013). The red squares represent the running mean with its respective standard deviation.
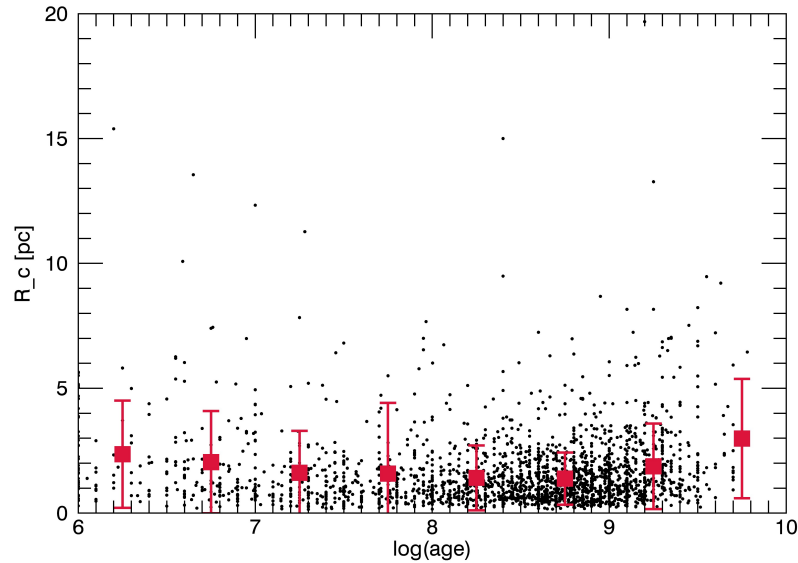
Figure 6: King's core radius as a function of age for the OCs in the catalogue of Kharchenko et al. (2013). The red squares represent the running mean with its respective standard deviation.

at $[Fe/H] \sim -0.3$ dex. This result is unfortunately biased by the low number of points with $H < -0.5$ kpc and $H > 0.5$ kpc, although e.g. Chen, Hou, and Wang (2003) and Pasquali and Perinotto (1993) also found a decrease in abundances (the former in $[Fe/H]$, the latter in $[O/H]$ and $[Ne/H]$) with distance from the plane. A detailed chemical analysis of these "extreme" clusters (in terms of their location in the disc) based on spectral data will throw new light on the question of the survival of old OCs: if the metallicities and chemical abundances of the old clusters will be found consistent with those expected from measurements of field stars located in the same environment, then the two populations probably share a very similar formation history, otherwise the scenario of their formation in the plane and of a subsequent migration should be investigated into more details.

As we will present in further detail in Chapter 2, the main problem with a study of this kind is the lack of high-resolution spectroscopic data for a large number of old OCs, mainly due to the difficulty in targeting cluster members without previous knowledge of their precise kinematics. For this reason, in the present work we concentrated our investigation on one very peculiar old open cluster: M67.
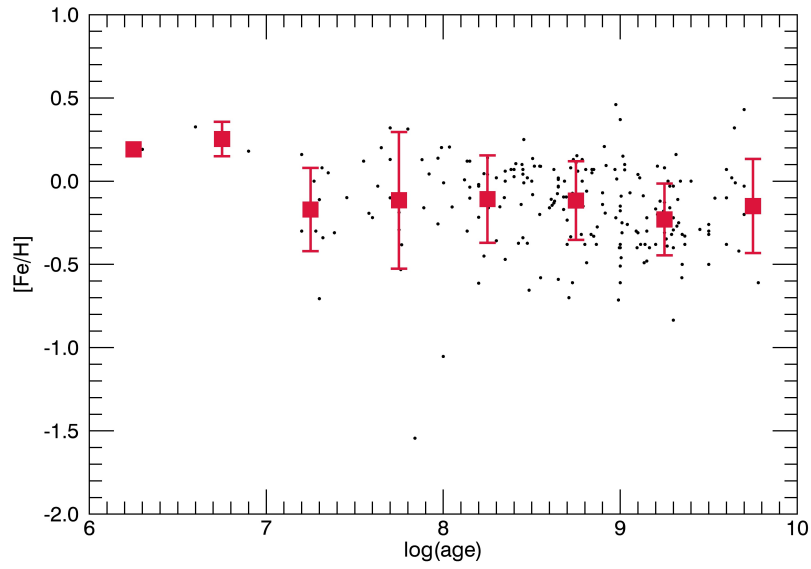
Figure 7: [Fe/H] as a function of age for a subsample of OCs in the catalogue of Kharchenko et al. (2013). The red squares represent the running mean with its respective standard deviation.
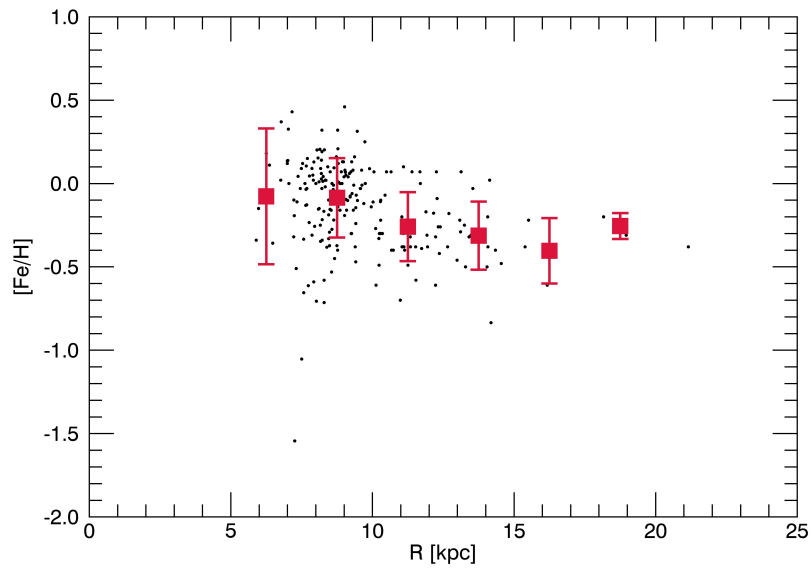
Figure 8: [Fe/H] as a function of Galactocentric distance for a subsample of OCs in the catalogue of Kharchenko et al. (2013). The red squares represent the running mean with its respective standard deviation.
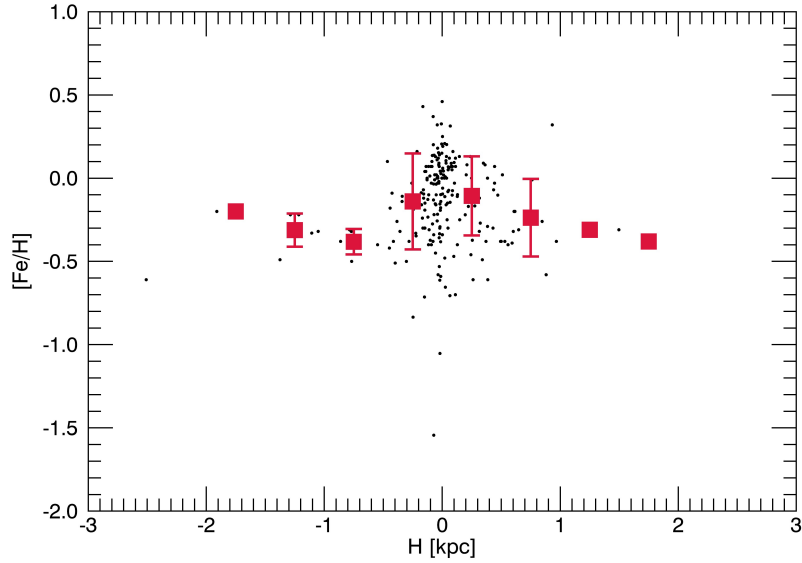
Figure 9: [Fe/H] as a function of distance from the Galactic plane for a subsample of OCs in the catalogue of Kharchenko et al. (2013). The red squares represent the running mean with its respective standard deviation.

1.2 M67: A TEXTBOOK CASE

Among the old OCs of the Milky Way, M67 (or NGC 2682) plays a special role for different reasons. First of all, with an age of 3.5-4 Gyr (see, e.g., Bellini et al. 2010b; Kharchenko et al. 2013; Sarajedini, Dotter, and Kirkpatrick 2009), M67 is one of the oldest OCs in the Galaxy. As a consequence of its old age, all evolutionary phases between the main sequence and the red clump are very well populated on the colour-magnitude diagram (CMD), which makes M67 the perfect target for studies of stellar evolution. Furthermore, it is located in the relative vicinity of the Sun, at 800-900 pc (see, e.g., Sarajedini, Dotter, and Kirkpatrick 2009), relatively high above the plane ($l = 215.70 \, \text{deg}, b = +31.90 \, \text{deg}$), and has a reddening $E(B - V)$ between 0.015 and 0.052 mag (see, e.g., Fan et al., 1996; Taylor, 2007), which makes it feasible to obtain high-resolution spectroscopic data at the expense of a reasonable amount of observational time. Moreover, M67 presents an approximately solar metallicity (see, e.g., Bertelli Motta et al., 2017; Önehag, Gustafsson, and Korn, 2014; Pace, Pasquini, and François, 2008; Randich et al., 2006; Shetrone and Sandquist, 2000; Tautvaišiene et al., 2000; Yong, Carney, and Teixera de Almeida, 2005) and is therefore considered a proxy for solar studies and used as a calibrator in many spectroscopic surveys. For all these reasons, several cluster members in different evolutionary phases have been targeted in high-resolution spectroscopic studies, making M67 an excellent test-case for studies of stellar evolution. This kind of data availability is very rare, since usually spectroscopic investigations of OCs concentrate only on red giant stars, mainly due to their luminosity.

M67 hosts several solar twins (see, e.g., Castro et al., 2011; Liu et al., 2016; Pasquini et al., 2008) and in particular M67-1194, a solar twin with one of the most

similar chemical compositions to the Sun discovered so far (Önehag et al., 2011). These findings led to the hypothesis that the Sun might have formed inside M67, although simulations have shown that in this scenario the protoplanetary disc or planetary system of the Sun should have been disrupted during the ejection from the cluster (see Pichardo et al. 2012).

Due to its peculiarities, M67 was studied in great detail in the past and a vast literature exist on various aspects of this OC. Davenport and Sandquist (2010) studied the dissolution of M67 with data from the Sloan Digital Sky Survey and found evidence of an asymmetric halo and mass segregation within the cluster. Already Bonatto and Bica (2003) had investigated the luminosity function of M67 from 2MASS data and concluded that mass segregation was present in the cluster. Zhao, Tian, and Su (1996) also came to the same conclusion analysing the internal kinematics of the cluster at different distances from the centre. Further studies on the kinematics of M67 were carried out, e.g., by Bellini et al. (2010a), Geller, Latham, and Mathieu (2015), Girard et al. (1989), and Sanders (1977). Rotation velocities in stars belonging to M67 were investigated by Barnes et al. (2016), who determined the rotation periods of several main sequence stars based on data from the K2 mission and found them to be correlated with their colour, and hence with their temperature. They use the rotational velocities of the stars to derive a gyrochronological age of 4.2 Gyr for M67. Melo, Pasquini, and De Medeiros (2001) analysed the rotational velocities of a sample containing M67 members in different evolutionary stages. They found results similar to those of Barnes et al. (2016), with the rotational velocity increasing along the main sequence, reaching a maximum at the turn-off, and decreasing again for red giant stars.

The white dwarf cooling sequence of M67 was studied e.g. by Richer et al. (1998), who used it to derive an age of 4.3 Gyr for the cluster, in good agreement with other age estimates. More recently, the study of Bellini et al. (2010b) also found that the age of M67 derived from the white dwarf cooling sequence is consistent with the results of isochrone fitting of the cluster turn-off. Carraro et al. (1996) and Tripicco, Dorman, and Bell (1993) investigated the evidences of mass-loss in red giant stars of M67.

From the point of view of the chemical composition of the cluster, several studies were dedicated to different chemical species: lithium (see, e.g., Balachandran, 1995; Canto Martins et al., 2006, 2011; Castro et al., 2016; Deliyannis et al., 1994; Pace et al., 2012; Pasquini, Randich, and Pallavicini, 1997; Spite et al., 1987), carbon and nitrogen (Bertelli Motta et al., 2017; Brown, 1987; Gilroy and Brown, 1991; Shetrone and Sandquist, 2000; Tautvaišiene et al., 2000), oxygen (see, e.g., Takeda and Honda, 2015), fluorine (see, e.g., Maiorca et al., 2014; Nault and Pilachowski, 2013), and berillium (see, e.g., Randich et al., 2007). More general investigations of the chemical composition of M67 stars can be found, e.g., in Friel, Jacobson, and Pilachowski (2010), Önehag, Gustafsson, and Korn (2014), Pace, Pasquini, and François (2008), Randich et al. (2006), Shetrone and Sandquist (2000), Tautvaišiene et al. (2000), and Yong, Carney, and Teixera de Almeida (2005). In particular, we discuss the findings of Önehag, Gustafsson, and Korn (2014), Shetrone and Sandquist (2000), and Tautvaišiene et al. (2000) in Chapter 3, 4, and 5.

M67 was recently subject to a survey searching for extrasolar planets around its member stars (Brucalassi et al. 2014, 2016, 2017; Nardiello et al. 2016a; Pasquini

et al. 2012). The authors found three hot jupiters and a giant planet, as well as two further planet candidates.

Furthermore, M67 hosts a large number of variable and active stars as well as peculiar stars such as blue stragglers, yellow stragglers and sub-subgiants. M67 was in fact one of the first open clusters in which a large population of blue straggler stars (BSS) was detected (Johnson and Sandage, 1955). Since then, numerous studies of these objects were carried out (see, e.g., Bruntt et al., 2007; Deng et al., 1999; Gilliland and Brown, 1992; Landsman et al., 1997; Leiner et al., 2016; Leonard and Linnell, 1992; Liu et al., 2008; Mathieu, Latham, and Griffin, 1990; Mathieu et al., 1986, 2003; Mathys, 1991; Pribulla et al., 2008; Sandquist and Shetrone, 2003; Sandquist et al., 2003; Shetrone and Sandquist, 2000; van den Berg et al., 2001, see Chapter 5 for a detailed discussion).

X-ray emission has been detected for several M67 members, mostly in variable stars such as, e.g., cataclysmic variables, contact binaries, and RS Canum Venaticorum variables (see, e.g., Belloni, Verbunt, and Mathieu, 1998; Belloni, Verbunt, and Schmitt, 1993; Mooley and Singh, 2015; Pasquini and Belloni, 1998; Pasquini, Belloni, and Abbott, 1994; van den Berg et al., 2002, 2004). Recently, the new incoming data from the Kepler mission have enabled many new studies based on asteroseismology, ranging from age to mass determinations, and to stellar variability (see, e.g., Barnes et al., 2016; Gonzalez, 2016a,b; Leiner et al., 2016; Nardiello et al., 2016a,b; Stello et al., 2016). Further works on peculiar members of M67 include studies on cataclysmic variables (Balaguer-Núñez et al., 2010; Williams et al., 2013), chromospheric activity in its members (Dupree, Whitney, and Pasquini, 1999; Giampapa et al., 2006; Reiners and Giampapa, 2009), binaries and other variables (see, e.g., Geller, Latham, and Mathieu, 2015; Kim et al., 1996; Mathieu, Latham, and Griffin, 1990; Qian et al., 2006; Sandquist, 2006; Yakut et al., 2009; Zhang, Zhang, and Deng, 2005). Some of this works are discussed in Chapter 5 in the context of a study of blue straggler stars in M67.

In this work, we investigate variations in the surface abundances of M67 members due to stellar evolution. Therefore, in the next section we summarise the main steps in the evolution of stars in the mass range of the M67 population.

1.3   THE LIFE OF A LOW-MASS STAR

Due to its old age, M67 is populated by low-mass stars, in the (initial) mass range $0.1 \sim 1.5 M_\odot$. We follow here the main steps in the evolution of such stars from their formation to their end on the white dwarfs cooling sequence (Fig. 10 shows the evolutionary track of a $1.4 M_\odot$ star from the pre-main sequence to the thermally pulsating asymptotic giant branch). For a detailed description of the processes mentioned in this section we refer to Salaris and Cassisi (2005).

Stars are born through the collapse of gas in large molecular clouds. In order for the gas to become unstable and collapse, it must reach a critical mass (the Jeans mass) that depends on temperature and density:

$$M_{Jeans} \propto T^{3/2} \rho^{-1/2} \tag{4}$$
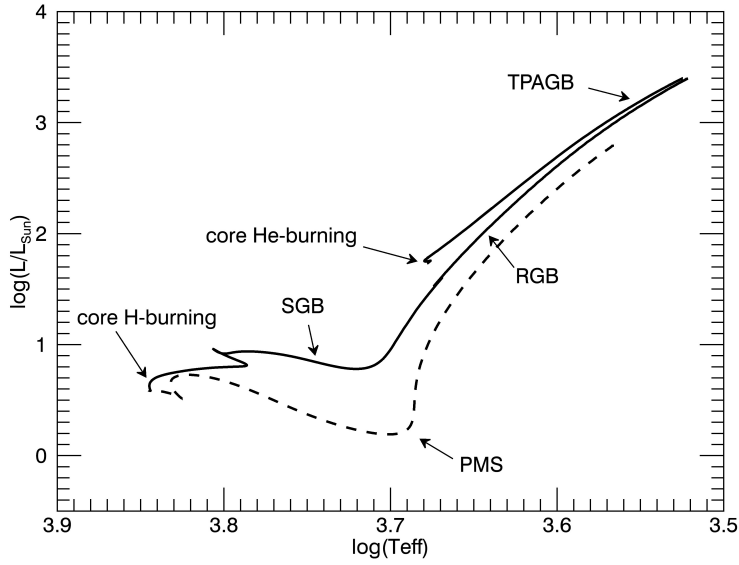
Figure 10: The evolution of a star with $1.4M_\odot$, $Z = 0.014$, and $Y = 0.273$ on the CMD from the pre-main sequence to the TPAGB phase. Plotted using PARSEC evolutionary tracks (Bressan et al., 2012).

After the collapse, the protostar is in hydrostatic equilibrium and follows the virial theorem, which states:

$$E_{pot} = -2E_{kin}. \tag{5}$$

This means that the total energy E_{tot} is negative and therefore the system is bound:

$$E_{tot} = E_{pot} + E_{kin} = -E_{kin} = \frac{1}{2}E_{pot}. \tag{6}$$

When the protostar starts loosing energy through radiation, since

$$L = -\frac{dE_{tot}}{dt} = -\frac{1}{2}\frac{dE_{pot}}{dt}, \tag{7}$$

the star has to contract in order to maintain the virial equilibrium. As a consequence, E_{pot} decreases and E_{kin} increases, leading to an increase in temperature, which, in turn, leads to the ionisation of H and He in the stellar interior. This process absorbs most of the energy deriving from the contraction and the object collapses. Only after the completion of the ionisation processes the star returns to hydrostatic equilibrium.

Stars that have reached this stage are fully convective and follow the so-called Hayashi track on the Herzsprung–Russell diagram (HRD), described by an nearly constant T_{eff} and decreasing luminosity due to the contraction of the star.

In this phase, when a temperature of at least $T \sim 10^6$ K is reached in the stellar interior, light elements such as D, Li, Be, B are processed into He. The increase in temperature leads to the formation of a radiative core, and as a consequence, the

star leaves the Hayashi track (which describes the locus of fully convective stars on the HRD). The star then moves towards the zero age main sequence (ZAMS) describing on the HRD a curve with little luminosity variation but increasing T_{eff}, the so-called pre-main sequence (PMS).

The main sequence (MS) corresponds to the position on the HRD occupied by stars burning hydrogen in their core, which can happen as soon as the core temperature reaches $\sim 10^7$ K. The period that the star spends on the main sequence is the longest phase in the evolution of a star and its duration depends on the mass of the object (Hansen and Kawaler, 1994):

$$t \approx \frac{10^{10}}{(M/M_\odot)^{2.5}} \, yr. \tag{8}$$

We note that protostellar objects with $M < 0.08 M_\odot$ never reach the ZAMS because their core becomes degenerate before reaching the temperature necessary to ignite hydrogen. Such objects become brown dwarfs or planets and progressively cool down.

Two processes are responsible for the nuclear processing of hydrogen into helium: the p–p chain and the CNO-cycle. The former consists in the transformation of four hydrogen nuclei into one ^{4}He nucleus through direct reactions, the latter uses other elements (carbon, nitrogen, and oxygen) as catalysts for the transformation of hydrogen into helium. In every star both processes are active, but the main channel depends on the temperature of the star (see Fig. 11). Their efficiency is described by:

$$\epsilon_{pp} \quad \propto \quad T_6^4 \tag{9}$$
$$\epsilon_{CNO} \quad \propto \quad T_6^{18} \tag{10}$$

where T_6 is the temperature expressed in millions of Kelvin. Indicatively, stars with $M < 1.2 M_\odot$ have radiative cores and convective envelopes and burn hydrogen through the p–p chain, while in stars with $M > 1.2 M_\odot$, which present convective cores and radiative envelopes, the CNO cycle is more efficient.

While convection has the characteristics of averaging out possible chemical inhomogeneities, radiative regions in the stellar interior are affected by atomic diffusion, i.e. a stratification in abundance of the different elements resulting from the combination of gravity and radiative acceleration. In stars with radiative cores this results in shorter life-times on the MS, since hydrogen is substituted by He sinking towards the centre of the star. We discuss atomic diffusion in stars of the mass range of M67 in detail in Chapter 4.

A further effect that MS stars with $M > 1.2 M_\odot$ are exposed to is core overshooting. In convective cores, the material approaching the boundary to the radiative envelope usually has a non-zero velocity. For this reason, material from the convective region can cross the boundary to the radiative region, de facto increasing the size of the core. This has the effect of increasing the amount of hydrogen in the core and thus to prolong the life on the MS.

When the fuel in the core is exhausted, hydrogen burning proceeds in the shells surrounding the inert, radiative He core. The star expands, the surface temperature decreases and the envelope becomes convective. As a consequence, the star leaves the MS and evolves along the subgiant branch (SGB). While its luminosity remains
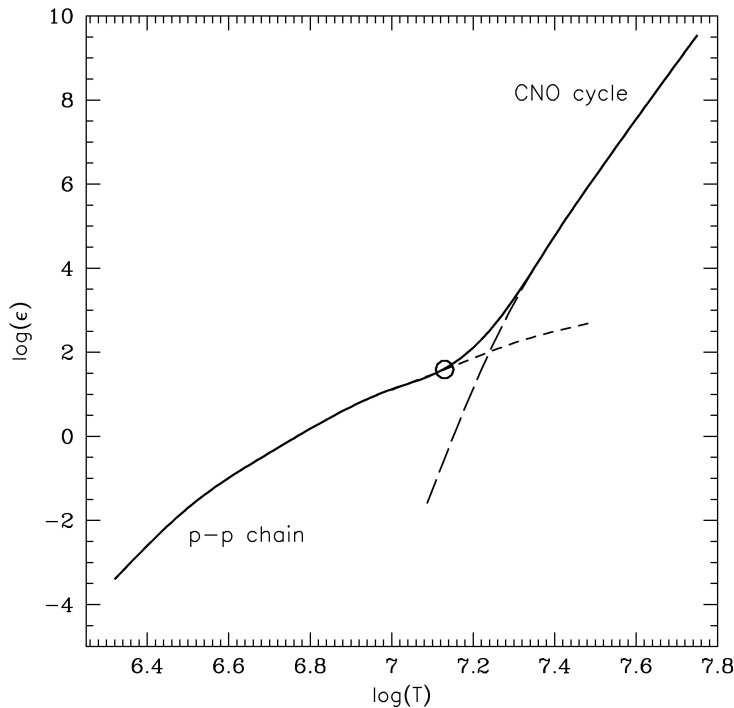
Figure 11: Efficiency as a function of temperature for the p–p chain and the CNO cycle. The black circle represents the position of the Sun. Figure from Salaris and Cassisi (2005), courtesy of Prof. M. Salaris.

nearly unchanged, its temperature decreases and its colour becomes redder. During this phase the convective envelope deepens into the stellar interior and induces mixing between the outer and inner layers of the star.

Since in the stellar interior the CNO-cycle is active, the abundances of carbon, nitrogen, and oxygen in the deep layers of the star are the equilibrium abundances resulting from the nuclear processes involved and are different from the surface chemical abundances. When the convective envelope deepens into the inner layers of the star, it brings to the surface the products of the CNO-cycle. This process is called first dredge-up (FDU) and changes the observable abundances of the elements involved: the abundance of carbon decreases, that of nitrogen increases, while that of oxygen remains almost unchanged. We discuss the effects of the FDU in M67 star in detail in Chapter 3.

The deepening of the convective envelope continues until the star reaches the limit of its Hayashi track, describing a fully convective object. As a consequence the luminosity increases and the star expands, thus moving along the red giant branch (RGB). Stars with $M < 2.3 M_\odot$ develop a degenerate He core after the MS. When hydrogen burning proceeds in the surrounding shells, more and more He is deposited on the He core. As the hydrogen-burning region moves towards the outer layer of the star, the convective envelope becomes thinner and thinner.

After the FDU, a discontinuity in molecular weight is left over at the boundary between the layers reached by the convective envelope and the hydrogen burning shell. As long as there is this discontinuity, there can be no mixing between these
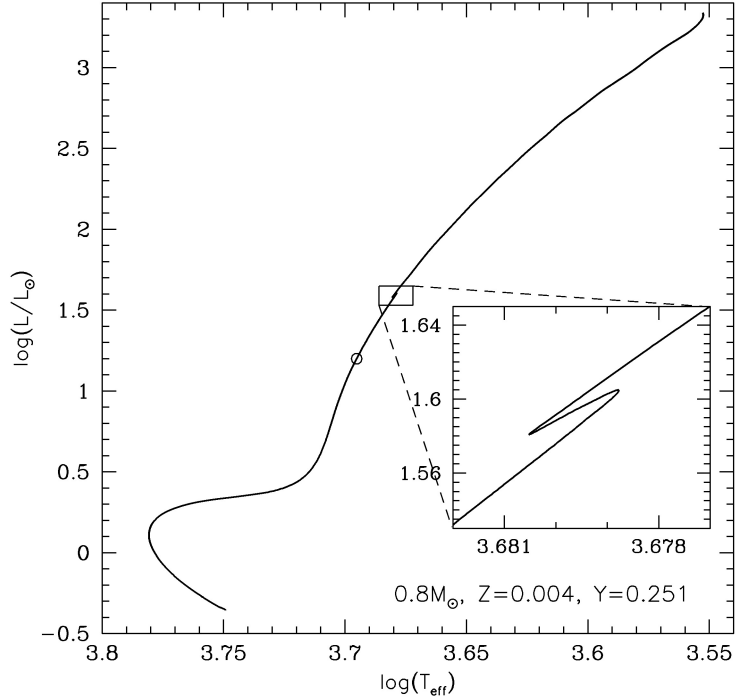
Figure 12: Evolutionary track of a $0.8 M_\odot$ star. The region of the RGB bump is zoomed-in in the small panel. The black circle represents the point on the RGB where the FDU is completed. Figure from Salaris and Cassisi (2005), courtesy of Prof. M. Salaris.

two regions of the star. When the hydrogen burning shell reaches the boundary, due to the relation between the molecular weight and the luminosity:

$$L \propto \mu^{7.5}, \tag{11}$$

the luminosity decreases first before increasing again. The same luminosity value is therefore crossed three times in a short time span and we therefore often see an overdensity of stars in this region, called the RGB bump (see Fig. 12). After the discontinuity is crossed, material from the H-burning shell can be mixed with the convective envelope. This is process is called extra-mixing and it has the consequence of enlarging the effects of the first dredge-up seen on the surface (see Chapter 3).

When the degenerate He core reaches a temperature of $\sim 10^8$ K helium ignites. Due to the degeneracy in the core, the energy produced by the He burning does not translate in an expansion and cooling of the core and as a consequence a thermal runaway occurs. This produces a drastic increase in the core luminosity, called He flash, which is mostly absorbed by the outer layers of the stars and translates in the removal of the degeneracy in the outer part of the core, where He was ignited. Several other less strong flashes follow, until the degeneracy is completely removed from the core.

After the He flash the RGB phase is terminated. At this point the luminosity decreases due to the expansion of the He core and the decrease in temperature of the surrounding H burning shell. The star reaches the zero age horizontal branch

(ZAHB), where quiescent He burning continues in the (convective) core through the so-called triple-α process, in which three He nuclei react almost simultaneously to become a carbon nucleus. In fact, the formation of a ^{12}C nucleus follows

$$^4\text{He} +^4\text{He} \quad \longrightarrow \quad ^8\text{Be} \tag{12}$$

$$^8\text{Be} +^4\text{He} \quad \longrightarrow \quad ^{12}\text{C} + \gamma. \tag{13}$$

^{8}Be is unstable and the capture of the third ^{4}He nucleus by the ^{8}Be nucleus must occur within $\sim 10^{-16}$ s, before the latter decays back into two ^{4}He nuclei.

Through further capture of ^{4}He nuclei, the so-called α-elements form during this phase. Of particular importance is the transformation of ^{12}C into ^{16}O through

$$^{12}\text{C} +^4\text{He} \longrightarrow^{16}\text{O} + \gamma. \tag{14}$$

After part of the He has been depleted in the core, this reaction becomes very relevant, since it is more likely to occur than the triple-α process. Thus, a CO inert core is progressively formed. Meanwhile, hydrogen burning through the CNO-cycle proceeds in a shell surrounding the core.

After He exhaustion, the CO core of low-mass stars becomes degenerate. At this point He-burning proceeds in a shell surrounding the core. This phase is referred-to as asymptotic giant branch (AGB) phase, as the star evolves at almost constant temperature and increasing luminosity, similar to the RBG. When He-burning ignites in the shell, the outer layers expand and cool down, thus inhibiting H-burning in the outer shells. When He is exhausted in the shell, the star contracts and the H-burning shell switches on again. The subsequent phase is called thermally pulsating AGB (TPAGB) phase. The H-burning shell produces He that feeds the inner layers surrounding the degenerate core. When enough He is accumulated, He burning switches on again in the semi-degenerate shell surrounding the core, resulting in a thermonuclear runaway. As a consequence, the outer layers expand and cool down, and the H-burning shell switches off. When He is exhausted again, the star contracts and H-burning switches on again, and so on.

The AGB phase is characterised by numerous interesting processes. During the thermal pulses, in particular when the He shell ignites and the outer layers expand and cool down, a convective envelope develops that penetrates progressively into the stellar interior. This process is called the third dredge-up (the second dredge-up occurs only in stars with $M > 3 - 5 M_\odot$ during the early AGB phase) and, bringing to the surface the products of He-burning, is responsible e.g. for the enhancement of carbon on the surface and thus for the creation of the so-called carbon stars. Furthermore, AGB stars are the environment in which s-elements form, through capture of neutrons by the existing elements. Neutrons can result from several nuclear interactions, but in low-mass stars ($M < 3 M_\odot$) only the temperature necessary for the reaction:

$$^{13}\text{C} +^4\text{He} \longrightarrow^{16}\text{O} + n \tag{15}$$
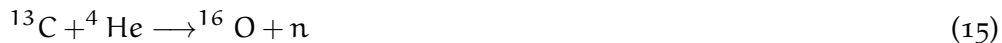
is reached. The s-elements are then brought to the surface through convection and released into the interstellar medium through mass loss. In fact, due to the expansion and decrease in temperature, layers of molecules and dust grains form at the surface of AGB stars. These are then blown away by the radiative pressure.

When a sufficient amount of mass has been ejected, the star is left with a thin H envelope, a He shell and a degenerate CO core. Stars with $0.3M_\odot < M < 8M_\odot$ cannot ignite carbon and therefore finish their life as white dwarfs. They first evolve towards higher temperature and, as a consequence, they are able to ionise the material ejected during the TPAGB, thus forming a planetary nebula. After this phase the remnat cools down following the white dwarf cooling sequence.

This work is organised as follows: in Chapter 2 we will present the membership analysis method used to identify stars belonging to a cluster and the results of this method applied to the fields surrounding known open clusters in a large spectroscopic survey. In Chapter 3 and 4 we present the effects of stellar evolution, and in particular of the first dredge-up and of atomic diffusion, on the stars of one particular open cluster, M67. In Chapter 5 we investigate the chemical composition of blue straggler stars and evolved blue straggler stars in M67. Finally, in Chapter 6 we discuss the possibilities of future studies on the kinematics of star forming regions and OB associations.

OPEN CLUSTERS IN SPECTROSCOPIC SURVEYS

The membership analysis method described in Section 2.1 was published in Bertelli Motta, C., M. Salaris, A. Pasquali, and E. K. Grebel (2017). 'Observing the products of stellar evolution in the old open cluster M67 with APOGEE'. In: MNRAS 466, pp. 2161–2174.

A major limitation on the retrieval of spectroscopic data regarding open clusters comes from the pre-selection of cluster members. In fact, since OCs are not as dense as GCs, the probability of observing a foreground or background star, and not a member of the cluster, when retrieving data in the field of the cluster is quite high. On the other hand, in order to know for sure which stars belong to a given cluster, a lot of information is needed and part of it comes from the spectra themselves. The criteria that are commonly used for the membership analysis of open cluster stars can be divided into kinematic, photometric, and chemical criteria.

First of all it is assumed that stars in the same open cluster move with approximately the same velocity in the 3-dimensional space. This means that their proper motions (PM), or tangential velocities, i.e. their velocity component projected onto the sky and measured by their displacement in time (mas/yr), should be approximately the same. The same holds for their radial velocity (RV), i.e. their velocity along the line of sight, which is measured through the Doppler shift of their spectral absorption features.

Secondly, it is assumed that open clusters are populated by a single stellar population. The member stars therefore populate a very specific locus in the colour-magnitude diagram (CMD), which is typically reproduced by an isochrone of given age and metallicity. If the photometry of the cluster area is available, it is possible to exclude the stars that do not lie on the isochrone within the photometric errors as non members of the clusters, although it must be noted that by doing so many peculiar stars, such as blue, red, and yellow straggler stars actually belonging to the cluster but not placed on the isochrone would be excluded. Also, a high degree of differential reddening might lead to a displacement of the stars from the isochrone.

The final assumption that is often made is that open clusters are chemically homogeneous at the present day because they are born from the same molecular cloud. As we will show in later chapters of this work, this assumption does not exactly hold since stellar evolution changes the surface chemical composition of stars. Nevertheless, different elements experience different variations in surface abundance and it can be assumed that, e.g., [Fe/H] is homogeneous up to ~ 0.1 dex (see, e.g., Chapter 4).

2.1   MEMBERSHIP ANALYSIS

For an investigation of the chemical composition of stars in open clusters and especially for the study of possible inhomogeneities arising from stellar evolution, a reliable determination of the membership probability of each star is essential. In fact, only if we can exclude contamination from field stars with (almost) absolute certainty, we can reasonably assume that potential variations in the chemical abundances of cluster stars are a product of either stellar evolution or of the star formation history within the cluster.

In order to select likely member stars in open clusters, we developed a code that analyses different properties of the candidate member sample. In the following, we illustrate in detail the membership analysis pipeline using the example of M67 with data from the twelfth Data Release of the Apache Point Observatory Galactic Evolution Experiment (hereafter APOGEE DR12, see Alam et al., 2015; Majewski et al., 2015) as part of the Sloan Digital Sky Survey III (SDSS-III see Eisenstein et al., 2011). The APOGEE spectrograph is mounted on the 2.5m Sloan telescope and operates in the near-infrared range from 1.51 to 1.7 µm with a spectroscopic resolution of R ∼ 22500. Stellar parameters such as T_{eff}, log g, [M/H], [C/M], [N/M], and [α/M], as well as the abundances of several elements are derived with the APOGEE Stellar Parameters and Chemical Abundances Pipeline (ASPCAP) (see García Pérez et al., 2016; Holtzman et al., 2015).

1. The first step consists in a crossmatch of the APOGEE stars in the SDSS DR12 with the central coordinates of M67, which we retrieve from Kharchenko et al. (2013). All stars are selected that lie within the cluster's outermost radius (1.03 deg), defined by Kharchenko et al. (2013) as the distance from the centre of the cluster at which the density of cluster stars cannot be distinguished from that of the field.

2. We expect that the member stars of a given open cluster share the same tangential velocities (as inferred from their proper motions in RA and Dec) and RV. Thus, after the spatial constraints set by step 1., we address the tangential velocities of the stars. In particular, we are interested in the absolute value of the PM vector, which we derive through the vectorial sum of the PM components in RA and Dec provided by the PPMXL catalogue (Roeser, Demleitner, and Schilbach, 2010), including the corrections by Vickers, Röser, and Grebel (2016). The following relation holds for the absolute value of the PM:

$$PM_{tot} = \sqrt{PM_{RA}^2 + PM_{Dec}^2}. \tag{16}$$

Plotting a histogram of the resulting PM_{tot} for all stars within the radius of the cluster, we expect the members of the cluster to show a distribution peaked at the mean PM_{tot} of the cluster and whose width is given by the PM errors from the PPMXL catalogue and by the internal scatter due to the progressive dissolution of the cluster. In order to exclude obvious outliers from the calculations, we select a first range by eye (red lines in the plots in Fig. 13, panel a). We then calculate the weighted mean PM_{tot} and its standard deviation within this range. All stars lying within 2σ from the mean are selected and considered in the next step of the analysis.

Due to the very large PM_{tot} errors for some of the stars in the PPMXL catalogue that we do not want to include in our sample, we calculate the mean error for the above selection and exclude stars whose PM_{tot} error is larger than the mean error (~ 1.8 mas/yr) $+1\sigma$ (~ 1.2 mas/yr).

3. In step 2, we consider only the absolute value of the PM_{tot} and thus lose information about the direction of the PM_{tot} vector. Therefore, it might happen that stars having by chance the same absolute PM_{tot} as the average proper motion of the cluster, but moving in a different direction, are considered members of the cluster. In order to correct for this effect, we consider in the next step the distribution of the angles of the PM_{tot} vector (see Figure 13, panel b). Also here, we calculate the mean weighted by the errors (mean error ~ 9.88 deg) and the standard deviation and select all objects within 2σ from the mean. The result of this selection can be seen in Figure 13, panel c: all stars move in the same direction in the RA-Dec plane, with proper motion vectors of the same length (within the errors).

4. In the next step we repeat the same procedure as in step 2 and 3, but with the RV of the stars resulting from the APOGEE analysis (Figure 13, panel d). Given that the typical errors of the APOGEE RV for stars in the radius of M67 are very small (~ 0.05km/s), we do not put any constraint on these errors, contrarily to step 1.

5. Once we have made sure that the kinematic properties of our selection of stars are consistent with them belonging to the same kinematic group, we proceed with the photometric criteria. For all selected stars we can retrieve 2MASS magnitudes. We use a distance modulus of $(m - M)_0 = 9.64$ mag, a reddening of E(B-V)=0.023 mag and an age estimate in the range between 3.75 and 4 Gyr (from Bellini et al., 2010b) to calculate the corresponding BaSTI isochrones (see Pietrinferni et al. 2004) with a metallicity of [Fe/H]=0.06 dex, including core overshooting during the main sequence. We then compare the isochrones reddened according to the Cardelli, Clayton, and Mathis (1989) extinction law with the 2MASS magnitudes of the stars plotted in a colour-magnitude diagram. We exclude the objects that do not cross any of the two isochrones corresponding to an age of 3.75 and 4 Gyr within three times their error in magnitude and colour. We repeat this step in the colour-magnitude diagrams described by J vs $(J - H)$ and K_s vs $(J - K_s)$ (see Figure 13, panel e and f).

We should note that by doing this we exclude blue straggler stars that are probably members of M67. While this is not relevant for the study of evolutionary effects such as the first dredge-up and atomic diffusion proposed in Chapter 3 and 4, when we want to investigate blue straggler stars (see e.g. Chapter 5) we need to proceed differently. Blue straggler stars are expected to share the same kinematic properties as the rest of the cluster, i.e. steps 1-4 should be in principle still applicable, but since they are often found in binary or multiple systems this statistical approach can be misleading. It is therefore necessary to carry out a very careful analysis of the stellar kinematics (see, e.g., Geller, Latham, and Mathieu 2015).

6. As a final step, we consider that stars belonging to a given open cluster, even in case of inhomogeneities in the abundances of certain elements, are expected to share the same [Fe/H] abundance. Thus, we repeat the same procedure as in steps 2.-4. for the iron abundance [Fe/H] calculated with the pipeline ASPCAP, and consider all stars within $2\sigma \approx 0.1$ dex from the mean [Fe/H] to be members of the cluster (see Figure 13, panel g). Typical [Fe/H] errors for this selection are ~ 0.03 dex.

We point out that the ASPCAP DR12 parameters for dwarf stars were not calibrated by the SDSS collaboration due to the difficulties of the pipeline in treating stars with high $\log(g)$, among others because stellar rotation was not included in the analysis (see, e.g, Holtzman et al., 2015). Therefore, in step 6 we exclude potential cluster members on the main sequence and turn-off of M67 from our selection because they do not have entries in the ASPCAP DR12 catalogue of calibrated abundances. For the study of the first dredge-up this is not very relevant, since our purpose is not to obtain a complete sample of M67 members but rather to select a number of highly probable members on the subgiant and red giant branch that allow us to investigate the effects of stellar evolution on the chemical composition of stars.

After the cluster members selection, we cleaned the sample from binaries known from the literature. We matched our sample with those of Yakut et al. (2009) and Geller, Latham, and Mathieu (2015). We did not find any stars in common with Yakut et al. (2009), but we did find two binaries from Geller, Latham, and Mathieu (2015) among our members, as shown in Fig. 14. We exclude these two stars from our sample, since being unresolved binaries, we cannot use their abundances to investigate the effects of stellar evolution on the surface chemistry of single cluster stars. All other stars from our sample are considered members by Geller, Latham, and Mathieu (2015), with the exception of one star that was not analysed in their work and another star that is not considered a member after their analysis.

Averaging over the resulting sample of 34 stars distributed across the subgiant branch, the lower red giant branch and the red clump, we find M67 to have an average radial velocity of RV = 33.806 ± 0.528 km/s, a proper motion in RA $\times \cos(\mathrm{Dec})$ of $\mathrm{PM_x} = -5.906 \pm 0.951$ mas/yr and in Dec of $\mathrm{PM_y} = -7.175 \pm 1.268$ mas/yr (using the corrected proper motions from Vickers, Röser, and Grebel 2016)[1], consistent with the literature within three times the errors (see Geller, Latham, and Mathieu 2015, RV = 33.64 ± 0.03 km/s; Yakut et al. 2009, RV = 33.67 ± 0.09 km/s, and Bellini et al. 2010a, $\mathrm{PM_x} = -9.6 \pm 1.1$ and $\mathrm{PM_y} = -3.7 \pm 0.8$ mas/yr). For the metallicity, we obtain [Fe/H] = 0.08 ± 0.04 dex, slightly higher than other literature values (see, e.g., Tautvaišiene et al. 2000, [Fe/H] = -0.03 ± 0.03 dex; Yong, Carney, and Teixera de Almeida 2005, [Fe/H] = 0.03 ± 0.15 dex; Randich et al. 2006, [Fe/H] = 0.03 ± 0.01 dex; Pace, Pasquini, and François 2008, [Fe/H] = 0.03 ± 0.04 dex) but still consistent with them within three times the errors. The cluster-wide parameters of M67 are summarized in Table 1.

---

1 Repeating the membership analysis with the non-corrected proper motions from PPMXL we find $\mathrm{PM_x} = -7.754 \pm 0.952$ mas/yr and $\mathrm{PM_y} = -5.613 \pm 1.276$ mas/yr.
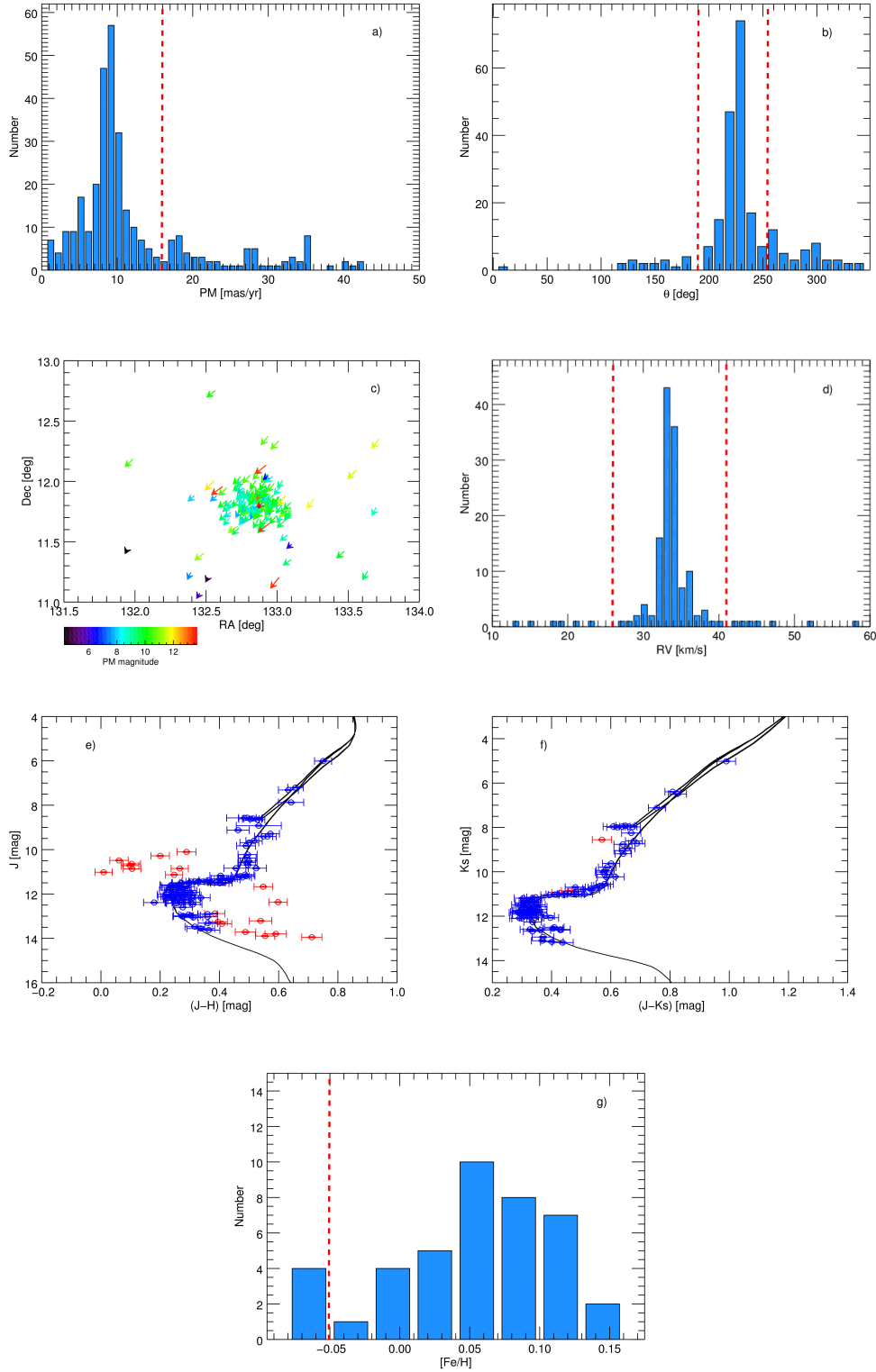
Figure 13: The membership analysis step by step. *Panel a*: histogram of PM_{tot} (mean error $PM_{err} \sim 1.8$ mas/yr); *panel b*: histogram of the proper motion angle ($\theta_{err} \sim 9.88$ deg); *panel c*: representation of the proper motion vector of the selected stars in the RA-Dec plane; *panel d*: histogram of the radial velocities ($RV_{err} \sim 0.05$ km/s); *panel e* and *f*: colour-magnitude diagram for J vs. $(J - H)$ and K_s vs. $(J - K_s)$, the rejected stars are highlighted in red; *panel g*: histogram of the [Fe/H] abundances of the selected stars ([Fe/H]$_{err} \sim 0.03$ dex). The red dashed lines represent the interval taken into account for the computation of the mean value and standard deviation of each distribution.
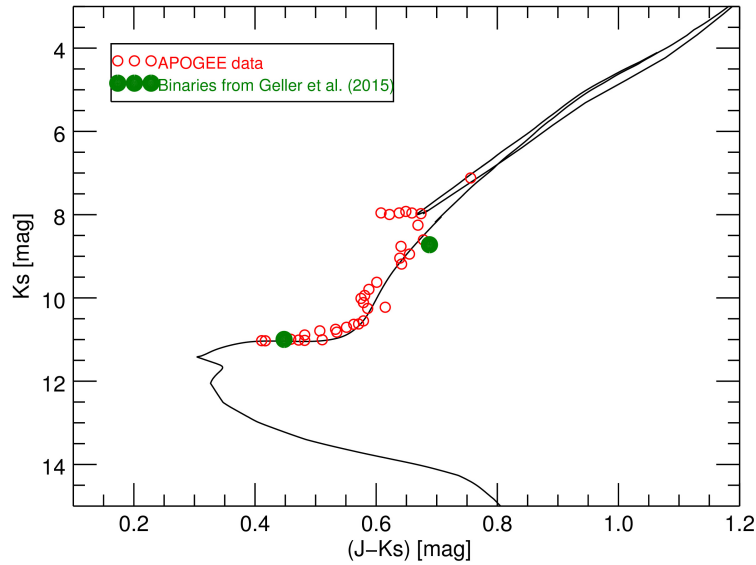
Figure 14: Our selection of members for M67 plotted on the BaSTI isochrone of age 3.75 Gyr. The green circles represent the members labeled as binaries in Geller, Latham, and Mathieu (2015). These stars are excluded from all further investigations.

Table 1: General parameters of M67. The central coordinates are taken from Kharchenko et al. (2013). The quoted radial velocity, the proper motions, and the metallicity are the mean values for the sample of cluster members selected in this study. The turn-off age range, as well as the reddening and the distance modulus are taken from Bellini et al. (2010b).

RA	Dec	RV	e_RV	PM_x	e_PM_x	PM_y	e_PM_y
08:51:23.4	+11:48:54	33.806	0.528	-5.906	0.951	-7.175	1.268

Age	E(B-V)	$(m-M)_0$	[Fe/H]	e_[Fe/H]
3.75-4.00	0.023	9.64	0.08	0.04

2.2 LARGE SPECTROSCOPIC SURVEYS

It is often assumed that large spectroscopic surveys contain a lot of information about open clusters. We searched the archives of the infrared ($1.51 - 1.70\mu$m), high-resolution (R ~ 22500) survey APOGEE DR12 looking for stars in open clusters. Similar to what was described in the previous section, we cross-matched the entire Kharchenko et al. (2013) catalogue with the survey archives, looking for stars within the radius of each cluster. We then applied our membership analysis method to each of the clusters, in this case using only one isochrone in step 5. The results of our search and analysis are summarised in Table 2: the first row indicates for how many clusters we find more than 1, 10, 20 or 50 stars within the radius in the APOGEE archive. The second row indicates for how many of these clusters we find more than three members after our analysis. We started from the clusters for which the field is most populated and found that only for 6 clusters out of 21 in APOGEE DR12 more than 3 probable members were observed (two further clusters have more than 3 members but no calibrated abundances, so we could not apply step 6 of our membership analysis). Analysing all clusters with more than 20 and less than 50 stars within their radius we find only one additional cluster with more than 3 members in APOGEE. We did not pursue the analysis for clusters with a less populated field, since our membership analysis becomes very difficult for low number statistics. While it is true that the criteria used for our membership analysis are very conservative, other studies have found comparable results. Frinchaboy et al. (2013), e.g., published a list of 28 open clusters from APOGEE DR10 from which they derive chemical gradients of the Galaxy. However, only 11 of these clusters have at least 3 members after their membership analysis.

We note that the stars found to be member of a cluster usually lie on the RGB or RC (especially for APOGEE), which together with the very low number of members makes it impossible to investigate the chemical homogeneity within the cluster. The only cluster for which a sufficient number of members in different evolutionary stages were observed is M67, which therefore became the subject of the investigations presented in this work.

With this introductory chapter we want to demonstrate that in order to carry out efficient spectroscopic observations of open cluster members, a careful membership analysis is needed beforehand. Unfortunately, often no information about the RV of the cluster is available a priori and since the PM at the researchers' disposal so far are still affected by large errors, a membership analysis only based on this information and on the photometry of the cluster is not very accurate. For future spectroscopic surveys, the input of the upcoming data releases of the Gaia mission will be of fundamental importance: thanks to the high-precision PM and parallaxes that will become available, it will be possible to perform an accurate membership analysis also without RV and metallicity and thus to choose targets that are very likely to be members of the clusters.

Table 2: Membership analysis results.

APOGEE	N > 1	N > 10	N > 20	N > 50
N clusters	437	135	61	21
N clusters$_{>3memb.}$			7	6

Part II

STUDYING THE EFFECTS OF STELLAR EVOLUTION IN THE STARS OF M67

Single stellar populations, being born from the same molecular cloud at virtually the same time, are often assumed to share the same chemical composition. While this assumption is quite accurate for the initial chemical composition of the stars, once stellar evolution sets in it does not hold any longer. Processes such as atomic diffusion, the first dredge-up and extra-mixing result in variations in the stellar surface chemical composition depending on their evolutionary stage. This has broad implications: e.g., atomic diffusion effects set a constraint to the precision achievable by chemical tagging methods, while the post-dredge-up [C/N] ratio can be used for the age-dating of field stars. Open clusters are ideal examples of single stellar populations and are therefore extremely useful for the study of stellar evolution. We present an investigation of stellar evolutionary effects in the well-known old open cluster M67 based on high-resolution spectra from APOGEE and the Gaia-ESO Survey, including a comparison with the predictions of theoretical models.

THE POST-DREDGE-UP [C/N] ABUNDANCE AS AN AGE INDICATOR

This chapter is a partially revised version of Bertelli Motta, C., M. Salaris, A. Pasquali, and E. K. Grebel (2017). 'Observing the products of stellar evolution in the old open cluster M67 with APOGEE'. In: MNRAS 466, pp. 2161–2174.

C. Bertelli Motta performed the analysis and the interpretation of the results with the help of A. Pasquali and M. Salaris and wrote most of the text. The abundances and stellar parameters analysed in this chapter were retrieved from the APOGEE twelfth and thirteenth data releases. M. Salaris provided the models of stellar evolution used for comparison as well as Fig. 21. He also contributed to the writing of the introduction and part of the discussion of the paper, which were revised by C. Bertelli Motta when writing this chapter. All authors contributed with comments to the realisation of this study.

3.1 INTRODUCTION

One of the challenges of modern astrophysics is the age-dating of field stars in the Milky Way. While determining the age of field stars is of great importance for our understanding of Galactic evolution, obtaining this information can be very difficult. First of all, precise measurements of stellar parameters and abundances are needed for stars in different evolutionary phases representing a possibly large range of the Galactic history. In this context, large spectroscopic surveys at high resolution, such as Gaia-ESO (see, e.g., Gilmore et al., 2012) and the Apache Point Observatory Galactic Evolution Experiment –APOGEE– (see, e.g., Holtzman et al., 2015) are very useful, since they observe and analyse homogeneously large samples of stars and in particular RGB and red clump (RC) stars. While on the one side red giant stars are very suitable for age-dating studies, being bright and covering a large age range (from $\sim$ 1 Gyr to approximately the age of the Universe), on the other side they are very sensitive to stellar parameters, and small variations in effective temperature T_{eff} at fixed gravity $\log g$ can lead to large errors in the determination of their mass, in the absence of asteroseismic measurements. Since mass and age are connected at fixed evolutionary stage, this translates in large uncertainties in the age determination.

Masseron and Gilmore (2015) used the [C/N] abundance in stars that have completed the first dredge-up (FDU) and that are fainter than the RGB bump (after which extra-mixing effects can take place, see Section 3.2.3) as an age indicator. In fact, as we know from stellar models, while stars are on the main sequence carbon and nitrogen are processed in the stellar interiors through the CNO-cycle (independently if the CNO-cycle is the most efficient mechanism in producing energy) and by the time the stars reach the turn-off (TO), the CN-cycle equilibrium values are reached in the inner layers partially processed by H-burning. These values correspond to a decrease in carbon and an increase in nitrogen with respect to

the initial abundances. When the stars leave the MS and the convective envelope, deepening into the stellar interior, reaches the layers that have been interested by H-burning, the processed material is brought to the surface, thus changing the observed [C/N] abundance of the star.

The decrease in surface [C/N] abundance due to the FDU depends on the stellar mass, and as a consequence on its age, since for stars of increasing mass a larger fraction of the total mass is interested by the FDU. More massive stars will thus experience a larger decrease in surface [C/N] abundance during the FDU than less massive ones, corresponding to older stellar populations.

Martig et al. (2016) used a sample of field stars for which masses from astero-seismic measurements are available, to build a semi-empirical calibration of the $[C/N]_{FDU}$-chemical composition-age relation (where $[C/N]_{FDU}$ is the post-FDU [C/N] abundance). They estimate the accuracy of the ages determined with this relation to be ∼ 40%.

Salaris et al. (2015) presented a theoretical calibration of the $[C/N]_{FDU}$-metallicity-age relation, which reaches an internal accuracy of ∼ 15% in the age determination of RGB stars. Since, however, using different sets of theoretical models was shown to produce large variations in the resulting $[C/N]_{FDU}$-metallicity-age relation (especially for ages < 10 Gyr), the authors conclude that it is necessary to test the validity of these calibrations with observational results. Open clusters are very useful in this context because their age can be independently estimated through isochrone fitting, and their $[C/N]_{FDU}$ can thus be compared with the theoretical predictions for RGB stars of the same age and metallicity.

In Salaris et al. (2015) the $[C/N]_{FDU}$ abundances of few open clusters were compared to the theoretical $[C/N]_{FDU}$-metallicity-age relation, including a spectroscopic estimate of the $[C/N]_{FDU}$ in M67 by Gilroy and Brown (1991). Nevertheless, the errors on this measured abundance were very large and as a consequence they did not constrain the theoretical relation very strongly. The aim of the study presented in this chapter is to follow the evolution of the [C/N] abundance along the SGB and the RGB and until the RC of M67 with data from APOGEE DR12 in order to obtain a more precise value for $[C/N]_{FDU}$ to be compared to the theoretical predictions and to investigate possible extra-mixing processes after the RGB bump.

This chapter is organised as follows. Section 3.2 describes the spectroscopic data, compares the APOGEE spectroscopic abundances with other estimates from the literature, with the predictions from theoretical models, and the $[C/N]_{FDU}$-age relation by Salaris et al. (2015). Finally, discussion and conclusions close the chapter.

3.2 DATA AND RESULTS

In this chapter, we analyse data from the Apache Point Observatory Galactic Evolution Experiment (APOGEE, see Majewski et al., 2015) as part of the Sloan Digital Sky Survey III (SDSS-III, DR12, see Alam et al., 2015; Eisenstein et al., 2011) using stellar parameters and abundances derived with the APOGEE Stellar Parameters and Chemical Abundances Pipeline (ASPCAP) (see García Pérez et al., 2016; Holtzman et al., 2015).

We carry out a membership analysis for the stars observed in APOGEE DR12 in the field of M67 as described in Chapter 1. For the selected sample, we then investigate the elemental abundances affected by stellar evolution, in particular [C/Fe] and [N/Fe] (Tables 3 and 6 contain information about the parameters and abundances of the 34 selected member stars). These effects are very well illustrated by Fig. 15 and Fig. 16. The [C/Fe] and [N/Fe] abundances of the M67 members vary along the isochrone, starting with pre-FDU abundances on the subgiant branch and gradually showing the effect of the FDU on the red giant branch. In addition, the [C/Fe] and [N/Fe] distributions exhibit two peaks representing the pre- and post-FDU abundances.

Some preliminary considerations are due before we compare the APOGEE carbon and nitrogen abundances of our sample with theoretical models. The results of the ASPCAP DR12 pipeline are extensively discussed in Holtzman et al. (2015), including tests on the homogeneity of the abundances within single clusters and the consistency with previous values from the literature. Under the assumption that members of a given cluster should share the same surface abundances, with the exception of C and N which vary due to mixing processes, they correct all trends found in T_{eff} for the measured abundances, except for C and N. They then conclude that the [X/H] abundances derived with ASPCAP DR12 for some elements might suffer from systematic offsets of the order of $0.1 - 0.2$ dex with respect to other values found in the literature. They suggest, however, that using [X/Fe] abundances calculated subtracting [Fe/H] from [X/H] should at least partially correct for possible trends and offsets present in the data. We therefore use in the following analysis only abundances in the form [X/Fe]. Given these considerations, it is important to compare the ASPCAP DR12results to other independent estimates of the C and N abundance in M67 from high-resolution spectroscopic measurements, in order to estimate how reliably we can compare the ASPCAP DR12 results to theoretical models.

3.2.1 *Comparison with high-resolution spectroscopy*

Unfortunately, not many high-resolution spectroscopic measurements of the C and N abundances in M67 stars are available in the literature. In the following we refer to abundances derived for a sample of TO stars by Shetrone and Sandquist (2000) and for RC and RGB stars after the RGB bump by Tautvaišiene et al. (2000) (see Fig. 17 and Table 7 and 8 for details about the selected stars). If we assume that the abundances do not vary between the TO and the SGB, we should find the results from Shetrone and Sandquist (2000) to be consistent with the C and N abundances from APOGEE DR12 before the start of the FDU.

In Fig. 18 we compare the ASPCAP DR12 [C/Fe], [N/Fe], and [O/Fe] abundances as a function of colour $(J - K_s)_0$ (corrected for the reddening $E(J - Ks) = 0.021$ mag) with the abundances derived by Shetrone and Sandquist (2000) and Tautvaišiene et al. (2000). We obtained the colours for the two samples from the literature matching the coordinates of the stars with the 2MASS catalogue (Skrutskie et al., 2006). The oxygen abundance was included in this comparison for reasons that will be explained later in this section.
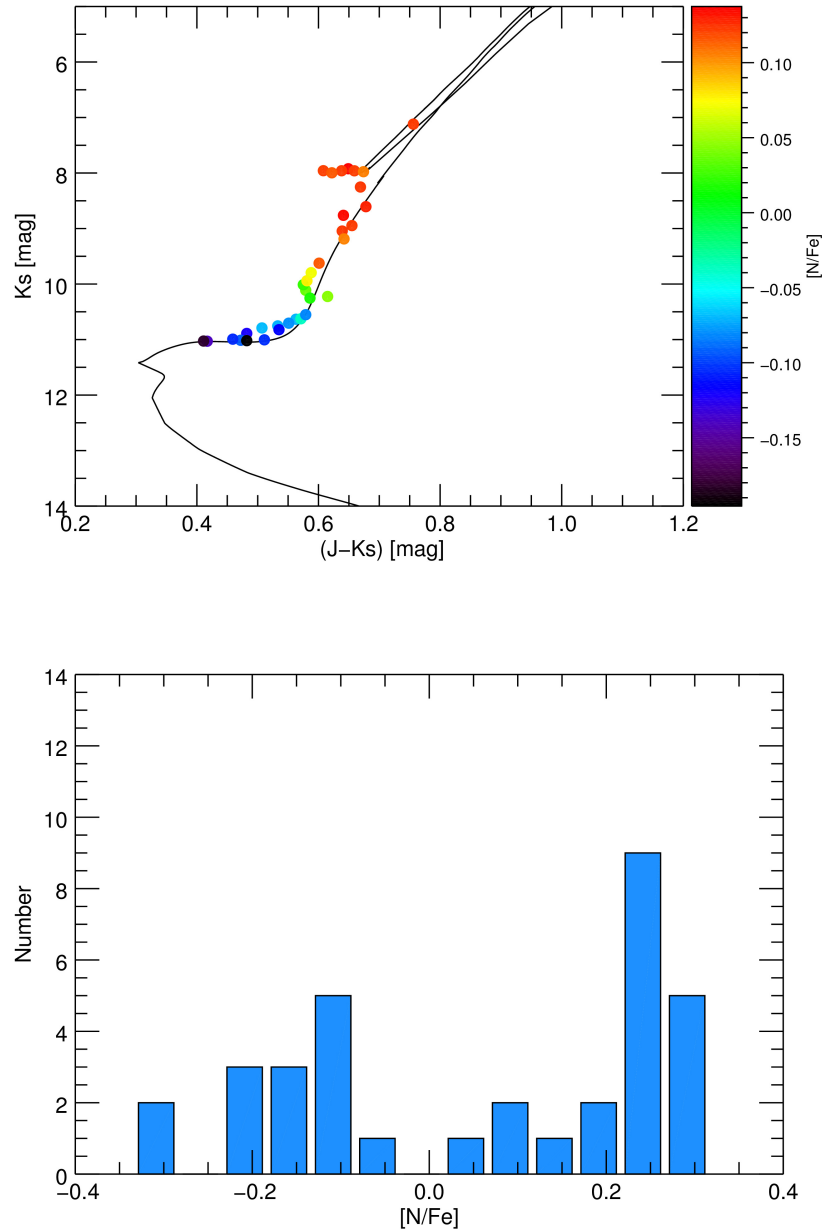
Figure 15: *Top panel:*Colour-magnitude diagram of the member stars of M67with an over-plotted 3.75 Gyr isochrone. The symbols representing the stars are colour-coded with their [N/Fe] abundance. The effect of the first dredge-up can be seen clearly at the transition between the SGB and the RGB. The N produced by the CNO cycle is brought to the surface, thus enhancing its abundance. *Bottom panel:* Histogram showing the [N/Fe] abundance distribution of the member stars of M67 (mean error [N/Fe]$_{err}$ ∼ 0.08 dex). The distribution does not represent the expectations for the chemical composition of the MS of an open cluster, i.e. a single peak with a small variation. The abundance distribution of the subgiants and giants shows instead two peaks in [N/Fe].
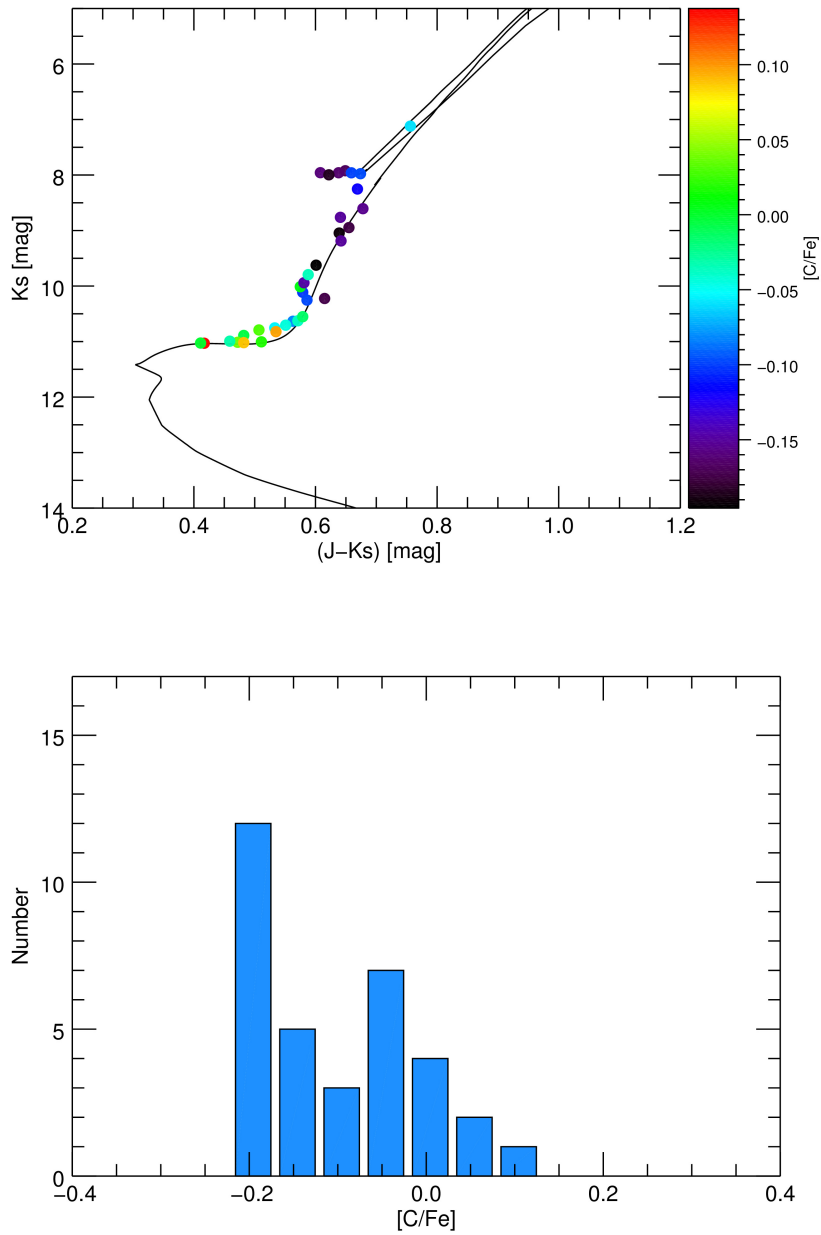
Figure 16: *Top panel:* A 3.75 Gyr isochrone is shown overplotted on the members of M67. The member stars are colour-coded according to their [C/Fe] abundance. In contrast to N, the abundance of C decreases during the CNO cycle, and as a consequence the surface abundance of [C/Fe] after the first dredge-up is depleted. *Bottom panel:* Histogram of the [C/Fe] abundance of the member stars of M67 (mean error [C/Fe]$_{err}$ ~ 0.06 dex). Also in this case, two peaks in the abundance distribution are visible, although not as distinctly as in the case of [N/Fe].

The averages of the [C/Fe], [N/Fe], and [O/Fe] abundances derived by Tautvaišiene et al. (2000) for the RC are -0.18 ± 0.02, 0.26 ± 0.06 and 0.01 ± 0.05 dex (the error bar corresponds to the σ dispersion around the mean), respectively. The average abundances derived by ASPCAP DR12 for the RC stars of M67, [C/Fe] = -0.15 ± 0.04, [N/Fe] = 0.29 ± 0.02, and [O/Fe] = 0.00 ± 0.02 dex, are consistent with the results of Tautvaišiene et al. (2000) within the errors. We point out that colours and effective temperatures of the RC stars correspond to those of stars on the RGB after the FDU is complete.

Similarly, the mean [C/Fe] and [O/Fe] abundance derived from the measurements of Shetrone and Sandquist (2000) (-0.01 ± 0.10 and -0.02 ± 0.08 dex, respectively) for TO stars, are consistent with the average abundances from ASPCAP DR12 ([C/Fe] = 0.04 ± 0.07 dex and [O/Fe] = 0.02 ± 0.02 dex) found for stars with $(J - K_s)_0 <0.47$, i.e. before the onset of the FDU.

In order to understand if the agreement between abundances at the TO and in more evolved SGB stars can be interpreted as a proof of the accuracy of the ASPCAP DR12 results for stars in this temperature range, we need to discuss the effects of atomic diffusion on the surface chemical composition of these stars.

Atomic diffusion is an evolutionary process that can alter the surface abundances of stars and that is active during the MS phase. It results from the combination of gravitational settling, thermal and chemical diffusion, and radiative acceleration and causes an increase or a decrease in surface abundance depending on the force prevailing on a given ion (gravity or radiative acceleration). This effect reaches its maximum at the TO, after which the deepening of the convective envelope during the SGB phase essentially restores the initial abundances(see, e.g., Cassisi and Salaris, 2013, and references therein).

In Michaud et al. (2004) the authors present stellar evolutionary models calculated for M67 taking into account the effect of atomic diffusion. As described there, the abundance of the elements in the oxygen group are expected to decrease during the MS phase, reaching a minimum at the TO, and then to increase again along the SGB. By the time the stars reach the RGB the surface abundances are almost the initial ones. The maximum variation at the TO is ~ 0.10 dex. Since, however, iron behaves in a similar way, reaching an under-abundance of ~ 0.08 dex at the TO, abundances in the form [X/Fe] should present smaller variations than [X/H] values.

A study of potential diffusion effects in the stars of M67 was carried out by Önehag, Gustafsson, and Korn (2014) who performed a differential analysis of the abundances in MS and TO stars with respect to early SGB stars, including elements such as C, O, and Fe (and others), but not N. They found differences in abundance between the groups of stars of the order of 0.02 dex, which seem to indicate the presence of diffusion, although the results are not conclusive. The stars in their subgiant sample have temperatures ~ 500 K hotter than the bluest subgiant in our APOGEE sample and average abundances [C/Fe] = -0.04 ± 0.05 dex and [O/Fe] = -0.04 ± 0.07 dex, which are consistent with the mean ASPCAP DR12 abundances obtained for the pre-FDU subgiants.

We thus conclude that there is no compelling evidence of a significant variation in [C/Fe] and [O/Fe] abundance between the TO and the pre-FDU SGB stars, since both the [C/Fe] and [O/Fe] mean abundances obtained by Shetrone and Sandquist

(2000) for a sample of TO stars and by Önehag, Gustafsson, and Korn (2014) for a sample of early SGB stars hotter than our APOGEE sample are consistent within the errors with the abundances obtained by ASPCAP DR12 for stars before the onset of the FDU. Later, in Chapter 4, we will present a detailed study of possible atomic diffusion effects in M67 with data from the Gaia-ESO Survey and we will show that the variations in surface abundances become sizeable when comparing upper-MS / TO stars with stars on the red giant branch.

Considering the above comparisons of the mean ASPCAP DR12 [C/Fe] and [O/Fe] abundances on the SGB and on the RC with independently derived abundances from the literature based on high-resolution spectroscopic data, there is no evidence that the APOGEE data need to be corrected for temperature trends and/or systematic offsets.

The situation for the [N/Fe] ASPCAP DR12 abundances along the SGB is, however, different. While [C/Fe] and [O/Fe] remain constant before the onset of the FDU, [N/Fe] displays a clear trend with colour (and as a consequence with T_{eff}), as can be seen in Fig. 18. The [N/Fe] decreases with bluer colours and increasing temperature and reaches ~ -0.3 dex for the hottest stars in our sample, a large depletion considering that M67 is known to have a chemical composition very similar to the solar one. In this case a comparison with literature estimates is harder since Önehag, Gustafsson, and Korn 2014 did not derive N abundances and the measurements of N in the TO stars of Shetrone and Sandquist (2000) were not very accurate and in two cases represent only upper limits. Nevertheless, they seem to rule out the abundances derived by ASPCAP DR12. Moreover, it is difficult to think of a process that would be capable of changing the surface N abundances along the SGB leaving C and O unchanged. We thus conclude that, since M67 is known to have an approximately solar metallicity, which is confirmed by the pre-FDU abundances of C and O, it is reasonable to assume that also the N abundance is constant and approximately solar before the onset of the FDU. In addition, a surface abundance of [N/Fe]=0.0 dex for the pre-FDU stars would be consistent with abundances (or upper limits) derived by Shetrone and Sandquist (2000).

In support of this interpretation of the ASPCAP DR12 results we refer to Masseron and Gilmore (2015). Studying field subgiant stars in the thin and thick disc within APOGEE, they found an offset of -0.2 dex in the [N/Fe] abundance at solar metallicity, similar to what we observe in our selection of member stars for M67. This suggests that we are dealing with a systematic problem in the APOGEE data, or of the ASPCAP DR12 pipeline, and not with a peculiarity of M67. What still remains to be clarified is whether this problem is confined to the SGB or whether it affects all stars within APOGEE. Due to the change of the surface C and N during and after the SGB, it is more difficult to determine deviations of the observed abundances from the predicted ones for field stars of which we do not know the mass. Masseron and Gilmore (2015) do not investigate the problem further and on the basis of the observed depletion in the SGB they shift the [N/Fe] abundances of the entire sample by $+0.2$ dex. While for the investigation of Masseron and Gilmore (2015) this does not affect the results, for our study it is important to investigate whether this systematic offset is real.

We have shown that the [N/Fe] abundances of our sample of red giant branch and red clump stars fit very well those of stars independently observed and ana-
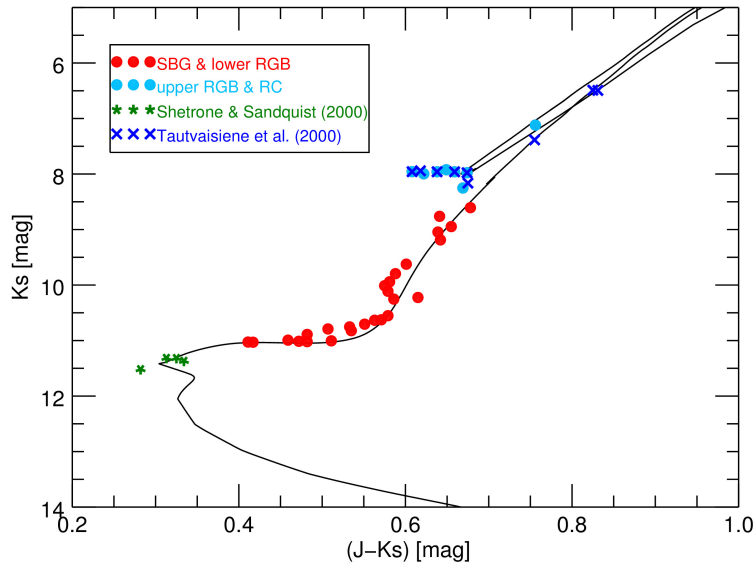
Figure 17: The plot shows our selection of M67 members from APOGEE together with stars analysed in other works. In particular, we consider the TO stars studied by Shetrone and Sandquist (2000) and the giant and clump stars from Tautvaišiene et al. (2000).

lysed by Tautvaišiene et al. (2000). Thus, we do not see any reason why the [N/Fe] abundances should be shifted by 0.2 dex for the entire sample of APOGEE stars. We claim that the reason for the systematic offset of [N/Fe] abundances in the APOGEE subgiant regime is due to the increasing temperature of the stars going from red to bluer colours. The [N/Fe] abundances in the ASPCAP DR12 pipeline are calculated from CN molecular lines. These become progressively weaker and more difficult to analyse as the effective temperature of the stars increases, thus leading to untrustworthy results in the subgiant region. We therefore will not consider stars bluer than $(J - Ks)_0 = 0.54$ mag (the approximate value at which the APOGEE [N/Fe] abundances reach the solar value), corresponding to a temperature hotter than $T_{eff} \sim 5000$ K.

3.2.2   *Comparison with the models*

After having found a reasonable explanation for the offset of [N/Fe] abundances in the SGB in DR12, we can proceed with the comparison between the APOGEE data and the predictions from stellar evolution models.

In Fig. 19, we plot the [C/N] abundance obtained for our sample of M67 members as a function of $(J - K_s)_0$ colour together with two different models for stars of the masses $1.40 M_{\odot}$ and $1.35 M_{\odot}$, [Fe/H] = 0.06 dex (from the BaSTI database). These correspond to an age of 4 and 3.75 Gyr, respectively, considered to be the TO age range of M67 following Bellini et al. (2010b), who also employed the same BaSTI models used in this work. The light-blue circles represent stars that might have undergone extra mixing and are therefore not suitable for the computation of the post-FDU [C/N] abundance. Finally, the orange diamonds represent the stars
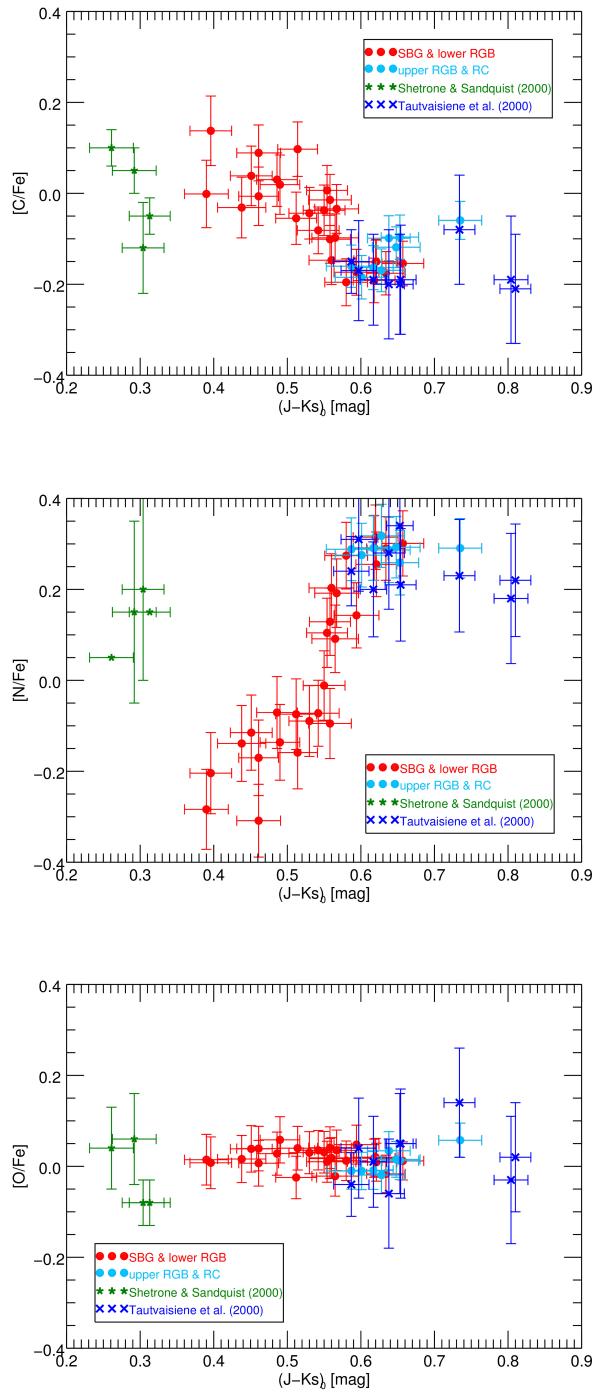
Figure 18: The [C/Fe], [N/Fe], and [O/Fe] abundances of the APOGEE sample and those from the literature are plotted as a function of colour. This picture confirms that the abundances from Shetrone and Sandquist (2000) and Tautvaišiene et al. (2000) agree well with the expectation for solar values before the first dredge-up and with the values derived with ASPCAP DR12 after the first dredge-up. While [C/Fe] and [O/Fe] for the APOGEE sample agree very well with the literature values, [N/Fe] appears to be depleted by ∼ 0.2 dex on the SGB.
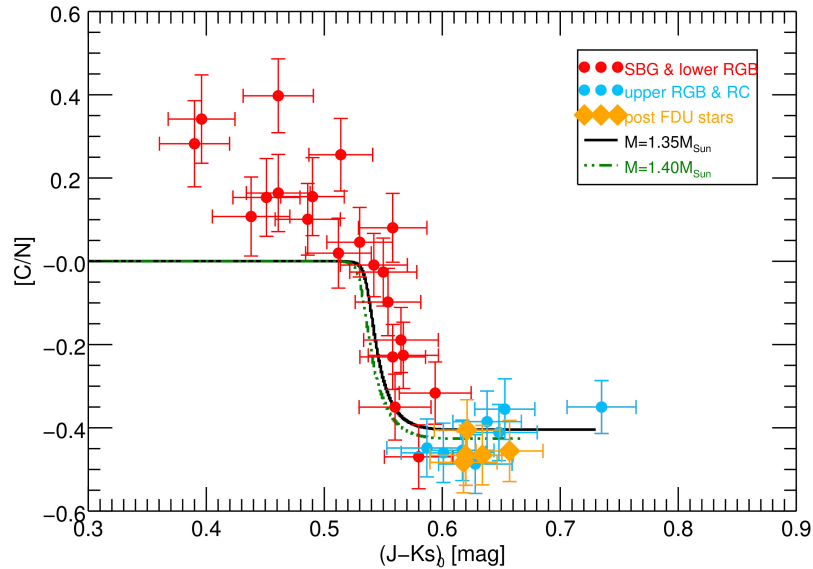
Figure 19: The plot shows the [C/N] abundances derived by ASPCAP DR12 as a function of the $(J-K_s)_0$ colour compared with two models characterised by different masses (solid black line for $1.35 M_\odot$ and green dash-dotted line for $1.40 M_\odot$). The light blue circles represent stars of the RGB and RC that are excluded from the computation of the post-dredge-up [C/N] abundance due to possible extra mixing in their interior. The orange diamonds are the stars used to calculate the mean value for the post-dredge-up [C/N] abundance.

that we used to compute the post-FDU mean [C/N] abundance, as we will explain later in this section. We selected them based on the colour at which the FDU is complete, $(J-K_s)_0 > 0.6$ mag, and excluding stars brighter than the red giant bump luminosity from the models, $K_s < 8.5$ mag.

The ASPCAP DR12 abundances for stars with $(J-K_s)_0 > 0.54$ mag are consistent with the predictions of the models representing the age range of M67. In Fig. 20 the [C/Fe] and [N/Fe] abundances of the M67 stars and the respective models are plotted separately as a function of the $(J-K_s)_0$ colour. Also in this case the data are in good agreement with the models, if we exclude the [N/Fe] depletion in the subgiant range. We also compared the ASPCAP DR12 results with models using different assumption regarding envelope overshooting in the SGB. We found that all models are consistent with the observational data and that we cannot distinguish between them within the errors (see Salaris et al. 2015 for details about the effect of envelope overshooting on $[C/N]_{FDU}$).

We use five stars to determine the mean [C/N] abundance in M67 after the FDU (orange diamonds in Fig. 19), which we then compare with the models from Salaris et al. (2015) for the age estimation of field stars (see Fig. 21). We obtain an abundance of $[C/N]_{FDU} = -0.46 \pm 0.03$ dex, which is consistent with the prediction of $[C/N]_{FDU} = -0.4$ dex for the models with stellar mass $M = 1.35 M_\odot$ and of $[C/N]_{FDU} = -0.43$ dex for $M = 1.4 M_\odot$.
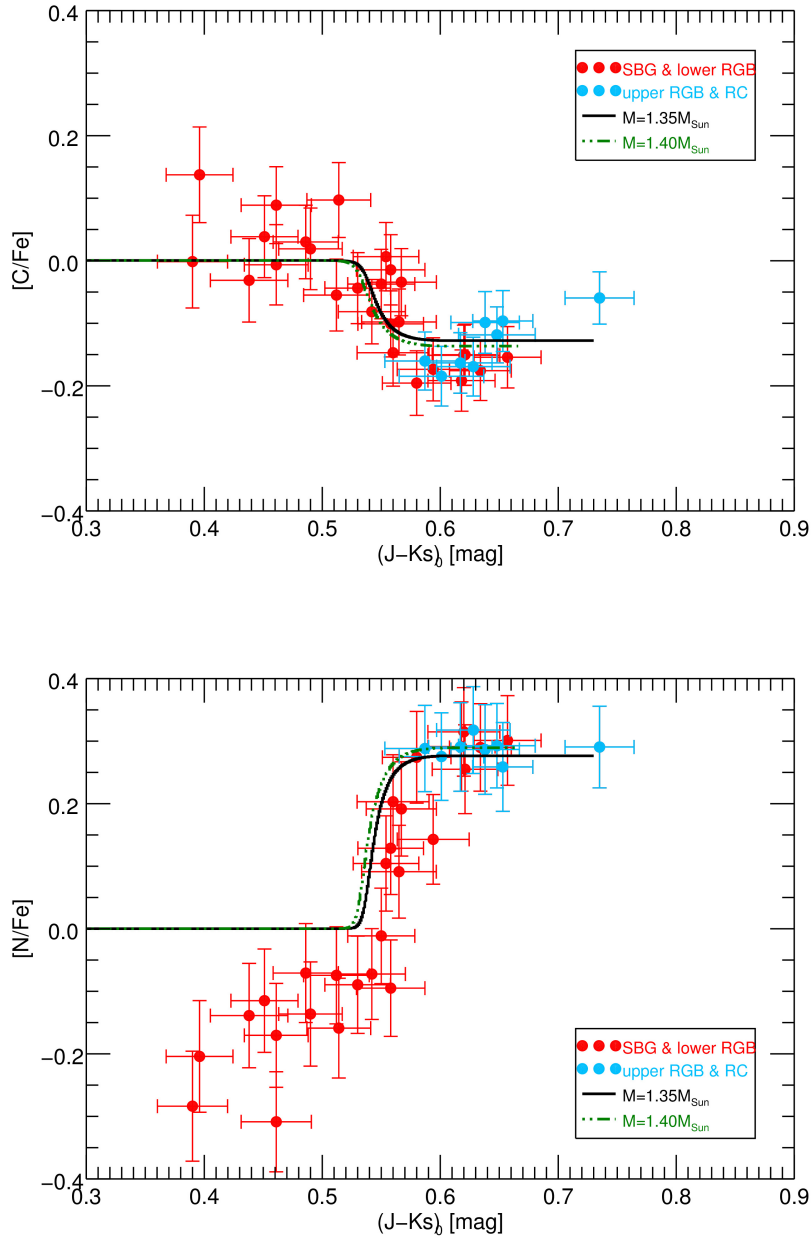
Figure 20: [C/Fe] and [N/Fe] as a function of the $(J - K_s)_0$ colour is plotted together with the respective model predictions. While the MS abundance of [C/Fe] derived with ASPCAP DR12 is consistent with a solar composition and with the models, the [N/Fe] abundance before the FDU is depleted and does not agree with the models.
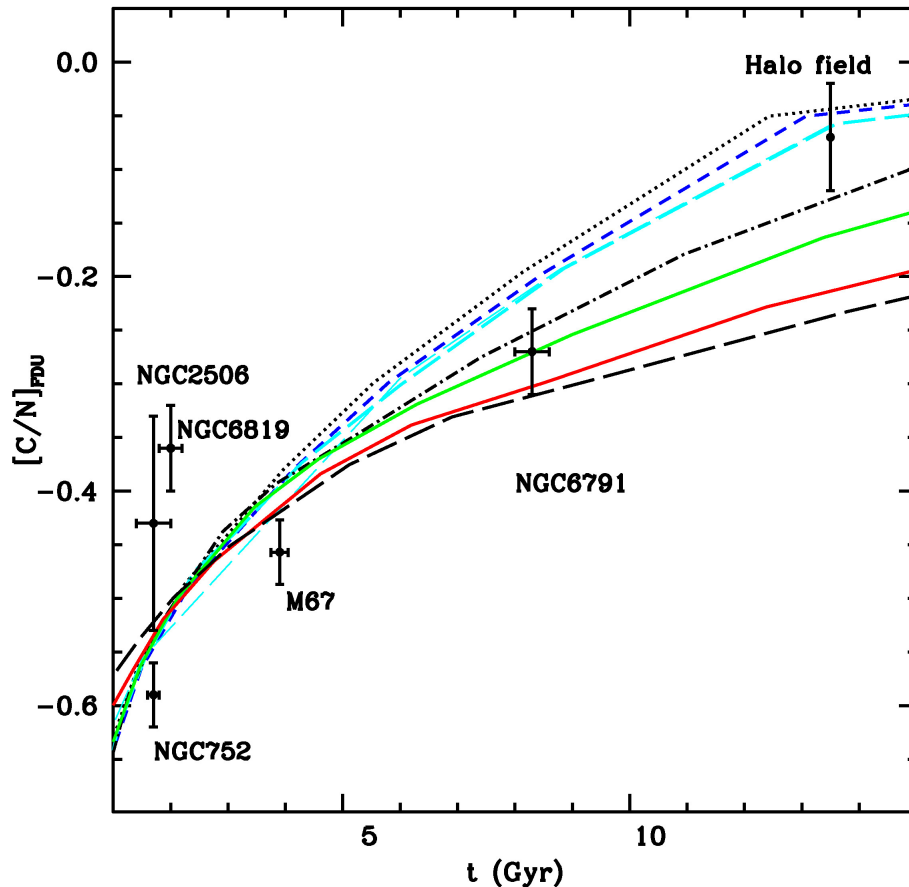
Figure 21: As Fig. 2 from Salaris et al. (2015): The plot shows the theoretical value of $[C/N]_{FDU}$ as a function of age for different metallicities. The curves shown computed for different [M/H]: -2.27 dex (black dotted line), -1.49 dex (blue short dashed), -1.27 dex (light blue long dashed), -0.66 dex (black dot-dashed), -0.35 dex (green solid), 0.06 dex (red solid) and 0.26 dex (black long dashed), respectively. Values for the $[C/N]_{FDU}$ of several Galactic open clusters and halo field stars available in the literature are also plotted (see Salaris et al. 2015 for details), together with the new $[C/N]_{FDU}$ value for M67 obtained in the current work.

Fig. 21 updates Fig. 2 in Salaris et al. (2015) with the $[C/N]_{FDU}$ of M67 obtained in this study. The errors are considerably smaller and the post-FDU $[C/N]_{FDU}$ is in better agreement with the models.

3.2.3   *Post-FDU extra mixing*

As mentioned above, we exclude bright RGB stars and RC stars to avoid problems related to possible extra mixing episodes that set in after the RGB bump. The mean molecular weight discontinuity left over by the FDU is expected to inhibit any extra-mixing below the convective envelope, but when this discontinuity is erased after the RGB bump, extra-mixing processes are possible, as shown for example by the evolution of the C^{12}/C^{13} ratio in field giants at various metallicities (Charbonnel and Balachandran, 2000, and references therein).These extra mixing processes
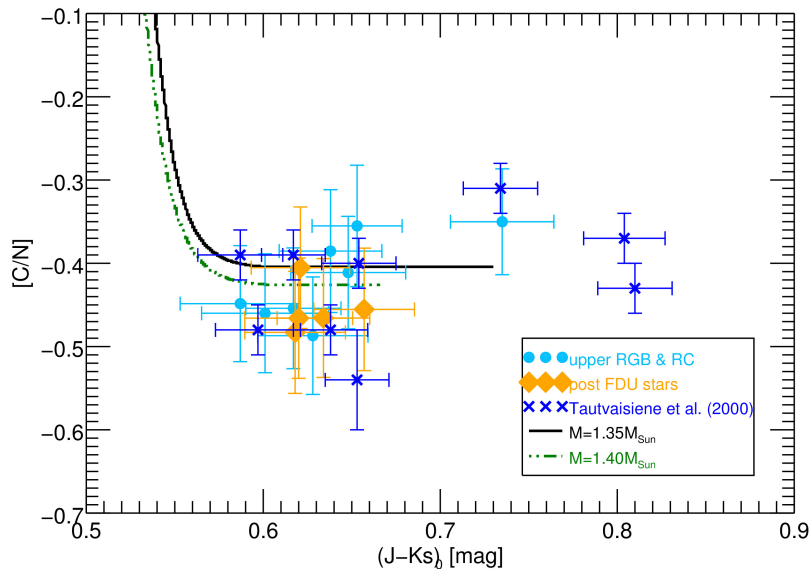
Figure 22: The plot shows the [C/N] abundances for the post-FDU (orange diamonds), and upper RGB and RC (light-blue circles) APOGEE stars in M67, as well as for the RGB and RC stars from Tautvaišiene et al. (2000). The data are compared to the models for stellar masses of $1.35M_\odot$ (black solid line) and $1.4M_\odot$ (green dashed-dotted line).

can also decrease the [C/N] ratio compared to the FDU value (N increases and C decreases), as seen, e.g., in field halo stars (Gratton et al., 2000).

Our sample of M67 members contains seven red clump stars as well as one bright red giant branch (or possibly AGB) star. Fig. 22 shows that the [C/N] abundances of the red clump stars are consistent with the post-FDU [C/N] abundance and do not appear to be affected by any extra mixing process. On the other hand, the [C/N] of the upper RGB star ($K_s < 8.5$ mag) is higher than $[C/N]_{FDU}$ and the value predicted by the models, contrarily to the drop in [C/N] expected from extra mixing. If we add the upper RGB and RC stars independently observed and analysed by Tautvaišiene et al. (2000) to this sample, we see this picture confirmed (see also Fig 6 in Tautvaišiene et al. 2000): RC stars have [C/N] abundances comparable to the $[C/N]_{FDU}$ value, while the [C/N] in upper RGB stars is slightly higher (see Fig. 22). This suggests that at the age and metallicity of M67 extra mixing after the red giant bump is not playing a significant role and that there might even be a different process taking place that has the opposite effect on the surface abundances of upper RGB stars.

We note that the study by Souto et al. (2016), analysing the chemical composition of six RC and six lower RGB stars in the ~ 2 Gyr old open cluster NGC 2420 from APOGEE spectra found similar results. The RC stars in NGC 2420 show the same $^{13}C/^{14}N$ as the lower RGB stars, suggesting that no extra-mixing is taking place after the luminosity bump.

Unfortunately, our sample of upper RGB stars (also taking into account the stars from Tautvaišiene et al. 2000) is very small, so that no statistically significant conclusion can be drawn. We argue that more high-resolution spectroscopic observa-

tions of upper RGB stars in M67 are necessary to assess the role of extra mixing in such stars.

3.3 APOGEE DR13

Shortly after our study was completed, the 13th data release of the Sloan Digital Sky Survey was made public. We performed the same analysis as for the DR12 data described in this chapter in order to determine the degree of agreement between the new results derived with the updated ASPCAP DR13 pipeline with the old ones.

In the DR13, some changes have been applied to the stellar parameter pipeline of APOGEE (see SDSS Collaboration et al. 2016, Holtzman et al. in prep.). For instance, different synthetic grids are now used for giants and dwarfs, allowing rotation for the latter. As a consequence, many TO and upper-main-sequence stars of M67, which had been previously excluded from our membership analysis, present now calibrated parameters from the ASPCAP DR13 pipeline. We thus find 78 member stars for M67, in contrast to the 34 found from the DR12 (see Fig. 23).

Plotting the [C/N] abundance as a function of $(J - Ks)_0$ with the DR13 data, we find that the main-sequence and TO stars are consistent with a solar chemical composition. The sub-giant and giant stars, on the other hand, show a very large scatter and the post-dredge-up average [C/N] value for the cluster is lower with respect to the DR12 and the high-resolution spectroscopic data found in Shetrone and Sandquist (2000) and Tautvaišiene et al. (2000) (see Fig. 24).

When looking at the different elemental abundances separately, the changes applied to the ASPCAP pipeline in the DR13 seem to have solved the problem of the depletion for the [N/Fe] abundances in the sub-giant branch (see Fig. 25, panel a). Nevertheless, while giant-branch and red-clump stars in the DR12 were consistent with the results of high-resolution spectroscopic studies found in the literature, in the DR13 the post-dredge-up values for [N/Fe] are systematically enhanced with respect to Tautvaišiene et al. (2000). In particular, the red clump and upper red giant branch stars of APOGEE DR13 have on average a [N/Fe] value that is 0.12 dex higher than in Tautvaišiene et al. (2000).

Plotting the DR13 results for the [C/Fe] and [O/Fe] abundances as a function of $(J - Ks)_0$, we observe a very large scatter of the data affecting the giant stars for the former and the main-sequence and TO stars for the latter (see Fig. 25, panel b and c). In comparison with Tautvaišiene et al. (2000) the [C/Fe] abundance in red clump and upper red giant stars in APOGEE DR13 is on average 0.10 dex higher, while the [O/Fe] abundance is only 0.05 dex lower.

In addition, we note that the stellar evolutionary models described in Sec. 3.2.2, representing a stellar mass of $1.4 M_\odot$ and an age of 3.75 Gyr, which were consistent with the results of the DR12, reproduce very poorly the abundances resulting from the DR13 (see Fig. 24 and Fig. 25). We run a χ^2 test to quantify and compare the goodness of the fit between the APOGEE DR12 and 13 data, with

$$\chi^2 = \sum_i \frac{(O_i - E_i)^2}{\sigma_i^2}, \tag{17}$$
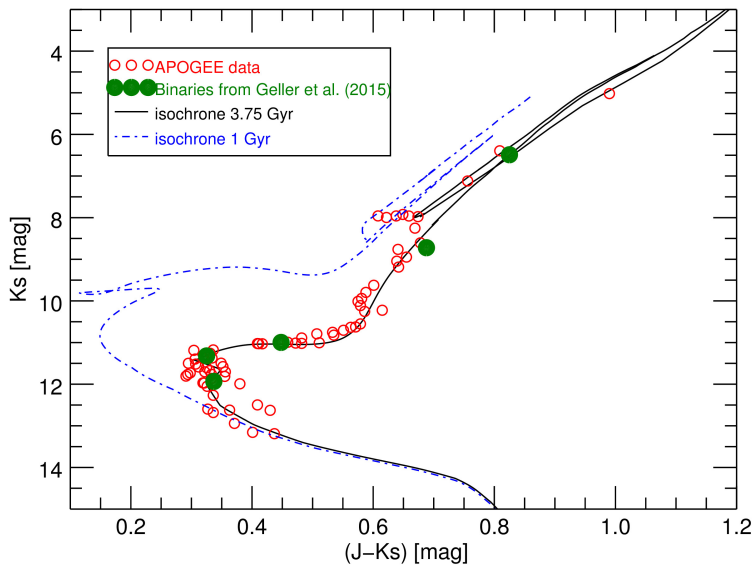
Figure 23: Selection of the members of M67 for the DR13. Binaries are highlighted in green and are excluded from further analysis. The 1 Gyr isochrone represents the age needed to fit the DR13 post-dredge-up [C/N] value with stellar evolutionary models.

where O_i are the observed values of [C/N], E_i the $[C/N]_{FDU}$ abundance predicted by the models, and σ_i the errors of the observations. We considered only stars that have already completed the first dredge-up, i.e. with $(J - Ks)_0 > 0.6$ and $Ks > 8.5$ mag (orange diamonds in Fig. 24), and found $\chi^2 = 1.5$ for the DR12 versus $\chi^2 = 164.6$ for the DR13.

If, in addition, we wanted to fit the mean $[C/N]_{FDU}$ obtained from the same selection of stars for the DR13 ([C/N] = −0.53 dex) with the same set of stellar evolutionary models, we would obtain a stellar mass corresponding to an age of ∼ 1 Gyr, which, however, is not consistent with the observed CMD of M67, as shown in Fig. 23.

   To summarise, the changes applied to the ASPCAP pipeline in DR13 seem to have improved the problem of the systematic depletion in [N/Fe] observed in hot stars in the DR12. Nevertheless, the overall results for the abundances of sub-giant and giant stars in the DR13 are in worse agreement with literature values than in the DR12. This would indicate that further adjustments have to be made to the ASPCAP pipeline in order to improve the abundance determination for certain elements at cooler temperatures and higher luminosities.

3.4   CONCLUSIONS

In this study we analyse the pre- and post-FDU [C/N] abundance in the old open cluster M67 and use it as a calibrator for the age-dating of field stars (see Salaris et al., 2015). In order to assess the accuracy of our analysis, we compare data obtained within the APOGEE DR12 survey and analysed by the stellar parameters and abundances pipeline ASPCAP with [C/Fe] and [N/Fe] values from the lit-
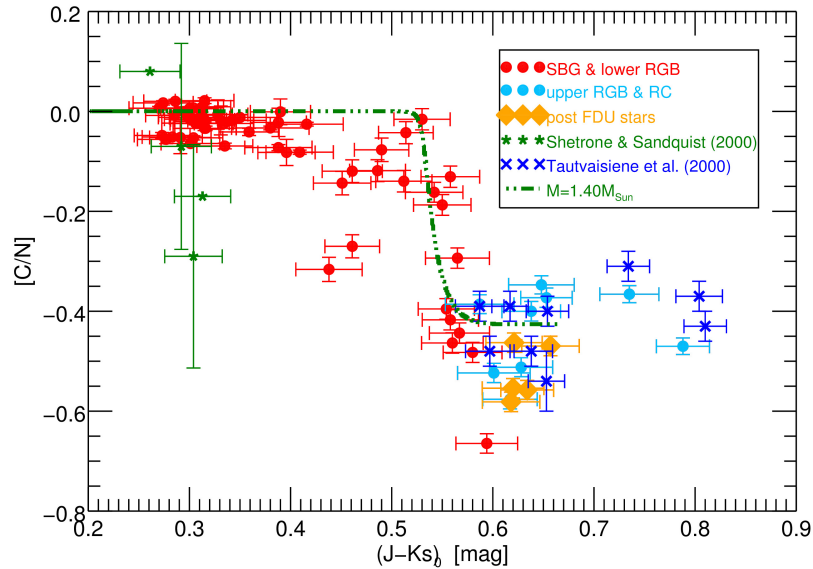
Figure 24: [C/N] abundance as a function of colour $(J − Ks)_0$. The orange diamonds indicate the stars that have completed the first dredge-up.

erature for TO (Shetrone and Sandquist, 2000), red giant branch, and red clump (Tautvaišiene et al., 2000) stars in M67.

We find the [C/Fe] abundances from ASPCAP DR12 to be in very good agreement with the literature, both before and after the FDU. Less straightforward are the results for [N/Fe]. While the values of our sample after the FDU are consistent within the errors with the results from Tautvaišiene et al. (2000), the abundances in the subgiant region appear systematically depleted and even show a trend with colour. Taking into account the results by Masseron and Gilmore (2015), we assert that the depletion of [N/Fe] in the subgiant region is a problem common to the entire sample of APOGEE stars, and not a characteristic of M67. Possibly, the offset shown by the data is a result of the decreasing precision of the [N/Fe] measurements in ASPCAP DR12 with increasing temperature due to the weakening of the molecular bands used for the abundance determination.

The problem of the systematic underestimation of [N/Fe] in the sub-giant branch seems to have been overcome in the recently published SDSS DR13 (see Appendix). This, however, happened on the expense of a much larger scatter in the overlall [N/Fe], [C/Fe], and [O/Fe] abundances. In addition, the post-FDU [N/Fe] abundance is not consistent any more with the other spectroscopic studies described in this work and with the evolutionary models (see Appendix for details).

We then compare the ASPCAP DR12 [C/N] abundances with stellar evolutionary models which include core-overshooting and find that the observational data match the theoretical predictions very well within the errors when taking into account the findings described in the above paragraph. We obtain a new estimate for the mean post-FDU [C/N] in M67 of $[C/N]_{FDU} = −0.46 \pm 0.03$ dex which is in good agreement and thus provides a stringent observational test of the
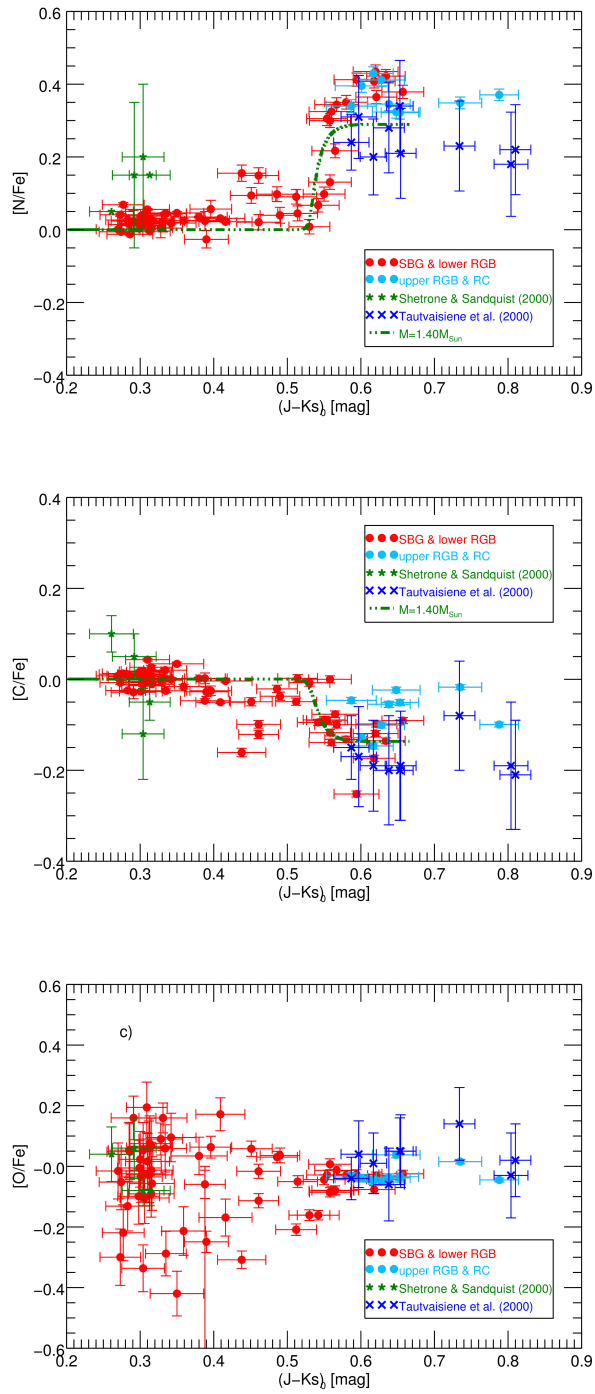
Figure 25: [N/Fe], [C/Fe], and [O/Fe] abundance as a function of colour $(J - Ks)_0$.

$[C/N]_{FDU} - t - [M/H]$ relation of Salaris et al. (2015) (see Fig. 21 as an updated version of Fig. 2 in Salaris et al. 2015).

Finally, we extend our analysis to APOGEE DR13 and find that the agreement between the new data and the results from the literature as well as the models is worse than for the DR12.

Table 3: List of the selected M67 members with their coordinates, radial velocities from APOGEE, proper motions from PPMXL and the respective errors.

Nr	RA (J2000) [hms]	Dec (J2000) [dms]	RV [km/s]	RV_err [km/s]	PMx [mas/yr]	PMy [mas/yr]	PM_tot [mas/yr]	PM_err [mas/yr]
1	08:50:36.134	+11:43:18.005	34.087	.010	-6.270	-5.136	8.105	1.000
2	08:50:49.949	+11:49:12.727	33.716	.015	-6.798	-6.952	9.724	1.100
3	08:50:58.162	+11:52:22.361	34.091	.010	-6.376	-5.451	8.389	1.300
4	08:51:08.390	+11:47:12.142	33.509	.008	-6.597	-6.657	9.372	1.000
5	08:51:12.697	+11:52:42.370	34.389	.002	-6.296	-6.079	8.752	1.900
6	08:51:15.641	+11:50:56.162	34.423	.021	-4.453	-6.784	8.115	1.000
7	08:51:17.040	+11:50:46.424	33.717	.003	-6.574	-7.855	10.243	2.200
8	08:51:18.773	+11:51:18.673	34.360	.012	-5.032	-7.796	9.279	1.100
9	08:51:18.972	+11:58:11.021	33.966	.007	-5.875	-8.473	10.311	1.000
10	08:51:21.564	+11:46:06.121	34.850	.003	-4.703	-6.857	8.315	2.000
11	08:51:26.186	+11:53:52.048	34.164	.002	-5.243	-5.835	7.845	1.856
12	08:51:28.988	+11:50:33.072	33.450	.002	-7.116	-6.483	9.626	.900
13	08:51:29.351	+11:45:27.558	33.095	.011	-4.876	-7.613	9.040	1.100
14	08:51:35.403	+11:57:56.455	33.449	.017	-5.298	-8.643	10.138	1.000
15	08:51:35.778	+11:53:34.714	34.006	.007	-6.155	-7.711	9.866	1.000
16	08:51:38.626	+12:20:14.183	33.755	.012	-6.782	-8.363	10.767	1.200
17	08:51:39.382	+11:51:45.659	34.523	.006	-5.272	-5.846	7.873	.900
18	08:51:42.342	+11:50:07.631	34.349	.004	-4.789	-8.241	9.531	.900

Table 4: Table 3 continued.

Nr	RA (J2000) [hms]	Dec (J2000) [dms]	RV [km/s]	RV_err [km/s]	PMx [mas/yr]	PMy [mas/yr]	PM_tot [mas/yr]	PM_err [mas/yr]
19	08:51:42.358	+11:51:23.098	33.600	.003	-5.744	-6.789	8.893	.900
20	08:51:43.888	+11:56:42.580	33.018	.002	-5.453	-7.740	9.468	1.867
21	08:51:44.013	+11:46:24.521	32.980	.017	-4.664	-7.249	8.619	1.000
22	08:51:44.741	+11:46:46.031	33.593	.011	-4.112	-8.268	9.234	1.100
23	08:51:45.078	+11:47:45.938	33.017	.004	-6.698	-8.237	10.617	1.900
24	08:51:48.838	+11:56:51.191	34.398	.011	-6.823	-8.132	10.615	1.100
25	08:51:55.672	+12:17:57.332	33.381	.015	-7.462	-7.867	10.844	1.200
26	08:51:56.117	+11:50:14.777	34.614	.010	-6.320	-7.828	10.060	1.200
27	08:51:59.522	+11:55:04.922	34.426	.002	-5.641	-6.780	8.820	.900
28	08:52:10.973	+11:31:49.152	33.892	.002	-6.773	-5.520	8.737	1.600
29	08:52:11.343	+11:45:38.023	33.108	.016	-5.249	-8.044	9.605	1.000
30	08:52:16.564	+11:19:38.017	33.769	.001	-7.710	-5.206	9.303	1.532
31	08:52:18.569	+11:44:26.304	33.725	.002	-4.994	-9.190	10.459	.900
32	08:52:20.030	+11:27:36.252	33.946	.007	-4.690	-3.923	6.114	1.900
33	08:52:56.250	+11:48:53.939	32.950	.007	-6.681	-9.800	11.861	1.000
34	08:53:46.727	+11:23:30.714	33.098	.005	-7.282	-6.598	9.827	.900

Table 5: Infrared colours from 2MASS and the respective errors for the list of selected M67 members.

Jmag [mag]	Hmag [mag]	Ksmag [mag]	e_Jmag [mag]	e_Hmag [mag]	e_Ksmag [mag]
11.131	10.644	10.552	.020	.022	.021
11.372	10.960	10.890	.021	.020	.017
11.197	10.707	10.626	.022	.020	.018
10.691	10.195	10.112	.022	.022	.017
8.650	8.122	7.976	.018	.018	.018
11.485	11.094	11.013	.022	.019	.018
9.284	8.712	8.606	.022	.021	.018
11.502	11.089	11.020	.022	.020	.020
10.587	10.095	10.012	.022	.020	.017
9.602	9.085	8.947	.019	.020	.018
8.619	8.113	7.960	.020	.020	.021
8.566	8.072	7.958	.024	.018	.024
11.287	10.864	10.754	.022	.020	.017
11.447	11.143	11.030	.021	.022	.019
10.522	10.023	9.941	.020	.020	.023
11.298	10.866	10.791	.021	.019	.018
10.383	9.889	9.795	.020	.022	.022
9.829	9.339	9.187	.022	.023	.017
9.403	8.854	8.762	.020	.023	.023
8.618	8.114	7.996	.018	.034	.031
11.438	11.110	11.027	.022	.022	.020
211.357	10.918	10.822	.021	.022	.017
9.684	9.183	9.045	.022	.023	.018
11.256	10.779	10.705	.022	.022	.017
11.516	11.115	11.005	.020	.024	.018
11.197	10.726	10.634	.022	.020	.018
8.597	8.084	7.959	.020	.024	.018
8.921	8.388	8.252	.027	.071	.018
11.452	11.082	10.993	.026	.034	.020
7.875	7.233	7.119	.023	.036	.018
8.572	8.087	7.923	.021	.057	.023
10.839	10.383	10.253	.026	.032	.018
10.839	10.315	10.224	.023	.026	.020
10.225	9.730	9.624	.019	.026	.022

Table 6: List of the ASPCAP DR12 abundances and their errors for our selection of M67 members.

Nr	[Fe/H] [dex]	e_[Fe/H] [dex]	[C/Fe] [dex]	e_[C/Fe] [dex]	[N/Fe] [dex]	e_[N/Fe] [dex]	[O/Fe] [dex]	e_[O/Fe] [dex]
1	.080	.034	-.014	.056	-.095	.077	.041	.046
2	.016	.035	-.006	.064	-.170	.083	.007	.050
3	.059	.033	-.037	.056	-.011	.076	.031	.046
4	.121	.033	-.101	.053	.129	.074	.017	.044
5	.079	.032	-.096	.049	.259	.071	.012	.042
6	.066	.035	.038	.065	-.115	.083	.038	.051
7	.086	.033	-.154	.049	.301	.072	.012	.042
8	.071	.034	.089	.061	-.309	.080	.039	.049
9	.029	.034	.007	.055	.104	.076	.010	.045
10	.140	.032	-.176	.048	.290	.070	-.017	.041
11	.059	.033	-.099	.049	.287	.072	.034	.042
12	.118	.032	-.160	.046	.288	.069	-.010	.040
13	.096	.034	-.055	.057	-.074	.078	-.024	.047
14	.009	.036	.137	.076	-.204	.089	.008	.057
15	.072	.033	-.147	.053	.203	.075	.019	.044
16	.030	.034	.030	.059	-.071	.079	.028	.047
17	.045	.033	-.034	.054	.192	.075	.035	.045
18	.120	.032	-.150	.049	.255	.071	.009	.042
19	.088	.032	-.151	.048	.315	.071	.020	.041
20	.128	.032	-.185	.048	.275	.070	-.010	.041
21	.043	.035	-.001	.074	-.284	.088	.015	.056
22	.023	.034	.097	.060	-.159	.080	.040	.048
23	.105	.033	-.192	.049	.291	.071	.018	.042
24	.056	.034	-.044	.057	-.090	.078	.030	.046
25	.009	.035	.019	.065	-.136	.083	.058	.051
26	.157	.033	-.081	.051	-.072	.073	.035	.043
27	.102	.032	-.163	.048	.291	.071	-.009	.042
28	.113	.032	-.118	.045	.293	.068	.015	.039
29	.068	.035	-.031	.067	-.139	.083	.016	.052
30	.049	.031	-.060	.042	.291	.065	.057	.038
31	.143	.032	-.169	.047	.318	.069	-.019	.041
32	.110	.033	-.098	.053	.091	.074	-.022	.044
33	.171	.032	-.174	.050	.143	.072	.048	.043
34	.112	.033	-.196	.052	.274	.073	.012	.043

Table 7: Stars from the literature used for comparison with our APOGEE/ASPCAP data. The stars from Shetrone and Sandquist (2000) follow the nomenclature from Sanders (1977), those from Tautvaišiene et al. (2000) follow Fagerholm (1906). The proper motions are from Frolov and Ananyevskaya (1986), and the magnitudes from 2MASS (Skrutskie et al., 2006).

Name	RA (J2000) [hms]	Dec (J2000) [dms]	PMx [mas/yr]	PMy [mas/yr]	Jmag [mag]	Hmag [mag]	Kmag [mag]	e_Jmag [mag]	e_Hmag [mag]	e_Kmag [mag]
Stars from Shetrone and Sandquist (2000)
S815	08:50:54.37	+11:56:28.8	-.003	-.001	11.706	11.435	11.372	.022	.019	.017
S1183	08:51:49.93	+11:33:18.5	-.007	-.000	11.632	11.372	11.319	.022	.022	.020
S1271	08:51:34.28	+11:49:43.9	-.004	-.003	11.804	11.569	11.522	.022	.022	.020
S821	08:50:51.80	+11:56:55.5	-.001	.001	11.646	11.382	11.321	.022	.020	.018
Stars from Tautvaišiene et al. (2000)
F84	08:51:12.70	+11:52:42.5	-.006	-.001	8.650	8.122	7.976	.018	.018	.018
F105	08:51:17.11	+11:48:15.9	-.003	-.004	8.140	7.526	7.385	.027	.018	.021
F108	08:51:17.48	+11:45:22.5	-.003	-.002	7.325	6.683	6.494	.021	.020	.021
F141	08:51:22.81	+11:48:01.7	-.005	-.006	8.560	8.075	7.942	.023	.033	.024
F151	08:51:26.19	+11:53:52.0	-.006	-.004	8.619	8.113	7.960	.020	.020	.021
F164	08:51:28.99	+11:50:32.9	-.005	-.003	8.566	8.072	7.958	.024	.018	.024
F170	08:51:29.91	+11:47:16.7	-.003	-.009	7.314	6.681	6.489	.020	.027	.023
F224	08:51:43.56	+11:44:26.3	-.003	-.004	8.838	8.294	8.163	.032	.020	.021
F266	08:51:59.54	+11:55:05.2	-.005	-.007	8.597	8.084	7.959	.020	.024	.018

Table 8: Abundances of the stars from the literature used for comparison with our APOGEE/ASPCAP data. The errors of the carbon and oxygen abundances in Tautvaišiene et al. (2000) are indeed lower limits to the errors, as the uncertainties for the [C/H] and [O/H] abundances were not provided and only the errors to the [Fe/H] abundances could be used in the computation.

[Fe/H] [dex]	e_[Fe/H] [dex]	[C/Fe] [dex]	e_[C/Fe] [dex]	[N/Fe] [dex]	e_[N/Fe] [dex]	[O/Fe] [dex]	e_[O/Fe] [dex]
Stars from Shetrone and Sandquist (2000)							
-.050	.040	-.050	.040	.150		-.080	.050
-.040	.080	.050	.050	.150	.200	.060	.100
-.070	.030	.100	.040	.050		.040	.090
-.040	.040	-.120	.100	.200	.200	-.080	.050
Stars from Tautvaišiene et al. (2000)							
-.020	.110	-.200	.110	.340	.125	.050	.110
-.050	.120	-.080	.120	.230	.124	.140	.120
-.020	.120	-.210	.120	.220	.124	.020	.120
-.010	.110	-.170	.110	.310	.114	.040	.110
.010	.120	-.200	.120	.280	.124	-.060	.120
.000	.070	-.150	.070	.240	.076	-.040	.070
-.020	.140	-.190	.140	.180	.143	-.030	.140
-.110	.120	-.190	.120	.210	.124	.050	.120
-.020	.100	-.190	.100	.200	.104	.010	.100

DIFFUSION EFFECTS IN M67?

This chapter was submitted for publication to MNRAS as Bertelli Motta, C. , A. Pasquali, J. Richer, G. Michaud, M. Salaris, A. Bragaglia, L. Magrini, S. Randich, E. K. Grebel, et al., "The Gaia-ESO Survey: Evidence of atomic diffusion in M67?".
C. Bertelli Motta performed the analysis and interpretation presented in this chapter with the help of A. Pasquali and wrote the text. The abundances analysed in this chapter were retrieved from the Gaia-ESO fifth internal data release and the models of stellar evolution including atomic diffusion used for comparison as well as Fig. 27 were provided by G. Michaud and J. Richer. All authors contributed with comments to the realisation of this study.

4.1 INTRODUCTION

Based on the commonly accepted knowledge that most stars form in associations or gravitationally bound clusters that dissolve with time and release their members into the field population (Lada and Lada, 2003), the suggestion that stars can be traced back to their parent cluster based on their chemical composition, the so-called chemical tagging (see, e.g., Freeman and Bland-Hawthorn 2002), has become very popular over the past years.

While chemical tagging is a potentially powerful tool for the understanding of the Galactic evolutionary history, there are limitations to this method that need to be accounted for. In fact, the common and reasonable assumption that stars born as a single stellar population from the same molecular cloud share the same chemical composition only holds for the *initial* surface abundances, which may vary as stars start following their evolutionary track. During the life of a star, several physical processes are at play in modifying its surface chemical composition. Although these changes are not dramatic, they do put constraints on the resolution achievable in studies of chemical tagging (see, e.g., Blanco-Cuaresma et al. 2015 for chemical tagging applied to open clusters). In addition, two stars formed from two different molecular clouds might happen to present the same surface abundances. This could be because the clouds of origin shared the same chemical composition or because the two objects have different mass and find themselves in different evolutionary stages, which might have led by chance to the same surface abundances, even if the initial ones were different (see, e.g., Dotter et al. 2017; Ness et al. 2017). In this scenario it would be impossible to tag the two stars back to a particular cluster of origin based on their present-day chemical composition alone. As Dotter et al. (2017) suggested, one would need to use stellar evolutionary models to infer the initial abundances of stars from the observed ones.

Stellar evolutionary effects are best studied with a sample of stars belonging to the same stellar population and most likely sharing the same initial chemical composition. While globular clusters are known to host two or more populations of stars with different light-element abundances among their members (see, e.g.,

Carretta et al. 2009; Gratton, Carretta, and Bragaglia 2012; Gratton, Sneden, and Carretta 2004; Kayser et al. 2008), this is not the case for open clusters (see, e.g., Bragaglia et al. 2012, 2014; Carraro et al. 2014), which are therefore ideal test benches for our study. Unfortunately, for most open clusters only the brighter stars in the red clump and upper-RGB are usually considered for spectroscopic studies, mainly because the MS and the TO regions are usually relatively faint and require very long exposure times. This makes it difficult to find in the literature suitable data for the investigation of evolutionary effects, which require stars at different evolutionary stages. Furthermore, we also need to test these effects in a range of metallicity and age (i.e., stellar mass). As explained in Chapter 1, the old open cluster M67 is an exception in this context and became for this reason the subject of our study.

Atomic diffusion (see Michaud, Alecian, and Richer 2015) is expected to alter the surface abundance of stars during the main-sequence phase due to the combined effect of gravitational settling, causing different elements to sink towards the interior of the star, and radiative acceleration working against it. In low-mass stars the overall trend is similar for all elemental species: surface abundances decrease along the MS with increasing stellar mass, reaching a minimum at the TO. The amplitude of the abundance variation between the early MS and the TO depends on the efficiency of radiative acceleration, i.e. on the degree of absorption of the outgoing photon flux for the different species. When the outer convective zone becomes deeper (after the TO), material from the stellar interior is brought to the surface. For most elements this means a recovery of the initial surface abundances, with the exception of species that undergo nuclear processing, such as ^{3}He, Li, Be, B, C, and N (see Chapter 3 and references therein). While metals sink towards the stellar interior, hydrogen is pushed into the outer layers, depriving the nucleus of fuel and thus shortening the life of the star on the MS (see, e.g., Jofré and Weiss 2011 and Salaris and Weiss 2001). This poses a further constraint on chemical tagging, since ages derived with models with and without diffusion can be significantly different.

Thus, in order to study atomic diffusion, stars along the MS, TO, SGB, and RGB are needed. In Chapter 3, we investigated the effects of the FDU affecting stars on the SGB and lower-RGB of M67 with data from APOGEE DR12 (see Majewski et al., 2015). M67 was furthermore included in the study of Smiljanic et al. (2016) where, using data from the Gaia-ESO Survey (GES, Gilmore et al., 2012; Randich, Gilmore, and Gaia-ESO Consortium, 2013), the authors investigated variations in Na and Al abundances as a consequence of mixing processes in the stellar interiors. In this chapter, we extend this study to the variations in surface abundances due to atomic diffusion by investigating the MS, TO, SGB, and RGB phase of M67 with GES data.

In Section 4.2 and 4.3 we present the data set and the models used for comparison in this study. In Section 4.4 we present the results and in Section 4.5 we discuss them together with possible caveats. Finally, in Section 4.6 we draw our conclusions.

One of the main goals of GES is the observation of a large number of open clusters covering a wide range in age, mass, metallicity, and Galactocentric distance. This is achieved by combining observations with FLAMES–GIRAFFE and FLAMES–UVES at the Very Large Telescope (VLT, see, e.g., Dekker et al. 2000; Pasquini et al. 2002). MS and TO stars in old open clusters were normally observed with the GIRAFFE set-ups HR9B ($514.3 - 535.6$ nm, R ~ 32000) and HR15N ($647 - 679$ nm, R ~ 20000). They cover a wavelength range that allows for precise measurements of the radial velocity, in addition to the abundances of Fe, Cr, and Ti for HR9B, and of Ca, Ti, Si, Al, and Li for HR15N, although with low precision. High-precision abundances of a large number of chemical species were calculated from FLAMES–UVES spectra generally obtained for stars on the MS, RGB, and on the red clump (RC) with the set-up U580 (200 nm around the central wavelength 580 nm, R ~ 47000).

M67 is included in the list of open clusters analysed within GES. The observations were collected from the ESO archive. In particular, they were part of the program 082.D–0726 (PI Gustafsson), which observed with FLAMES–UVES 25 stars in the field of M67 in all evolutionary stages between the MS and the lower-RGB (see Table 9). Thus, M67 is one of the few clusters in GES for which detailed chemical abundances from high-resolution spectroscopy are available for stars on the MS, TO, and RGB.

Fourteen of the stars distributed on the MS, TO, and early SGB branch were analysed in Önehag, Gustafsson, and Korn (2014) who searched the data for possible diffusion effects. They found differences in abundance between stars at the upper MS and TO and stars on the SGB of the order of ~ 0.02 dex (we note that they divide the sample that we define as TO in this work into TO and early SGB and compare the abundances of the first two with those of the third group). Although their results were not conclusive, also due to the small variation in abundances predicted by the models between these groups of stars, they seemed to support the presence of atomic diffusion.

We used the recommended results of the GES fifth internal data release (GES iDR5) for all the 25 stars and performed a membership analysis based on their radial velocities. We first excluded all stars known as binaries from Geller, Latham, and Mathieu (2015). We then computed the mean radial velocity of the remaining 17 stars ($\mathrm{RV}_{\mathrm{mean}} = 34.54 \pm 0.83\,\mathrm{km\,s^{-1}}$) and found that all stars lie within 3σ from this value. The mean error on the radial velocity ($0.36\,\mathrm{km\,s^{-1}}$) is smaller than the internal dispersion. This result is consistent with other mean radial velocity determinations of M67 known from the literature (see, e.g., Geller, Latham, and Mathieu 2015; Yadav et al. 2008) within few σ. In addition, we cross-matched the sample with the HSOY catalogue (Altmann et al., 2017) in order to check also the mean PM of the cluster ($\bar{\mu}_{\mathrm{RA}} = -9.67 \pm 0.64\,\mathrm{mas\,yr^{-1}}$, $\bar{\mu}_{\mathrm{Dec}} = -3.35 \pm 0.88\,\mathrm{mas\,yr^{-1}}$). We excluded one star that does not have an entry in the HSOY catalogue, and one because its PM is inconsistent with that of the cluster. Moreover, we verified that the 2MASS photometry (Skrutskie et al., 2006) of the remaining 15 stars is consistent with a 3.75 Gyr PARSEC isochrone (Bressan et al. 2012) calculated with $(m - M)_0 = 9.64$ mag, $E(B - V) = 0.023$ mag, and [Fe/H] = 0.06 dex (Bellini et al.

2010b; see Fig. 26; a list of the selected members and their parameters can be found in Table 14). This leaves 11 stars in common between our sample and the sample from Önehag, Gustafsson, and Korn (2014). We excluded 3 of their stars during our membership analysis (one as a binary and two because of PM criteria) and gained 4 additional ones along the SGB and lower RGB (see Table 9 and Fig. 26). In particular, the inclusion of three RGB stars into our analysis is of great importance for the study of diffusion effects. In fact, in absence of stars in their early main-sequence phase and thus still unaffected by diffusion, RGB stars are the only objects in our sample that show a surface chemical abundance similar to the initial one (except for C, N, and Li) and that can thus be compared to stars on the upper MS and TO, where diffusion effects reach their peak.

For all the 15 stars in our sample the chemical analysis was performed by GES working group (WG) 11, responsible for the analysis of UVES F, G, K stars (see Smiljanic et al. 2014 for a description of the abundances derivation and Sacco et al. 2014 for details about the reduction of UVES data).

In the GES iDR5 archive abundances are given in the form:

$$A(X) = \log(X/H) + 12, \tag{18}$$

and we transformed them for our purposes into

$$[X/H] = \log(X/H) - \log(X_{1194}/H_{1194}) \tag{19}$$

subtracting the GES abundances of the solar twin M67-1194 (ID 08510080+1148527, $A(X)_{1194}$) from $A(X)$.

4.3   MODELS

We compared the results with the stellar evolutionary models calculated in Michaud et al. (2004) (with an extension of the calculation to a slightly older age for the 1.35 solar mass model) for stars of solar metallicity, ages of 3.7-4 Gyr, and masses ranging from 0.5 to $1.4 M_\odot$. The calculations follow the description of Turcotte et al. (1998) and Richard, Michaud, and Richer (2001), including gravitational settling and radiative acceleration. Whereas all chemical species are affected by gravitational settling during the MS, different elements experience a varying amount of radiative acceleration, depending on the fraction of the total photon flux they absorb. After the TO the convective envelope deepens into the stellar interior and the effects of atomic diffusion are subverted, thus restoring in most cases the original surface abundances.

The models from Michaud et al. (2004) are divided into two sets of calculations. While the first one does not include turbulent transport, the second one is calculated including a density-dependent turbulent diffusion coefficient that is 400 times the He diffusion coefficient at $\log T = 6.09$, and that decreases inwards from there as ρ^{-3} (hereafter we will refer to this calculation as T6.09). This parametrisation of turbulent transport was chosen by Michaud et al. (2004) since it showed a minimisation of the Li depletion in Pop II stars (see Richard et al. 2002). The presence of turbulence reduces the effects of gravitational settling and as a consequence also the under-abundances at the TO, as can be seen in Fig. 28, where

Table 9: All stars in the field of M67 included in GES iDR5 from the observing program 082.D–0726 (PI Gustafsson). In the last column we include the results of our membership analysis combined with the information from Geller, Latham, and Mathieu (2015): single members (SM), binary members (BM), and non-members (NM).

ID	RA (J2000)	Dec (J2000)	Memb.
08505182+1156559[b]	08:50:51.82	+11:56:55.9	BM
08505600+1153519[a]	08:50:56.00	+11:53:51.9	SM
08505891+1148192[a]	08:50:58.91	+11:48:19.2	SM
08510017+1154321	08:51:00.17	+11:54:32.1	SM
08510080+1148527[a]	08:51:00.80	+11:48:52.7	SM
08510325+1145473[a]	08:51:03.25	+11:45:47.3	SM
08510524+1149340[a]	08:51:05.24	+11:49:34.0	SM
08510838+1147121	08:51:08.38	+11:47:12.1	SM
08510969+1159096	08:51:09.69	+11:59:09.6	NM
08511267+1150345[c]	08:51:12.67	+11:50:34.5	NM
08511799+1145541	08:51:17.99	+11:45:54.1	NM
08511854+1149214[a]	08:51:18.54	+11:49:21.4	SM
08511868+1147026	08:51:18.68	+11:47:02.6	NM
08511901+1150056	08:51:19.01	+11:50:05.6	NM
08512012+1146417[a]	08:51:20.12	+11:46:41.7	SM
08512291+1148493	08:51:22.91	+11:48:49.3	NM
08512940+1154139	08:51:29.40	+11:54:13.9	NM
08513045+1148582	08:51:30.45	+11:48:58.2	NM
08513322+1148513[c]	08:51:33.22	+11:48:51.3	NM
08513577+1153347	08:51:35.77	+11:53:34.7	SM
08513740+1150052[a]	08:51:37.40	+11:50:05.2	SM
08514081+1149055[a]	08:51:40.81	+11:49:05.5	SM
08514122+1154290[a]	08:51:41.22	+11:54:29.0	SM
08514507+1147459	08:51:45.07	+11:47:45.9	SM
08514995+1149311[a]	08:51:49.95	+11:49:31.1	SM

[a]: stars in common with the selection of Önehag, Gustafsson, and Korn (2014) and ours.
[b]: stars from the selection of Önehag, Gustafsson, and Korn (2014) excluded from our analysis since they are binaries (Geller, Latham, and Mathieu, 2015).
[c]: stars from the selection of Önehag, Gustafsson, and Korn (2014) excluded from our analysis because of PM criteria.
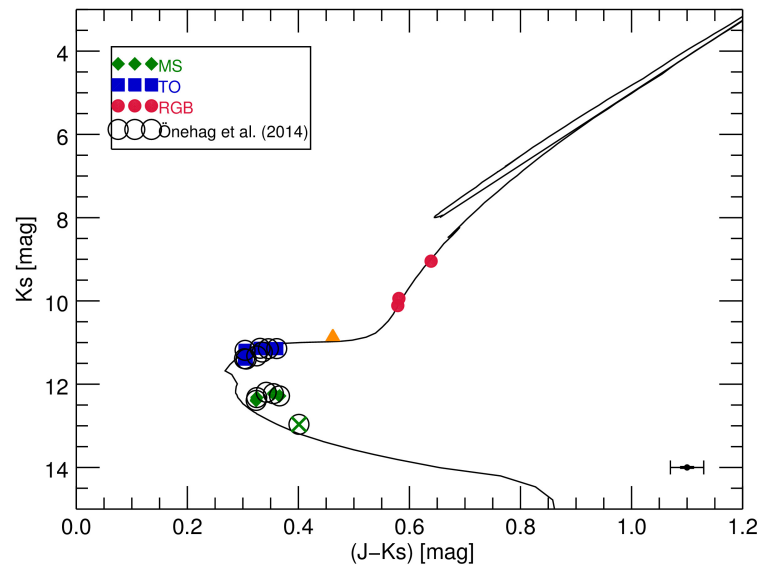
Figure 26: CMD of the M67 members selected from the GES archive plotted using 2MASS photometry. Main-sequence stars are plotted as green diamonds, TO stars as blue squares, and RGB stars as red circles. The star S806 is plotted as an orange triangle. The solar twin M67 1194 is plotted as a green cross. The mean error bar is shown at the bottom-right of the figure. The stars selected in Önehag, Gustafsson, and Korn (2014) are plotted as black circles. The solid line represents a PARSEC isochrone for an age of 3.75 Gyr and the parameters for M67 listed in the text.

the models are plotted as isochrones, each data point representing a different mass (see Table 10 for a summary of the T_{eff} and $\log g$ corresponding to each mass). The turbulent mixing efficiency necessary to match the observed variations in surface abundances due to atomic diffusion has been shown to vary for different globular clusters, more metal-rich clusters needing more efficient mixing (see, e.g., Gruyters et al. 2013; Korn et al. 2007). In the models, the pressure as a function of T is obtained using an approximate $T-\tau$ relationship and integrating the pressure equation from $\tau = 0$ to at least $\tau = 2/3$. For details see Krishna Swamy (1966) and VandenBerg et al. (2008)

In this study, we decided to focus on the models reaching the age range 3.7–4.0 Gyr. This is necessary to see the effects of deep mixing present in the lower-RGB stars of M67. Unfortunately, the calculations with turbulence only evolved as far as 3.74 Gyr for the most massive star (with a mass of $1.35M_{\odot}$). We recall that an age of 3.7-4.0 Gyr is consistent with the age estimations for M67 (see, e.g., Bellini et al. 2010b).

As can be seen in Fig. 28, for the calculations with turbulent transport the last data point, representing a model with mass $1.35M_{\odot}$, does not have the same $\log g$ as the calculations without turbulence. In fact, the model with $1.35M_{\odot}$ did not reach the same age as the calculation without turbulence, but rather stopped at 3.74 Gyr. Nevertheless, we expect that the surface abundances after 3.6 Gyr will be the same regardless of the inclusion of turbulence in the models. This can be proven by inspecting Fig. 27. Here, we show two calculations for a star of mass $1.35M_{\odot}$ as a function of age, including the two models considered in this work, with and without turbulence. Fig. 27 shows how the two models converge after 3.5 Gyr. We thus expect the $1.35M_{\odot}$ model with turbulence to have the same surface chemical composition as the model not including turbulent transport after 3.6 Gyr.

4.4 RESULTS

In the following, we present the results of our study and compare the measured abundances from the GES data with the models of Michaud et al. (2004). In Fig. 28 and 29 the elemental abundances of stars from the MS, SGB, and RGB are plotted as a function of $\log g$. The abundances shown and discussed in this chapter refer to the elements in their neutral state. We present and discuss in this work only elements for which we have both the measured abundances from GES iDR5 and the predictions from the models by Michaud et al. (2004). The star with GES-ID 08510017+1154321 is highlighted as an orange triangle for the reasons explained in subsection 4.5.1. The solar twin M67-1194 is plotted as a green cross and is not included in the calculations when computing the average abundances of the MS stars. In fact, M67-1194 lies on the 'lower' MS with respect to the rest of the sample and presents for most elements an abundance more similar to the RGB than to the MS and TO samples, as predicted by the models of Michaud et al. (2004) for stars of the same mass. Models of stellar evolution including turbulent diffusion are shown as a black, solid line, while models without turbulence are displayed as a dashed, black line.

Since the effect of diffusion on the stellar surface chemical composition is very small (typically less than ~ 0.1 dex for stars in the mass range of M67 members)

Table 10: T_{eff} and log g for the models presented in this work in the age range 3.7–4.0 Gyr.

| $M^*/M_{\odot NoTurb}$	$T_{effNoTurb}$[K]	log g_{NoTurb}
0.500	3907.8	4.843
0.600	4078.7	4.741
0.700	4421.7	4.660
0.900	5404.7	4.557
1.000	5780.2	4.467
1.060	5956.0	4.394
1.070	5981.2	4.378
1.075	5994.9	4.371
1.080	6004.8	4.365
1.081	6006.9	4.363
1.082	6008.1	4.365
1.083	6010.8	4.360
1.085	6014.5	4.360
1.090	6023.2	4.350
1.150	6083.1	4.267
1.200	6083.3	4.201
1.250	6221.3	4.065
1.300	5977.2	3.886
1.350	4933.1	3.240
$M^*/M_{\odot NoTurb}$	$T_{effNoTurb}$[K]	log g_{NoTurb}
0.500	3907.6	4.844
0.600	4078.0	4.742
0.700	4420.6	4.661
0.800	4928.1	4.618
0.900	5399.5	4.560
1.000	5781.3	4.469
1.050	5934.5	4.414
1.100	6055.1	4.350
1.150	6116.0	4.283
1.200	6114.5	4.212
1.250	6095.3	4.129
1.300	6111.6	3.938
1.350	5059.9	3.525
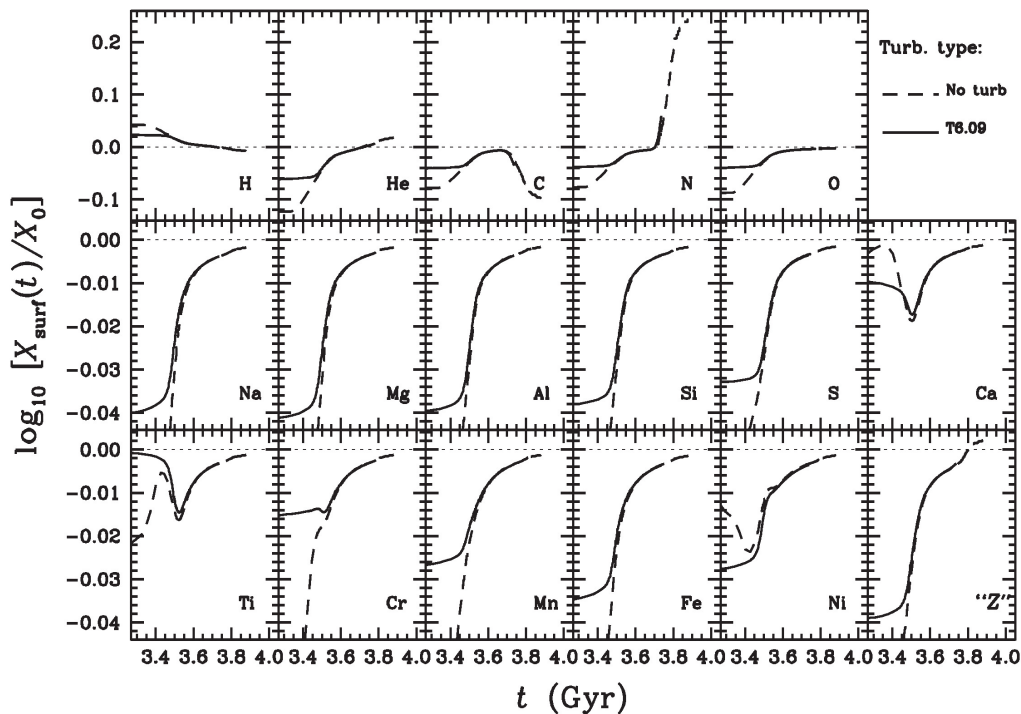
Figure 27: Comparison of the surface abundances of two different models with (solid black line) and without (dashed black line) turbulence for a star of $1.35M_\odot$ as a function of time.

precise measurements are required. Indeed, if the scatter of the observationally derived abundances is larger than or even comparable to the expected variation, no sensible conclusion can be drawn. For this reason, we performed a statistical analysis of the abundances aimed at determining which of the elements derived within GES clearly show trends consistent with the effects of atomic diffusion predicted by the models of Michaud et al. (2004).

Table 11 summarizes the mean elemental abundances and relative standard deviations obtained within GES for two groups of stars in M67: the upper MS and the RGB stars. Table 12 shows the difference in surface chemical abundances between these two groups for the species studied in this work, its error calculated as

$$err\_\Delta[X/H] = \sqrt{\sigma_{ms}^2 + \sigma_g^2} \tag{20}$$

where σ_{ms} and σ_g are the standard deviations of the abundance distributions of the upper MS and RGB stars, respectively; the last two columns show the maximum difference in surface abundance predicted by the models (calculated between a mass of 1.2 and 1.35 $M_\odot$). TO stars were excluded from this discussion because the maximum abundance variation predicted by the models is reached at the log g corresponding to the upper MS ($\sim 1.2M_\odot$ in the models).

For Al, Si, Ca, Ti, Cr, Mn, and Ni, $\Delta[X/H]$ is larger than $3 \times err\_\Delta[X/H]$, while for Fe $\Delta[X/H]$ is larger than $2 \times err\_\Delta[X/H]$. We conclude that for these elements the presence of a trend in log g is clear and the offset in surface abundance between upper MS and RGB can be considered statistically significant. $\Delta[X/H]$ is larger than $1 \times err\_\Delta[X/H]$ for C, O, and Na making the offset between the two samples less clear, but still visible. For Mg $\Delta[X/H]$ is lower than $err\_\Delta[X/H]$ and [S/H] is

available only for stars on the upper MS and on the TO. We will thus exclude Mg and S from the following discussion, although the distribution of [Mg/H] as a function of log g can be seen in Fig. 28.

For the elements of the oxygen group (O, Na, Mg, Al, Si, and S), the models predict the largest difference between initial surface abundance and values at the TO. This is due to the little radiative acceleration that these elements experience below the surface convection zone (for details, see Michaud et al. 2004, Fig. 3). As shown in Fig. 28, the models are consistent with GES [Na/H] and [Si/H] abundances of the M67 stars within $1 - 2 \times$ err_Δ[X/H]. For Al the difference between Δ[X/H] and the offset predicted by the models is larger than $3 \times$ err_Δ[X/H]. As explained above, the measured [O/H] abundances present a large scatter, even if Δ[X/H] is consistent with the predictions of the models.

Species between P and Ti are expected to experience a larger radiative acceleration as compared to lighter elements (see Fig. 3 in Michaud et al. 2004). This reduces the effect of gravitational settling, resulting in a much smaller difference between the surface abundances of TO and RGB stars as compared to Al or O. Fig. 29 shows how the [Ca/H] and [Ti/H] both suffer from an offset with respect to the model abundances, which is more prominent for [Ti/H] than for [Ca/H]. Nevertheless, looking at Table 11 and 12 one can see that a trend in log g is present for Ca and Ti and is slightly more pronounced than predicted by the models, but still consistent within $3 \times$ err_Δ[X/H].

Elements of the iron group (Cr, Mn, Fe, Ni) are predicted to experience less radiative acceleration as compared to Ca or Ti, but more than the elements in the oxygen group, resulting in very similar but slightly smaller under-abundances at the TO. Cr is systematically under-abundant compared to the theoretical predictions. The trend between MS and RGB is consistent with the models in the case of Cr and slightly smaller for Fe. A similar trend between the TO and the SGB/low-RGB was also found for [Fe/H] by Casey (2016), analysing lower resolution spectra. For Mn and Ni Δ[X/H] differs by $3 \times$ err_Δ[X/H] or more from the abundance differences predicted by the models.

We note that, since we are interested in a relative comparison between two groups of stars analysed within GES iDR5 rather than in the absolute abundances of the stars, err_Δ[X/H] is calculated only from the internal scatter of the measured abundances and does not take into account the error of the measurements.

4.5   DISCUSSION

In the following we discuss the interpretation of the results presented so far as well as possible caveats, such as corrections for NLTE effects, abundance trends in a cluster for which we do not expect to see diffusion effects, and trends of the abundances of M67 with temperature derived from APOGEE infrared spectra.

4.5.1   *S806*

Figure 28 and 29 show that one star (GES-ID: 08510017+1154321, S806 in the notation from Sanders 1977) in M67 presents for almost all elements investigated in this work higher abundances with respect to its companions. The star matches
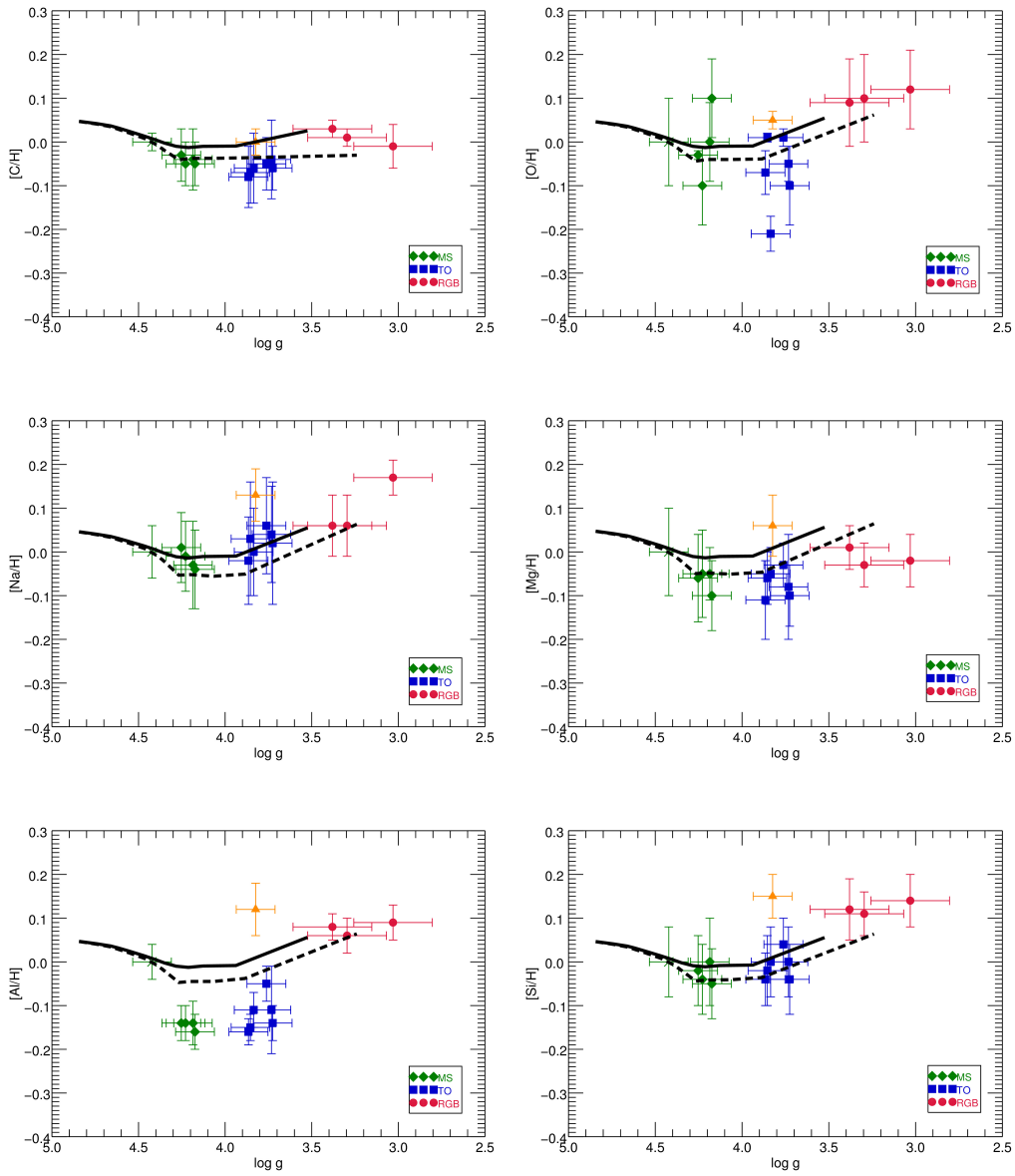
Figure 28: The different panels show from top to bottom and from left to right the abundances of C, O, Na, Mg, Al, and Si as a function of log g. The symbols are the same as in Fig. 26. We also overplotted models of stellar evolution with (black solid line) and without (dashed black line) turbulence in the stellar interior. Note that the lowest log g point of the dashed lines could be horizontally shifted to the left to the same log g as the solid lines. The large shift is due to the rapid variation of log g with age for the 1.35 solar mass model at that evolutionary stage and the slight age difference between the models with and without turbulence.
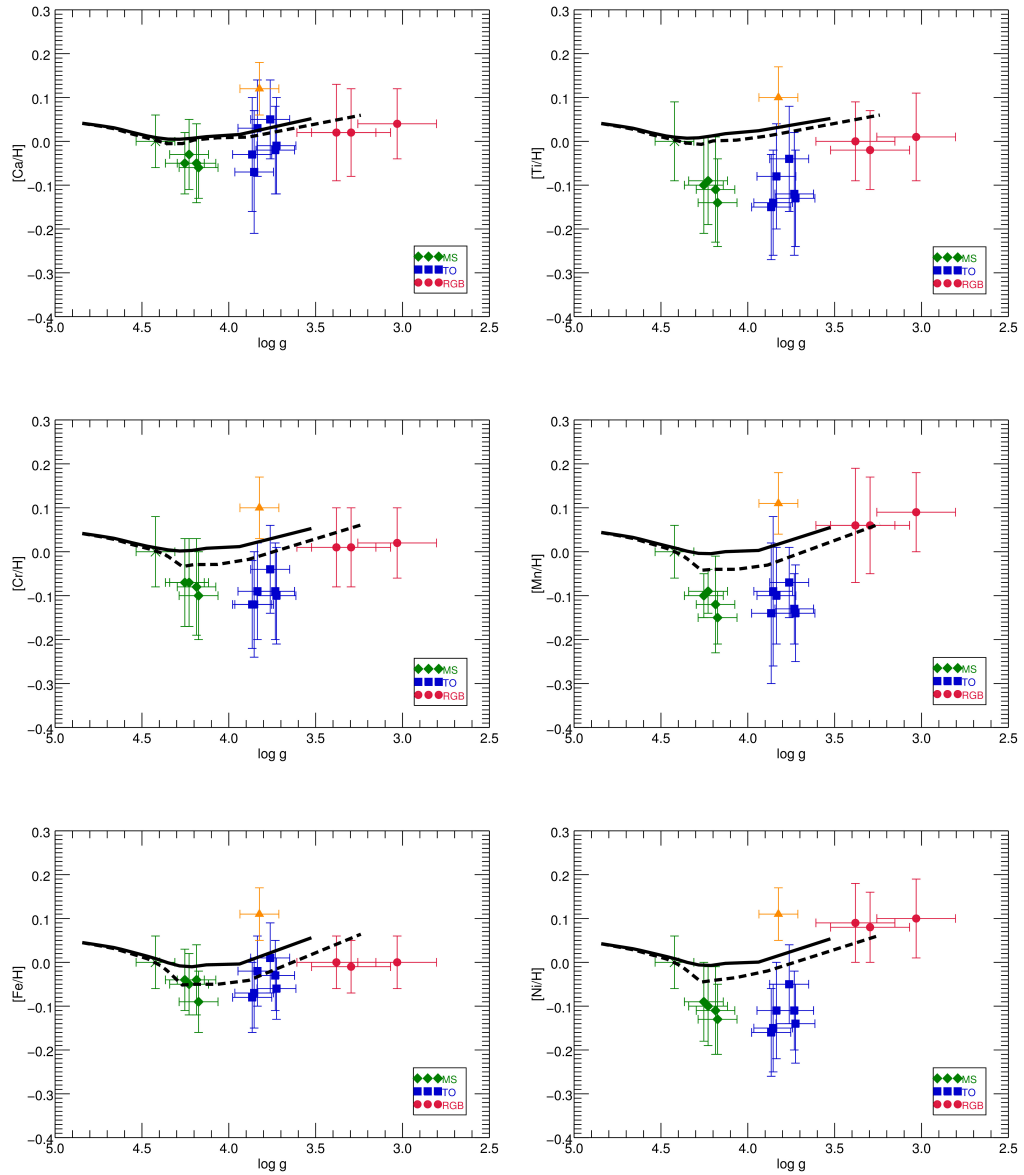
Figure 29: Fig. 28 continued. GES abundances of Ca, Ti, Cr, Mn, Fe, and Ni and a function of log g.

Table 11: Mean surface chemical abundances and standard deviations for stars on the MS and TO ([X/H]$_{MS}$) and giant stars ([X/H]$_{RGB}$) in M67.

X	[X/H]$_{MS}$	σ_{MS}	[X/H]$_{RGB}$	σ_{RGB}
C	-0.043	0.008	-0.01	0.016
O	-0.008	0.072	0.103	0.013
Na	-0.018	0.019	0.097	0.052
Mg	-0.065	0.021	-0.013	0.017
Al	-0.145	0.009	0.077	0.013
Si	-0.028	0.019	0.123	0.013
Ca	-0.048	0.011	0.027	0.009
Ti	-0.110	0.019	-0.003	0.013
Cr	-0.080	0.012	0.013	0.005
Mn	-0.115	0.023	0.070	0.014
Fe	-0.055	0.021	-0.003	0.005
Ni	-0.108	0.015	0.090	0.008

Table 12: Difference between the mean abundances on the upper-MS and on the RGB as compared to the difference in abundance between the 1.2M$_\odot$ and 1.35M$_\odot$ models, both with and without turbulence.

X	Δ[X/H]	err_Δ[X/H]	Δ[X/H]$_{NoTurb}$	Δ[X/H]$_{Turb}$
C	0.033	0.018	0.007	0.018
O	0.111	0.073	0.102	0.075
Na	0.115	0.084	0.116	0.078
Mg	0.052	0.055	0.113	0.078
Al	0.222	0.016	0.109	0.077
Si	0.151	0.023	0.105	0.075
Ca	0.075	0.014	0.057	0.053
Ti	0.107	0.023	0.059	0.049
Cr	0.093	0.013	0.090	0.058
Mn	0.185	0.027	0.104	0.068
Fe	0.052	0.022	0.114	0.074
Ni	0.198	0.017	0.103	0.069

all criteria (kinematic and photometric) considered in the membership analysis of the cluster, but its chemical composition is not consistent with that of other cluster members with the same gravity.

Of course the possibility exists that S806 is not a member of M67, although this is not very likely given the perfect match with the clusters kinematics. Nevertheless, the surface abundances measured in S806 cannot be explained by simple stellar evolutionary processes. We therefore need to explain its position in the SGB and its peculiar chemical composition.

A possible explanation for the peculiar surface abundances of S806 (with respect to its $\log g$) is that the star might be part of a binary system initially composed of one massive companion, and a secondary companion with a mass of approximately $1.3 M_\odot$ now lying on the SGB. If the massive companion evolved into an AGB star and expelled part of its envelope, the surface of the secondary companion would have been polluted by the ejected material (the s-element abundances for S806 are also higher than in the other cluster members). At an age of ~ 4 Gyr, the massive companion would have evolved into a white dwarf and thus would not contribute significantly to the luminosity of the binary system. In this scenario the binary would have to be face-on, since S806 has been classified as a single star in Geller, Latham, and Mathieu (2015). Alternatively, the system could have been disrupted by encounters with other stars within the cluster. In this case we would only be observing the low-mass companion.

4.5.2 *NLTE effects*

The abundances of GES iDR5 are calculated for 1D-atmospheres and LTE. It is therefore interesting to discuss how corrections for NLTE would affect the abundances of the elements under study and if these alone can account for the abundance trends observed.

The upper-MS stars of M67 have a mean $T_{eff} = 6031$ K and $\log g = 4.21$ dex. For the giant stars we find a mean $T_{eff} = 4875$ K and $\log g = 3.24$. In Lind et al. (2011) this corresponds to corrections for the Na abundance of -0.15 dex for the 568.2 nm line and of -0.1 dex for the 615.4 nm line for both dwarfs and giants, thus leaving the offset between the two groups unchanged.

For Al, Nordlander and Lind (2017) predict a correction of -0.1 dex for the MS stars and of -0.2 for the RGB stars. This would indeed diminish the offset observed between MS and RGB in the GES Al abundances, but a clear trend in $\log g$ would still be visible.

Zhang et al. (2017) predicts for Mg a correction of +0.01 dex for the MS group. In the sample of stars analysed by these authors we could not find any star with the temperature and gravity of the M67 giants. The most similar one has $T_{eff} = 4901$K and $\log g = 2.76$ and corresponds to a correction of -0.02 dex. Thus, in the case of magnesium the NLTE correction would not significantly change the difference in abundance between MS and RGB.

Similarly, for Si the corrections would be -0.01 dex and -0.04 dex for the MS and the RGB, respectively (using the same objects as for Mg).

Going to heavier elements, NLTE corrections are available only for Fe from Lind, Bergemann, and Asplund (2012). The authors calculate corrections of $\sim +0.01$ dex

and ~ +0.0 dex for the MS and RGB respectively. These corrections would not change significantly the overall difference in abundance between the two groups.

4.5.3 NGC 6633

In the previous section we have discussed how the abundance trends visible in the stars of M67 cannot be explained by NLTE effects, which remain unaccounted for in the GES iDR5 analysis. In order to be reasonably confident that the trends we observe are indeed due to diffusion effects, we need to rule out systematic offsets deriving from the analysis of stars in different evolutionary stages. We therefore choose a second cluster, NGC 6633, for which stars both on the MS and on the RGB/RC have been observed and analysed in GES iDR5. This cluster is much younger than M67, with an age of ~ 540 Myr (Randich et al. 2017, subm.) and has a slightly sub-solar metallicity of [Fe/H] =: -0.05 ± 0.06 dex (Jacobson et al., 2016).

After performing a membership analysis of the stars observed with UVES in the field of NGC 6633 based on radial velocities and HSOY proper motions, we found 5 MS stars and 3 stars that could be RGB or RC stars based on their position on the CMD. These are plotted as green and red dots, respectively, in Fig. 30, together with a Padova isochrone with age 540 Myr, [Fe/H] = -0.05 dex, distance modulus $(m - M)_0 = 8.07$ mag, and reddening $E(B - V) = 0.182$ mag (Randich et al., subm.). We find also three further stars on the MS that are probable members of the cluster based on their kinematic properties (orange triangles in Fig. 30), but that we do not take into consideration for our analysis due to the following reasons. One of them, 18265591+0635559, is flagged as a binary in GES iDR5. The log g of 18264026+0637500 is on the grid edge and the star is therefore flagged for "suspicious stellar parameters". 18272787+0620520 has abundances and errors on the abundances very different from the cluster distribution for most elements. Since it lies on the edge of the proper motion distribution of our sample, it is probably not a member of the cluster.

Due to its young age, we do not expect to find diffusion effects in the observed stars of NGC 6633, since there was not enough time for diffusion to become efficient in those MS stars. Besides, we do not have any stars at the TO where we could in principle observe diffusion effects, if any. Stars on the MS and on the giant branch are expected to present the same abundances and if they do not it would mean that there are systematic offsets between the abundances of dwarf and giant stars that are due to the analysis alone.

Figure 31 and 32 show, similarly to Fig. 28 and 29, the abundances of several elements as a function of log g. For elements of the Ca and Fe group, we do not find any significant offsets between the MS and the giant stars. As shown in Table 13 the mean abundances of the two groups are consistent with each other within one sigma.

This is not the case for lighter elements of the oxygen group. Na in particular presents a large difference (0.278 dex) between the mean MS abundance and the average abundance of the giant stars. Nevertheless, this offset could be a physical effect: for stars in the mass range of the NGC 6633 giants (~ $2.5 M_\odot$) we expect to see an enhancement in Na due to mixing effects after the dredge-up (see, e.g., Smiljanic et al. 2016 and references therein). Besides, also NLTE effects might play
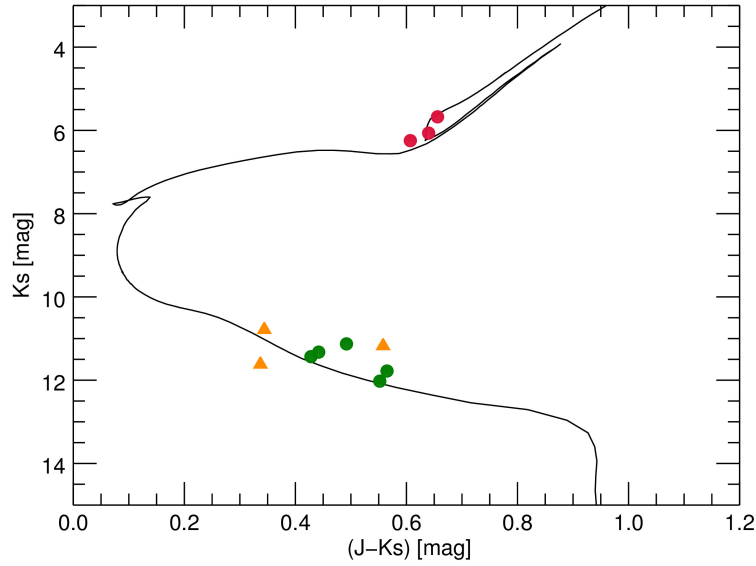
Figure 30: CMD of the stars selected as members of NCG 6633. Green circles are stars on the MS, red circles represent giant stars and orange triangle stars with flags that we do not take into account in our analysis.

a role: Lind et al. (2011) predict a correction for NLTE effects of the Na abundance between -0.1 and -0.15 dex for the T_{eff} and $\log g$ of the NGC 6633 MS stars and of -0.2 dex for the giant stars for the 568.2 nm line at solar metallicity. For the 615.4 nm line the correction would be -0.1 dex for both groups.

For Mg, Al, and Si an offset is also present, although not as pronounced as for Na. While the effects of mixing for Al should not be visible in stars less massive than $3M_\odot$ (Smiljanic et al., 2016), this offset would disappear or at least become less significant if NLTE effects were taken into account in the abundance analysis. Nordlander and Lind (2017) predict for Al a difference in correction between dwarf and giant stars similar to that for Na from Lind et al. (2011). For Mg we do not expect NLTE effects to have a strong influence on the abundances. Zhang et al. (2017) calculate corrections of the order of ± 0.01 dex for stellar parameters similar to our NGC 6633 sample. Similarly, Zhang et al. (2016) predict corrections of the order of -0.06 – -0.01 dex for Si.

4.5.4 *APOGEE DR14*

The recent fourteenth data release of the Apache Point Observatory Galactic Evolution Experiment (hereafter APOGEE DR14, see Abolfathi et al., 2017; Majewski et al., 2015) contains very important results concerning the abundances of M67 stars. In APOGEE DR14 stars in every evolutionary stage of M67 have been observed and analysed, from the MS to the RC. We decided to be as conservative as possible in the choice of the stars to take into consideration and we selected only those with STARFLAG, ASPCAPFLAG, and the ELEMFLAG of the element under
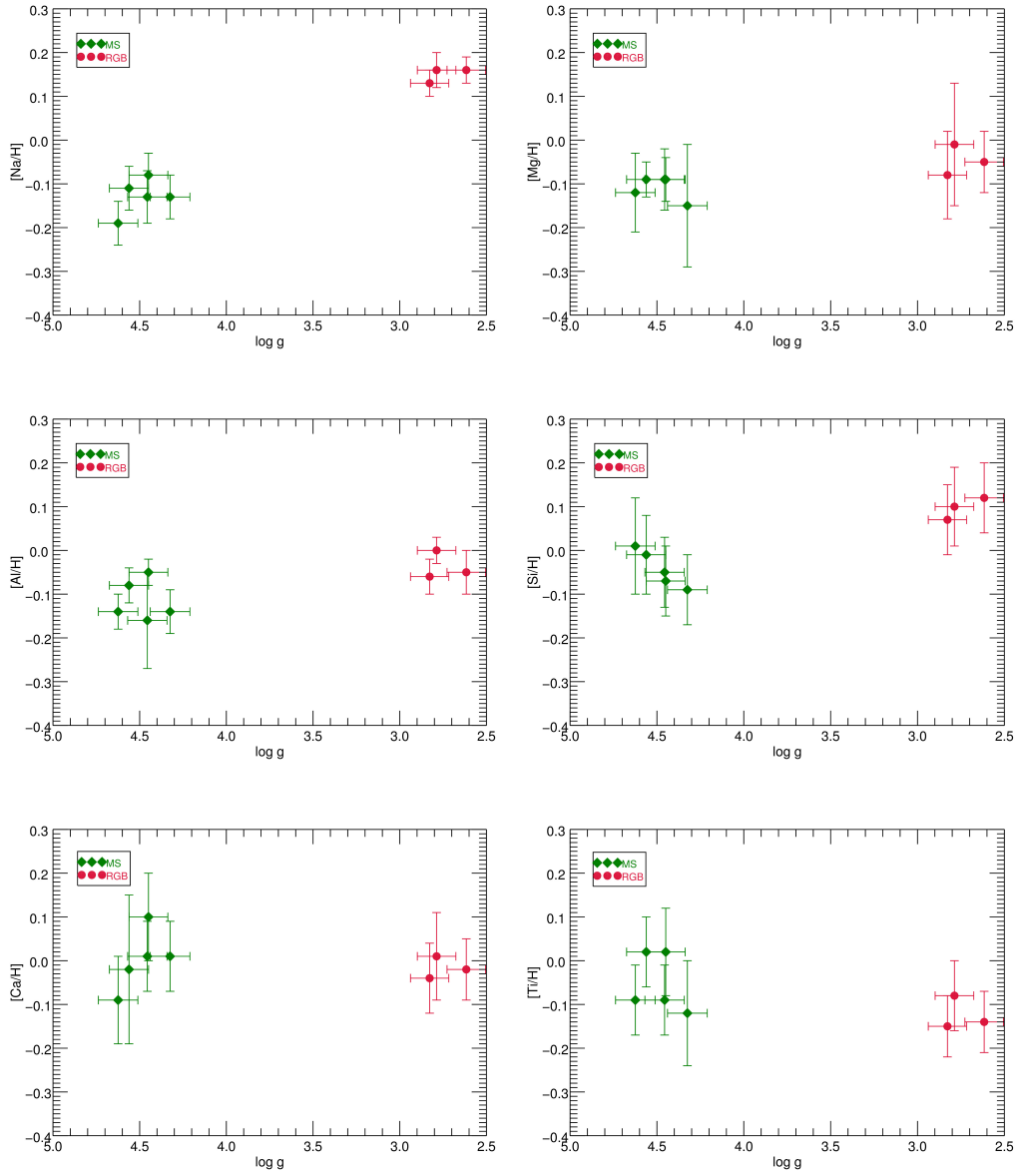
Figure 31: The different panels show from top to bottom and from left to right the abundances of Na, Mg, Al, Si, Ca, and Ti as a function of $\log g$ in NGC 6633. The symbols are the same as in Fig. 30.
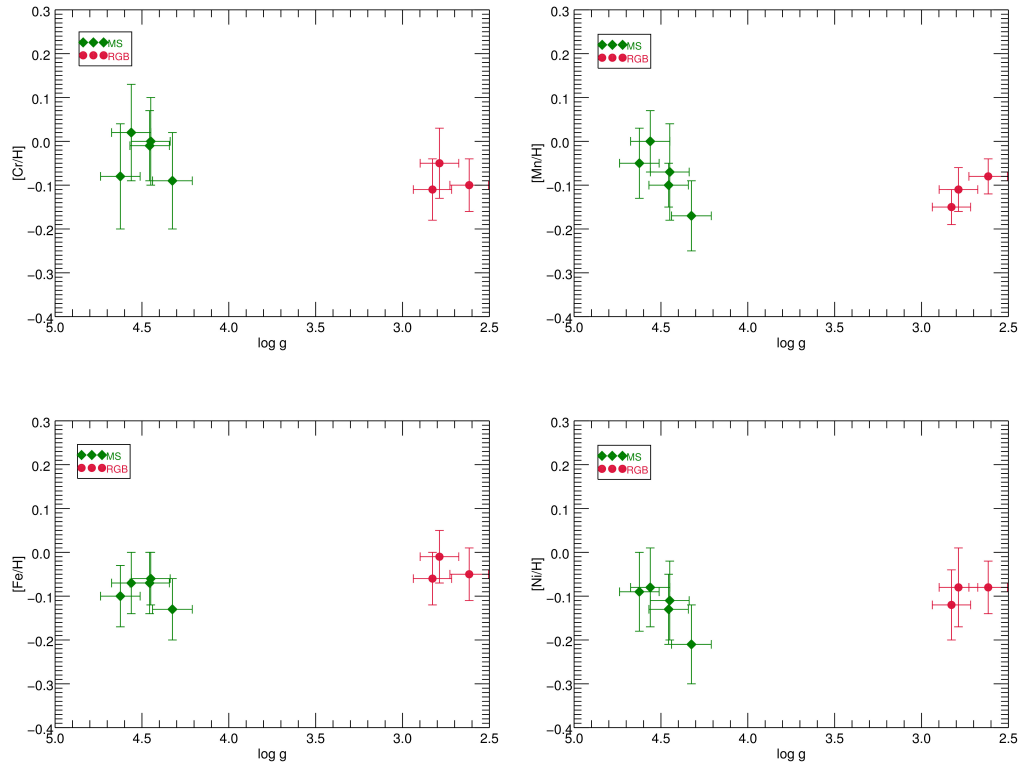
Figure 32: Fig. 31 continued. GES abundances of Cr, Mn, Fe, and Ni and a function of log g.

Table 13: Mean surface chemical abundances and standard deviations for stars on the MS ([X/H]$_{MS}$) and RGB ([X/H]$_{RGB}$) in NGC 6633.

X	[X/H]$_{MS}$	σ_{MS}	[X/H]$_{RGB}$	σ_{RGB}
C	0.072	0.098	-0.200	0.036
Na	-0.128	0.036	0.015	0.014
Mg	-0.108	0.024	-0.047	0.029
Al	-0.114	0.042	-0.037	0.026
Si	-0.042	0.037	0.097	0.021
Ca	0.002	0.061	-0.017	0.021
Ti	-0.052	0.060	-0.123	0.031
Cr	-0.032	0.045	-0.087	0.026
Mn	-0.078	0.056	-0.113	0.029
Fe	-0.086	0.026	-0.040	0.022
Ni	-0.124	0.046	-0.093	0.019

study equal to zero. By doing so we aim at excluding as many possible biases due to unreliable results as possible.

APOGEE DR14 contains the abundances determined by the APOGEE Stellar Parameters and Chemical Abundances Pipeline (ASPCAP) (see García Pérez et al., 2016; Holtzman et al., 2015) as well as calibrated abundances. These are calculated under the assumption that abundances of open cluster members should be homogeneous and that therefore any trend with temperature must be corrected for. Since for our purposes it is important to take into consideration any trend of the chemical abundances as a function of temperature, we decided to use the uncalibrated abundances. We present the results in the form [X/H]. For the elements that were calculated as [X/M] we add the uncalibrated [M/H] of the star. The error bars only represent the errors on the fit of the uncalibrated abundances presented in the APOGEE DR14 catalogue (for the uncalibrated [M/H] no errors are given). These are very small and are not to be considered realistic errors.

Figure 33 shows the CMD of the sample selected after a membership analysis based on radial velocity, proper motion, photometry and metallicity (similar to the procedure described in Chapter 1), and after all stars with the flags listed above not equal to zero were excluded. The stars are colour-coded based on their iron abundance. It is already clear from this plot that [Fe/H] on the TO is lower than on the RGB and on the RC. Since no calibrated $\log g$ is available for dwarf stars in APOGEE DR14, we plotted in Fig. 34 [Fe/H] as a function of the effective temperature together with the models from Michaud et al. (2004). The abundances obtained by APOGEE DR14 are consistent with the predictions of stellar evolutionary models that include atomic diffusion. Figure 35 shows the results obtained for a list of other species. Most of them are consistent with the models, although, as in GES iDR5, for some of them it would be necessary to apply a systematic shift to the models in order to match the observations. This is a very important result for our study, since it shows that abundances computed with a completely independent method from infrared rather than optical spectra yield results consistent with those obtained within GES iDR5.

4.6 SUMMARY

We studied the surface chemical composition of member stars in the old open cluster M67 analysed by the Gaia-ESO Survey, searching for evidence of atomic diffusion processes. We compared the abundances of C, O, Al, Na, Si, Ca, Ti, Cr, Mn, Fe, and Ni with different stellar evolutionary models calculated by Michaud et al. (2004) for the age and metallicity of M67 and found them to be consistent with each other. Our results support the findings of Önehag, Gustafsson, and Korn (2014), although the inclusion of three RGB stars compared to the sample of Önehag, Gustafsson, and Korn (2014) renders the results more conclusive, since in RGB stars the initial surface abundances are essentially restored, after the effects of atomic diffusion have been cancelled by convection. Furthermore, the predicted abundance variations between upper MS and RGB are larger than between upper MS and TO/early SGB and thus easier to measure. Also Casey (2016) found a variation in metallicity [Fe/H] of ~ 0.05 dex between TO and SGB/low-RGB stars of M67 from lower resolution spectra. Although we find strong indications
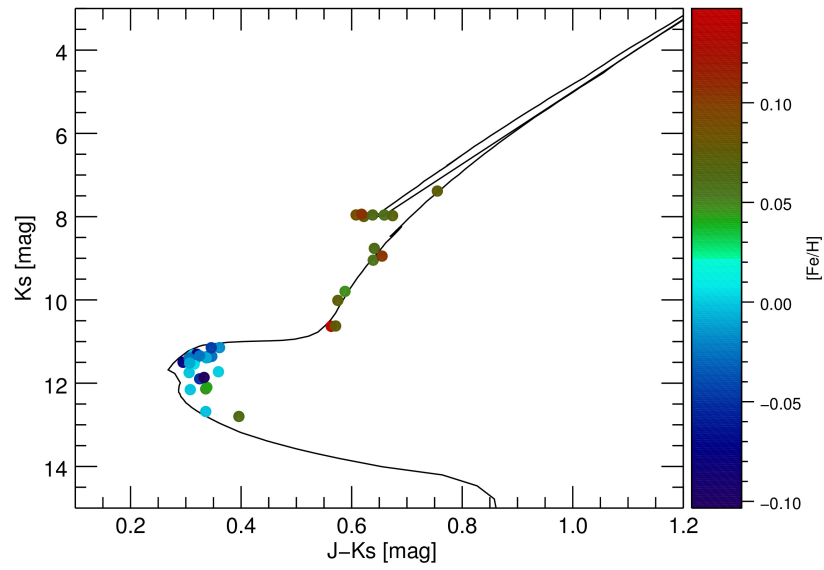
Figure 33: CMD of the stars selected as members of M67 from APOGEE DR14. Stars with STARFLAG, ASPCAPFLAG or FE_H_FLAG not equal to zero were excluded from the plot. The stars are colour coded by their iron abundance.
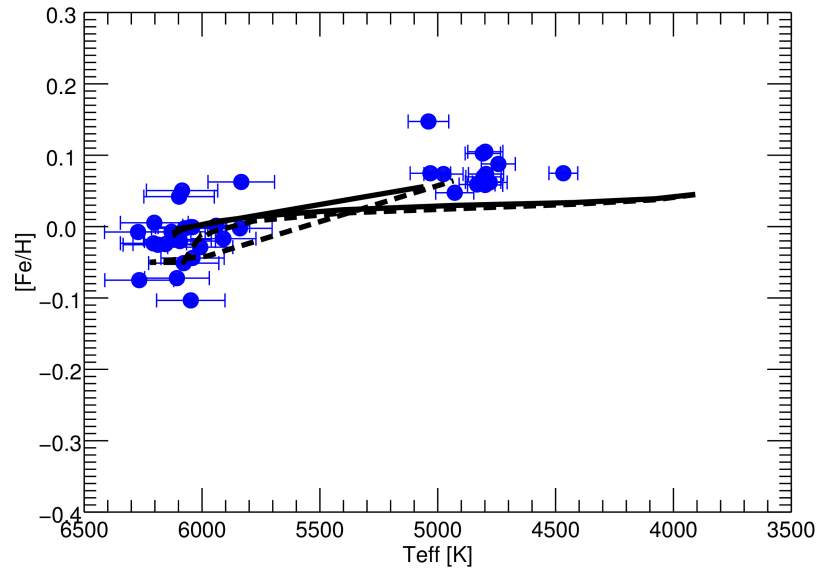
Figure 34: Uncalibrated iron abundance from APOGEE DR14 for M67 stars as a function of their (calibrated) effective temperature compared to models of stellar evolution.
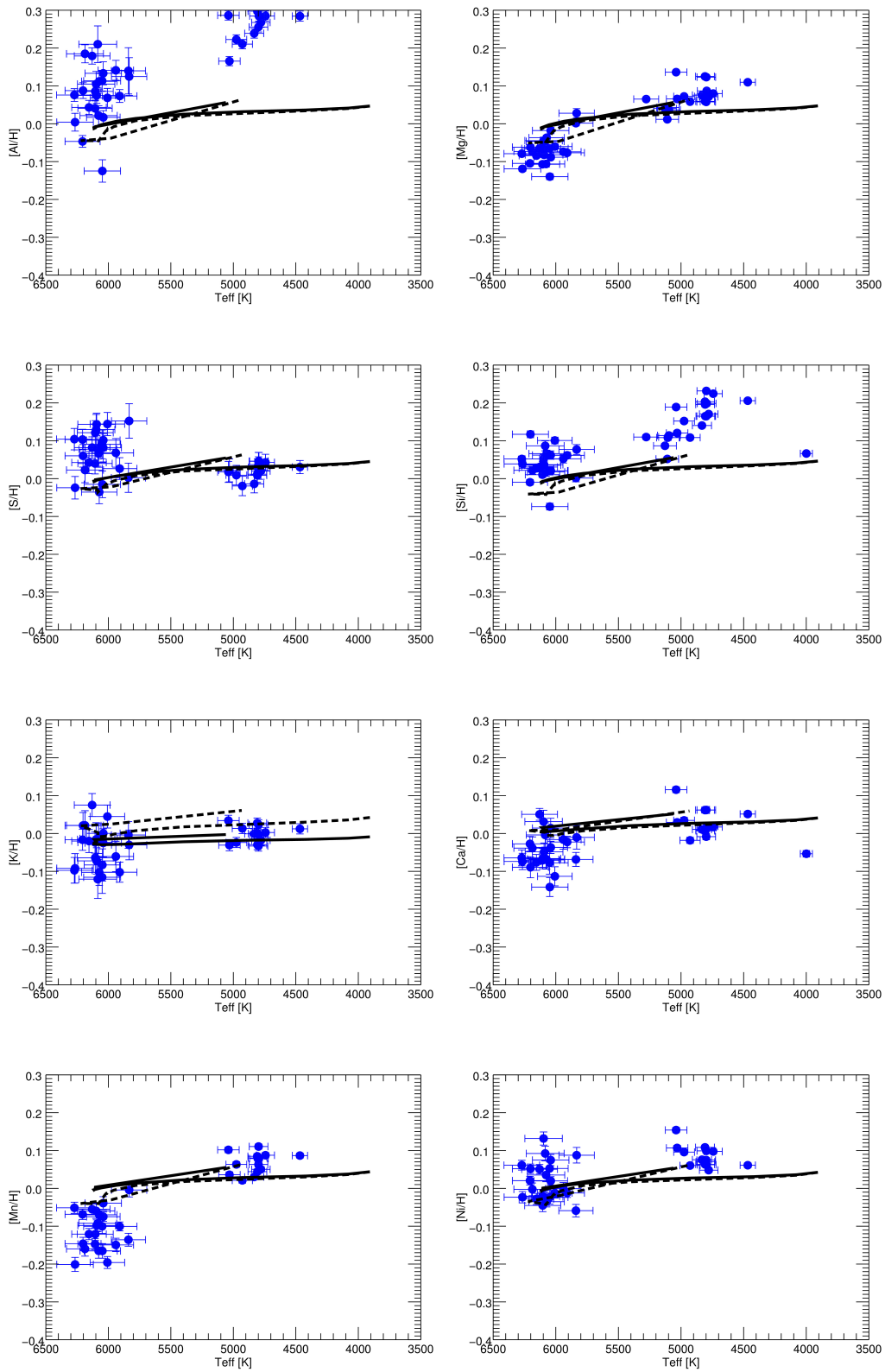
Figure 35: As in Fig. 34, the plot shows the chemical abundances obtained by APOGEE DR14 as a function of T_{eff} compared to models of stellar evolution.

of ongoing diffusion processes, it is not possible to state whether the models with or without turbulent diffusion better represent the data, given the spread and the errors on the measured abundances at the upper MS and TO.

We have also shown that the star S806 systematically presents higher surface abundances than its cluster companions. We suggest as a possible explanation that this star might be part of a binary system and have undergone accretion of expelled material from a putative evolved more massive companion.

We have investigated the abundances in stars of the MS and RGB/RC of NGC 6633, a cluster young enough that we do not expect any signs of diffusion effects in the stars included in GES iDR5. As expected, for most elements the abundances of the two groups are consistent with each other within one sigma, except for few light elements of the Na group. In some cases the offset can be explained by mixing processes and NLTE effects, while at least for Si the measured abundance difference between dwarfs and giants might be enhanced due to analysis effects. Taking this into account in the M67 analysis would actually bring the measurements into better agreement with the model predictions (Fig. 28).

We found that the newest APOGEE data release DR14 presents results for the stars of M67 that are consistent with the results from GES iDR5. Since the APOGEE abundances were derived with an independent method and furthermore from infrared instead of optical spectra, this supports the claim that the offsets in abundance that we are observing are of physical nature and not artefacts due to the analysis method.

The evidence of variations in the surface abundances of stars due to stellar evolutionary effects have strong implications for the field of Galactic archaeology, since it puts a constraint on the precision achievable with chemical tagging of the order of ~ 0.1 dex, similar to what was indicated in Dotter et al. (2017). As a consequence, future studies will need to re-think chemical tagging methods taking into account stellar evolution or they will be applicable only to stars in the same evolutionary stage.

Table 14: List of the GES stars selected as members of M67 and their principal parameters: coordinates, proper motions from the HSOY catalogue, radial velicities, temperatures and gravities as derived by the GES pipelines.

ID	RA [hms]	Dec [dms]	Teff [K]	e_Teff [K]	logg	e_logg	RV [km/s]	e_RV [km/s]	pmra [mas/yr]	pmde [mas/yr]	e_pmra [mas/yr]	e_pmde [mas/yr]
08514507+1147459	08:51:45.07	+11:47:45.9	4798	146	3.031	0.226	33.609	0.364	-11.08	-1.55	0.85	0.86
08513577+1153347	08:51:35.77	+11:53:34.7	4913	147	3.296	0.228	34.472	0.364	-9.70	-3.43	0.65	0.68
08510838+1147121	08:51:08.38	+11:47:12.1	4915	147	3.381	0.227	33.887	0.364	-10.11	-3.20	0.65	0.65
08510017+1154321	08:51:00.17	+11:54:32.1	5423	56	3.824	0.112	34.591	0.364	-9.53	-3.66	0.66	0.66
08510080+1148527	08:51:00.80	+11:48:52.7	5733	57	4.422	0.112	34.690	0.364	-8.68	-1.98	0.85	0.85
08511854+1149214	08:51:18.54	+11:49:21.4	5873	57	3.732	0.111	35.739	0.364	-10.02	-3.15	0.72	0.77
08510325+1145473	08:51:03.25	+11:45:47.3	5887	57	3.762	0.112	35.455	0.364	-9.58	-3.10	0.65	0.65
08514995+1149311	08:51:49.95	+11:49:31.1	5915	56	3.726	0.112	33.675	0.364	-10.07	-3.23	0.72	0.76
08513740+1150052	08:51:37.40	+11:50:05.2	5946	56	3.835	0.112	32.802	0.364	-10.03	-3.79	0.65	0.65
08510524+1149340	08:51:05.24	+11:49:34.0	6001	56	4.174	0.112	35.750	0.364	-9.76	-5.37	0.95	1.07
08514081+1149055	08:51:40.81	+11:49:05.5	6022	57	4.253	0.112	34.439	0.364	-10.42	-3.29	0.71	0.71
08505891+1148192	08:50:58.91	+11:48:19.2	6036	57	4.229	0.112	35.408	0.364	-9.26	-2.73	0.77	0.71
08505600+1153519	08:50:56.00	+11:53:51.9	6064	56	4.186	0.111	35.828	0.364	-8.77	-4.52	0.71	0.75
08514122+1154290	08:51:41.22	+11:54:29.0	6065	56	3.854	0.111	33.997	0.365	-9.27	-3.53	0.65	0.65
08512012+1146417	08:51:20.12	+11:46:41.7	6069	57	3.865	0.113	34.409	0.364	-8.78	-3.66	0.65	0.65

Table 15: List of the GES stars selected as members of M67 together with the respective abundances derived within GES and investigated in this work.

ID	C	e_C	O	e_O	Na	e_Na	Mg	e_Mg	Al	e_Al	Si	e_Si
08514507+1147459	8.22	0.05	8.72	0.09	6.31	0.04	7.51	0.06	6.42	0.04	7.57	0.06
08513577+1153347	8.24	0.02	8.70	0.10	6.20	0.07	7.50	0.05	6.39	0.04	7.54	0.05
08510838+1147121	8.26	0.02	8.69	0.10	6.20	0.07	7.54	0.05	6.41	0.03	7.55	0.07
08510017+1154321	8.23	0.03	8.65	0.02	6.27	0.06	7.59	0.07	6.45	0.06	7.58	0.05
08510080+1148527	8.23	0.02	8.60	0.10	6.14	0.06	7.53	0.10	6.33	0.04	7.43	0.08
08511854+1149214	8.19	0.09	8.55	0.04	6.18	0.11	7.45	0.12	6.22	0.10	7.43	0.08
08510325+1145473	8.18	0.06	8.61	0.02	6.20	0.11	7.50	0.05	6.28	0.04	7.47	0.06
08514995+1149311	8.17	0.05	8.50	0.09	6.16	0.14	7.43	0.07	6.19	0.04	7.39	0.08
08513740+1150052	8.17	0.08	8.39	0.04	6.14	0.10	7.48	0.06	6.22	0.04	7.43	0.08
08510524+1149340	8.18	0.05	8.70	0.09	6.10	0.09	7.43	0.08	6.17	0.04	7.38	0.08
08514081+1149055	8.20	0.06	8.57	0.01	6.15	0.08	7.47	0.10	6.19	0.04	7.41	0.08
08505891+1148192	8.18	0.05	8.50	0.09	6.13	0.08	7.48	0.10	6.19	0.04	7.39	0.08
08505600+1153519	8.19	0.07	8.60	0.09	6.11	0.10	7.48	0.06	6.19	0.05	7.43	0.10
08514122+1154290	8.16	0.07	8.61	0.01	6.17	0.13	7.47	0.06	6.18	0.03	7.41	0.08
08512012+1146417	8.15	0.07	8.53	0.05	6.12	0.10	7.42	0.09	6.17	0.03	7.39	0.06

ID	Ca	e_Ca	Ti	e_Ti	Cr	e_Cr	Mn	e_Mn	Fe	e_Fe	Ni	e_Ni
08514507+1147459	6.46	0.08	4.91	0.10	5.62	0.08	5.48	0.09	7.43	0.06	6.30	0.09
08513577+1153347	6.44	0.10	4.88	0.09	5.61	0.09	5.45	0.11	7.42	0.06	6.28	0.08
08510838+1147121	6.44	0.11	4.90	0.09	5.61	0.09	5.45	0.13	7.43	0.06	6.29	0.09
08510017+1154321	6.54	0.06	5.00	0.07	5.70	0.07	5.50	0.07	7.54	0.06	6.31	0.06
08510080+1148527	6.42	0.06	4.90	0.09	5.60	0.08	5.39	0.06	7.43	0.06	6.20	0.06
08511854+1149214	6.40	0.10	4.78	0.14	5.51	0.11	5.26	0.08	7.40	0.08	6.09	0.09
08510325+1145473	6.47	0.09	4.86	0.12	5.56	0.10	5.32	0.08	7.44	0.08	6.15	0.09
08514995+1149311	6.41	0.11	4.77	0.11	5.50	0.11	5.25	0.11	7.37	0.07	6.06	0.09
08513740+1150052	6.45	0.11	4.82	0.12	5.51	0.11	5.29	0.11	7.41	0.08	6.09	0.11
08510524+1149340	6.36	0.07	4.76	0.10	5.50	0.10	5.24	0.06	7.34	0.07	6.07	0.08
08514081+1149055	6.37	0.07	4.80	0.11	5.53	0.10	5.29	0.05	7.39	0.07	6.11	0.09
08505891+1148192	6.39	0.08	4.81	0.10	5.53	0.10	5.30	0.05	7.38	0.07	6.10	0.09
08505600+1153519	6.37	0.09	4.79	0.12	5.52	0.11	5.27	0.11	7.39	0.08	6.09	0.10
08514122+1154290	6.35	0.14	4.76	0.12	5.48	0.12	5.30	0.17	7.36	0.08	6.05	0.10
08512012+1146417	6.39	0.13	4.75	0.12	5.48	0.10	5.25	0.16	7.35	0.08	6.04	0.10

Part III

BLUE STRAGGLER STARS IN M67

Within the variety of objects populating stellar clusters, blue straggler stars (BSSs) are among the most puzzling ones. BSSs are commonly found in globular clusters, but they are also known to populate old open clusters of the Milky Way. Two main theoretical scenarios (collision and mass transfer) have been suggested to explained their formation, although finding observational evidence in support of either of them represents a challenging task. Among the APOGEE observations of the old open cluster M67, we found 8 BSS candidates known from the literature, two known evolved BSSs and a new BSS candidate selected by its kinematic properties. We carried out an independent chemical analysis of 5 stars out of the sample and we found that the un-evolved BSS candidates have surface abundances similar to those of stars on the turn-off of M67. Especially the absence of any anomaly in their carbon abundances seems to support a collisional formation scenario for these stars. Furthermore, we note that the abundances of the evolved BSSs S1040 and S1237 are consistent with the abundances of the red clump stars of M67. In particular, they show a depletion in carbon by ~ 0.2dex, which could be either interpreted as the signature of mass transfer or as the product of stellar evolutionary processes.

THE CHEMICAL PROPERTIES OF BLUE STRAGGLER STARS IN M67

The contents of this chapter are planned to be submitted for publication to MNRAS as Bertelli Motta, C., A. Pasquali, E.Caffau, M. Salaris, and E. K. Grebel, 'A chemical study of Blue straggler stars in M67 with APOGEE'.
C. Bertelli Motta performed the analysis and interpretation of the results with the help of A. Pasquali and wrote the text. The spectra and stellar parameters used in this study were retrieved from the APOGEE fourteenth data release. The abundances used for the analysis presented in this chapter were calculated by E. Caffau with MyGIsFOS (Sbordone et al., 2014) and the models of stellar evolution used for comparison were provided by M. Salaris.

5.1 INTRODUCTION

Among the variety of objects that populate stellar clusters, blue straggler stars (BSSs) are surely among those still presenting many riddles to astronomers. They are more luminous and bluer than the cluster TO, but their spread in the CMD cannot be explained by a younger single stellar population. BSSs were first discovered by Sandage (1953) in the CMD of the globular cluster M3. Shortly after, many old open clusters, e.g. NGC 7789 (Burbidge and Sandage, 1958), M67 (Johnson and Sandage, 1955), NGC 188 (Sandage, 1962), and NGC 6791 (Kinman, 1965), were found or at least suspected to host a BSSs population (for a review of the historical discoveries of BSSs see Cannon 2015). Nowadays BSSs are known to populate a large number of open and globular clusters (for a catalogue, see Ahumada and Lapasset 2007 and Fusi Pecci, Ferraro, and Cacciari 1993, respectively).

In order to appear 'younger' than the age of their hosting cluster, BSSs must have undergone processes that led to an increase in mass, e.g. through interactions with other stars, thus prolonging their life on the MS. There are several BSS formation scenarios predicted by theoretical studies. The first is mass transfer or mergers in close binary systems (McCrea, 1964; Strom and Strom, 1970): when one of the stars in a close binary system fills its Roche lobe, e.g. after expansion due to its evolution along the SGB, material from this star is accreted onto its companion, thus increasing its mass and extending its hydrogen burning phase for a longer time than its initial core mass would have allowed. Under some circumstances, it might even come to a merger of the two stars. The second scenario involves dynamically induced stellar collisions between single stars or multiple systems that lead to the formation of a BSS (Hills and Day, 1976). Recently, a third formation channel has been suggested, namely the merger of binaries in hierarchical triple systems caused by Kozai cycles and tidal friction (Naoz and Fabrycky, 2014; Perets and Fabrycky, 2009). In this scenario a close binary system, also called inner binary, acts as a companion to a third star. The dynamical interactions within the hierarchical triple system lead to oscillations in the eccentricity and inclination of the
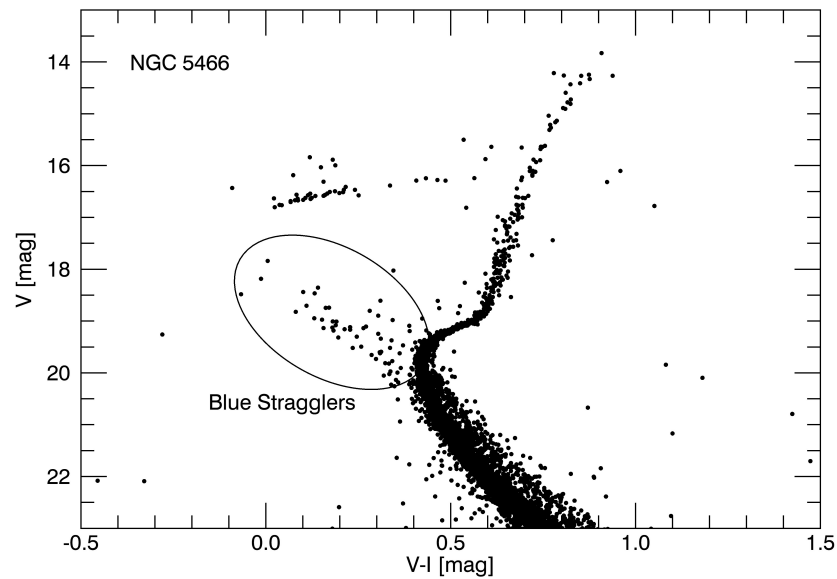
Figure 36: CMD of the globular cluster NGC 5466. The ellipse indicates the locus of blue straggler stars on the CMD. Photometry from the Hubble Space Telescope (HST) survey of globular clusters (Sarajedini et al., 2007, http://www.astro.ufl.edu/~ata/public_hstgc/databases.html)

inner close binary (Kozai oscillations or Kozai cycles, first proposed in Kozai 1962), which might then merge into a BSS. This scenario would, among other things, explain the presence of BSSs in long-period binaries.

If BSSs form through mass accretion, the material that is accreted last comes from the inner layers of the donor, where e.g. the CNO cycle has taken place and the abundance of lithium is depleted. We thus expect the BSSs surface abundances of elements such as C, N, O, and Li to be different from those of the parental cloud and consequently of the un-evolved cluster members (see, e.g., Sarna and De Greve 1996). If, instead, BSSs form through the dynamical collision of two stars, simulations do not predict that significant mixing happens in the stellar interior and the surface abundances are expected to be the same as in the rest of the cluster (see, e.g., Lombardi, Rasio, and Shapiro 1995). Thus, investigating the surface chemical composition of BSSs can hint at the circumstances under which they formed.

The measurement of surface abundances in BSSs belonging to globular clusters is difficult because of their faintness, but in recent years several studies have been carried out trying to determine the chemical composition of these objects and thus to constrain their formation history. Ferraro et al. (2006) studied the chemical composition of BSSs in 47 Tuc and found a substantial fraction of stars depleted in C and O. Nevertheless, 47 Tuc is the only cluster in which such a high number of depleted BSSs has been observed. In M4, M30, and ω Centauri a maximum of $1 - 2$ stars with a CO signature have been detected (see, e.g., Lovisi et al., 2010, 2013; Mucciarelli et al., 2014). This leads to the conclusion that either the mass transfer

formation channel is not very efficient in globular clusters or the surface C and O depletion expected in this scenario is only a temporary feature (Ferraro et al., 2015, and references therein).

BSSs are often observed as variable stars. In some cases this can give us hints about the formation history of the BSSs. Mass transfer BSSs are classical examples of Algol-type systems, eclipsing binaries formed by a MS star as a primary and an evolved star that has lost part of its mass through mass transfer after filling its Roche-lobe (McCrea, 1964). Also several BSSs are found to be W Ursae Majoris variables, contact binaries with a common envelope that are eventually going to merge. Some BSSs positioned on the Cepheid instability strip are observed as δ Scuti variables (see, e.g., Pribulla et al., 2008), although in this case their variable nature does not tell us how they formed. There is also the case of BSSs observed as companions to RS Canum Venaticorum (RS CVn) variables, showing chromospheric activity and presenting large spots which typically produce variations in the stellar luminosity (see, e.g., Sandquist et al., 2003).

Another characteristic of BSSs is their (sometimes) high rotational velocity $v \sin i$. Unfortunately, $v \sin i$ does not help us to disentangle the possible formation scenarios, since from theory stellar collisions (Sills, Adams, and Davies, 2005), as well as mass transfer (Webbink, 1976) and coalescence (Eggleton, 2011) can lead to rapid rotation. The studies carried out on the rotation velocities of BSSs in globular clusters found a correlation between the number of fast rotating BSSs and the density of the cluster: more sparse clusters (e.g. M4, ω Centauri) have a high concentration of rapid rotating BSSs ($\sim$ 33%), while in denser clusters (47 Tuc, NGC 6397, M30) the fraction is $\sim$ 4% (Ferraro et al., 2015, and references therein).

The old open cluster M67 ($\sim$ 4 Gyr) is known to host a relatively large population of BSSs and has been one of the first clusters in which BSSs have been discovered (Johnson and Sandage, 1955). The M67 BSSs have since then been extensively studied observationally both from a photometric (e.g. Gilliland et al., 1991; Pribulla et al., 2008; Sandquist and Shetrone, 2003; Sandquist et al., 2003; Stassun et al., 2002; van den Berg et al., 2002) and spectroscopic point of view (e.g. Geller, Latham, and Mathieu, 2015; Latham and Milone, 1996; Liu et al., 2008; Mathieu, Latham, and Griffin, 1990; Mathieu et al., 1986; Mathys, 1991; Shetrone and Sandquist, 2000), and also theoretically (e.g. Hurley et al., 2001, 2005; Tian et al., 2006). Although dynamical collisions are expected to be a more relevant formation channel in denser environments, N-body simulations have shown that cluster dynamics plays an important role in the formation of the BSSs population found in M67, although also a large number of primordial close binaries is necessary to account for the number of BSSs observed in M67 (Hurley et al., 2001, 2005). Both formation scenarios (mass transfer and collisions) thus seem to concur in the formation of BSSs in M67, at least from the point of view of numerical simulations.

Furthermore, M67 hosts red straggler and yellow straggler stars (YSS). The first ones, also known as sub-subgiants, are objects less luminous than the SGB and redder than the MS, but consistent with the kinematics of the cluster. Mathieu et al. (2003) found two of these objects in the field of M67, S1113 and S1063 (naming from Sanders 1977), which revealed themselves as binaries composed of a SGB star and a main-sequence star and whose origin and low luminosity are still unexplained. YSS are objects more luminous than the SGB, but bluer than the RGB.

Two of the YSS present in M67 are known to be evolved BSSs, S1040 and S1237. The first has been studied in detail by Landsman et al. (1997), who found it to be composed by a red giant and a He-core white dwarf companion. S1237 was subject to a study carried out by Leiner et al. (2016) based on Kepler asteroseismic data (Howell et al., 2014). The authors derived the asteroseismic mass and radius of the primary companion of the binary system, that was found to be much more massive ($\sim 2.9 M_\odot$) than the M67 RC. A third star, S1072, is listed in the literature as a candidate BSS but is actually redder than the TO, and is thus thought to be evolving along its SGB.

Previous investigations of the chemical composition (Fe, Li, C, N, Na, Mg, Ca, Ni, Ba) of 7 BSSs in M67 (Mathys 1991; Shetrone and Sandquist 2000) found that the surface abundances of these stars are consistent with those of TO stars, which would suggest a collisional formation scenario. We perform an independent chemical analysis of the infrared spectra of 3 candidate BSSs and 2 evolved BSSs in the field of M67. We then present the derived abundances together with information collected from previous studies, and discuss whether they can give us clues about the BSSs formation mechanisms in M67.

5.2 DATA AND METHOD

Within the field of M67, 24 stars are known as candidate BSSs from Deng et al. (1999) (see Table 16). Balaguer-Núñez, Galadí-Enríquez, and Jordi (2007) suggested S1466 together with S489 as further BSS candidates. Nevertheless, in the kinematic study of M67 carried out by Geller, Latham, and Mathieu (2015), S1466 is listed as non-member, while S489 is considered a single member of the cluster based on its kinematics, but not a BSS.

Liu et al. (2008) performed a spectroscopic study of 19 stars from the list of BSS candidates and derived their T_{eff} and log g. Sandquist and Shetrone (2003) studied the light curves of 20 of these stars, indicating several variable stars among them that will be discussed later in more detail. Pribulla et al. (2008) investigated the variability of all the 24 BSS candidates with the MOST (*Microvariability and Oscillations of STars*) satellite. Geller, Latham, and Mathieu (2015) included all 24 objects in a larger list of targets for their study of the kinematics of M67. For each of them they determined their membership probability and binarity. Furthermore, they exclude some of these stars from the list of BSSs based either on their kinematic properties or on their position on the CMD. In Table 16 we summarise the findings of the previous studies: for each star we list if it is considered member and a blue straggler by Geller, Latham, and Mathieu (2015) and a variable by Pribulla et al. (2008) and Sandquist and Shetrone (2003).

Out of the 24 BSS candidates from Deng et al. (1999), 12 are included in the fourteenth data release of the Apache Point Observatory Galactic Evolution Experiment (hereafter APOGEE DR14, see Abolfathi et al., 2017; Majewski et al., 2015). Four of them have the ASPCAP flag set to STAR_BAD [1] and we therefore do not take these stars into further consideration. The other stars have, if any, only flags

---

[1] "BAD overall for star: set if any of TEFF, LOGG, CHI2, COLORTE, ROTATION, SN error are set, or any parameter is near grid edge (GRIDEDGE_BAD is set in any PARAMFLAG"
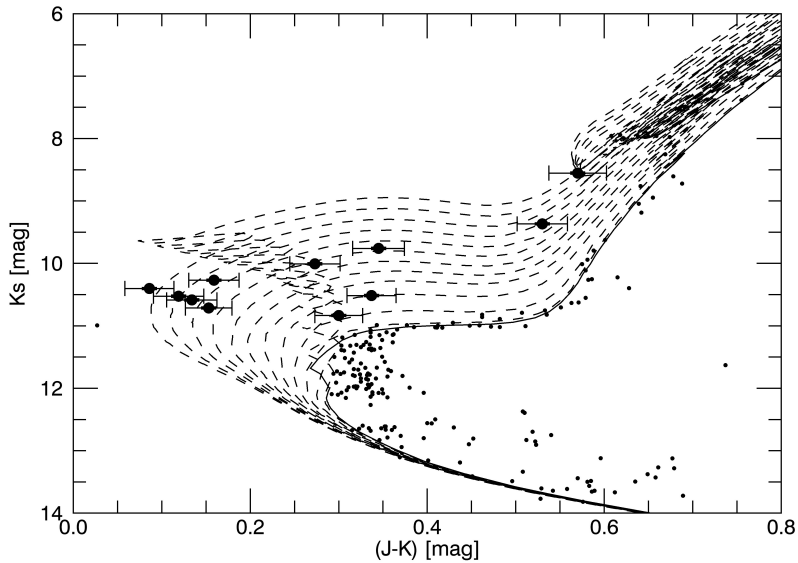
Figure 37: CMD of M67 where the kinematic members of the cluster are represented as small black dot and the 8 BSS candidates as well as the two evolved BSS considered in this studied are plotted as large black dots. We also show a sequence of PARSEC isochrones (Bressan et al., 2012) ranging from 1 to 4 Gyr.

signalising warnings. In addition, APOGEE DR14 also observed two evolved BSSs, S1040 and S1237.

We use the effective temperatures, gravities, and microturbulences (when available) derived with the APOGEE Stellar Parameters and Chemical Abundances Pipeline (ASPCAP) (see García Pérez et al., 2016; Holtzman et al., 2015) as an input for our independent chemical analysis performed with MyGIsFOS (Sbordone et al., 2014). The code MyGIsFOS uses a pre-computed synthetic stellar grid to determine stellar parameters and abundances. Although the code allows for the determination of stellar parameters such as T_{eff}, $\log g$, V_{micro}, and $[\alpha/Fe]$, we decided to keep the stellar parameters fixed, using the values derived by ASPCAP for T_{eff}, $\log g$, V_{micro} and assuming $[\alpha/Fe] = 0$ (see Table 17). Since for dwarf stars no calibrated $\log g$ values are available in APOGEE DR14, we used $\log g$ values derived comparing the position of the stars on the CMD with the closest isochrone (see Fig. 37). MyGIsFOS then computes the element abundances fitting the different line profiles with the synthetic spectra along the [Fe/H]–dimension of the grid. We chose not to use the abundances derived from ASPCAP in order to have a better understanding of the systematics involved in the abundance determination and in order to be able to carry out tests, e.g. on the dependence of the obtained abundances on T_{eff}, $\log g$, and the persistence (i.e. residual flux from previous exposures) present in some of the APOGEE spectra (Holtzman et al., 2015).

Table 16: The 24 candidate BSSs from Deng et al. (1999) are listed together with their membership probability and confirmed BSS nature from Geller, Latham, and Mathieu (2015) (G15), their variability as detected by Sandquist and Shetrone (2003) (S&S03) and Pribulla et al. (2008) (P08). DS: δ scuti variable, EB: eclipsing binary, Poss. LA: possible low amplitude. In the last column we indicate which stars are present in APOGEE DR14.

Name	Memb. G15	BSS G15	Var. S&S03	Var. P08	APOGEE DR14
S977	BLM	Y	N	–	Y
S1434	BLM	Y	–	–	Y
S1066	BLM	Y	N	–	Y
S1267	BM	Y	N	–	Y
S1284	BM	Y	DS	DS	Y
S1263	SM	Y	Poss. LA	–	Y
S968	SM	Y	Poss. LA, Am	–	Y
S975	BM	Y	Faint comp.	–	–
S1082	BM	Y	RS CVn var.	EB	Y
S752	BM	Y	Am, poss. flare	–	Y
S1072	BM	?	N	–	Y
S1280	BLM	Y	DS	DS	–
S997	BM	Y	N	–	–
S1195	BM	Y	N	–	–
S792	SM	N	N	–	Y
S277	BM	N	–	–	–
S2226	SM	Y	–	–	–
S1273	SM	N	N	–	–
S984	SM	N	N	–	Y
S1005	BM	N	N	–	–
S751	SM	N	N	–	–
S1036	BLM	N	W UMa var.	EB	–
S145	SN	N	–	–	–
S2204	SM	N	N	–	–

Table 17: Input parameters used for the chemical analysis with MyGIsFOS: the calibrated temperatures, gravities, and microturbulences from APOGEE DR14, the photometric temperatures, and the gravities from the isochrones (used when no calibrated gravities from APOGEE DR14 were available). The last column indicated if the analysed spectra are affected by persistence.

Name	$T_{eff,DR14}$ [K]	$\log g_{DR14}$ [dex]	$v_{micro,DR14}$ [km/s]	$T_{eff,photo}$ [K]	$\log g_{iso}$ [dex]	Persistence
S792	5947	–	0.67	5943	3.65	N
S984	5963	–	0.75	6118	3.8	Y
S1072	5776	–	1.00	5915	3.4	N
S1237	5030	3.15	1.04	5022	2.9	Y
S1040	5063	3.03	1.12	5157	3.2	N

5.3 ANALYSIS AND RESULTS

We performed a membership analysis of the stars observed by APOGEE DR14 in the field of the old open cluster M67 based only on their proper motions and radial velocities, as in the first 4 steps of the membership analysis described in Chapter 2. In Fig. 38 we compare the radial velocity (RV) distribution of the BSS candidates found in APOGEE with the RV distribution found for M67 members after our analysis. Two stars lie outside of the cluster distribution and would have been eliminated by our selection. The RV obtained by APOGEE for the BSS candidates are also in some cases significantly different from the ones derived by Geller, Latham, and Mathieu (2015) (see Table 18), so we suggest that the peculiar velocities might be due to variations caused by the radial projection of the binary orbit. Nevertheless, the proper motions that we retrieve from HSOY (the proper motion catalogue obtained combining the information from the first Gaia data release – Gaia DR1 – and the PPMXL catalogue, see Altmann et al. 2017) for the BSS candidates are consistent with the mean proper motion of M67 (see Fig. 39), except for S1082 that does not have an entry in HSOY. After our membership analysis we find also one further star, S1373, which to our knowledge has never been considered as a BSS candidate before, but which is consistent with the kinematic properties of M67 (although at the edge of the PM distribution, see Fig. 39) and is bluer and more luminous than the TO stars. In our study, we also consider two objects located above the SGB of M67 and known from the literature as evolved BSS, S1040 (Landsman et al., 1997) and S1237 (Leiner et al., 2016). The complete sample, containing in total 11 stars, is displayed in Fig. 40, the 8 candidate BSSs as blue diamonds, the evolved BSSs as orange diamonds, and S1373 as a magenta diamond.

We performed an independent analysis of the chemical composition of 5 of the 11 stars with MyGIsFOS (S984, S792, S1072, S1237, and S1040; see spectra in Fig. 41) and obtained the abundances of C, Al, Mg, Si, S, Fe, and Ni. The remaining BSS candidates could not be analysed because they are too hot or rotating too fast. The stars for which elemental abundances were obtained are circled in Fig. 40. We se-

Table 18: The rotation velocities and radial velocities of the 11 stars of our sample derived by APOGEE DR14 compared to the radial velocities from Geller, Latham, and Mathieu (2015).

Name	$v \sin i$ [km/s]	AP RV [km/s]	AP RV_e [km/s]	G15 RV [km/s]	G15 RV_e [km/s]
S792	3.63	34.08	0.01	33.49	0.1
S752	76.26	25.68	0.14	31.29	0.35
S984	8.00	33.49	0.02	31.89	0.19
S1072	13.88	34.88	0.02	32.72	0.13
S1040	6.09	31.69	0.01	33.01	0.08
S1263	25.56	32.67	0.07	32.22	0.07
S1284	79.45	34.42	0.15	31.92	0.37
S1267	60.90	38.71	0.44	33.76	0.23
S1237	–	37.33	0.003	33.58	0.06
S1082	13.99	34.42	0.04	33.68	0.09
S1373	53.05	31.05	0.05	–	–
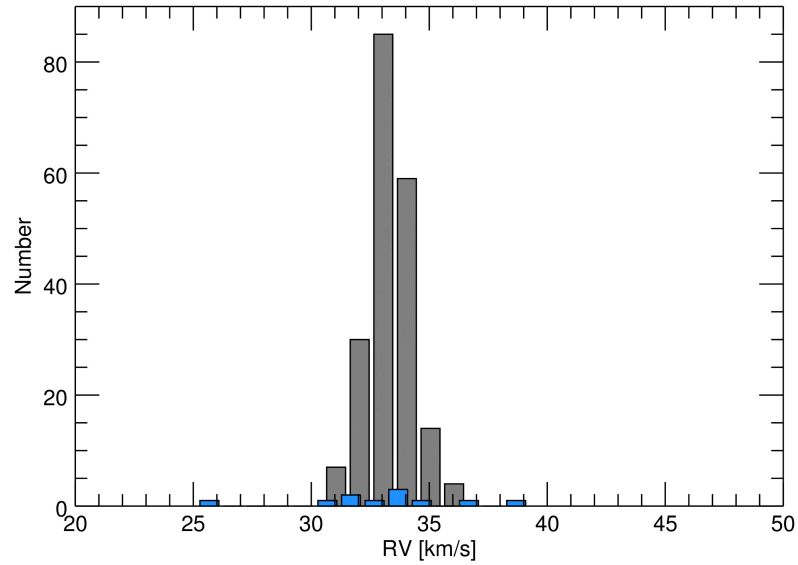
Figure 38: The grey histogram representing the radial velocities of stars considered members based on their kinematic properties. The blue histogram shows the radial velocities obtained in APOGEE DR14 for the 8 BSS candidates, the 2 evolved BSSs, and our new candidate S1373.
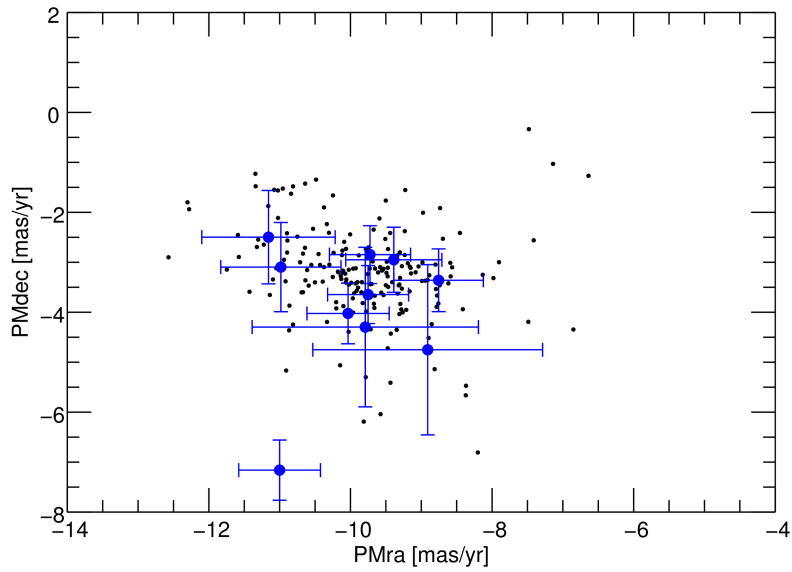
Figure 39: Proper motion in RA and Dec of our sample of stars. Colours and symbols are as in Fig. 38. Black dots are stars selected through our membership analysis.
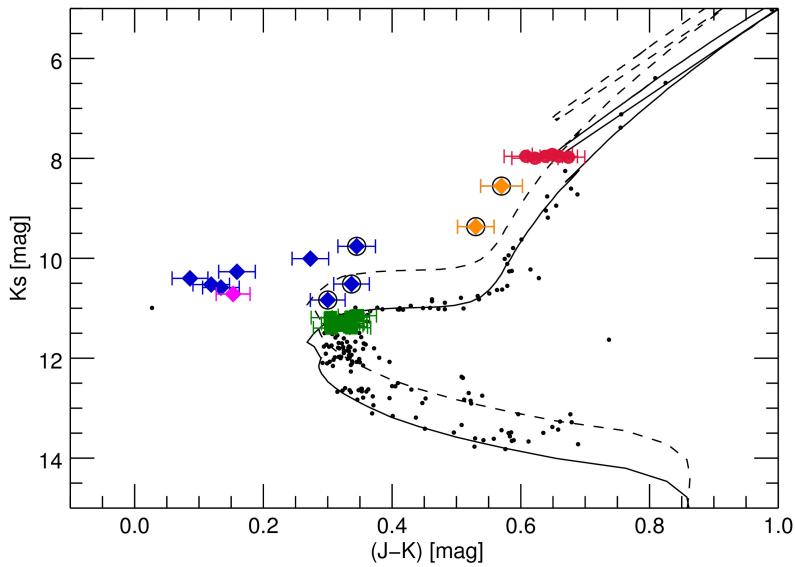
Figure 40: The plot shows the position on the CMD of the stars involved in our study. The BSS candidates known from the literature and found in APOGEE DR14 are plotted as blue diamonds, the new BSS candidate proposed in this work is plotted as magenta diamond, while the two evolved BSSs are shown as orange diamonds. The two control samples on the TO and on the RC are shown as green squares and red dots respectively. The stars for which we obtained chemical abundances are circled in black. We show a 4 Gyr PARSEC isochrone as a solid black line and the position of the equal-mass binaries as a dashed line.

lected two further samples of 10 stars in the TO region and 6 stars on the RC of M67 (see Fig. 40) in order to compare the chemical abundances of the BSS candidates with the abundances found in dwarfs (green squares) and evolved giants (red dots).

For all elements under study, the un-evolved BSS candidates in M67 present surface abundances in good agreement with the stars in the TO sample (see Fig. 43).

The two evolved BSSs present surface abundances consistent with those of the RC. For most elements these correspond to the abundances at the TO, except for the species that are processed during stellar evolution, such as C. The carbon abundance of the evolved BSSs is depleted by $\sim$ 0.25 dex (see Fig. 42), consistent with the RC abundances derived from our analysis. The carbon abundance is depleted in the RC due to the effect of the FDU and possibly of extra-mixing processes (see Chapter 3). Fig. 42 also shows the predicted effect of the FDU with models of mass $1.4 M_\odot$ (dashed line), $2 M_\odot$ (solid line), and $2.9 M_\odot$ (dotted line) with [Fe/H] = 0.06 dex from the BaSTI database. The first model represents the mass of the lower RGB in M67, the second that of the S1237 from the closest isochrone and the third that of S1237 from asteroseismic measurements. The mean [C/H] abundance measured in both evolved BSSs and RC is lower than the post-FDU abundance for all three models, although all of them are included in the error bars. Unfortunately we could not measure N abundances for the stars under study, due to the high temperature and the consequent weakness of the molecular bands from which they are derived.

Some of the stars were observed in several visits by APOGEE and the spectra were then combined before being analysed with ASPCAP. The blue chip of the APOGEE detector is known to suffer from persistence (see, e.g., Holtzman et al. 2015) and the spectra affected by this problem are flagged in the APOGEE archive. In order to reduce possible errors deriving from the presence of persistence in the spectra under study, we retrieved the spectra of the single visits and combined and analysed only those without persistence, when possible. For S984 and S1237 all visits were affected by high persistence. We therefore tested the influence of persistence on the derivation of the chemical composition in the case of S1040. For this star visits both with and without persistence are available. We separated the spectra with and without persistence and created two combined spectra that we then analysed (see. Fig. 44). We found that the presence of persistence in the spectra causes small variations in the abundances derived with our analysis, that are 1 order of magnitude smaller than the errors. We thus conclude that the abundances derived from spectra affected by persistence are reliable, at least in the case of the stars under study.

In addition, we considered two different sets of temperature in order to test the dependence of our results on the input parameters. For one set we adopted the calibrated effective temperature obtained by ASPCAP, while for the second set we calculated the photometric temperature of the stars following the equation of González Hernández and Bonifacio (2009):

$$\theta_{eff} = b_0 + b_1 X + b_2 X^2 + b_3 X[Fe/H] + b_4[Fe/H] + b_5[Fe/H]^2, \tag{21}$$

where $\theta_{eff} = 5040/T_{eff}$, X is the infrared colour (we use $J - K_s$), and $b_{0..5}$ are the coefficient of the fit. When using $J - K_s$, for dwarf stars holds $b_0 = 0.6524$,

Table 19: Abundances obtained for the 5 analysed BSSs with MyGiSFOS.

Name	[C/H]	e_[C/H]	[Mg/H]	e_[Mg/H]	[Al/H]	e_[Al/H]
S792	-0.02	0.23	-0.05	0.46	0.3	0.15
S984	-0.00	0.18	0.14	0.52	0.37	0.056
S1072	0.02	0.15	0.07	0.33	0.29	0.14
S1237	-0.22	0.19	0.04	0.34	0.37	0.18
S1040	-0.28	0.20	0.29		0.38	0.23

[Si/H]	e_[Si/H]	[S/H]	e_[S/H]	[Fe/H]	e_[Fe/H]	[Ni/H]	e_[Ni/H]
0.19	0.15	-0.25	0.16	-0.07	0.19	-0.25	0.15
0.21	0.13	-0.16		0.06	0.2	0.03	
0.13	0.16	-0.19	0.16	-0.04	0.15		
0.2	0.2	0.07	0.23	0.05	0.16	-0.12	0.24
0.06	0.12	-0.22		-0.10	0.19	-0.28	0.18

$b_1 = 0.5813$, $b_2 = 0.1225$, $b_3 = -0.0646$, $b_4 = 0.0370$, and $b_5 = 0.0016$, while for giants $b_0 = 0.6517$, $b_1 = 0.6312$, $b_2 = 0.0168$, $b_3 = -0.0381$, $b_4 = 0.0256$, and $b_5 = 0.0013$. Both sets of temperatures are listed in Table 17. As we show in Fig. 45, there is a trend of the resulting [Fe/H] abundance with temperature, but this effect is smaller than the error on the abundances and thus should be of no further concern. We also tested the effects of variations in $\log g$ and v_{micro}. Changing e.g. $\log g$ by ~ 0.25 dex or v_{micro} by 0.04 km/s leads to variations in the abundances that are smaller than their errors.

Table 20: Abundances obtained for the 10 TO stars analysed with MyGiSFOS.

Name	[C/H]	e_[C/H]	[Al/H]	e_[Al/H]	[Mg/H]	e_[Mg/H]
S815	-0.07	0.32	0.16	0.22	-0.12	0.41
S598	0.03	0.08	0.39	0.15	0.06	0.37
S756	-0.01	0.21	0.29	0.11	0.11	0.37
S1076	-0.01	0.17	0.21	0.10	-0.21	0.37
S1083	-0.03	0.25	0.18	0.17	-0.11	0.45
S1310	-0.01	0.16	0.25	0.18	-0.06	0.53
S1268	0.0	0.20	0.19	0.21	0.01	0.42
S1456	-0.1	0.27	0.16	0.24	-0.02	0.39
S1429	0.11	0.12	0.14	0.19	-0.05	0.36
S1589	-0.02	0.18	0.18	0.1513	-0.05	0.34

[Si/H]	e_[Si/H]	[S/H]	e_[S/H]	[Fe/H]	e_[Fe/H]	[Ni/H]	e_[Ni/H]
0.15	0.17	-0.2	0.19	-0.12	0.16		
0.2	0.13	-0.08	0.24	0.01	0.16	0.03	0.20
0.21	0.11	-0.12	0.18	-0.03	0.15	0.05	0.20
0.02	0.06	-0.26	0.18	-0.19	0.17	-0.07	0.19
0.12	0.11	-0.25	0.18	-0.11	0.17	-1.13	
0.15	0.14	-0.14	0.17	-0.08	0.14		
0.1	0.16	-0.24	0.15	-0.11	0.18	-0.07	0.23
0.05	0.17	-0.26	0.10	-0.2	0.13	-0.46	
0.08	0.11	-0.15	0.16	-0.12	0.17		
0.1	0.14	-0.18	0.12	-0.14	0.1603	0.09	

Table 21: Abundances obtained for the 6 RC stars analysed with MyGiSFOS.

Name	[C/H]	e_[C/H]	[Al/H]	e_[Al/H]	[Mg/H]	e_[Mg/H]
S1074	-0.29	0.21	0.39	0.32	0.14	0.23
S1084	-0.27	0.24	0.36	0.30	0.05	0.15
S1279	-0.31	0.26	0.36	0.30	0.26	0.19
S1316	-0.34	0.24	0.33	0.31	0.16	0.22
S1479	-0.30	0.17	0.37	0.31	0.16	0.23
S1592	-0.24	0.17	0.35	0.32	0.2	0.23

[Si/H]	e_[Si/H]	[S/H]	e_[S/H]	[Fe/H]	e_[Fe/H]	[Ni/H]	e_[Ni/H]
0.14	0.08	-0.02	0.40	-0.04	0.17	-0.23	0.17
0.14	0.09	0.15	0.14	-0.03	0.19	-0.23	0.20
0.16	0.09	-0.01	0.39	-0.03	0.17	-0.2	0.15
0.14	0.10	0.14	0.11	-0.05	0.18	-0.26	0.16
0.11	0.11	0.14	0.12	-0.05	0.16	-0.25	0.19
0.15	0.13	0.0	0.37	0.0	0.18	-0.23	0.18
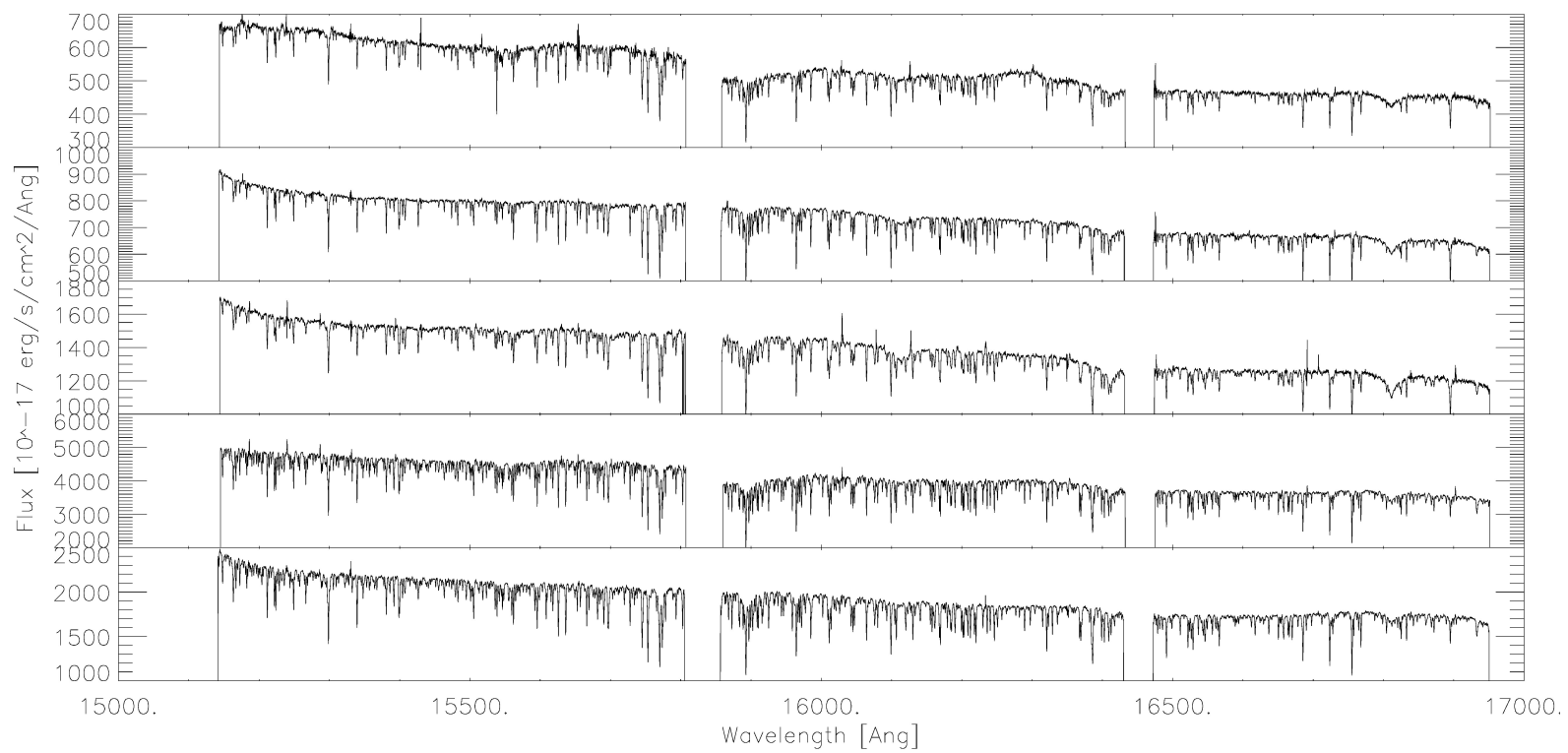
Figure 41: Spectra of the five BSSs analysed in our work. From top to bottom: S984, S792, S1072, S1237, and S1040.

5.4 DISCUSSION

In the following we first discuss the general characteristics of BSSs in M67 from APOGEE DR14 data, such as their rotational velocity and spatial distribution, and then summarise the properties of the BSS candidates observed in APOGEE DR14 one by one including our chemical analysis, when available. The properties of the different BSSs are summarised in Tables 16,17,18,19.

5.4.1 *Spatial distribution*

As can be seen in Fig. 46, the spatial distribution of the 8 BSS candidates considered in this work (blue diamonds) and of the 2 evolved BSSs (orange diamonds) is concentrated in the central region of the cluster, while S1373 (magenta diamond) lies at a larger distance from the centre of the cluster. This is not inconsistent with the BSSs distribution observed in other clusters (see discussion below), but together with its position in the PM diagram this could mean that S1373 is not a member of M67. The complete sample of the 24 BSS candidates from Deng et al. (1999) is shown as large black dots and presents 3 stars outside the central region of the cluster. We show stars considered members based on radial velocity and proper motions as small dots.

The distribution of the BSSs distances from the centre of the hosting cluster presents different shapes. Globular clusters have been shown to present three different types of spatial distribution (flat, bimodal, or centrally concentrated) that are correlated with the dynamical age of the cluster (see,e.g., Ferraro et al. 1997, 2012). In the case of open clusters, while BSSs in NGC 188 have been shown to have a bimodal spatial distribution (Geller et al., 2008), the density of BSSs in M67, as shown in Geller, Latham, and Mathieu (2015), decreases rapidly with distance from the cluster centre, although we point out that two out of three of the candidate BSSs lying further away from the cluster centre, as well as S1373, (see Fig. 46) are not considered in the BSSs list compiled by Geller, Latham, and Mathieu (2015). On the other hand, as discussed in Geller, Latham, and Mathieu (2015) the study of NGC 188 extended to a much larger distance from the cluster centre than the surveys that have been carried out so far for M67. It is therefore possible that also for M67 BSSs present a bimodal distribution that has not been discovered yet.

5.4.2 *Rotation velocity*

One of the outputs of the ASPCAP pipeline is the rotation velocity of the analysed star, $v \sin i$. In the sample of BSS candidates observed by APOGEE DR14, five stars have rotational velocities higher than 20 km/s and up to $\sim$ 80 km/s. $v \sin i$ is plotted in Fig. 47 as a function of the calibrated effective temperature derived with ASPCAP. All fast rotators have temperatures higher than 6400 K, although there is one star hotter than 7000 K with rotational velocity lower than 20 km/s. Unfortunately, we could not derive the surface chemical composition of any of these objects due to the line broadening caused by rotation. The stars that we analysed have all $v \sin i < 20$km/s, and especially S792 and S984 have rotational velocities similar to the TO stars and close to zero. For the RC sample no rotational velocities
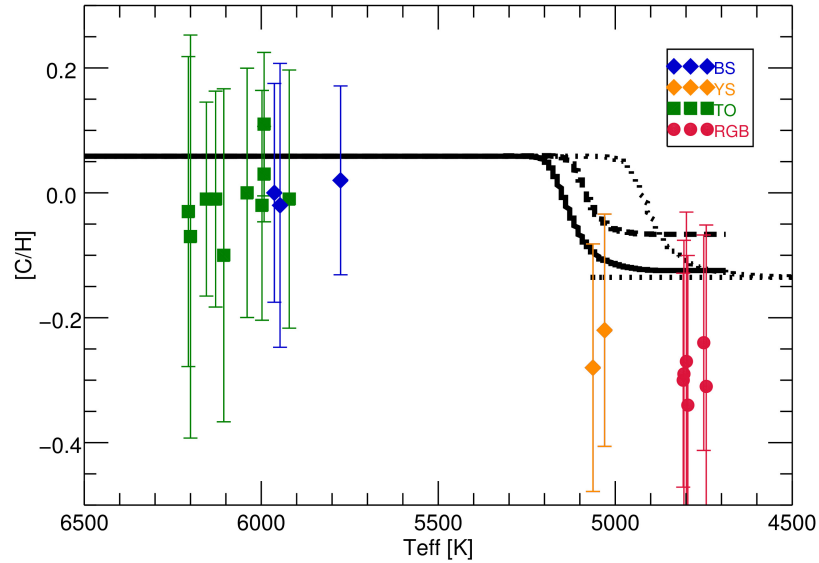
Figure 42: Carbon abundances obtained with our analysis for the BSSs and the control samples. Colours and symbols are the same as in Fig. 40. We also overplot models of stellar evolution calculated for $[Fe/H] = 0.06$ dex and a mass $1.4M_\odot$ (dashed line), $2.0M_\odot$ (solid line) and $2.9M_\odot$ (dotted line).

were measured with ASPCAP. As shown in Mathieu and Geller (2009) also many BSSs in NGC 188 and NGC 6819 present high rotational velocities, although the highest value that they derive is ~ 50km/s. In contrast to the results of Mathieu and Geller (2009), we do not find a trend in effective temperature for the measured rotational velocities, although no star cooler than 6400K is a fast rotator. As described in Sec. 5.1, fast rotating BSSs are mostly found in low-density globular clusters. These findings are consistent with the presence of a large number of fast rotating BSSs found in sparse environments such as that of M67.

5.4.3 *Chemical composition*

To our knowledge, the only previous studies of the chemical composition of BSS candidates in M67 were carried out by Shetrone and Sandquist (2000) and Mathys (1991). They performed a chemical analysis of 7 BSS candidates in total and only one of them (S984) is in common with the sample that we analysed with MyGiS-FOS (their results for the C and Fe abundances are summarised in Table 22). In the following, we will discuss in more detail the information available from the literature about each star for which infrared spectra were retrieved by APOGEE DR14, complementing it with the stellar parameters derived by ASPCAP and the results from our analysis.

The stars observed by APOGEE DR14 but excluded from our study because of their flags are: S977, considered a likely binary member by Geller, Latham, and Mathieu (2015) who also include it in their list of confirmed BSSs; S1434, also considered a likely binary member and a BSS by Geller, Latham, and Mathieu (2015).
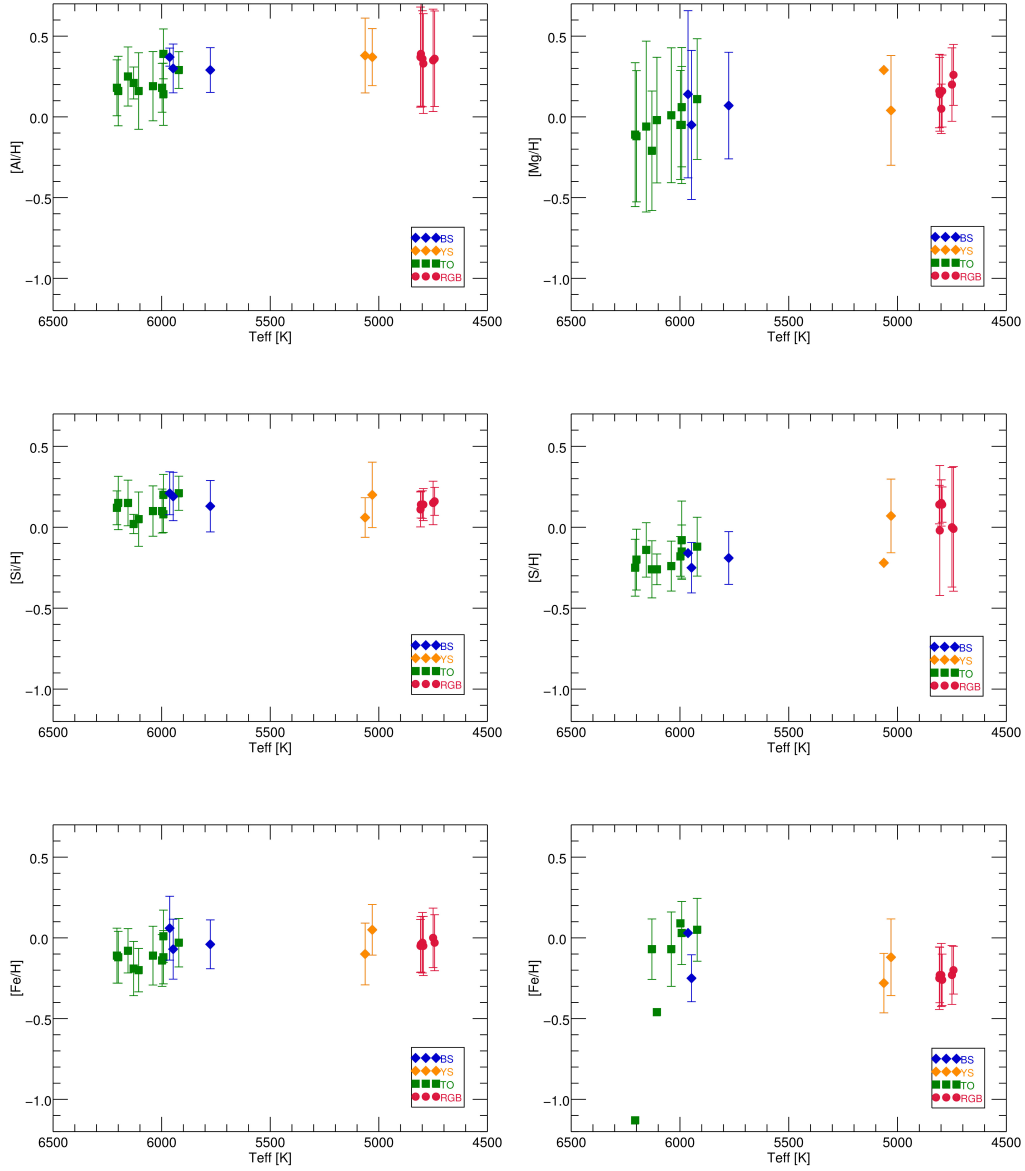
Figure 43: Abundances derived from our analysis as a function of the APOGEE DR14 calibrated effective temperature $T_{e}ff$. Colours and symbols are the same as in Fig. 40.
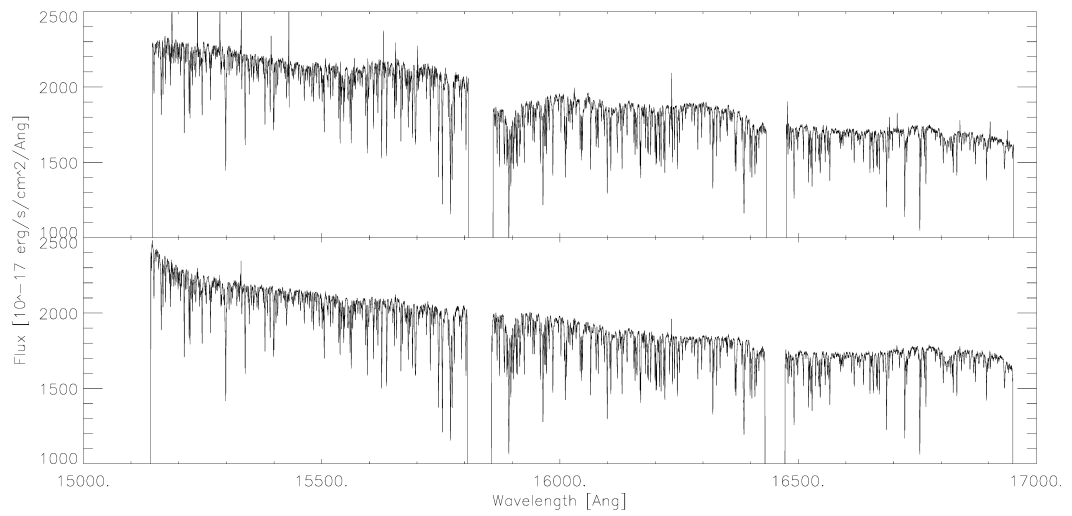
Figure 44: Combination of S1040 spectra with (top panel) and without persistence (bottom panel).
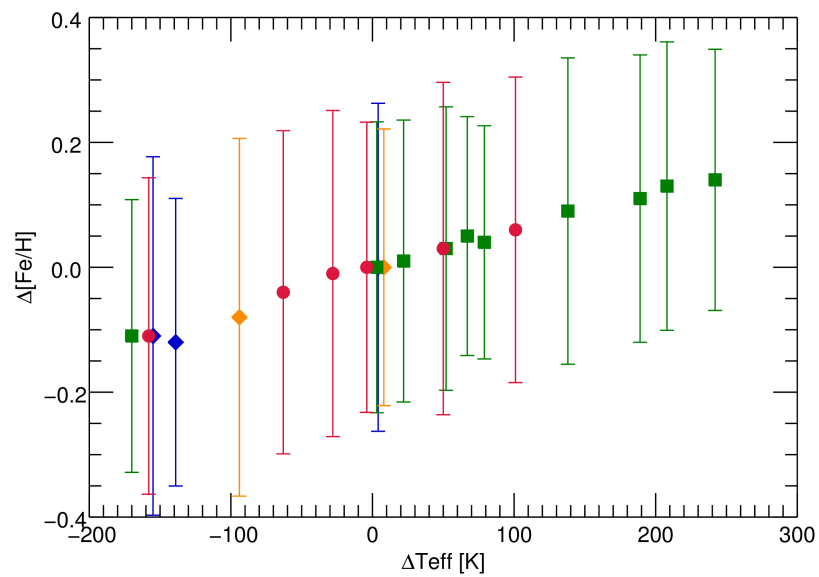
Figure 45: Difference in abundance obtained using two different sets of temperature as a function of the temperature difference. Colours and symbols are as in Fig. 40.
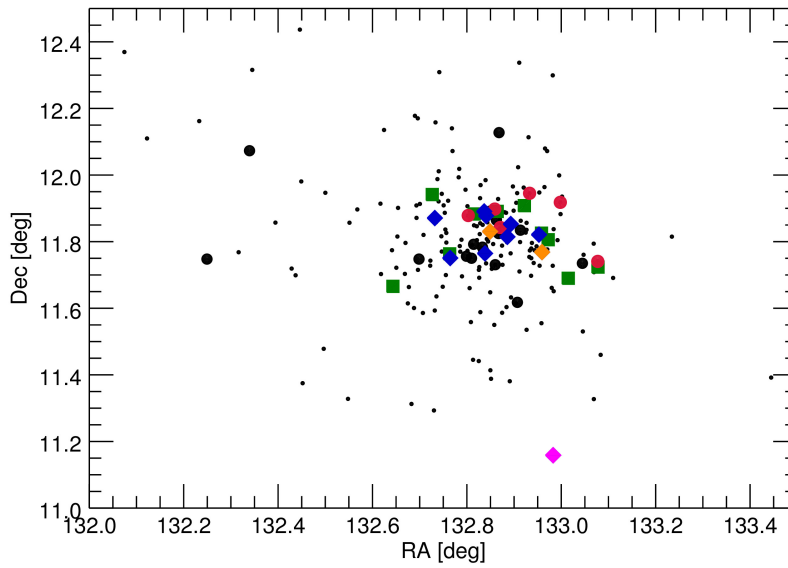
Figure 46: Distribution in equatorial coordinates of the stars considered in this study. Kinematic members and full members of M67 are plotted with small and large dots, respectively. BSSs, evolved BSSs, TO, and RC stars are displayed with the same colours and symbols as in Fig. 40.
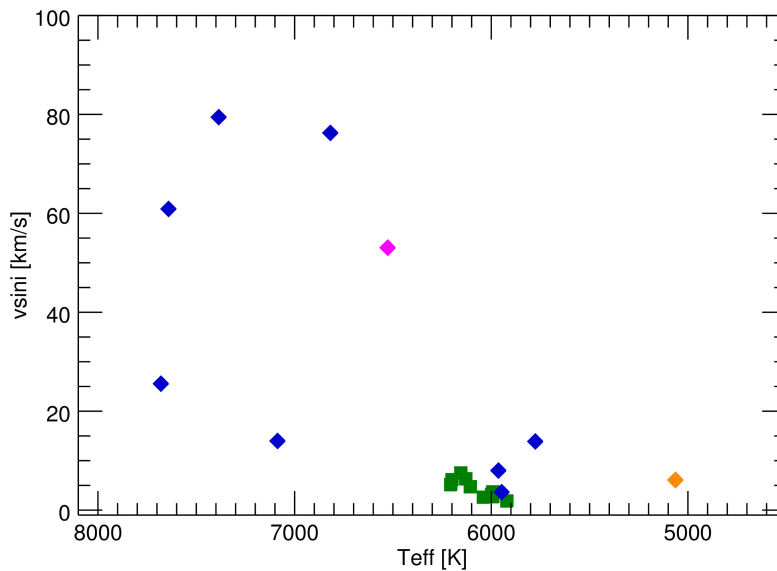
Figure 47: Rotational velocity $v \sin i$ as a function of the uncalibrated ASPCAP effective temperature. Colours and symbols are the same as in Fig. 40.

Table 22: C and Fe abundances obtained by Shetrone and Sandquist (2000) and Mathys (1991) for 7 BSSs.

Name	[C/Fe]	e_[C/Fe]	[Fe/H]	e_[Fe/H]
Stars from Shetrone and Sandquist (2000)				
S984	-0.14	0.08	0.08	0.03
S2204	0.05	0.06	-0.05	0.06
S975	-0.09	0.09	0.02	0.06
S997	-0.03	0.08	-0.06	0.03
S1082	-0.01	0.05	-0.25	0.05
Stars from Mathys (1991)				
S968	-0.75	0.23	0.03	0.16
S1263	-0.64	0.21	0.09	0.19

S1434 is likely to be a rapidly rotating binary for which the authors obtained only a preliminary orbital solution. According to Balaguer-Núñez, Galadí-Enríquez, and Jordi (2007) the membership of S1434 is uncertain; S1066 is listed as a likely binary member and a BSS by Geller, Latham, and Mathieu (2015). Sandquist and Shetrone (2003) do not detect any variation in the light curve of this star, so it cannot be considered an eclipsing binary; S968 is also considered a BSS and a single star member by Geller, Latham, and Mathieu (2015). Sandquist and Shetrone (2003) report it as an Am star and a possible low amplitude variable. S968 was analysed by Mathys (1991) and, similarly to S1263 (see below), was found to be under-abundant in C and O. Nevertheless, the author points out that the O abundance of S968, a known Am star, is consistent with that of other dwarf Am stars in his sample.

The first star included in our sample is S1267. It is found to be a binary member and a BSS by Geller, Latham, and Mathieu (2015), although Balaguer-Núñez, Galadí-Enríquez, and Jordi (2007) consider its membership uncertain. Sandquist and Shetrone (2003) do not find signs of variability for this star. Nevertheless, S1267 is known to be a spectroscopic binary with a period of 846d and eccentricity $e = 0.475 \pm 0.125$ from Latham and Milone (1996). The radial velocity RV = 38.7km/s derived with ASPCAP is higher than the cluster mean and the value obtained by Geller, Latham, and Mathieu (2015), RV = 33.76 ± 0.23 km/s. It is a fast rotator ($v\sin i = 60.9$km/s) and has $T_{eff} = 7598.7$K.

S1284 is a δ Scuti star. Its variable nature is discussed e.g. in Gilliland et al. (1991), Pribulla et al. (2008), and Sandquist and Shetrone (2003). Geller, Latham, and Mathieu (2015) lists it as a binary member of M67 and a BSS. Latham et al. (1992) reports a binary period of 4.1828d and $e = 0.266 \pm 0.045$. Its radial velocity is consistent with the cluster mean and, with $T_{eff} = 7343.0$K, it is among the hotter BSSs of the sample. Its rotation velocity is very high, $v\sin i = 79.5$km/s.

S1263 is a single star member of M67 and a BSS according to Geller, Latham, and Mathieu (2015). Sandquist and Shetrone (2003) state that it might be a variable star with low amplitude, while Pribulla et al. (2008) do not find any sign of variability for this object. It has a radial velocity consistent with the cluster, it seems to rotate

much slower than the BSSs discussed so far ($vsini = 25$km/s), and it has $T_{eff} = 7599.0$K. S1263 is one of the BSSs analysed by Mathys (1991) who found it to be depleted in both C and O although with iron abundance consistent with that of the cluster ([Fe/H] $= 0.09 \pm 0.19$dex).

S1082 is the best studied BSS in M67. It is known to be a system composed of a close binary with a BSS and a TO star and a second component, probably a BSS itself. The spectroscopic study of van den Berg et al. (2001) revealed the presence of three components in the system. X-ray emission found by Belloni, Verbunt, and Mathieu (1998) suggests that the close system might be a magnetically active RS CVn-type eclipsing binary. In Sandquist et al. (2003), the light curve of this stellar system was studied in detail and the authors confirmed S1082 to be formed by a close binary with orbital period 1.08 d and a second component which is either a spatial superposition, or a third star dynamically bound but on a large eccentricity orbit with a period of 1189 d. Pribulla et al. (2008) further studied the asymmetry of the light-curve of S1082, probably caused by photospheric spots in the non-BSS companion in the close binary. Leigh and Sills (2011) developed an analytic method based on energy conservation in stellar encounters to determine the formation scenario of multiple stellar systems. They analysed the specific case of S1082 and came to the conclusion that, if the close binary and the second component are indeed dynamically connected, they must have formed through a single 3+3 encounter. Since such encounters are very rare considering the present density of M67, they conclude that the second component of S1082 is probably only spatially overlapping the close binary. If, on the other hand, one takes into consideration that M67 might have lost part of its mass due to evaporation and interaction with the disc and that its density might have been a factor of 2 higher in the past, then the probability for the encounter of two triple systems is much higher. S1082 was part of the study of Shetrone and Sandquist (2000), who found its abundances to be on average 0.2 dex lower than the cluster mean. The effective temperature derived in APOGEE DR14 is $T_{eff} = 7086.89$K, much higher than its photometric temperature $T_{eff} = 6317.77$K, but it is not a fast rotator ($vsini = 13.99$km/s).

S752 is considered an Am star with a possible flare detected by Sandquist and Shetrone (2003). It was found to be a long-period binary with 1003d and $e = 0.317 \pm 0.123$ by Latham and Milone (1996). Geller, Latham, and Mathieu (2015) list it as a binary member and a BSS. Its radial velocity is not consistent with the cluster mean (RV $= 25.68 \pm 0.14$ km/s) and lower than the value derived by Geller, Latham, and Mathieu (2015) (RV $= 31.29 \pm 0.35$ km/s). It is a fast rotator ($vsini = 77$km/s), and has $T_{eff} = 6630.7$K.

S792 and S984 are considered single members of M67 by Geller, Latham, and Mathieu (2015), although they comment that these two stars might possibly be binaries with a very long period that could not be detected in their survey. The authors argue that these two stars are not BSSs since their position on the CMD is too close to the TO, in a region that is expected to be populated by binaries consisting of MS stars. Indeed, Fig. 40 shows how they are included in the area between the single-star isochrone of M67 and the equal-mass binary isochrone, obtained shifting the former by -0.75 mag. Sandquist and Shetrone (2003) also do not find any variability in the light curve of these two stars. Their RVs are consistent with the cluster mean and their rotational velocities are low, $vsini =$

3.6 km/s and $vsini = 8$ km/s respectively, consistent with the rotation velocities measured for TO stars. Their temperatures ($T_{eff} = 5910.2$K and $T_{eff} = 5926.6$K) are also consistent with the TO, as are the abundances that we obtain in our analysis. Similar results were obtained by Shetrone and Sandquist (2000) for S984, who found its Li abundance to be consistent with that of the TO. They combined their derived RV with other data from Mathieu et al. (1986) and inferred a possible orbital period of ~ 1.5d for this star. They argue that if the system is indeed a close binary it should be tidally locked, but in that case its lithium abundance is too low. Since Geller, Latham, and Mathieu (2015) did not find any sign of such an orbital period, S984 can be either a binary with long period that they could not detect and composed by TO stars, as they suggest, or a BSS formed through collision. The same holds for S792, for which the measured C abundance is consistent with that of the TO and therefore hints at a main-sequence binary or a collisional BSS (unfortunately, Li measurements are not available for this star).

S1072 is listed as a spectroscopic binary member and a yellow giant of M67 by Geller, Latham, and Mathieu (2015). Sandquist and Shetrone (2003) did not find any variation in its light curve. Liu et al. (2008) analysed S1072 and found it to have log g lower than 4 dex. Its peculiar position above the SGB and its colour being much redder than the other BSSs in the sample could indicate that S1072 is a BSS in the process of evolving to a giant. Mathieu, Latham, and Griffin (1990) discovered that it is a binary with a 1495 d period and $e = 0.32 \pm 0.07$. van den Berg et al. (2002) found that S1072, as well as S1040 and S1237 (see below), presents an unexplained X-ray emission. Its radial velocity is consistent with the cluster distribution and it has a low rotational velocity ($vsini = 13.88$ km/s). The abundances that we derive are consistent with those of the TO, and also C is not depleted. The absence of carbon depletion would rule out a formation through mass accretion, although as Ferraro et al. (2006) point out, the C depletion expected in BSSs with a mass transfer history might be a transient one and, if indeed S1072 is already evolving along its SGB, the mass-transfer event would have happened in the non-recent past. If S1072 is a long-period and high-eccentricity binary composed of a BSS and a further companion, the original system must have been formed by at least 3 stars. We therefore suggest that S1072 might have formed through Kozai cycles in a hierarchical triple system (Perets and Fabrycky, 2009).

S1040, most likely an evolved BSS, lies bluewards of the M67 RGB. Mathieu, Latham, and Griffin (1990) found this object to be a binary with period 42.8d. Landsman et al. (1997) carried out a detailed study of this object based on spectro-scopic and photometric data and identified it as a binary system with a He white dwarf as a secondary companion. This indicates that part of the mass of the He WD was stripped from the star before it could reach the He burning phase and was accreted onto the primary companion. Thus, S1040 can be considered a typical example of an evolved BSS formed through mass accretion. Sandquist and Shetrone (2003) find a drop in luminosity corresponding to the passage of the white dwarf in front of the giant, but they comment that this variability cannot be caused by an eclipse and it is probably due to other effects due to the passage of the WD. We find that S1040 has abundances consistent with those of the RC stars. This also includes C, which is found to be depleted by ~ 0.25 dex with respect to the TO. This could be the C depletion expected from mass-transfer BSSs, although it

would mean that the signature has remained visible for a long time after the accretion event, given the evolved nature of S1040. Another possibility is that we are observing the effects of classical stellar evolution taking place after the formation of the BSS, and in particular the FDU.

S1237 is an evolved BSS situated between the SGB and the RC of M67, with a slightly bluer colour than the RGB (see Fig. 40) and $\sim$ 1 mag more luminous in Ks than S1040. This star has been studied in detail by Leiner et al. (2016) who, based on asteroseismological data from the Kepler K2 mission (Howell et al., 2014), found S1237 to be a binary system whose primary has $M = 2.97 \pm 0.24 M_\odot$ and $R = 9.27 \pm 0.19 R_\odot$. Considering that the TO mass of M67 is $\sim 1.3 M_\odot$, these results seem to indicate that S1237 had an uncommon evolution history and is most likely an evolved blue straggler star. Despite the fact that the spectrum of S1237, similarly to other MS stars of M67, shows a FUV excess, SED fitting indicates that the secondary companion is probably an upper-MS star or a BSS close to the TO of M67. As for the formation history of S1237, Leiner et al. (2016) suggest that a collision scenario as well as a Kozai-cycle-induced merger are possible mechanisms. Similarly to S1040, S1237 is depleted in C consistently with the RC. If for this object a mass-transfer scenario is excluded we can only explain the carbon depletion with stellar evolution.

5.5 SUMMARY

We analyse the chemical composition of three candidate BSSs as well as of two known evolved BSSs in the old open cluster M67 and we discuss the results together with information gathered from the literature. We find that un-evolved BSSs share the same surface abundances as TO stars. Based on their position in the CMD and on past studies on their variability, the BSS candidates S792 and S984 are either long-period binaries formed by two TO stars or single BSSs. If the second is true, the measured abundances, similar to those of the TO stars, hint at a collisional formation scenario.

S1072 also shares the same chemical composition as the dwarf stars of M67 and presents no C depletion. A possible explanation for the absence of a chemical signature indicating mass transfer can be found in Ferraro et al. (2006), where the authors suggest that the signature might be visible only for a short time, before the mixing in the stellar interior averages it out. On the other side, if S1072 indeed is a BSS in binary with an orbital period of 1495d and eccentricity of 0.32, it cannot have undergone mass transfer with the present companion. We suggest that S1072 could have formed through a Kozai-cycle-induced merger in a hierarchical triple system.

S1040 is known to be an evolved BSS with a He-core companion and thus it most likely formed through mass accretion. We measure a depletion in C but, if this is the signature of a mass-accretion event and such signatures are transient as suggested by Ferraro et al. (2006), it would be strange to observe it in a star that has already evolved so far along the RGB. On the other hand the C depletion is higher (although consistent within the errors) than the theoretical predictions of the FDU for stars in the mass range $1.4 - 2.9 M_\odot$.

A similar line of thought holds for S1237, except that for this object Leiner et al. (2016) have excluded a formation scenario through mass accretion. Thus, in this case the C depletion that we measure must be due to evolutionary effects rather than formation processes.

In summary, we find a depletion in carbon only for the evolved BSSs known in M67, S1040, and S1237, but we argue that this is most likely due to processes of stellar evolution rather than to a mass transfer history, although measurements of the nitrogen and lithium abundances of these stars would be necessary to confirm our picture. Our results confirm the findings of globular cluster studies, where very few carbon depleted BSSs are found. [C/H] estimations in the hotter BSSs would be necessary in order to obtain a complete picture and an estimate of the significance of mass transfer in the formation of BSSs.

Part IV

DYNAMICAL PROPERTIES OF OB ASSOCIATIONS

The following chapter is meant as a proof of concept regarding the future exploitation of the Gaia mission with respect to the formation and evolution of stellar clusters. We analyse two star forming complexes, the Cygnus and the Cepheus regions, with proper motions and parallaxes taken from the Tycho-Gaia astrometric solution (TGAS). While being limited by incompleteness and still large errors, these data can serve as test-bench for what will be possible to achieve with the future Gaia data releases.

THE KINEMATICS OF OB ASSOCIATIONS

The thin disc of the Milky Way hosts numerous star forming regions harbouring young stellar clusters of different masses, OB associations, and HII regions. Due to their very young age, these environments are laboratories for studies concerning the evolution of massive stars, the effects of feedback and stellar winds, as well as the processes involved in the formation of stellar clusters. In this chapter, meant as a methodological experiment, we present a preliminary study of the kinematic properties of star forming regions based on data from the Tycho-Gaia astrometric solution (TGAS) catalogue (Michalik, Lindegren, and Hobbs, 2015). This catalogue contains positions, parallaxes and proper motions for ~2 million stars and was obtained combining the first Gaia data release (hereafter Gaia DR1; Gaia Collaboration et al. 2016) with the Tycho-2 catalogue (Høg et al., 2000). We use the TGAS data to investigate two star forming regions located in the Cygnus and Cepheus constellations. In the case of Cygnus OB2/OB9 we cross-match a list of member stars from the literature with the TGAS catalogue and then calculate the peculiar velocities from their TGAS proper motions. For the Cepheus region, instead, we use the TGAS parallaxes to select stars at the distance of the star forming complex and then derive the peculiar velocities of the stars. The goal of the experiment is to test the potential of the future Gaia data releases in the study of the dynamical evolution of OB associations and young clusters present in these regions.

6.1 THE CYGNUS REGION

The Cygnus region is one of the biggest star-forming complexes of the Galaxy. It is composed of a large number of star forming regions, young stellar clusters and OB associations (see, e.g., Reipurth and Schneider, 2008, and references therein). One of the best-known components of the Cygnus region is Cyg OB2 (see Knödlseder 2003 for a review). Cyg OB2 has been studied extensively since the discovery of the first early type stars by Münch and Morgan (1953). The large number of massive stars populating this area of the sky ($\sim$ 100 O-type stars for a total mass of $4 - 10 \cdot 10^4 M_\odot$ Knödlseder 2000) led researchers to think that Cyg OB2 might be even the progenitor of a globular cluster (Comerón et al., 2002; Knödlseder, 2000; Reddish, Lawrence, and Pratt, 1966), although Hanson (2003) suggests that its mass might be overestimated due to the presence of foreground and background stars. Furthermore, Cyg OB2 lies in the centre of the so-called Cygnus super-bubble, a giant X-ray emitting bubble characterising the Cygnus region (Cash et al., 1980). The origin of the super-bubble is still debated between those who claim that it originated through supernovae explosions of very massive members of Cyg OB2 and those who think that the bubble is in reality a superposition of features distributed along the line of sight (see, e.g., Reipurth and Schneider, 2008, and references

therein). The stellar content of Cyg OB2 also includes a large number of peculiar stars, e.g. the evolved contact binary V729 Cyg, Luminous Blue Variables (LBV), and Wolf-Rayet stars (see, e.g., Comerón and Pasquali, 2012; Knödlseder, 2003, and references therein). Cyg OB2 is situated at a distance of 1.4 kpc from the Sun (Rygl et al., 2012) and suffers from high extinction ($A_v = 4 - 7$mag, Wright, Drew, and Mohr-Smith 2015). The most recent age determinations of Cyg OB2 suggest that the association has an age of $1 - 6$ Myr (Berlanas et al. 2017; Comerón and Pasquali 2012; Wright, Drew, and Mohr-Smith 2015) and that star formation has been active over a large time span.

In Comerón and Pasquali (2012) and Comerón et al. (2002, 2008) the authors present an extensive study of the Cygnus region both photometric and spectroscopic. They developed an empirical method for the differentiation of reddened OB stars earlier than B0-B2 from evolved red giants based solely on a combination of visual and infrared photometry and independent of reddening. The criterion reads:

$$Q_{BJK} = 0.196(B - J) - 0.981(J - K) - 0.098 > 0 \tag{22}$$

$$Q_{JHK} = 0.447(J - H) - 0.894(H - K) - 0.089 < 0 \tag{23}$$

Stars with $K_s > 9$ mag and $B > 16$ mag are not considered in order to reduce possible background contamination and obtain a sample bright enough to be spectroscopically confirmed with a 2m-class telescope.

Spectroscopic follow-ups have shown that this empirical photometric criterion has a success rate of about $70 - 80\%$ in the search for OB stars. The authors confirmed the nature of 60 OB stars and provided a list of ~ 60 further candidates. Furthermore, Comerón and Pasquali (2012) estimated masses and ages for the stars subject of their study and found an age gradient that possibly indicates star formation propagation from Cygnus OB9 (situated to the north-west with respect to Cyg OB2) to Cyg OB2, being Cyg OB9 on average older than the bulk of Cyg OB2.

More recently, Berlanas et al. (2017), extended the sample of known Cyg OB2 members with stars from the surroundings of the OB association and spectroscopically classifying candidate OB stars from Comerón and Pasquali (2012). They validate 42 further members of the association. They also confirm the age trend in Galactic longitude found by Comerón and Pasquali (2012).

6.1.1 *Age spread, parallaxes, and peculiar velocities in Cyg OB2 and OB9*

Given the age spread found by Berlanas et al. (2017) and Comerón and Pasquali (2012), an interesting question about Cyg OB2 and OB9 is whether the different age groups that are found among their OB stars are linked or rather represent different star-forming regions, whose projected spatial distributions possibly overlap. We address this issue by analysing their kinematics, in terms of their peculiar velocities, and parallaxes, i.e. the apparent displacement of an object in the sky as a consequence of the movement of the Earth on its orbit. The parallax (pxl) is correlated to the distance (d) of the observer from the object as $pxl[arcsec] = 1/d[pc]$ for small angles. Specifically, we have cross-matched the list of OB stars from Comerón
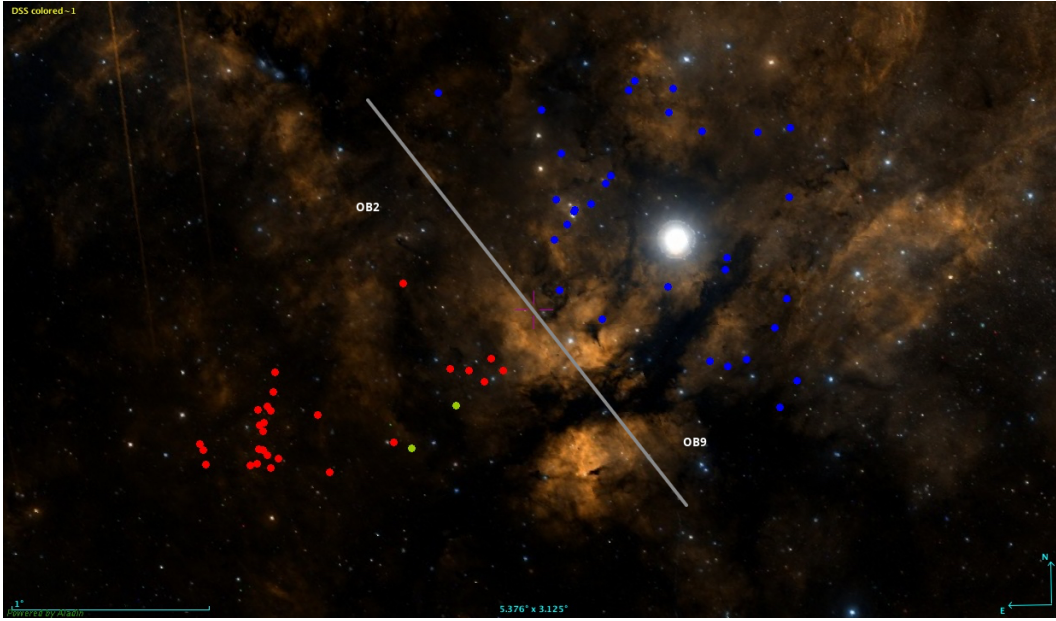
Figure 48: DSS sky view of the Cygnus region created with the help of "Aladin sky atlas" (Boch and Fernique, 2014; Bonnarel et al., 2000). The OB stars belonging to Cyg OB2 from the cross-match between Comerón and Pasquali (2012) and TGAS are plotted as red dots, the Cyg OB9 stars as blue dots. The two stars from Berlanas et al. (2017), are plotted as green dots.

and Pasquali (2012) and from Berlanas et al. (2017), with the TGAS catalogue. We found 58 stars belonging to Cygnus OB2 and Cygnus OB9 from the sample of Comerón and Pasquali (2012), as well as 2 stars from Berlanas et al. (2017), located in the 1° radius area drawn by Comerón and Pasquali (2012) around Cygnus OB2. We intentionally excluded field stars listed in both works from this analysis. We could not find any match in TGAS for stars fainter than B = 13.6 mag. Our sample is shown in Fig. 48, the stars in Cyg OB2 are plotted as red dots, those in Cyg OB9 as blue dots and the 2 stars from Berlanas et al. (2017) as green dots. The grey line indicates the approximate limit between Cyg OB2 and Cyg OB9. The coordinates of the objects included in the present analysis can be found in Table 23, 25, and 26 as well as their observed proper motions in RA and Dec direction from TGAS, and the parallaxes from TGAS.

Fig. 49 shows the peculiar velocities of our sample as arrows in the plane of the sky as defined by the stars' Galactic coordinates, derived correcting the observed proper motions for the reflected solar motion and for the Galactic rotation as described in Mdzinarishvili and Chargeishvili (2005): we first transform the observed proper motions (pm_α, pm_δ) from equatorial coordinates into Galactic coordinates:

$$pm_l = pm_\alpha \cos\psi + pm_\delta \sin\psi \tag{24}$$

$$pm_b = -pm_\alpha \sin\psi + pm_\delta \cos\psi \tag{25}$$

where

$$\cos\psi = \frac{\sin\delta_G \cos\delta - \cos\delta_G \sin\delta \cos(\alpha - \alpha_G)}{\cos b} \tag{26}$$

$$\sin\psi = \frac{\sin(\alpha - \alpha_G)\cos\delta_G}{\cos b}, \tag{27}$$

with the J2000 coordinates of the Galactic North Pole being $\alpha_G = 192.85951 \, \text{deg}$ and $\delta_G = 27.12834 \, \text{deg}$, respectively (Reid&Brunthaler 2004).

The observed tangential velocities of the stars can be calculated as

$$v_{lt} = K r pm_l \tag{28}$$
$$v_{bt} = K r pm_b \tag{29}$$

where $K = 4.740$ is a constant deriving from the change of units and $r = 1.4 \, \text{kpc}$ the distance of Cygnus from the Sun (Rygl et al., 2012). Considering that the observed tangential velocities are the sum of the peculiar velocities of the stars, the reflected Solar motion and the Galactic rotation, we get:

$$v_{ltpec} = v_{lt} - v_{lt\odot} - v_{ltG} \tag{30}$$
$$v_{btpec} = v_{bt} - v_{bt\odot} - v_{btG}. \tag{31}$$

We can calculate the reflected Solar motion using

$$v_{lt\odot} = U_\odot \sin l - V_\odot \cos l \tag{32}$$
$$v_{bt\odot} = U_\odot \cos l \sin b + V_\odot \sin l \sin b - W_\odot \cos b \tag{33}$$

where $U_\odot, V_\odot, W_\odot$ are the Galactic space velocities of the Sun, $U_\odot = 8.5 \pm 0.29 \, \text{km/s}$, $V_\odot = 13.38 \pm 0.43 \, \text{km/s}$, and $W_\odot = 6.49 \pm 0.26 \, \text{km/s}$, respectively (Coşkunoğlu et al., 2011).

In order to compute the velocity component representing the Galactic rotation, we first need to calculate the distance of Cygnus from the Galactic centre:

$$R^2 = R_0^2 + r^2 \cos b^2 - 2 r R_0 \cos b \cos l \tag{34}$$

We then have

$$v_{ltG} = R_0 (\omega - \omega_0) \cos l - r \omega \cos b \tag{35}$$
$$v_{btG} = -R_0 (\omega - \omega_0) \sin l \sin b \tag{36}$$

with $\omega_0 = V_0 / R_0$, where $V_0 = 220 \, \text{km/s}$ is the velocity of the Galactic rotation and $R_0 = 8.5 \, \text{kpc}$ the Galactocentric distance of the Sun (Kerr and Lynden-Bell, 1986), and $\omega = V_0 / R$.

The colour-coding in Fig. 49 represents the ages of the stars derived in Berlanas et al. (2017), when using non-rotating Geneva stellar models: yellow for stars older than 10 Myr, purple for stars between 5 and 10 Myr, and finally brown for objects that are younger than 5 Myr. The 2 new Cygnus OB2 stars from Berlanas et al. (2017), are displayed in red for clarity, but they belong to the 5 - 10 Myr age bin. A few high-velocity stars can be seen in Fig. 49. These could either be field stars contaminating the sample or runaway stars that are being expelled from the association. In particular, the star with the highest peculiar velocity has $v_{pec} \sim 54$ km/s. Comerón and Pasquali (2007) confirmed the existence of a runaway star in Cyg OB2 with $v_{pec} = 39.8 \pm 9.8$ km/s, which is consistent within two times the error with our findings. On average, both star forming regions are moving in approximately the same direction, with median $v_{ltpec} = -15.35 \pm 3.00, v_{btpec} = 4.03 \pm 2.83 \, \text{km/s}$ for OB9 and $v_{ltpec} = -5.95 \pm 2.53, v_{btpec} = 1.15 \pm 2.95 \, \text{km/s}$ for
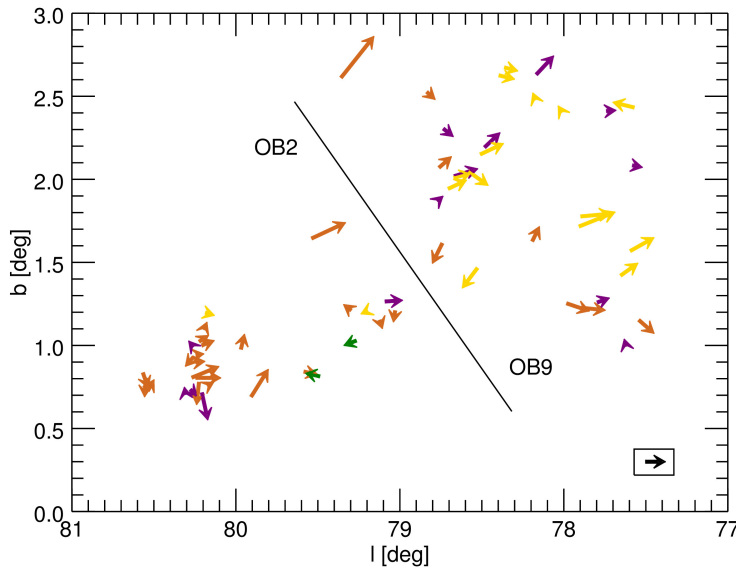
Figure 49: Galactic coordinates of the Cyg OB2 and OB9 stars selected for our kinematic study. The arrows represent the proper motions of the stars from TGAS and trasformed into the galactic coordinate system. The colours represent different age bins: red for stars older than 10 Myr, green for ages between 5 and 10 Myr and blue for stars younger than 5 Myr. The black arrows represent the mean proper motion of the stars in OB2 and OB9.

OB2. This seems to indicate that the older Cyg OB9 and the younger Cyg OB2 have similar kinematic properties and that there are no clear signs of dissolution in the associations, but the scatter in the TGAS data is still too high to draw significant conclusions.

In Fig. 50 the parallaxes of the stars are plotted as a function of their Galactic latitude. Stars belonging to Cygnus OB9 are shown as empty circles, while stars in Cygnus OB2 are plotted as filled circles. The presence of stars with negative parallaxes can be explained by their error bars: these stars have most probably very small parallaxes and the solution of the astrometric fit happens to fall below zero. Although a negative parallax is clearly unphysical, these points are consistent with a positive parallax within one sigma. Nevertheless, we exclude these objects in computing the bulk parallax of Cygnus OB2 and OB9. The mean parallax of the Cygnus OB9 stars is p = 0.65 ± 0.25 mas, corresponding to an average distance of 1538^{+962}_{-427} pc; for Cygnus OB2 we find p = 0.63 ± 0.41 mas and consequently a mean dstance of 1587^{+2958}_{-625} pc. The mean distances are consistent with each other and with the distance modulus of 10.8 mag for Cyg OB2/OB9 adopted in the literature (see, e.g, Comerón and Pasquali, 2012; Hanson, 2003; Rygl et al., 2012), although the errors are of the same order of magnitude than the distance. Also in the case of the parallaxes, the TGAS data are still too imprecise to obtain conclusive results, but the future Gaia data releases ought to confirm if the two OB associations lie at the same distance, as suggested by their CMDs, or if their vicinity is only a spatial projection.
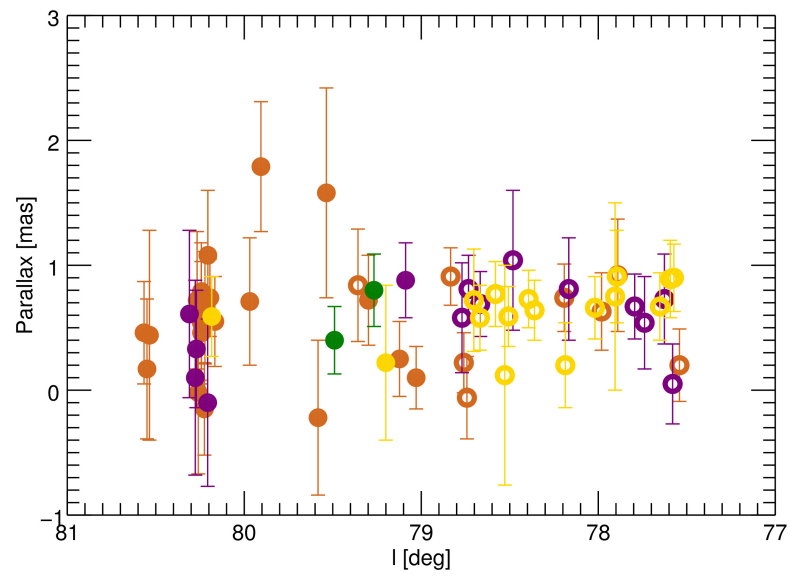
Figure 50: The TGAS parallax of the stars selected for the analysis as a fuction of their Galactic latitude. Open circles represent Cyg OB9, filled circles Cyg OB2 stars.

Table 23: List of Cyg OB2 stars from Comerón and Pasquali (2012) analysed in this study.

RA (J2000) [deg]	Dec (J2000) [deg]	l [deg]	b [deg]	PM_RA [mas/yr]	PM_Dec [mas/yr]	e_PM_RA [mas/yr]	e_PM_Dec [mas/yr]	Parallax [mas]	e_Parallax [mas]
307.751	+40.83	79.583	0.842	-2.781	-6.132	3.569	1.117	-0.22	0.62
308.325	+41.309	80.225	0.777	+1.034	-5.957	1.497	1.109	-0.15	0.37
308.378	+41.256	80.207	0.713	+0.877	-7.417	2.425	2.005	-0.1	0.67
308.189	+41.427	80.260	0.929	-0.106	-4.064	1.620	1.570	-0.02	0.65
306.932	+40.595	79.029	1.207	-0.39	-5.020	1.054	0.672	+0.1	0.25
308.413	+41.324	80.277	0.733	-1.743	-5.630	2.598	2.468	+0.1	0.78
308.556	+41.584	80.550	0.802	+0.455	-5.760	2.119	1.364	+0.17	0.56
307.064	+40.735	79.201	1.207	-1.038	-3.782	1.335	1.143	+0.22	0.62
307.064	+40.639	79.123	1.151	-1.145	-5.301	1.179	0.777	+0.25	0.3
308.116	+41.481	80.271	1.006	-2.084	-3.582	1.945	1.276	+0.33	0.47
308.623	+41.529	80.536	0.729	-3.807	-3.952	3.660	2.831	+0.44	0.84
308.535	+41.616	80.566	0.834	-0.578	-6.210	1.486	1.250	+0.46	0.41
308.161	+41.421	80.242	0.942	-2.743	-5.025	1.703	1.139	+0.46	0.38
308.208	+41.396	80.243	0.899	-2.825	-5.209	1.958	1.292	+0.54	0.49
308.295	+41.252	80.166	0.761	-2.722	-4.567	0.117	0.103	+0.55	0.36
307.842	+41.525	80.184	1.197	-2.379	-5.504	1.312	1.385	+0.59	0.32
308.449	+41.345	80.310	0.723	-2.36	-3.769	2.137	1.644	+0.61	0.67
308.058	+41.453	80.222	1.024	-3.477	-4.777	2.047	1.051	+0.66	0.45
307.906	+41.222	79.969	0.979	-4.052	-3.327	2.208	1.558	+0.71	0.51
307.133	+40.817	79.298	1.213	-1.939	-2.863	0.583	0.529	+0.72	0.36

Table 24: Table 23 continued.

RA (J2000) [deg]	Dec (J2000) [deg]	l [deg]	b [deg]	PM_RA [mas/yr]	PM_Dec [mas/yr]	e_PM_RA [mas/yr]	e_PM_Dec [mas/yr]	Parallax [mas]	e_Parallax [mas]
308.325	+41.36	80.267	0.807	-5.76	-6.531	2.129	1.682	+0.72	0.55
307.957	+41.474	80.194	1.097	-3.039	-3.946	1.196	0.656	+0.74	0.31
308.309	+41.339	80.243	0.805	-4.196	-7.285	1.571	1.181	+0.79	0.39
306.916	+40.677	79.088	1.265	-3.58	-6.303	1.132	0.727	+0.88	0.3
308.069	+41.427	80.206	1.001	-3.588	-5.277	1.820	1.065	+1.08	0.52
306.851	+41.263	79.536	1.645	-6.905	-7.077	4.716	2.075	+1.58	0.84
308.163	+41.002	79.906	0.693	-6.881	-3.845	1.921	1.469	+1.79	0.52

Table 25: List of Cyg OB2 stars from Berlanas et al. (2017) analysed in this work.

RA (J2000) [deg]	Dec (J2000) [deg]	l [deg]	b [deg]	PM_RA [mas/yr]	PM_Dec [mas/yr]	e_PM_RA [mas/yr]	e_PM_Dec [mas/yr]	Parallax [mas]	e_Parallax [mas]
307.306	+40.684	79.267	1.028	-.0235	-3.177	0.958	1.431	0.8	0.29
307.708	+40.738	79.490	0.814	-1.047	-2.118	1.046	0.703	0.4	0.27

Table 26: List of Cyg OB9 stars from Comerón and Pasquali (2012) analysed in this work.

RA (J2000) [deg]	Dec (J2000) [deg]	l [deg]	b [deg]	PM_RA [mas/yr]	PM_Dec [mas/yr]	e_PM_RA [mas/yr]	e_PM_Dec [mas/yr]	Parallax [mas]	e_Parallax [mas]
306.277	+40.597	78.742	1.613	1.480	-4.802	1.791	0.712	-0.060	0.33
304.902	+39.912	77.580	2.084	-2.417	-5.687	1.194	0.918	0.050	0.32
306.275	+40.337	78.528	1.465	1.950	-4.160	4.822	1.054	0.120	0.88
304.886	+40.654	78.186	2.513	-1.923	-4.177	1.512	0.979	0.200	0.34
305.869	+39.35	77.541	1.152	-1.526	-7.376	1.109	0.910	0.200	0.29
305.795	+40.875	78.760	2.072	-4.282	-4.860	0.061	0.065	0.220	0.24
304.666	+40.227	77.738	2.411	-2.711	-5.412	0.032	0.037	0.540	0.37
305.794	+40.765	78.668	2.010	-3.915	-5.992	1.079	0.708	0.580	0.26
306.021	+40.768	78.770	1.870	-2.912	-4.528	1.619	1.356	0.580	0.44
305.519	+40.714	78.508	2.151	-5.228	-6.247	1.176	1.017	0.590	0.24
306.090	+39.768	77.981	1.253	-2.913	-7.818	1.104	1.148	0.630	0.31
304.840	+40.888	78.360	2.673	-2.526	-6.232	0.061	0.070	0.640	0.24
304.866	+40.462	78.019	2.417	-2.129	-3.659	1.293	0.636	0.660	0.25
305.664	+39.595	77.652	1.422	-4.897	-5.387	0.985	0.748	0.670	0.27
305.943	+39.619	77.794	1.260	-3.435	-5.402	1.036	1.052	0.670	0.26
305.782	+40.769	78.667	2.020	-4.848	-6.580	1.158	0.740	0.690	0.26
305.891	+40.756	78.703	1.944	-4.522	-5.801	1.747	1.141	0.720	0.41
304.917	+40.889	78.394	2.626	-2.689	-6.549	0.880	0.665	0.730	0.23
306.074	+39.342	77.626	1.018	-2.172	-3.942	1.472	1.313	0.730	0.36
305.845	+40.156	78.192	1.629	-4.287	-3.924	1.006	0.881	0.740	0.27

Table 27: Table 26 continued.

RA (J2000) [deg]	Dec (J2000) [deg]	l [deg]	b [deg]	PM_RA [mas/yr]	PM_Dec [mas/yr]	e_PM_RA [mas/yr]	e_PM_Dec [mas/yr]	Parallax [mas]	e_Parallax [mas]
305.537	+39.971	77.905	1.717	-6.840	-7.591	4.771	1.495	0.750	0.75
305.687	+40.715	78.581	2.048	-1.810	-8.005	0.043	0.049	0.770	0.26
305.523	+40.986	78.733	2.304	-1.728	-6.160	0.045	0.050	0.810	0.27
304.741	+40.705	78.166	2.633	-5.665	-4.900	1.026	0.860	0.810	0.41
305.657	+41.675	79.358	2.614	-10.015	-4.792	1.885	1.365	0.840	0.45
305.463	+39.631	77.593	1.570	-5.606	-6.138	1.357	0.743	0.890	0.31
304.521	+40.102	77.573	2.433	-.674	-1.191	0.776	0.683	0.900	0.27
305.358	+41.194	78.834	2.525	-1.635	-5.914	0.794	0.609	0.910	0.23
305.465	+39.997	77.895	1.777	-4.840	-7.878	1.551	1.026	0.910	0.37
306.049	+39.678	77.890	1.227	-3.638	-7.483	1.136	1.061	0.920	0.45
305.453	+40.717	78.482	2.194	-5.002	-4.948	3.313	0.944	1.040	0.56

6.2 THE CEPHEUS REGION

We applied a similar study to the star forming region situated in the Cepheus constellation, which hosts several young stellar clusters and OB associations (see Kun, Kiss, and Balog, 2008, and references therein for a review). In particular, we concentrated on the OB associations Cep OB2, OB3, and OB4 (see Fig. 51).

Cep OB2 is an extended area ($96 < l < 108$ deg and $-1 < b < 12$ deg, according to de Zeeuw et al. 1999) on the sky at a distance of ~ 800 pc (Kun, Kiss, and Balog, 2008). Cep OB2 is usually divided into two sub-regions, as suggested by Simonson and van Someren Greve (1976). Cep OB2a is characterised by the so-called Cepheus bubble, an expanding ring-shaped infrared-emitting feature, possibly formed via a supernova explosion (Kun, Balazs, and Toth, 1987). Studies of its CO and HI content (Ábrahám, Balázs, and Kun, 2000; Patel et al., 1998) concluded that the Cepheus bubble is a HI expanding shell of ~ 120 pc in diameter associated with molecular clouds and HII regions whose size and expansion velocity are consistent with the model of a supernova explosion occurred ~ 1.7 yr ago. The authors conclude that the bubble probably originated from the supernova explosion of a massive member of the already existing association, which triggered further star formation in the compressed surrounding gas. The outer ring of the Cepheus bubble is in fact characterised by a large number of HII regions and infrared sources (Balazs and Kun, 1989). In the centre of the bubble is situated the open cluster NGC 7160, with an age of ~ 10Myr (see, e.g., Sicilia-Aguilar et al., 2005).

The second sub-region, Cep OB2b, is situated to the south-west of the Cepheus bubble and hosts the young star cluster Trumpler 37 (~ 4 Myr, Sicilia-Aguilar et al. 2005) and the HII region IC 1396 with the well-known Elephant Trunk nebula and numerous star forming globules. Also IC1396 is characterised by an expanding molecular ring (Patel et al., 1998), driven by the wind of the O-star HD206267, although of much smaller size (~ 12 pc) compared to the Cepheus bubble. Tr37, being one of the youngest known open cluster, has been extensively studied in the past together with the neighbouring cluster NGC 7160 under several aspects, from its pre-main sequence to the surrounding star forming activity, X-ray emission, and extinction (see, e.g., Clayton and Fitzpatrick, 1987; Errmann et al., 2013; Getman et al., 2007, 2012; Marschall, Karshner, and Comins, 1990; Marschall and van Altena, 1987; Mercer et al., 2009; Morbidelli et al., 1997; Nakano et al., 2012; Saurin, Bica, and Bonatto, 2012; Schulz, Berghoefer, and Zinnecker, 1997; Sicilia-Aguilar, Henning, and Hartmann, 2010; Sicilia-Aguilar et al., 2004, 2005, 2006, 2011, 2014, 2015)

Cep OB3 is situated to the east of Cep OB2, at $108 < l < 113$ deg and $1 < b < 7$ deg (de Zeeuw et al., 1999), at a distance of 725 pc (Blaauw, Hiltner, and Johnson, 1959) and is also commonly subdivided into two sub-regions Cep OB3a and Cep OB3b (Blaauw, 1964) of different ages, 7.5 and 5.5 Myr respectively (Jordi, Trullols, and Galadi-Enriquez, 1996). The younger group Cep OB3b is associated with the HII region S155 and its most luminous members maintain the ionisation state of the surrounding region. Sargent (1977, 1979) found and studied a molecular cloud complex in the region of Cep OB3 presenting numerous sub-clumps. Cep OB3 and its associated molecular cloud have been subject to a large number of studies, but the details of these investigations go beyond the scope of the present work.
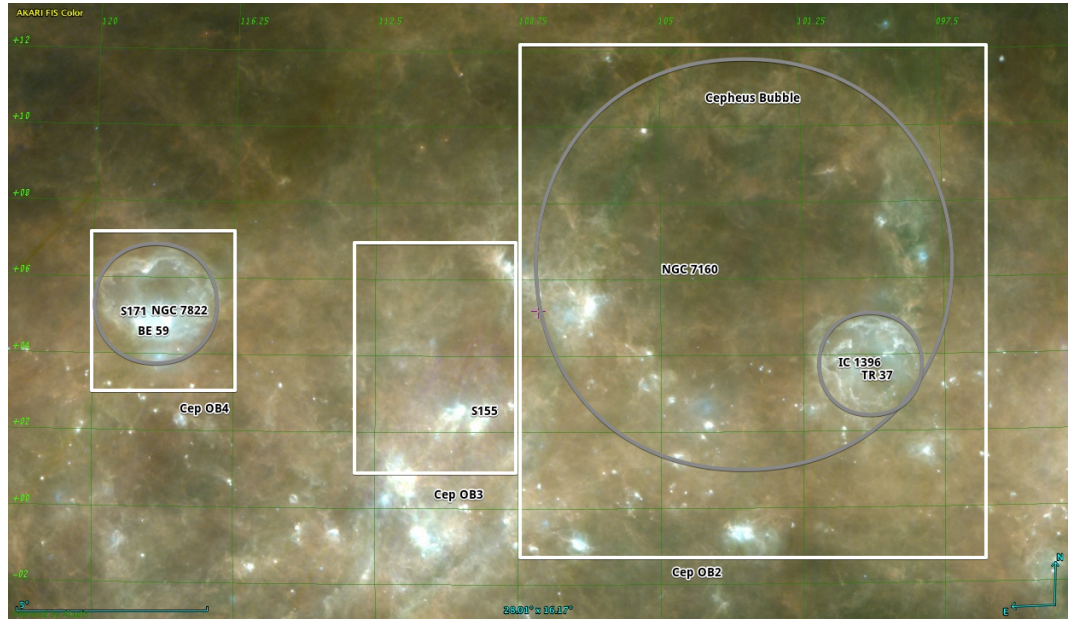
Figure 51: An AKARI view of the Cepheus region created with the help of "Aladin sky atlas" (Boch and Fernique, 2014; Bonnarel et al., 2000). The areas representing the three OB associations discussed in this work are shown as white rectangles following the coordinates from de Zeeuw et al. (1999). The approximate positions of the expanding bubbles are shown as grey circles as well as the approximate position of the most notable clusters and HII regions are marked with their names.

We refer to Kun, Kiss, and Balog (2008) and the references therein for a detailed review.

Cep OB4 lies to the east of Cep OB3 ($116 < l < 120$ deg and $3 < b < 7$ deg, de Zeeuw et al. 1999) It is characterised by a large cloud and the presence of the open cluster Berkeley 59 as well as the HII regions S171 and NGC 7822 (Lozinskaya, Sitnik, and Toropova, 1987). Lozinskaya, Sitnik, and Toropova (1987) also found two expanding shells associated with OB4, a smaller one with radius 0.7 deg, probably driven by the luminous stars in its interior, and a larger one with radius 1.5 deg possibly resulting from a supernova explosion. Olano, Meschin, and Niemela (2006) also suggests the presence of an expanding shell with a radius of ~ 100 pc situated at $l = 122$ deg and $b = +10$ deg that would be connected to Cep OB4. The estimated age for the Cep OB4 region is of 0.6–6 Myr (MacConnell, 1968), its distance from Hipparcos parallaxes 800–1000 pc (de Zeeuw et al., 1999). It furthermore presents high extinction ($A_V = 3$ mag, MacConnell, 1968). For further details of the star-forming processes in Cep OB4 we refer to Kun, Kiss, and Balog (2008) and references therein.

6.2.1 *Parallaxes and peculiar velocities in Cep OB2,OB3, and OB4*

We selected all stars observed with TGAS in the area of Cep OB2 , Cep OB3 and Cep OB4 using the coordinates given in de Zeeuw et al. (1999) (see Fig. 51).

As a first step, we selected all stars with a parallax error smaller than 0.25 mas in order to clean our sample as much as possible from spurious contamination. The

still very large errors of the TGAS parallaxes have as a consequence the exclusion of the vast majority of the stars (see Fig. 52).

As a further step, we used the TGAS parallaxes to limit the analysis to stars that realistically lie at the distance of the Cepheus region. From the parallax distribution (see Fig. 53) we select stars in three bins with width 0.25 mas representing the centre of the distribution, from 0.75 to 1.5 mas, which correspond to the distance range known for the Cepheus region from the literature. From Fig. 52 it appears that the majority of stars in Cep OB4 lie in the parallax bin 0.75–1.00 mas, corresponding to a distance of 1000–1333 pc, larger than the one known from the literature. For Cep OB3 the bulk of the stars is enclosed in the central bin, i.e. at a distance of 800–1000 pc, also larger than the 725 pc predicted from the literature. For Cep OB2 we find that the two more distant bins contain almost the same amount of stars. This would translate in a large spread in distances for the members of this associations. We will discuss this in more detail looking at the spatial distribution of the stars.

Figure 54 shows the selected sample for each parallax bin, starting from the closest (blue) and proceeding with the intermediate (green) and most distant bin (red), on a sky map of the infrared survey AKARI (Murakami et al., 2007), highlighting dust emission and thus embedded star forming regions (compare with Fig. 51 for the position of the different components of the associations). From these images it is confirmed that the central region of Cep OB4 lies at a distance of 1000-1333 pc. Although stars in all bins are present, the star-forming region S155 appears to be located between 800 and 1000 pc from the Sun. Within Cep OB2, the central region of the young cluster Trumpler 37 and the HII region IC1396, together with the Elephant trunk region appear closer (667–800 pc) than the ring around this region (1000–1333 pc). The ring around the Cepheus bubble is most populated in the 800–1000 pc bin, while the inner part of the bubble is similarly populated in all three bins.

We now overplot the galactic coordinates of our sample with the corresponding peculiar velocities calculated as described in Section 6.1 for the three different parallax bins (Fig. 55 increasing the distance from top to bottom, the approximate positions of the expanding bubbles are shown as grey circles). The overall motion of the three OB associations shows a relatively large scatter, although it is possible to distinguish some sub-structures. The stars in the region of Tr 37 and IC 1396 including all three distance bins, e.g., have a mean velocity $v_{\mathrm{ltpec}} = -10.6818 \pm 3.53$, $v_{\mathrm{btpec}} = 1.10 \pm 3.84 \mathrm{km/s}$. The stars in the most distant bin of Cep OB4 and inside the expanding bubble have $v_{\mathrm{ltpec}} = -6.38 \pm 1.57$, $v_{\mathrm{btpec}} = 3.12 \pm 3.08 \mathrm{km/s}$. In all distance bins we can see several stars with a larger peculiar velocity compared with the bulk of the stars. These could be explained by foreground and background contamination or as runaway stars expelled from the associations because of dynamical encounters. As explained in the beginning of this section, these regions contain different clusters and star forming regions of different age and since the number of objects that we retrieve at the end of our analysis is quite small, it is not possible at the present time to compare their position on a CMD with theoretical isochrones or to asses , e.g., if there is in these regions any sign of mass segregation.

As we have shown, this kind of study is affected by the still high errors associated with Gaia DR1 parallaxes and proper motions and small number statistics.

Nevertheless, with this experiment we want to highlight the potential of the future Gaia data releases, that will probably allow a selection of the members of a given OB association or young open cluster based alone on the parallax, thus avoiding the use of the proper motion as a selection criterion and allowing a detailed study of possible inhomogeneities in the kinematics of these regions and their future evolution.
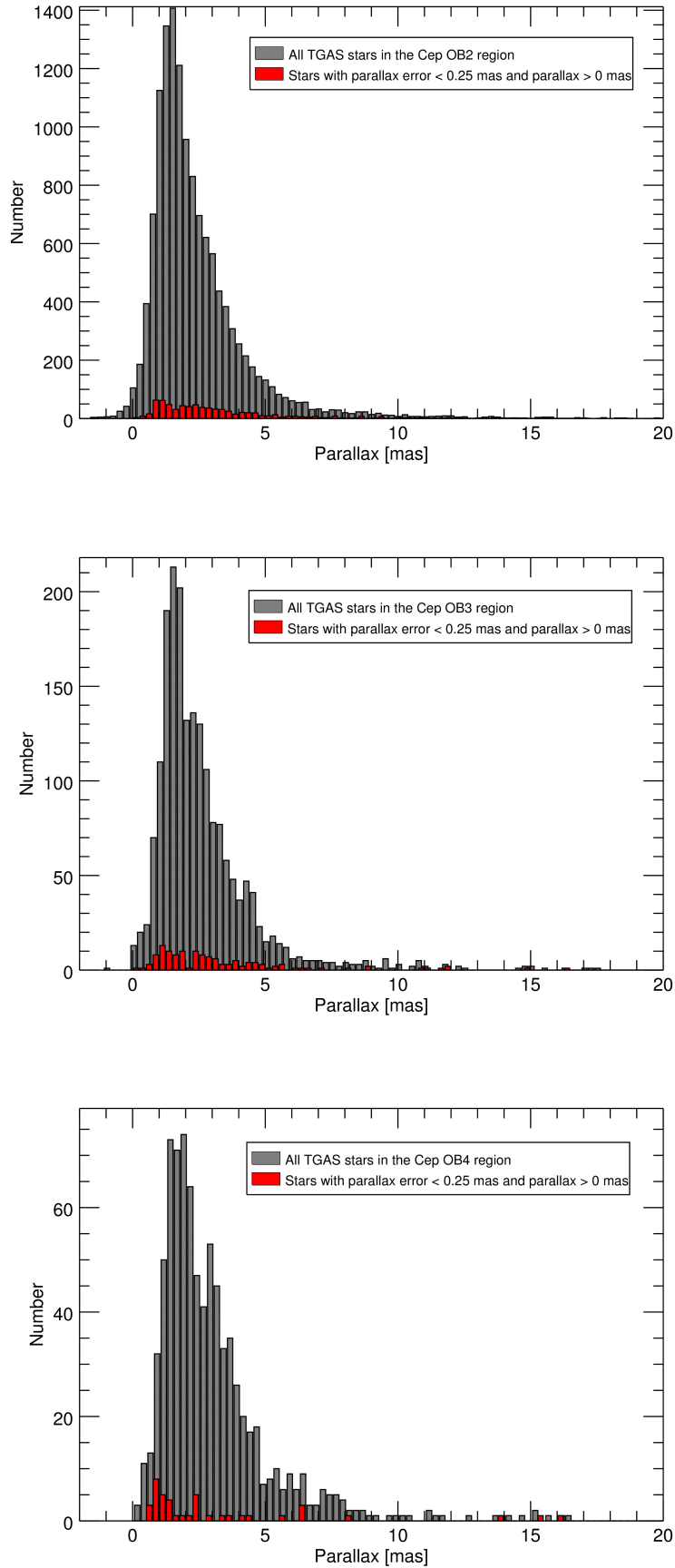
Figure 52: Histogram of the TGAS parallaxes measured for all stars in the Cep OB2, Cep OB3 and Cep OB4 regions (grey columns). We plot in red the stars with a parallax error smaller than 0.25 mas.
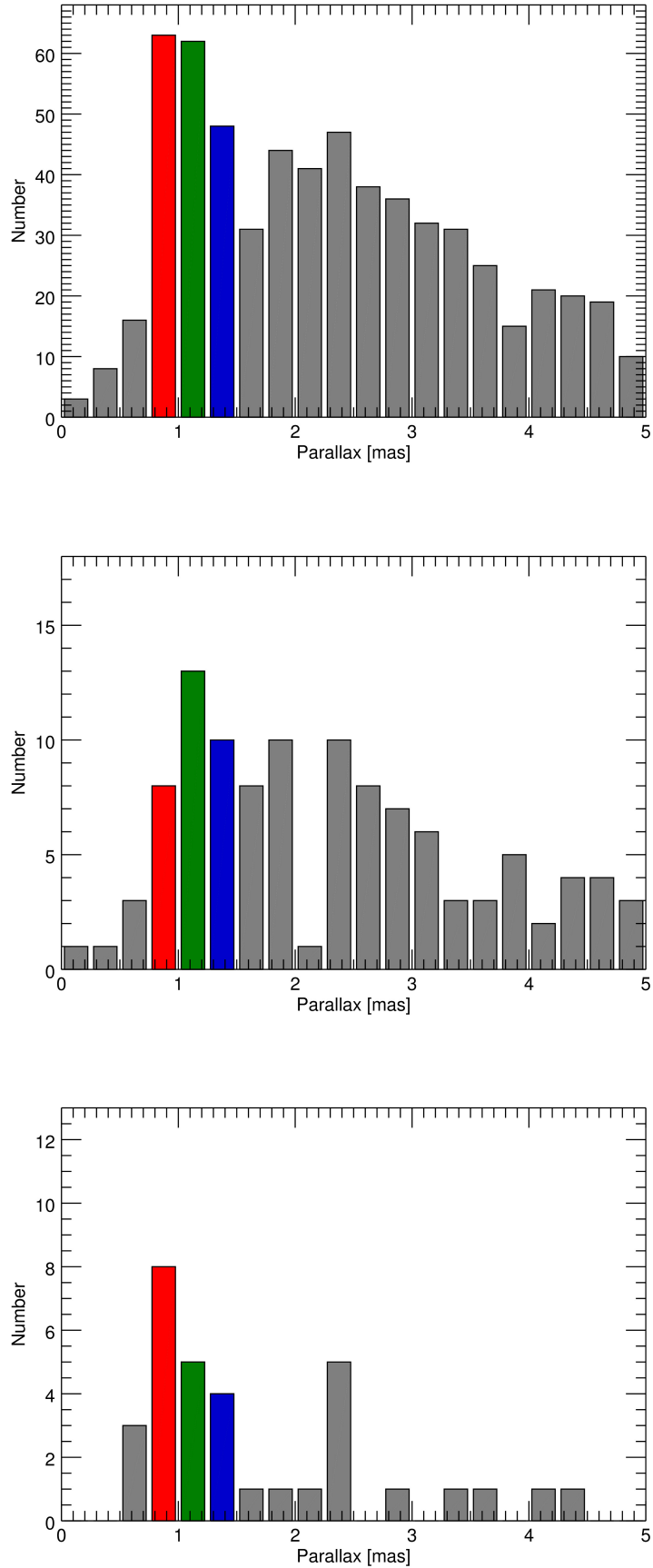
Figure 53: Histogram of the parallaxes of the stars in Cep OB2, Cep OB3, and Cep OB4 with parallax error smaller than 0.25 mas. We select the stars in three bin corresponding to a distance of 667–800 pc (blue), 800–1000 pc (green), and 1000–1333 pc (red).
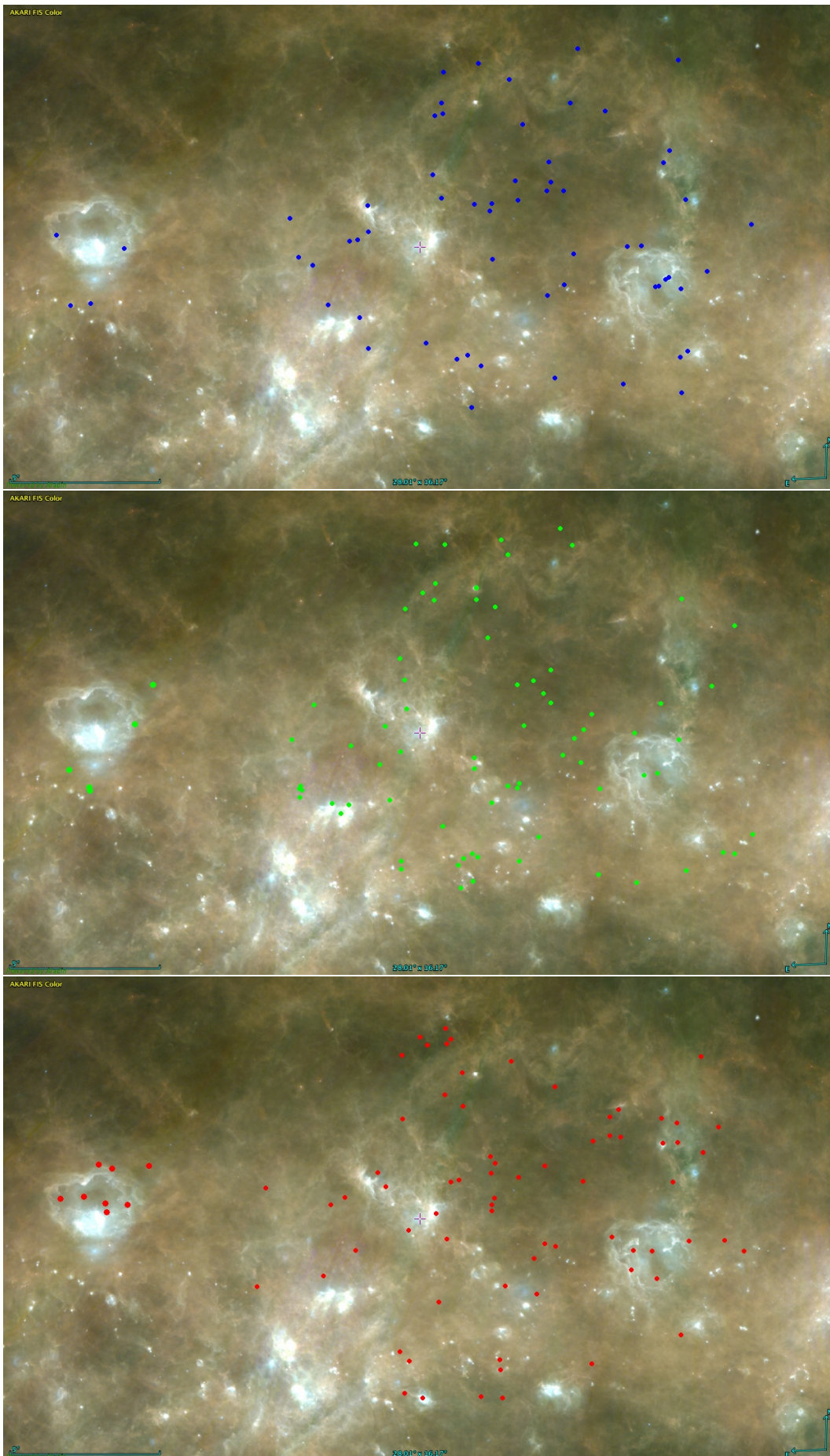
Figure 54: AKARI sky map overplotted with the stars selected in the three different distance bins: 667–800 pc (blue), 800–1000 pc (green), and 1000–1333 pc (red). Created with the help of "Aladin sky atlas" (Boch and Fernique, 2014; Bonnarel et al., 2000)
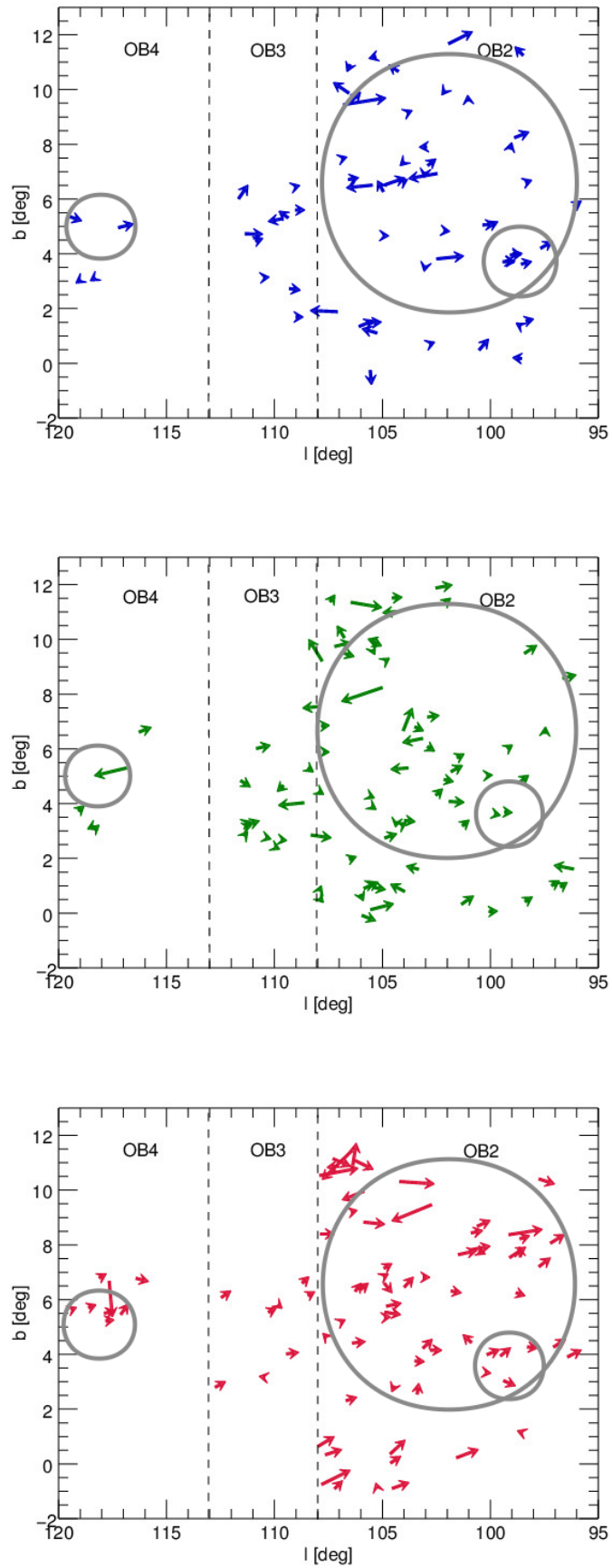
Figure 55: Peculiar velocity vectors of the stars selected in the three different distance bins plotted at the location of their Galactic coordinates. The grey circles indicate the approximate position of the expanding bubbles in the different associations.

Table 28: List of Cep OB2 stars in the three distance bins discussed in this work.

RA (J2000) [deg]	Dec (J2000) [deg]	l [deg]	b [deg]	PM_RA [mas/yr]	PM_Dec [mas/yr]	e_PM_RA [mas/yr]	e_PM_Dec [mas/yr]	Parallax [mas]	e_Parallax [mas]
332.001	+63.736	105.997	+6.375	-2.598	-1.692	0.071	0.065	0.753	0.222
337.613	+56.855	104.537	-0.894	-4.495	-3.355	0.676	0.563	0.758	0.238
331.116	+62.408	104.883	+5.541	-3.008	-4.845	0.065	0.06	0.762	0.228
320.793	+58.983	98.799	+6.25	-1.422	-4.538	0.096	0.106	0.766	0.227
329.034	+63.704	104.923	+7.143	-2.505	-2.174	0.08	0.074	0.775	0.231
337.203	+63.272	107.680	+4.705	+0.021	-1.291	0.852	0.608	0.788	0.245
319.814	+61.962	100.599	+8.683	-3.616	-3.455	0.086	0.077	0.795	0.226
329.765	+63.263	104.908	+6.595	-0.286	-4.957	0.074	0.067	0.801	0.237
330.700	+62.54	104.807	+5.761	-3.618	-3.601	0.128	0.108	0.805	0.217
337.997	+60.701	106.674	+2.309	-2.827	-2.702	0.096	0.093	0.807	0.237
336.543	+57.982	104.631	+0.368	-5.118	-1.45	1.02	0.526	0.817	0.244
316.115	+59.072	97.205	+8.066	-4.295	-3.649	0.139	0.136	0.833	0.223
322.670	+61.837	101.474	+7.646	-4.257	-4.553	0.071	0.063	0.837	0.226
341.957	+58.147	107.204	-0.899	-2.66	-1.5	0.136	0.113	0.858	0.236
326.546	+57.793	100.222	+3.335	-1.288	-3.514	0.21	0.193	0.86	0.225
342.855	+58.553	107.808	-0.749	-7.928	-2.287	1.179	0.563	0.86	0.243
338.700	+57.25	105.247	-0.854	-0.443	-1.364	0.11	0.102	0.867	0.238
326.782	+55.056	98.561	+1.156	+0.138	-1.83	0.134	0.124	0.874	0.222
322.887	+65.618	104.191	+10.313	-6.059	-8.102	0.17	0.163	0.878	0.227
328.361	+62.587	103.981	+6.461	-3.551	-1.504	0.124	0.108	0.883	0.228

Table 29: Table 28 continued.

RA (J2000)	Dec (J2000)	l	b	PM_RA	PM_Dec	e_PM_RA	e_PM_Dec	Parallax	e_Parallax
[deg]	[deg]	[deg]	[deg]	[mas/yr]	[mas/yr]	[mas/yr]	[mas/yr]	[mas]	[mas]
324.809	+57.801	99.526	+3.948	-3.591	-2.68	0.133	0.145	0.891	0.235
332.783	+66.461	107.868	+8.399	-2.952	-3.622	0.098	0.103	0.892	0.215
320.598	+61.989	100.879	+8.438	-2.784	-3.751	0.907	0.758	0.901	0.25
329.522	+68.187	107.899	+10.534	-8.68	-5.928	1.092	0.608	0.904	0.245
333.637	+59.956	104.452	+2.839	+1.061	-3.067	0.743	0.557	0.907	0.248
318.040	+58.894	97.742	+7.21	-3.916	-3.092	0.103	0.105	0.907	0.228
329.058	+63.433	104.762	+6.924	-0.468	-1.976	0.942	0.704	0.915	0.249
329.832	+60.298	103.115	+4.227	-3.463	-1.868	0.051	0.051	0.915	0.226
325.717	+57.017	99.377	+3.035	-1.769	-5.438	0.079	0.084	0.915	0.24
326.142	+59.057	100.880	+4.436	-0.044	+0.416	0.084	0.073	0.92	0.243
318.690	+59.761	98.609	+7.56	-1.97	-0.535	0.068	0.063	0.921	0.222
329.371	+60.032	102.770	+4.156	-2.487	-4.027	0.13	0.116	0.921	0.227
321.080	+61.271	100.529	+7.77	-1.009	-3.833	0.068	0.069	0.922	0.248
322.691	+57.2	98.277	+4.271	-2.044	-4.518	0.065	0.064	0.93	0.239
332.566	+63.831	106.257	+6.308	-2.609	-1.122	1.02	0.476	0.933	0.247
331.984	+56.158	101.558	+0.227	-5.882	-4.086	0.978	0.658	0.934	0.246
327.214	+68.273	107.281	+11.144	-2.189	-5.562	0.596	0.622	0.935	0.223
328.766	+66.254	106.442	+9.206	-1.559	-2.295	0.762	0.508	0.938	0.245
321.853	+64.006	102.730	+9.463	+9.524	+2.105	0.779	0.587	0.941	0.226
325.072	+61.083	101.812	+6.315	-1.913	-4.226	0.744	0.641	0.944	0.236

Table 30: Table 28 continued.

RA (J2000)	Dec (J2000)	l	b	PM_RA	PM_Dec	e_PM_RA	e_PM_Dec	Parallax	e_Parallax
[deg]	[deg]	[deg]	[deg]	[mas/yr]	[mas/yr]	[mas/yr]	[mas/yr]	[mas]	[mas]
325.640	+58.244	100.150	+3.99	-3.531	-3.51	0.139	0.138	0.944	0.219
332.240	+59.114	103.388	+2.553	-2.133	-0.424	0.83	0.559	0.947	0.247
324.974	+67.932	106.412	+11.44	+10.109	-1.805	0.772	0.513	0.948	0.247
331.003	+60.147	103.489	+3.756	-2.07	-3.781	1.151	0.794	0.951	0.249
326.482	+66.464	105.865	+9.954	+5.205	+0.254	0.797	0.498	0.951	0.247
319.389	+60.1	99.101	+7.54	-4.994	-3.459	0.076	0.074	0.955	0.236
334.801	+63.243	106.749	+5.26	-0.347	-1.932	0.809	0.506	0.958	0.244
321.569	+61.571	100.909	+7.818	-4.489	-4.907	0.075	0.071	0.961	0.248
341.603	+59.442	107.636	+0.335	-4.252	-2.95	0.097	0.086	0.964	0.238
321.097	+56.362	97.063	+4.272	-3.909	-3.409	0.087	0.083	0.964	0.228
336.839	+57.691	104.612	+0.037	-3.177	-2.341	1.027	0.542	0.965	0.244
318.209	+60.696	99.134	+8.373	-6.994	-7.487	0.131	0.125	0.971	0.223
327.190	+67.911	107.035	+10.874	+2.191	+0.115	0.902	0.689	0.973	0.236
320.728	+55.65	96.415	+3.911	-4.073	-3.935	0.066	0.065	0.974	0.239
317.740	+60.221	98.623	+8.221	-2.601	-3.589	0.104	0.106	0.975	0.223
325.807	+67.517	106.368	+10.92	-4.404	+1.956	0.949	0.646	0.977	0.243
335.159	+62.338	106.388	+4.413	-3.035	-3.424	0.084	0.085	0.982	0.238
325.296	+67.548	106.241	+11.073	-1.999	-6.071	0.944	0.719	0.983	0.246
331.385	+62.262	104.897	+5.349	-1.468	-2.759	0.085	0.07	0.988	0.237
313.201	+60.981	97.740	+10.407	-1.852	-6.101	0.083	0.086	0.993	0.235

Table 31: Table 28 continued.

RA (J2000)	Dec (J2000)	l	b	PM_RA	PM_Dec	e_PM_RA	e_PM_Dec	Parallax	e_Parallax
[deg]	[deg]	[deg]	[deg]	[mas/yr]	[mas/yr]	[mas/yr]	[mas/yr]	[mas]	[mas]
326.427	+62.308	103.109	+6.818	-1.533	-3.16	0.045	0.04	0.993	0.235
328.242	+65.596	105.854	+8.83	-3.882	-5.407	0.747	0.523	0.996	0.236
341.904	+59.87	107.968	+0.646	-4.677	-1.854	0.778	0.499	0.998	0.238
334.834	+65.142	107.814	+6.836	-2.664	-3.108	0.654	0.901	1.002	0.245
335.879	+64.302	107.729	+5.888	-1.916	-2.997	0.904	0.542	1.009	0.242
327.124	+61.615	102.911	+6.077	-1.298	-5.078	0.991	1.082	1.009	0.24
341.660	+60.002	107.920	+0.818	-1.604	-0.823	0.913	0.441	1.009	0.23
338.003	+63.192	107.949	+4.451	-1.071	-3.855	0.451	0.39	1.01	0.227
338.242	+58.245	105.536	+0.13	-8.565	-4.756	1.054	0.488	1.013	0.24
327.083	+61.997	103.142	+6.382	+6.332	+1.466	0.862	0.573	1.019	0.247
318.578	+58.258	97.467	+6.571	-2.26	-1.055	0.099	0.098	1.028	0.22
328.271	+58.36	101.289	+3.194	-3.602	-2.318	0.084	0.099	1.039	0.232
325.601	+57.736	99.801	+3.62	-1.679	-4.3	0.038	0.038	1.043	0.249
324.864	+57.484	99.337	+3.69	-2.391	-4.572	0.07	0.075	1.07	0.229
327.474	+60.203	102.137	+4.88	-2.463	-5.067	0.097	0.097	1.07	0.239
324.641	+53.723	96.747	+0.959	-3.427	-3.316	0.089	0.086	1.073	0.238
317.762	+64.853	102.112	+11.325	-3.187	-2.274	0.72	0.536	1.076	0.231
326.603	+60.22	101.815	+5.171	-4.983	-3.259	0.925	0.683	1.078	0.236
341.900	+59.755	107.914	+0.544	-0.643	-4.263	0.794	0.564	1.081	0.238
331.544	+56.106	101.329	+0.328	-5.683	-2.747	0.954	0.642	1.084	0.242

Table 32: Table 28 continued.

RA (J2000)	Dec (J2000)	l	b	PM_RA	PM_Dec	e_PM_RA	e_PM_Dec	Parallax	e_Parallax
[deg]	[deg]	[deg]	[deg]	[mas/yr]	[mas/yr]	[mas/yr]	[mas/yr]	[mas]	[mas]
338.503	+58.958	106.012	+0.677	+0.081	-4.809	1.086	0.627	1.085	0.246
321.673	+59.104	99.209	+6.018	-2.701	-2.845	0.115	0.113	1.087	0.231
325.598	+62.431	102.897	+7.162	-3.864	-4.377	1.065	0.871	1.097	0.245
335.073	+57.992	103.979	+0.794	+2.605	+2.649	0.132	0.119	1.097	0.247
328.784	+59.998	102.517	+4.311	-3.671	-1.954	0.058	0.056	1.101	0.232
337.346	+59.04	105.541	+1.051	-1.73	-2.671	0.763	0.435	1.102	0.244
321.863	+66.197	104.298	+11.019	+3.974	+1.834	0.87	0.619	1.102	0.239
325.101	+54.03	97.153	+1.009	-3.735	-3.449	0.092	0.089	1.119	0.226
324.224	+58.985	100.089	+5.034	-1.55	-3.346	0.995	0.656	1.126	0.246
327.357	+54.382	98.387	+0.424	-3.521	-3.199	0.081	0.069	1.132	0.217
325.549	+65.229	104.749	+9.276	-0.976	-1.884	0.788	0.565	1.145	0.237
334.179	+65.814	107.963	+7.546	+5.027	+1.126	0.915	0.61	1.147	0.244
314.651	+58.976	96.635	+8.575	-4.594	-5.397	0.135	0.139	1.147	0.219
327.076	+68.535	107.415	+11.376	-3.115	-0.621	0.785	0.596	1.15	0.24
332.225	+60.131	103.973	+3.385	-3.204	-4.868	0.791	0.581	1.151	0.245
330.018	+55.129	100.054	+0.058	-2.96	-4.479	0.091	0.092	1.154	0.227
328.025	+67.124	106.769	+10.065	-0.931	+3.443	0.906	0.665	1.159	0.239
334.181	+61.405	105.486	+3.889	-0.924	-3.837	0.829	0.465	1.162	0.245
317.407	+65.519	102.519	+11.879	-5.131	-5.547	0.1	0.081	1.165	0.245
332.529	+60.051	104.050	+3.232	-1.604	-2.351	0.816	0.585	1.166	0.248

Table 33: Table 28 continued.

RA (J2000) [deg]	Dec (J2000) [deg]	l [deg]	b [deg]	PM_RA [mas/yr]	PM_Dec [mas/yr]	e_PM_RA [mas/yr]	e_PM_Dec [mas/yr]	Parallax [mas]	e_Parallax [mas]
321.409	+66.714	104.540	+11.513	-3.016	-4.07	0.088	0.083	1.166	0.226
325.709	+66.11	105.391	+9.892	-1.468	-4.579	0.752	0.529	1.166	0.236
329.620	+61.578	103.817	+5.303	+5.067	+1.364	0.76	0.592	1.169	0.233
326.328	+65.833	105.398	+9.518	+0.007	-2.559	0.215	0.209	1.173	0.225
328.129	+59.437	101.907	+4.079	-4.46	-6.092	0.099	0.088	1.178	0.244
338.090	+60.335	106.527	+1.97	-2.842	-2.64	0.072	0.069	1.179	0.232
339.109	+58.26	105.938	-0.086	-3.529	-6.52	0.998	0.564	1.181	0.242
337.163	+58.846	105.360	+0.934	-3.213	-5.041	0.071	0.066	1.194	0.226
333.207	+58.304	103.334	+1.602	+2.694	+1.113	0.947	0.588	1.195	0.245
338.001	+59.074	105.848	+0.907	-5.837	-2.997	0.763	0.424	1.198	0.242
325.192	+67.887	106.443	+11.352	-7.3	-10.516	0.808	0.667	1.202	0.244
329.391	+67.14	107.198	+9.744	-5.588	-4.079	0.559	0.576	1.205	0.245
328.164	+62.783	104.034	+6.67	-8.055	+2.305	1.051	0.601	1.208	0.234
331.424	+67.081	107.798	+9.216	-0.919	+7.714	0.785	0.527	1.22	0.249
325.506	+60.424	101.534	+5.68	-3.205	-2.899	0.932	0.878	1.22	0.238
323.150	+53.807	96.149	+1.612	+3.871	+2.965	0.083	0.077	1.225	0.231
327.071	+62.541	103.490	+6.803	-1.762	-5.195	0.123	0.112	1.225	0.216
315.527	+60.909	98.414	+9.491	-5.63	-3.825	0.083	0.091	1.228	0.224
322.473	+57.816	98.616	+4.799	-4.366	-2.96	0.093	0.089	1.23	0.231
333.753	+61.692	105.478	+4.242	-0.719	-2.901	0.068	0.06	1.237	0.227

RA (J2000)	Dec (J2000)	l	b	PM_RA	PM_Dec	e_PM_RA	e_PM_Dec	Parallax	e_Parallax
[deg]	[deg]	[deg]	[deg]	[mas/yr]	[mas/yr]	[mas/yr]	[mas/yr]	[mas]	[mas]
325.612	+66.129	105.373	+9.932	+0.959	+0.499	0.728	0.454	1.242	0.24
334.459	+60.122	104.886	+2.748	-4.731	-3.391	1.097	0.717	1.246	0.247
329.011	+66.715	106.811	+9.504	-2.457	-5.157	0.855	0.642	1.247	0.238
332.950	+60.288	104.358	+3.306	+0.924	-3.377	0.954	0.529	1.249	0.247
327.616	+64.611	105.015	+8.237	+14.564	+3.843	0.88	0.587	1.25	0.248
323.856	+58.884	99.879	+5.086	-2.417	-3.036	0.897	0.629	1.254	0.239
339.170	+60.543	107.093	+1.884	+8.932	+3.58	1.018	0.588	1.257	0.232
324.171	+57.502	99.071	+3.952	-4.374	-5.244	0.715	0.518	1.265	0.243
327.539	+60.18	102.147	+4.843	-1.903	-3.928	0.053	0.051	1.268	0.234
324.140	+64.536	103.829	+9.163	-2.097	-2.478	0.083	0.086	1.269	0.229
328.164	+62.747	104.012	+6.642	-2.011	-2.272	1.062	0.655	1.27	0.249
323.330	+67.026	105.312	+11.207	+2.21	-0.358	0.748	0.577	1.275	0.234
316.856	+64.951	101.927	+11.677	-10.083	-5.841	0.906	0.71	1.275	0.245
324.559	+59.168	100.339	+5.054	-3.967	-5.323	0.099	0.095	1.277	0.223
332.128	+65.136	106.868	+7.479	-2.075	-2.365	0.772	0.559	1.287	0.245
324.745	+57.487	99.291	+3.735	-2.603	-5.314	0.083	0.089	1.29	0.243
332.215	+61.694	104.879	+4.66	-1.4	-2.975	0.09	0.074	1.296	0.241
319.708	+58.926	98.363	+6.608	-2.722	-3.594	0.05	0.044	1.299	0.247
324.945	+57.548	99.412	+3.709	-4.194	-5.474	0.749	0.528	1.299	0.236
332.611	+64.341	106.570	+6.712	-3.837	-3.55	0.076	0.066	1.302	0.218

Table 35: Table 28 continued.

RA (J2000) [deg]	Dec (J2000) [deg]	l [deg]	b [deg]	PM_RA [mas/yr]	PM_Dec [mas/yr]	e_PM_RA [mas/yr]	e_PM_Dec [mas/yr]	Parallax [mas]	e_Parallax [mas]
319.036	+62.887	101.026	+9.581	-1.887	-0.344	1.107	1.075	1.305	0.243
337.938	+59.566	106.071	+1.347	-6.256	-3.066	0.778	0.565	1.306	0.247
328.409	+66.537	106.509	+9.516	-6.192	-1.037	0.751	0.492	1.323	0.219
318.020	+56.719	96.131	+5.736	-3.988	-3.454	0.068	0.077	1.334	0.242
333.318	+57.26	102.791	+0.709	-2.19	-2.983	1.028	0.817	1.342	0.235
323.933	+57.468	98.952	+4.013	-2.148	-5.135	0.565	0.55	1.347	0.25
338.663	+57.92	105.564	-0.264	+2.201	-7.496	1.013	0.412	1.35	0.247
327.937	+66.848	106.563	+9.875	+1.83	+5.454	0.097	0.09	1.354	0.238
326.584	+55.235	98.590	+1.365	+0.263	-0.695	1.346	0.905	1.369	0.249
329.824	+63.189	104.883	+6.52	-8.219	-4.675	1.128	0.71	1.37	0.247
320.384	+63.911	102.200	+9.854	+0.355	-2.059	0.822	0.622	1.373	0.237
318.043	+60.419	98.872	+8.244	-5.9	-5.009	0.764	0.613	1.376	0.244
325.249	+61.978	102.473	+6.93	+9.44	+3.852	0.731	0.482	1.391	0.246
326.054	+55.21	98.343	+1.542	-3.243	-4.068	0.095	0.091	1.399	0.238
318.948	+60.291	99.087	+7.83	-2.707	-1.082	0.703	0.492	1.402	0.243
325.488	+62.478	102.890	+7.231	-4.357	-2.225	1.188	1.063	1.403	0.24
330.280	+63.043	104.959	+6.279	-0.943	+2.784	1.199	0.537	1.409	0.246
330.632	+59.646	103.040	+3.466	+0.591	-3.06	0.906	0.544	1.415	0.246
330.203	+55.75	100.513	+0.49	-5.93	-1.456	1.008	0.62	1.421	0.246
323.878	+56.918	98.560	+3.625	-4.132	-4.651	1.052	0.671	1.422	0.248

Table 36: Table 28 continued.

RA (J2000) [deg]	Dec (J2000) [deg]	l [deg]	b [deg]	PM_RA [mas/yr]	PM_Dec [mas/yr]	e_PM_RA [mas/yr]	e_PM_Dec [mas/yr]	Parallax [mas]	e_Parallax [mas]
322.421	+65.925	104.267	+10.666	+0.656	+2.703	0.089	0.086	1.43	0.249
330.879	+63.535	105.473	+6.509	+8.617	+3.374	0.071	0.06	1.433	0.244
327.416	+63.295	104.098	+7.281	+0.698	-2.043	1.018	0.702	1.439	0.25
329.072	+66.662	106.797	+9.448	-14.971	-10.026	0.811	0.587	1.447	0.247
327.849	+54.293	98.553	+0.174	+2.126	-0.284	0.104	0.109	1.453	0.239
336.822	+58.942	105.259	+1.108	+3.871	+2.207	0.139	0.127	1.454	0.211
329.338	+59.585	102.481	+3.814	-9.426	-7.987	0.178	0.163	1.461	0.225
337.198	+59.483	105.706	+1.469	-5.227	-4.83	0.751	0.458	1.469	0.233
326.145	+62.354	103.039	+6.938	+1.046	-3.209	0.742	0.544	1.469	0.23
324.612	+63.028	102.957	+7.908	+1.886	-0.214	1.026	0.645	1.493	0.225
312.763	+62.081	98.485	+11.254	-1.072	+2.402	0.846	0.634	1.494	0.247
326.092	+67.592	106.502	+10.904	+2.506	-2.762	1.111	0.833	1.495	0.248
321.957	+56.728	97.660	+4.205	-5.635	-3.885	0.813	0.465	1.497	0.239

Table 37: List of Cep OB3 stars in the three distance bins discussed in this work.

RA (J2000) [deg]	Dec (J2000) [deg]	l [deg]	b [deg]	PM_RA [mas/yr]	PM_Dec [mas/yr]	e_PM_RA [mas/yr]	e_PM_Dec [mas/yr]	Parallax [mas]	e_Parallax [mas]
341.428	+65.274	110.273	+5.54	-2.118	-1.674	0.127	0.115	0.838	0.224
349.265	+63.789	112.737	+2.801	-2.71	-1.393	0.07	0.063	0.85	0.231
344.351	+63.26	110.511	+3.172	+0.906	-1.241	1.149	0.606	0.863	0.226
345.644	+66.712	112.455	+6.08	-2.666	-0.996	0.735	0.577	0.877	0.238
336.922	+65.43	108.711	+6.608	-2.307	-1.23	0.096	0.099	0.896	0.238
340.159	+65.263	109.798	+5.782	-0.4	-2.714	0.075	0.07	0.896	0.228
336.956	+64.903	108.444	+6.152	-2.011	-1.802	0.727	0.412	0.911	0.236
341.361	+63.539	109.436	+4.019	-2.824	-2.89	0.798	0.531	0.993	0.243
345.834	+63.551	111.237	+3.161	-1.303	-1.993	0.068	0.068	1.004	0.238
339.788	+63.172	108.638	+4.032	+8.641	+1.874	0.804	0.513	1.023	0.244
345.756	+63.698	111.266	+3.309	-1.296	-1.903	0.055	0.057	1.028	0.246
344.197	+62.727	110.221	+2.72	-0.374	-2.25	0.068	0.067	1.03	0.236
340.989	+64.175	109.590	+4.657	+3.002	-2.633	1.016	0.453	1.088	0.237
343.927	+62.306	109.927	+2.393	-0.933	-3.091	0.055	0.055	1.094	0.245
342.081	+65.95	110.827	+6.015	-5.022	-2.883	0.115	0.101	1.123	0.233
340.373	+61.971	108.294	+2.851	-6.068	-6.415	0.786	0.468	1.131	0.243
345.937	+63.626	111.310	+3.211	-5.026	-2.267	0.726	0.57	1.143	0.249
344.920	+65.211	111.562	+4.836	-2.205	-5.206	1.05	0.482	1.144	0.241
343.127	+62.441	109.652	+2.676	-1.483	-2.953	0.06	0.064	1.159	0.237
346.189	+63.351	111.303	+2.914	-0.661	-1.441	0.95	0.654	1.169	0.246

Table 38: Table 37 continued.

RA (J2000)	Dec (J2000)	l	b	PM_RA	PM_Dec	e_PM_RA	e_PM_Dec	Parallax	e_Parallax
[deg]	[deg]	[deg]	[deg]	[mas/yr]	[mas/yr]	[mas/yr]	[mas/yr]	[mas]	[mas]
337.988	+64.172	108.445	+5.297	-1.066	-4.041	0.821	0.551	1.222	0.237
342.814	+61.268	108.999	+1.691	-2.556	-3.303	0.771	0.491	1.26	0.241
337.807	+65.466	109.046	+6.448	-1.943	-2.164	0.137	0.134	1.27	0.234
344.581	+65.03	111.355	+4.732	-6.166	-4.765	0.146	0.152	1.274	0.232
344.060	+63.166	110.352	+3.143	-0.835	-2.169	1.267	0.694	1.289	0.231
343.822	+64.583	110.870	+4.467	-2.983	-2.009	0.772	0.486	1.303	0.241
338.782	+64.72	109.021	+5.597	-3.229	-3.525	0.873	1.023	1.342	0.244
339.820	+64.651	109.373	+5.317	+1.812	+2.326	1.248	0.582	1.423	0.246
340.398	+64.746	109.637	+5.281	+5.416	-0.01	0.852	0.529	1.432	0.231
343.900	+66.321	111.656	+6.019	-5.548	+1.629	0.148	0.139	1.449	0.213
342.402	+62.333	109.303	+2.729	-3.588	-4.472	0.108	0.104	1.465	0.223

Table 39: List of Cep OB4 stars in the three distance bins discussed in this work.

RA (J2000) [deg]	Dec (J2000) [deg]	l [deg]	b [deg]	PM_RA [mas/yr]	PM_Dec [mas/yr]	e_PM_RA [mas/yr]	e_PM_Dec [mas/yr]	Parallax [mas]	e_Parallax [mas]
1.204	+68.189	118.606	+5.709	-1.426	-1.046	0.083	0.089	0.769	0.23
359.305	+69.162	118.115	+6.798	-1.453	-0.707	0.143	0.137	0.786	0.223
354.740	+68.726	116.407	+6.777	-2.37	-2.943	0.06	0.055	0.792	0.246
359.403	+67.845	117.874	+5.503	-2.227	-1.401	0.092	0.093	0.808	0.246
3.363	+68.248	119.410	+5.637	-0.809	-1.078	0.166	0.177	0.824	0.215
357.481	+67.637	117.115	+5.463	-2.014	+0.614	0.104	0.104	0.9	0.23
359.386	+67.554	117.807	+5.22	-1.587	-1.614	0.074	0.074	0.911	0.241
358.137	+68.934	117.655	+6.667	+1.683	-10.092	0.13	0.126	0.936	0.223
1.748	+65.539	118.348	+3.063	-1.57	-0.448	0.2	0.187	1.024	0.225
3.247	+66.322	119.079	+3.738	-1.821	-0.071	0.143	0.134	1.048	0.231
354.484	+68.531	116.262	+6.617	-4.392	-0.936	0.688	0.712	1.081	0.236
1.798	+65.654	118.388	+3.173	+2.784	-2.297	0.225	0.2	1.089	0.231
356.967	+67.419	116.870	+5.299	+12.441	-1.318	0.694	0.553	1.215	0.247
358.051	+67.169	117.219	+4.956	-5.636	-1.373	0.109	0.103	1.263	0.23
1.671	+65.588	118.325	+3.117	+2.403	-2.469	0.229	0.213	1.309	0.229
3.813	+68.006	119.541	+5.373	-4.367	-4.02	0.179	0.185	1.341	0.227
3.351	+65.613	119.015	+3.031	+2.221	-2.505	0.155	0.13	1.363	0.231

Part V

CONCLUSION

SUMMARY AND OUTLOOK

7.1 SUMMARY

The aim of this work is a study of the chemical properties of the old Galactic open cluster M67 especially from the point of view of stellar evolution. This kind of study is unfortunately limited by the scarcity of data concerning member stars in open clusters. As we discuss in Chapter 2, the observations of open clusters are more problematic in terms of membership than those of globular clusters due to the high contamination by field stars, given the low density of these environments. Consequently, in the absence of precise kinematic information about the stars in the field of interest, it is very difficult to select members a priori. In addition, due to practical reasons such as the highly time-consuming observations of faint MS and TO stars with high-resolution spectrographs, observations are often limited to the luminous red giants and RC stars. We thus performed a detailed study of the chemical properties of one open cluster which, due to its Sun-like age and metallicity, has been extensively observed in different evolutionary phases from the MS to the RC: M67. Since open cluster are not expected to present multiple stellar populations like those observed in globular clusters, possible chemical inhomogeneities must have different origins. They might be due to inhomogeneities in the parent molecular cloud or they can result from evolutionary processes (such as atomic diffusion or dredge-ups) taking place in the stellar interior.

In Chapter 3 we investigate the effects of the process known as first dredge-up. The convective envelope deepening into the inner layers of the star after the TO brings to the surface the material processed by the CNO cycle and thus changes the measurable surface abundances of carbon and nitrogen with respect to the abundances of the birth environment. We used APOGEE DR12 observations of M67 to study the evolution of the [C/N] abundance along the SGB and the RGB. We compare the observations with models of stellar evolution for masses comparable to the SGB and lower-RGB mass of M67 and found them to be consistent with each other. We derived a post-FDU [C/N] abundance of -0.46 ± 0.03 dex. We do not find any evidence of extra-mixing effects in the stars beyond the RGB bump, although we are limited by low-number statistics.

In Chapter 4 we used Gaia-ESO iDR5 data to study the effects of a further evolutionary process: atomic diffusion. In this case, the evolutionary phases involved are the MS and the SGB/lower-RGB. Atomic diffusion is active in the radiative cores of low-mass stars on the MS, where both gravity and radiative acceleration act on the atoms. Depending if the former or the latter is stronger, a given element will sink into the stellar interior or rise towards the outer layers, changing the surface abundance of the star. After the TO, the effect is cancelled by the deepening of the convective envelope into the stellar interior. For stars in the mass range represented in M67 the effect is small (~ 0.1 dex), but measurable. We find that M67 presents trends in $\log g$ for most elements that are consistent with the predictions

of stellar evolutionary models. We find similar trends in the abundances obtained for M67 by APOGEE DR14.

We extended our study of the chemical characteristics of M67 to peculiar objects populating the cluster in Chapter 5. We conducted an independent analysis of the APOGEE DR14 infrared spectra of three candidate blue straggler stars and two evolved blue straggler stars, as well as of ten TO and six RC stars as control samples. The aim of this study was to find in the surface chemical abundances of BSS possible hints at their formation history, such as carbon depletion caused by a mass transfer event in a close binary system. We found that only the two evolved BSS are depleted in carbon, in a similar way as the RC stars of M67. We conclude that the surface [C/H] under-abundance is more likely to be caused by stellar evolution, and in particular the FDU, than by mass transfer.

In the last chapter, we set aside the old open cluster M67 and dedicated ourselves to the investigation of the kinematic properties of the very young OB associations Cyg OB2 and OB9 and Cep OB2, OB3, and OB4. We proposed an approach in which the selection of candidate members is solely based on photometric data and/or parallaxes, so that we do not introduce any bias related to the motion of the stars. We are thus able to examine the proper motions of stars in extended star forming regions and to study their dynamical properties. We present our method with proper motions and parallaxes retrieved from the TGAS catalogue, although conclusive results will only be possible with the future Gaia data releases.

7.2   OUTLOOK

The studies presented in this work have several implications that go beyond the understanding of stellar evolution alone, especially in the field of Galactic archaeology. As presented in Chapter 3, the post-FDU [C/N] abundance can be used to determine the age of field stars, a task that can be otherwise very difficult. In order to calibrate the [C/N]-age-metallicity relation, though, it is necessary to obtain an estimate of the post-FDU [C/N] abundance for as many stellar clusters as possible in a large range of ages and metallicities. So far, not many clusters have high-resolution spectra of stars located on the lower RGB, before the RGB bump. We have applied for observational time in order to observe the TO, SGB and lower-RGB of two OCs, NGC 2243 and NGC 6253, with similar age ($\sim$ 3 Gyr) but different metallicity (respectively [Fe/H] $\sim$ +0.50 dex and [Fe/H] $\sim$ −0.40 dex, see, e.g., Carretta, Bragaglia, and Gratton 2007; François et al. 2013; Sestito, Randich, and Bragaglia 2007). These observations will allow us to test if indeed the post-FDU [C/N] abundance is rather insensitive to variations in metallicity at the age of these clusters as predicted by stellar evolution theory. (see Fig. 21).

As can be seen in Fig. 21, metallicity starts playing a more important role on the post-FDU [C/N] abundance at older ages (> 5 Gyr). Unfortunately, very few OCs exist with ages > 5 Gyr and none above $\sim$ 10 Gyr (Salaris, Weiss, and Percival, 2004). The only possibility to test the [C/N]-age-metallicity relation in clusters of these ages would be to use stars in globular clusters. This presents a series of problems: first, GCs contain multiple stellar populations. It is therefore necessary to first disentangle the different population and to then treat them separately when measuring [Fe/H]$_{FDU}$. Secondly, the effect of the FDU decreases with decreasing

mass of the star under analysis. This means that the effect that we want to measure becomes smaller and smaller and requires an increasingly high precision of the abundances as we go to higher ages. Finally, GCs are usually very faint due to their large distances from the Sun. Obtaining high-resolution and high-S/N spectra of stars on the lower-RGB is therefore very expensive in terms of observing time. Possible variations in the surface [C/H] and [N/H] abundance of SGB and lower RGB stars in a GC are presented e.g. in Marino et al. (2016) for the case of 47 Tuc. The authors find small trends opposite to what expected from theory but argue that at the metallicity of 47 Tuc ([Fe/H] = −0.77 dex, Carretta et al. 2009) the effects of the FDU should be almost negligible.

The investigation of atomic diffusion effects are very important in the context of Galactic archaeology and in particular in the application of chemical tagging methods. As we explain in Chapter 4 in detail, the variations in surface abundance due to atomic diffusion limit the resolution achievable when trying to trace stars in different evolutionary stages back to the cluster in which they were born. The theory of stellar evolution should therefore become part of the chemical tagging method. In this context it is important to use stellar clusters to test the effects of atomic diffusion on stars of different age and metallicity. A large effort has already been made to test these effects in globular clusters (see, e.g., Gruyters, Nordlander, and Korn, 2014; Gruyters et al., 2013, 2016; Korn et al., 2007; Lind et al., 2008; Nordlander et al., 2012), and in open clusters (see, e.g., Casey, 2016; Fossati et al., 2007, 2011; Kılıçoğlu et al., 2016; Martin et al., 2017; Önehag, Gustafsson, and Korn, 2014; Pasquini, Randich, and Pallavicini, 2001). Both for several globular and open clusters indications of active diffusion processes have been found, but due to the very small amplitude of these effects it is still difficult to disentangle them from other possible biases or trends deriving from the assumptions made during the analysis. It is therefore important to keep extending this kind of studies to new clusters with different ages and metallicities, but at the same time to improve our understanding of spectroscopy and stellar atmospheres.

In Chapter 5 we analysed the abundances of two evolved blue straggler stars in M67 and we found that they are depleted in carbon similarly to the RC stars. We then discussed how this depletion can be interpreted as a result of classical stellar evolution. This kind of study could lead to important insights into the evolution of BSSs. It is usually assumed that, after they are formed, BSSs follow the classical evolutionary path of stars with the same mass. Studying processes such as the first-dredge-up in these stars might help understanding if this assumption is indeed correct. On the other hand an investigation of this kind is made problematic by the small number of evolved BSSs present in clusters, by the difficulty in identifying these objects as evolved BSSs, and by the many still unclear details about their formation history, which might also lead to variations in the surface abundances.

Finally, the experiment presented in Chapter 6 and based on TGAS data will become of larger interest once the new Gaia DR2 will become available. The precise proper motions and parallaxes will be an unprecedented asset in the study of the dynamical evolution of stellar agglomerates such as stellar clusters and OB associations.

Part VI

APPENDIX

PUBLICATIONS

The following publications were used in this thesis:

- Bertelli Motta, C., M. Salaris, A. Pasquali, and E. K. Grebel (2017). 'Observing the products of stellar evolution in the old open cluster M67 with APOGEE'. In: MNRAS 466, pp. 2161–2174.

- Bertelli Motta, C., A. Pasquali, J. Richer, G. Michaud, M. Salaris, A. Bragaglia, L. Magrini, S. Randich, E. K. Grebel, et al. 'The Gaia-ESO Survey: Evidence of atomic diffusion in M67?'. Subm. to MNRAS.

I am also first author or co-author in the following publications which are not included in this thesis:

- Bertelli Motta, C., P. C. Clark, S. C. O. Glover, R. S. Klessen, and A. Pasquali (2016). 'The IMF as a function of supersonic turbulence'. In: MNRAS 462, pp. 4171-4182

- Berlanas, S. R., A. Herrero, F. Comerón, A. Pasquali, C. Bertelli Motta, and A. Sota (2017). 'New massive members of Cygnus OB2'. Accepted for publication in A&A. In: ArXiv e-prints. arXiv: 1711.06945

- Chen, B., E. D'Onghia, S. Pardy, A. Pasquali, C. Bertelli Motta, B. Hanlon and E. K. Grebel (2017). 'Chemo-Dynamical Clustering applied to APOGEE data: Re-Discovering Globular Clusters', subm. to ApJ, arXiv: 1709.03987

Abolfathi, B. et al. (2017). 'The Fourteenth Data Release of the Sloan Digital Sky Survey: First Spectroscopic Data from the extended Baryon Oscillation Sky Survey and from the second phase of the Apache Point Observatory Galactic Evolution Experiment'. In: *ArXiv e-prints*. arXiv: 1707.09322.

Ábrahám, P., L. G. Balázs, and M. Kun (2000). 'Morphology and kinematics of the Cepheus Bubble'. In: *A&A* 354, pp. 645–656.

Ahumada, J. A. and E. Lapasset (2007). 'New catalogue of blue stragglers in open clusters'. In: *A&A* 463, pp. 789–797. DOI: 10.1051/0004-6361:20054590.

Alam, S. et al. (2015). 'The Eleventh and Twelfth Data Releases of the Sloan Digital Sky Survey: Final Data from SDSS-III'. In: *ApJ Suppl.* 219, 12, p. 12. DOI: 10.1088/0067-0049/219/1/12. arXiv: 1501.00963 [astro-ph.IM].

Altmann, M., S. Roeser, M. Demleitner, U. Bastian, and E. Schilbach (2017). 'Hot Stuff for One Year (HSOY). A 583 million star proper motion catalogue derived from Gaia DR1 and PPMXL'. In: *A&A* 600, L4, p. L4. DOI: 10.1051/0004-6361/201730393. arXiv: 1701.02629.

Balachandran, S. (1995). 'The Lithium Dip in M67: Comparison with the Hyades, Praesepe, and NGC 752 Clusters'. In: *ApJ* 446, p. 203. DOI: 10.1086/175779.

Balaguer-Núñez, L., D. Galadí-Enríquez, and C. Jordi (2007). 'uvby - H_β CCD photometry and membership segregation of the open cluster NGC 2682 (M 67)'. In: *A&A* 470, pp. 585–596. DOI: 10.1051/0004-6361:20067003. arXiv: 0704.2887.

Balaguer-Núñez, L., D. Galadí-Enríquez, C. Jordi, and S. Sánchez (2010). 'Spectroscopy of Pre-CV Candidates in the Open Cluster M 67'. In: *Astrophysics and Space Science Proceedings* 14, p. 373. DOI: 10.1007/978-3-642-11250-8_85.

Balazs, L. G. and M. Kun (1989). 'Star-forming processes in Cepheus OB2'. In: *Astronomische Nachrichten* 310, pp. 385–388. DOI: 10.1002/asna.2113100519.

Barnes, S. A., J. Weingrill, D. Fritzewski, K. G. Strassmeier, and I. Platais (2016). 'Rotation Periods for Cool Stars in the 4 Gyr old Open Cluster M67, The Solar-Stellar Connection, and the Applicability of Gyrochronology to at least Solar Age'. In: *ApJ* 823, 16, p. 16. DOI: 10.3847/0004-637X/823/1/16. arXiv: 1603.09179 [astro-ph.SR].

Bellini, A., L. R. Bedin, B. Pichardo, E. Moreno, C. Allen, G. Piotto, and J. Anderson (2010a). 'Absolute proper motion of the Galactic open cluster M 67'. In: *A&A* 513, A51, A51. DOI: 10.1051/0004-6361/200913882. arXiv: 1005.0840 [astro-ph.GA].

Bellini, A. et al. (2010b). 'The end of the white dwarf cooling sequence in M 67'. In: *A&A* 513, A50, A50. DOI: 10.1051/0004-6361/200913721. arXiv: 1001.3827 [astro-ph.SR].

Belloni, T., F. Verbunt, and R. D. Mathieu (1998). 'X-rays from old open clusters: M 67 and NGC 188'. In: *A&A* 339, pp. 431–439. eprint: astro-ph/9808329.

Belloni, T., F. Verbunt, and J. H. M. M. Schmitt (1993). 'ROSAT detection of stellar X-ray sources in the old open cluster M 67'. In: *A&A* 269, pp. 175–180.

Berlanas, S. R., A. Herrero, F. Comerón, A. Pasquali, C. Bertelli Motta, and A. Sota (2017). 'New massive members of Cygnus OB2'. In: *ArXiv e-prints*. arXiv: 1711.06945 [astro-ph.SR].

Bertelli Motta, C., M. Salaris, A. Pasquali, and E. K. Grebel (2017). 'Observing the products of stellar evolution in the old open cluster M67 with APOGEE'. In: *MNRAS* 466, pp. 2161–2174. DOI: 10.1093/mnras/stw3252. arXiv: 1701.00979 [astro-ph.SR].

Blaauw, A. (1964). 'The O Associations in the Solar Neighborhood'. In: *ARA&A* 2, p. 213. DOI: 10.1146/annurev.aa.02.090164.001241.

Blaauw, A., W. A. Hiltner, and H. L. Johnson (1959). 'Photoelectric Photometry of the Association III Cephei.' In: *ApJ* 130, p. 69. DOI: 10.1086/146697.

Blanco-Cuaresma, S. et al. (2015). 'Testing the chemical tagging technique with open clusters'. In: *A&A* 577, A47, A47. DOI: 10.1051/0004-6361/201425232. arXiv: 1503.02082 [astro-ph.SR].

Blanton, M. R. et al. (2017). 'Sloan Digital Sky Survey IV: Mapping the Milky Way, Nearby Galaxies, and the Distant Universe'. In: *Astron. J.* 154, 28, p. 28. DOI: 10.3847/1538-3881/aa7567. arXiv: 1703.00052.

Boch, T. and P. Fernique (2014). 'Aladin Lite: Embed your Sky in the Browser'. In: *Astronomical Data Analysis Software and Systems XXIII*. Ed. by N. Manset and P. Forshay. Vol. 485. Astronomical Society of the Pacific Conference Series, p. 277.

Bonatto, C. and E. Bica (2003). 'Mass segregation in M 67 with 2MASS'. In: *A&A* 405, pp. 525–530. DOI: 10.1051/0004-6361:20030205.

Bonnarel, F., P. Fernique, O. Bienaymé, D. Egret, F. Genova, M. Louys, F. Ochsenbein, M. Wenger, and J. G. Bartlett (2000). 'The ALADIN interactive sky atlas. A reference tool for identification of astronomical sources'. In: *A&AS* 143, pp. 33–40. DOI: 10.1051/aas:2000331.

Bragaglia, A., R. G. Gratton, E. Carretta, V. D'Orazi, C. Sneden, and S. Lucatello (2012). 'Searching for multiple stellar populations in the massive, old open cluster Berkeley 39'. In: *A&A* 548, A122, A122. DOI: 10.1051/0004-6361/201220366. arXiv: 1211.1142.

Bragaglia, A., C. Sneden, E. Carretta, R. G. Gratton, S. Lucatello, P. F. Bernath, J. S. A. Brooke, and R. S. Ram (2014). 'Searching for Chemical Signatures of Multiple Stellar Populations in the Old, Massive Open Cluster NGC 6791'. In: *ApJ* 796, 68, p. 68. DOI: 10.1088/0004-637X/796/1/68. arXiv: 1409.8283 [astro-ph.SR].

Bressan, A., P. Marigo, L. Girardi, B. Salasnich, C. Dal Cero, S. Rubele, and A. Nanni (2012). 'PARSEC: stellar tracks and isochrones with the PAdova and TRieste Stellar Evolution Code'. In: *MNRAS* 427, pp. 127–145. DOI: 10.1111/j.1365-2966.2012.21948.x. arXiv: 1208.4498 [astro-ph.SR].

Brown, J. A. (1987). 'Carbon-to-nitrogen ratios along the evolutionary sequence of M67'. In: *ApJ* 317, pp. 701–709. DOI: 10.1086/165316.

Brucalassi, A., L. Pasquini, R. Saglia, M. T. Ruiz, P. Bonifacio, L. R. Bedin, K. Biazzo, C. Melo, C. Lovis, and S. Randich (2014). 'Three planetary companions around M 67 stars'. In: *A&A* 561, L9, p. L9. DOI: 10.1051/0004-6361/201322584. arXiv: 1401.4905 [astro-ph.SR].

Brucalassi, A. et al. (2016). 'Search for giant planets in M67. III. Excess of hot Jupiters in dense open clusters'. In: *A&A* 592, L1, p. L1. DOI: 10.1051/0004-6361/201527561. arXiv: 1606.05247 [astro-ph.EP].

Brucalassi, A. et al. (2017). 'Search for giant planets in M67 IV: survey results'. In: *ArXiv e-prints*. arXiv: 1703.04296 [astro-ph.EP].

Bruntt, H. et al. (2007). 'Multisite campaign on the open cluster M67 - III. δ Scuti pulsations in the blue stragglers'. In: *MNRAS* 378, pp. 1371–1384. DOI: 10.1111/j.1365-2966.2007.11865.x. arXiv: 0704.3884.

Burbidge, E. M. and A. Sandage (1958). 'The Color-Magnitude Diagram for the Galactic NGC 7789.' In: *ApJ* 128, p. 174. DOI: 10.1086/146535.

Cannon, R. D. (2015). 'Blue Straggler Stars: Early Observations That Failed to Solve the Problem'. In: *Ecology of Blue Straggler Stars*. Ed. by H. M. J. Boffin, G. Carraro, and G. Beccari, p. 17. DOI: 10.1007/978-3-662-44434-4_2.

Canto Martins, B. L., A. Lèbre, P. de Laverny, C. H. F. Melo, J. D. Do Nascimento Jr., O. Richard, and J. R. de Medeiros (2006). 'S1242: a lithium-rich subgiant star in the open cluster M 67'. In: *A&A* 451, pp. 993–997. DOI: 10.1051/0004-6361:20053334.

Canto Martins, B. L., A. Lèbre, A. Palacios, P. de Laverny, O. Richard, C. H. F. Melo, J. D. Do Nascimento Jr., and J. R. de Medeiros (2011). 'Lithium abundances and extra mixing processes in evolved stars of M 67'. In: *A&A* 527, A94, A94. DOI: 10.1051/0004-6361/201015015. arXiv: 1101.3757 [astro-ph.SR].

Cardelli, J. A., G. C. Clayton, and J. S. Mathis (1989). 'The relationship between infrared, optical, and ultraviolet extinction'. In: *ApJ* 345, pp. 245–256. DOI: 10.1086/167900.

Carraro, G., L. Girardi, A. Bressan, and C. Chiosi (1996). 'Mass loss from red giant stars in M 67: Is there any evidence for a metallicity dependence?' In: *A&A* 305, p. 849.

Carraro, G., G. de Silva, L. Monaco, A. P. Milone, and R. Mateluna (2014). 'Updated properties of the old open cluster Melotte 66: Searching for multiple stellar populations'. In: *A&A* 566, A39, A39. DOI: 10.1051/0004-6361/201423714. arXiv: 1404.6748.

Carretta, E., A. Bragaglia, and R. G. Gratton (2007). 'The chemical abundance of the very metal-rich old open clusters NGC 6253 and NGC 6791'. In: *A&A* 473, pp. 129–141. DOI: 10.1051/0004-6361:20065213. arXiv: 0706.2780.

Carretta, E., A. Bragaglia, R. Gratton, V. D'Orazi, and S. Lucatello (2009). 'Intrinsic iron spread and a new metallicity scale for globular clusters'. In: *A&A* 508, pp. 695–706. DOI: 10.1051/0004-6361/200913003. arXiv: 0910.0675.

Casey, A. R. (2016). 'sick: The Spectroscopic Inference Crank'. In: *ApJ Suppl.* 223, 8, p. 8. DOI: 10.3847/0067-0049/223/1/8. arXiv: 1603.03043 [astro-ph.IM].

Cash, W., P. Charles, S. Bowyer, F. Walter, G. Garmire, and G. Riegler (1980). 'The X-ray superbubble in Cygnus'. In: *ApJL* 238, pp. L71–L76. DOI: 10.1086/183261.

Cassisi, S. and M. Salaris (2013). *Old Stellar Populations: How to Study the Fossil Record of Galaxy Formation*. Wiley, New York.

Castro, M., J. D. Do Nascimento Jr., K. Biazzo, J. Meléndez, and J. R. de Medeiros (2011). 'Solar twins in M 67: evolutionary status and lithium abundance'. In: *A&A* 526, A17, A17. DOI: 10.1051/0004-6361/201015034. arXiv: 1011.1276 [astro-ph.SR].

Castro, M., T. Duarte, G. Pace, and J.-D. do Nascimento (2016). 'Mass effect on the lithium abundance evolution of open clusters: Hyades, NGC 752, and M 67'. In: *A&A* 590, A94, A94. DOI: 10.1051/0004-6361/201527583. arXiv: 1603.08809 [astro-ph.SR].

Charbonnel, C. and S. C. Balachandran (2000). 'The Nature of the lithium rich giants. Mixing episodes on the RGB and early-AGB'. In: *A&A* 359, pp. 563–572. eprint: astro-ph/0005280.

Chen, L., J. L. Hou, and J. J. Wang (2003). 'On the Galactic Disk Metallicity Distribution from Open Clusters. I. New Catalogs and Abundance Gradient'. In: *Astron. J.* 125, pp. 1397–1406. DOI: 10.1086/367911. eprint: astro-ph/0212542.

Clayton, G. C. and E. L. Fitzpatrick (1987). 'Anomalous dust in the open cluster Trumpler 37'. In: *Astron. J.* 93, pp. 157–162. DOI: 10.1086/114293.

Coşkunoğlu, B. et al. (2011). 'Local stellar kinematics from RAVE data - I. Local standard of rest'. In: *MNRAS* 412, pp. 1237–1245. DOI: 10.1111/j.1365-2966.2010.17983.x. arXiv: 1011.1188.

Comerón, F. and A. Pasquali (2007). 'A very massive runaway star from Cygnus OB2'. In: *A&A* 467, pp. L23–L27. DOI: 10.1051/0004-6361:20077304. arXiv: 0704.0676.

— (2012). 'New members of the massive stellar population in Cygnus'. In: *A&A* 543, A101, A101. DOI: 10.1051/0004-6361/201219022.

Comerón, F., A. Pasquali, G. Rodighiero, V. Stanishev, E. De Filippis, B. López Martí, M. C. Gálvez Ortiz, A. Stankov, and R. Gredel (2002). 'On the massive star contents of Cygnus OB2'. In: *A&A* 389, pp. 874–888. DOI: 10.1051/0004-6361:20020648.

Comerón, F., A. Pasquali, F. Figueras, and J. Torra (2008). 'The outskirts of Cygnus OB2'. In: *A&A* 486, pp. 453–466. DOI: 10.1051/0004-6361:200809917. arXiv: 0806.1891.

Davenport, J. R. A. and E. L. Sandquist (2010). 'Death of a Cluster: The Destruction of M67 as Seen by the Sloan Digital Sky Survey'. In: *ApJ* 711, pp. 559–572. DOI: 10.1088/0004-637X/711/2/559. arXiv: 1001.1198.

Dekker, H., S. D'Odorico, A. Kaufer, B. Delabre, and H. Kotzlowski (2000). 'Design, construction, and performance of UVES, the echelle spectrograph for the UT2 Kueyen Telescope at the ESO Paranal Observatory'. In: *Optical and IR Telescope Instrumentation and Detectors*. Ed. by M. Iye and A. F. Moorwood. Vol. 4008. Proc.SPIE, pp. 534–545. DOI: 10.1117/12.395512.

Deliyannis, C. P., J. R. King, A. M. Boesgaard, and S. G. Ryan (1994). 'Lithium in a short-period tidally locked binary of M67: Implications for stellar evolution, Galactic Lithium evolution, and cosmology'. In: *ApJL* 434, pp. L71–L74. DOI: 10.1086/187577.

Deng, L., R. Chen, X. S. Liu, and J. S. Chen (1999). 'The Blue Stragglers in M67 and Single-Population Synthesis'. In: *ApJ* 524, pp. 824–830. DOI: 10.1086/307832.

Dotter, A., C. Conroy, P. Cargile, and M. Asplund (2017). 'The Influence of Atomic Diffusion on Stellar Ages and Chemical Tagging'. In: *ApJ* 840, 99, p. 99. DOI: 10.3847/1538-4357/aa6d10. arXiv: 1704.03465 [astro-ph.SR].

Dupree, A. K., B. A. Whitney, and L. Pasquini (1999). 'Evolution of Chromospheric Activity: M67 Red Giants'. In: *ApJ* 520, pp. 751–762. DOI: 10.1086/307504.

Eggleton, P. (2011). *Evolutionary Processes in Binary and Multiple Stars*.

Eisenstein, D. J. et al. (2011). 'SDSS-III: Massive Spectroscopic Surveys of the Distant Universe, the Milky Way, and Extra-Solar Planetary Systems'. In: *Astron. J.* 142, 72, p. 72. DOI: 10.1088/0004-6256/142/3/72. arXiv: 1101.1529 [astro-ph.IM].

Errmann, R. et al. (2013). 'The stellar content of the young open cluster Trumpler 37'. In: *Astronomische Nachrichten* 334, pp. 673–681. DOI: 10.1002/asna.201311890. arXiv: 1305.4860 [astro-ph.SR].

Fagerholm, E. (1906). 'Ueber den Sternhaufen Messier 67'. PhD thesis. , Uppsala Univ., (1906).

Fan, X. et al. (1996). 'Deep Wide-Field Spectrophotometry of the Open Cluster M67'. In: *Astron. J.* 112, p. 628. DOI: 10.1086/118039. eprint: astro-ph/9604178.

Ferraro, F. R., B. Paltrinieri, F. Fusi Pecci, C. Cacciari, B. Dorman, R. T. Rood, R. Buonanno, C. E. Corsi, D. Burgarella, and M. Laget (1997). 'HST observations of blue Straggler stars in the core of the globular cluster M 3.' In: *A&A* 324, pp. 915–928. eprint: astro-ph/9703026.

Ferraro, F. R. et al. (2006). 'Discovery of Carbon/Oxygen-depleted Blue Straggler Stars in 47 Tucanae: The Chemical Signature of a Mass Transfer Formation Process'. In: *ApJL* 647, pp. L53–L56. DOI: 10.1086/507327. eprint: astro-ph/0610081.

Ferraro, F. R. et al. (2012). 'Dynamical age differences among coeval star clusters as revealed by blue stragglers'. In: *Nature* 492, pp. 393–395. DOI: 10.1038/nature11686. arXiv: 1212.5071 [astro-ph.SR].

Ferraro, F. R., B. Lanzoni, E. Dalessandro, A. Mucciarelli, and L. Lovisi (2015). 'Blue Straggler Stars in Globular Clusters: A Powerful Tool to Probe the Internal Dynamical Evolution of Stellar Systems'. In: *Ecology of Blue Straggler Stars*. Ed. by H. M. J. Boffin, G. Carraro, and G. Beccari, p. 99. DOI: 10.1007/978-3-662-44434-4_5.

Fossati, L., S. Bagnulo, R. Monier, S. A. Khan, O. Kochukhov, J. Landstreet, G. Wade, and W. Weiss (2007). 'Late stages of the evolution of A-type stars on the main sequence: comparison between observed chemical abundances and diffusion models for 8 Am stars of the Praesepe cluster'. In: *A&A* 476, pp. 911–925. DOI: 10.1051/0004-6361:20078320. arXiv: 0710.0579.

Fossati, L., C. P. Folsom, S. Bagnulo, J. H. Grunhut, O. Kochukhov, J. D. Landstreet, C. Paladini, and G. A. Wade (2011). 'A detailed spectroscopic analysis of the open cluster NGC 5460'. In: *MNRAS* 413, pp. 1132–1144. DOI: 10.1111/j.1365-2966.2011.18199.x. arXiv: 1012.3050 [astro-ph.SR].

François, P., L. Pasquini, K. Biazzo, P. Bonifacio, and R. Palsa (2013). 'Lithium abundance in the metal-poor open cluster NGC 2243 '. In: *A&A* 552, A136, A136. DOI: 10.1051/0004-6361/201220958. arXiv: 1303.3027 [astro-ph.SR].

Freeman, K. and J. Bland-Hawthorn (2002). 'The New Galaxy: Signatures of Its Formation'. In: *ARA&A* 40, pp. 487–537. DOI: 10.1146/annurev.astro.40.060401.093840. eprint: astro-ph/0208106.

Friel, E. D. (1995). 'The Old Open Clusters Of The Milky Way'. In: *ARA&A* 33, pp. 381–414. DOI: 10.1146/annurev.aa.33.090195.002121.

Friel, E. D., H. R. Jacobson, and C. A. Pilachowski (2010). 'Abundances of Red Giants in Old Open Clusters. V. Be 31, Be 32, Be 39, M 67, NGC 188, and NGC 1193'. In: *Astron. J.* 139, pp. 1942–1967. DOI: 10.1088/0004-6256/139/5/1942.

Frinchaboy, P. M. et al. (2013). 'The Open Cluster Chemical Analysis and Mapping Survey: Local Galactic Metallicity Gradient with APOGEE Using SDSS DR10'. In: *ApJL* 777, L1, p. L1. DOI: 10.1088/2041-8205/777/1/L1. arXiv: 1308.4195.

Froebrich, D., S. Schmeja, D. Samuel, and P. W. Lucas (2010). 'Old star clusters in the FSR catalogue'. In: *MNRAS* 409, pp. 1281–1288. DOI: 10.1111/j.1365-2966.2010.17390.x. arXiv: 1007.3410.

Frolov, V. N. and Y. K. Ananyevskaya (1986). 'Photometry and Proper Motions of Stars in the Open Cluster M67 = NGC2682'. In: *Astronomicheskij Tsirkulyar* 1432, p. 4.

Fusi Pecci, F., F. R. Ferraro, and C. Cacciari (1993). 'Blue Stragglers in Galactic Globular Clusters: A Revised Catalog, the Special Case of M3; and Some General Remarks'. In: *Blue Stragglers*. Ed. by R. A. Saffer. Vol. 53. Astronomical Society of the Pacific Conference Series, p. 97.

Gaia Collaboration et al. (2016). 'Gaia Data Release 1. Summary of the astrometric, photometric, and survey properties'. In: *A&A* 595, A2, A2. DOI: 10.1051/0004-6361/201629512. arXiv: 1609.04172 [astro-ph.IM].

García Pérez, A. E. et al. (2016). 'ASPCAP: The APOGEE Stellar Parameter and Chemical Abundances Pipeline'. In: *Astron. J.* 151, 144, p. 144. DOI: 10.3847/0004-6256/151/6/144. arXiv: 1510.07635 [astro-ph.SR].

Geller, A. M., D. W. Latham, and R. D. Mathieu (2015). 'Stellar Radial Velocities in the Old Open Cluster M67 (NGC 2682). I. Memberships, Binaries, and Kinematics'. In: *Astron. J.* 150, 97, p. 97. DOI: 10.1088/0004-6256/150/3/97. arXiv: 1507.01949 [astro-ph.SR].

Geller, A. M., R. D. Mathieu, H. C. Harris, and R. D. McClure (2008). 'WIYN Open Cluster Study. XXXII. Stellar Radial Velocities in the Old Open Cluster NGC 188'. In: *Astron. J.* 135, pp. 2264–2278. DOI: 10.1088/0004-6256/135/6/2264. arXiv: 1512.04983 [astro-ph.SR].

Getman, K. V., E. D. Feigelson, G. Garmire, P. Broos, and J. Wang (2007). 'X-Ray Study of Triggered Star Formation and Protostars in IC 1396N'. In: *ApJ* 654, pp. 316–337. DOI: 10.1086/509112. eprint: astro-ph/0607006.

Getman, K. V., E. D. Feigelson, A. Sicilia-Aguilar, P. S. Broos, M. A. Kuhn, and G. P. Garmire (2012). 'The Elephant Trunk Nebula and the Trumpler 37 cluster: contribution of triggered star formation to the total population of an H II region'. In: *MNRAS* 426, pp. 2917–2943. DOI: 10.1111/j.1365-2966.2012.21879.x. arXiv: 1208.1471 [astro-ph.SR].

Giampapa, M. S., J. C. Hall, R. R. Radick, and S. L. Baliunas (2006). 'A Survey of Chromospheric Activity in the Solar-Type Stars in the Open Cluster M67'. In: *ApJ* 651, pp. 444–461. DOI: 10.1086/507624. eprint: astro-ph/0607313.

Gilliland, R. L. and T. M. Brown (1992). 'The oscillating blue stragglers in the open cluster M67'. In: *Astron. J.* 103, pp. 1945–1954. DOI: 10.1086/116203.

Gilliland, R. L., T. M. Brown, D. K. Duncan, N. B. Suntzeff, G. W. Lockwood, D. T. Thompson, R. E. Schild, W. A. Jeffrey, and B. E. Penprase (1991). 'Time-resolved CCD photometry of an ensemble of stars in the open cluster M67'. In: *Astron. J.* 101, pp. 541–561. DOI: 10.1086/115703.

Gilmore, G. et al. (2012). 'The Gaia-ESO Public Spectroscopic Survey'. In: *The Messenger* 147, pp. 25–31.

Gilroy, K. K. and J. A. Brown (1991). 'Carbon isotope ratios along the giant branch of M67'. In: *ApJ* 371, pp. 578–583. DOI: 10.1086/169922.

Girard, T. M., W. M. Grundy, C. E. Lopez, and W. F. van Altena (1989). 'Relative proper motions and the stellar velocity dispersion of the open cluster M67'. In: *Astron. J.* 98, pp. 227–243. DOI: 10.1086/115139.

González Hernández, J. I. and P. Bonifacio (2009). 'A new implementation of the infrared flux method using the 2MASS catalogue'. In: *A&A* 497, pp. 497–509. DOI: 10.1051/0004-6361/200810904. arXiv: 0901.3034 [astro-ph.SR].

Gonzalez, G. (2016a). 'A revised gyro-age for M67 from Kepler/K2-Campaign-5 light curves'. In: *MNRAS* 463, pp. 3513–3519. DOI: 10.1093/mnras/stw2237. arXiv: 1609.00601 [astro-ph.SR].

— (2016b). 'Variability among stars in the M 67 field from Kepler/K2-Campaign-5 light curves'. In: *MNRAS* 459, pp. 1060–1068. DOI: 10.1093/mnras/stw700. arXiv: 1603.06638 [astro-ph.SR].

Gratton, R. G., E. Carretta, and A. Bragaglia (2012). 'Multiple populations in globular clusters. Lessons learned from the Milky Way globular clusters'. In: *A&ARv* 20, 50, p. 50. DOI: 10.1007/s00159-012-0050-3. arXiv: 1201.6526 [astro-ph.SR].

Gratton, R. G., C. Sneden, E. Carretta, and A. Bragaglia (2000). 'Mixing along the red giant branch in metal-poor field stars'. In: *A&A* 354, pp. 169–187.

Gratton, R., C. Sneden, and E. Carretta (2004). 'Abundance Variations Within Globular Clusters'. In: *ARA&A* 42, pp. 385–440. DOI: 10.1146/annurev.astro.42.053102.133945.

Gruyters, P., T. Nordlander, and A. J. Korn (2014). 'Atomic diffusion and mixing in old stars. V. A deeper look into the globular cluster NGC 6752'. In: *A&A* 567, A72, A72. DOI: 10.1051/0004-6361/201423590. arXiv: 1405.6543 [astro-ph.SR].

Gruyters, P., A. J. Korn, O. Richard, F. Grundahl, R. Collet, L. I. Mashonkina, Y. Osorio, and P. S. Barklem (2013). 'Atomic diffusion and mixing in old stars. IV. Weak abundance trends in the globular cluster NGC 6752'. In: *A&A* 555, A31, A31. DOI: 10.1051/0004-6361/201220821. arXiv: 1305.1774 [astro-ph.SR].

Gruyters, P., K. Lind, O. Richard, F. Grundahl, M. Asplund, L. Casagrande, C. Charbonnel, A. Milone, F. Primas, and A. J. Korn (2016). 'Atomic diffusion and mixing in old stars. VI. The lithium content of M30'. In: *A&A* 589, A61, A61. DOI: 10.1051/0004-6361/201527948. arXiv: 1603.01565 [astro-ph.SR].

Hansen, C. J. and S. D. Kawaler (1994). *Stellar Interiors. Physical Principles, Structure, and Evolution.* P. 84.

Hanson, M. M. (2003). 'A Study of Cygnus OB2: Pointing the Way toward Finding Our Galaxy's Super-Star Clusters'. In: *ApJ* 597, pp. 957–969. DOI: 10.1086/378508. eprint: astro-ph/0307540.

Hills, J. G. and C. A. Day (1976). 'Stellar Collisions in Globular Clusters'. In: *Astrophysical Lett.* 17, p. 87.

Høg, E., C. Fabricius, V. V. Makarov, S. Urban, T. Corbin, G. Wycoff, U. Bastian, P. Schwekendiek, and A. Wicenec (2000). 'The Tycho-2 catalogue of the 2.5 million brightest stars'. In: *A&A* 355, pp. L27–L30.

Holtzman, J. A. et al. (2015). 'Abundances, Stellar Parameters, and Spectra from the SDSS-III/APOGEE Survey'. In: *Astron. J.* 150, 148, p. 148. DOI: 10.1088/0004-6256/150/5/148. arXiv: 1501.04110.

Howell, S. B. et al. (2014). 'The K2 Mission: Characterization and Early Results'. In: *PASP* 126, p. 398. DOI: 10.1086/676406. arXiv: 1402.5163 [astro-ph.IM].

Hurley, J. R., C. A. Tout, S. J. Aarseth, and O. R. Pols (2001). 'Direct N-body modelling of stellar populations: blue stragglers in M67'. In: *MNRAS* 323, pp. 630–650. DOI: 10.1046/j.1365-8711.2001.04220.x. eprint: astro-ph/0012113.

Hurley, J. R., O. R. Pols, S. J. Aarseth, and C. A. Tout (2005). 'A complete N-body model of the old open cluster M67'. In: *MNRAS* 363, pp. 293–314. DOI: 10.1111/j.1365-2966.2005.09448.x. eprint: astro-ph/0507239.

Jacobson, H. R. et al. (2016). 'The Gaia-ESO Survey: Probes of the inner disk abundance gradient'. In: *A&A* 591, A37, A37. DOI: 10.1051/0004-6361/201527654. arXiv: 1605.04899.

Janes, K. A. and R. L. Phelps (1994). 'The galactic system of old star clusters: The development of the galactic disk'. In: *Astron. J.* 108, pp. 1773–1785. DOI: 10.1086/117192.

Jofré, P. and A. Weiss (2011). 'The age of the Milky Way halo stars from the Sloan Digital Sky Survey'. In: *A&A* 533, A59, A59. DOI: 10.1051/0004-6361/201117131. arXiv: 1105.2022.

Johnson, H. L. and A. R. Sandage (1955). 'The galactic cluster M67 and its significance for stellar evolution'. In: *ApJ* 121, p. 616. DOI: 10.1086/146027.

Jordi, C., E. Trullols, and D. Galadi-Enriquez (1996). 'Cepheus OB3 association: faint members.' In: *A&A* 312, pp. 499–507.

Kayser, A., M. Hilker, E. K. Grebel, and P. G. Willemsen (2008). 'Comparing CN and CH line strengths in a homogeneous spectroscopic sample of 8 Galactic globular clusters'. In: *A&A* 486, pp. 437–452. DOI: 10.1051/0004-6361:200809446. arXiv: 0805.1067.

Kerr, F. J. and D. Lynden-Bell (1986). 'Review of galactic constants'. In: *MNRAS* 221, pp. 1023–1038. DOI: 10.1093/mnras/221.4.1023.

Kharchenko, N. V., A. E. Piskunov, E. Schilbach, S. Röser, and R.-D. Scholz (2013). 'Global survey of star clusters in the Milky Way. II. The catalogue of basic parameters'. In: *A&A* 558, A53, A53. DOI: 10.1051/0004-6361/201322302. arXiv: 1308.5822.

Kılıçoğlu, T., R. Monier, J. Richer, L. Fossati, and B. Albayrak (2016). 'Chemical Composition of Intermediate-mass Star Members of the M6 (NGC 6405) Open Cluster'. In: *Astron. J.* 151, 49, p. 49. DOI: 10.3847/0004-6256/151/3/49. arXiv: 1510.05385 [astro-ph.SR].

Kim, S.-L., M. Y. Chun, B.-G. Park, and S.-W. Lee (1996). 'Variable stars in a Field of the Old Open Cluster M67: Photometric Precision of the BOAO 1.8m Telescope'. In: *Journal of Korean Astronomical Society* 29, pp. 43–51.

Kinman, T. D. (1965). 'The Star Cluster NGC 6791.' In: *ApJ* 142, p. 655. DOI: 10.1086/148329.

Knödlseder, J. (2000). 'Cygnus OB2 - a young globular cluster in the Milky Way'. In: *A&A* 360, pp. 539–548. eprint: astro-ph/0007442.

— (2003). 'Cygnus OB2 at all wavelengths'. In: *A Massive Star Odyssey: From Main Sequence to Supernova*. Ed. by K. van der Hucht, A. Herrero, and C. Esteban. Vol. 212. IAU Symposium, p. 505.

Korn, A. J., F. Grundahl, O. Richard, L. Mashonkina, P. S. Barklem, R. Collet, B. Gustafsson, and N. Piskunov (2007). 'Atomic Diffusion and Mixing in Old

Stars. I. Very Large Telescope FLAMES-UVES Observations of Stars in NGC 6397'. In: *ApJ* 671, pp. 402–419. DOI: 10.1086/523098. arXiv: 0709.0639.

Kozai, Y. (1962). 'Secular perturbations of asteroids with high inclination and eccentricity'. In: *Astron. J.* 67, p. 591. DOI: 10.1086/108790.

Krishna Swamy, K. S. (1966). 'Profiles of Strong Lines in K-Dwarfs'. In: *ApJ* 145, p. 174. DOI: 10.1086/148752.

Kun, M., L. G. Balazs, and I. Toth (1987). 'Giant infrared bubble in Cepheus'. In: *Ap&SS* 134, pp. 211–217. DOI: 10.1007/BF01094933.

Kun, M., Z. T. Kiss, and Z. Balog (2008). 'Star Forming Regions in Cepheus'. In: *Handbook of Star Forming Regions, Volume I*. Ed. by B. Reipurth, p. 136.

Lada, C. J. and E. A. Lada (2003). 'Embedded Clusters in Molecular Clouds'. In: *ARA&A* 41, pp. 57–115. DOI: 10.1146/annurev.astro.41.011802.094844. eprint: astro-ph/0301540.

Landsman, W., J. Aparicio, P. Bergeron, R. Di Stefano, and T. P. Stecher (1997). 'S1040 in M67: A Post–Mass Transfer Binary with a Helium Core White Dwarf'. In: *ApJL* 481, pp. L93–L96. DOI: 10.1086/310654. eprint: astro-ph/9703053.

Latham, D. W. and A. A. E. Milone (1996). 'Spectroscopic Binaries Among the M67 Blue Stragglers'. In: *The Origins, Evolution, and Destinies of Binary Stars in Clusters*. Ed. by E. F. Milone and J.-C. Mermilliod. Vol. 90. Astronomical Society of the Pacific Conference Series, p. 385.

Latham, D. W., R. D. Mathieu, A. A. E. Milone, and R. J. Davis (1992). 'Spectroscopic Binaries in the Open Cluster M67'. In: *IAU Colloq. 135: Complementary Approaches to Double and Multiple Star Research*. Ed. by H. A. McAlister and W. I. Hartkopf. Vol. 32. Astronomical Society of the Pacific Conference Series, p. 152.

Leigh, N. and A. Sills (2011). 'An analytic technique for constraining the dynamical origins of multiple star systems containing merger products'. In: *MNRAS* 410, pp. 2370–2384. DOI: 10.1111/j.1365-2966.2010.17609.x. arXiv: 1009.0461 [astro-ph.SR].

Leiner, E., R. D. Mathieu, D. Stello, A. Vanderburg, and E. Sandquist (2016). 'The K2 M67 Study: An Evolved Blue Straggler in M67 from K2 Mission Asteroseismology'. In: *ApJL* 832, L13, p. L13. DOI: 10.3847/2041-8205/832/1/L13. arXiv: 1611.01158 [astro-ph.SR].

Leonard, P. J. T. and A. P. Linnell (1992). 'On the possibility of a collisional origin for the blue stragglers and contact binaries in the old open clusters M67 and NGC 188'. In: *Astron. J.* 103, pp. 1928–1944. DOI: 10.1086/116202.

Lind, K., M. Bergemann, and M. Asplund (2012). 'Non-LTE line formation of Fe in late-type stars - II. 1D spectroscopic stellar parameters'. In: *MNRAS* 427, pp. 50–60. DOI: 10.1111/j.1365-2966.2012.21686.x. arXiv: 1207.2454 [astro-ph.SR].

Lind, K., A. J. Korn, P. S. Barklem, and F. Grundahl (2008). 'Atomic diffusion and mixing in old stars. II. Observations of stars in the globular cluster NGC 6397 with VLT/FLAMES-GIRAFFE'. In: *A&A* 490, pp. 777–786. DOI: 10.1051/0004-6361:200810051. arXiv: 0809.0317.

Lind, K., M. Asplund, P. S. Barklem, and A. K. Belyaev (2011). 'Non-LTE calculations for neutral Na in late-type stars using improved atomic data'. In:

A&A 528, A103, A103. DOI: 10.1051/0004-6361/201016095. arXiv: 1102.2160 [astro-ph.SR].

Liu, F., M. Asplund, D. Yong, J. Meléndez, I. Ramírez, A. I. Karakas, M. Carlos, and A. F. Marino (2016). 'The chemical compositions of solar twins in the open cluster M67'. In: *MNRAS* 463, pp. 696–704. DOI: 10.1093/mnras/stw2045. arXiv: 1608.03788 [astro-ph.SR].

Liu, G. Q., L. Deng, M. Chávez, E. Bertone, A. H. Davo, and M. D. Mata-Chávez (2008). 'A spectroscopic study of the blue stragglers in M67'. In: *MNRAS* 390, pp. 665–674. DOI: 10.1111/j.1365-2966.2008.13741.x. arXiv: 0811.2553.

Lombardi C. Jr., J., F. A. Rasio, and S. L. Shapiro (1995). 'On blue straggler formation by direct collisions of main sequence stars'. In: *ApJL* 445, pp. L117–L120. DOI: 10.1086/187903. eprint: astro-ph/9502106.

Lovisi, L. et al. (2010). 'Fast Rotating Blue Stragglers in the Globular Cluster M4'. In: *ApJL* 719, pp. L121–L125. DOI: 10.1088/2041-8205/719/2/L121. arXiv: 1007.2343.

Lovisi, L., A. Mucciarelli, B. Lanzoni, F. R. Ferraro, E. Dalessandro, and L. Monaco (2013). 'Flames and XSHOOTER Spectroscopy along the Two Blue Straggler Star Sequences of M30'. In: *ApJ* 772, 148, p. 148. DOI: 10.1088/0004-637X/772/2/148. arXiv: 1306.0839.

Lozinskaya, T. A., T. G. Sitnik, and M. S. Toropova (1987). 'Gas-Dust Complex NGC7822+171/W:1 Connected with the Association CEPHEUS-OB4'. In: *Soviet Astr.* 31, p. 493.

MacConnell, D. J. (1968). 'A Study of the Cepheus IV Association'. In: *ApJ Suppl.* 16, p. 275. DOI: 10.1086/190175.

Magrini, L. et al. (2017). 'The Gaia-ESO Survey: radial distribution of abundances in the Galactic disc from open clusters and young field stars'. In: *ArXiv e-prints*. arXiv: 1703.00762.

Maiorca, E., H. Uitenbroek, S. Uttenthaler, S. Randich, M. Busso, and L. Magrini (2014). 'A New Solar Fluorine Abundance and a Fluorine Determination in the Two Open Clusters M67 and NGC 6404'. In: *ApJ* 788, 149, p. 149. DOI: 10.1088/0004-637X/788/2/149. arXiv: 1404.5755 [astro-ph.SR].

Majewski, S. R. et al. (2015). 'The Apache Point Observatory Galactic Evolution Experiment (APOGEE)'. In: *ArXiv e-prints*. arXiv: 1509.05420 [astro-ph.IM].

Marino, A. F. et al. (2016). 'Chemical abundances in the multiple sub-giant branch of 47 Tucanae: insights on its faint sub-giant branch component'. In: *MNRAS* 459, pp. 610–623. DOI: 10.1093/mnras/stw611. arXiv: 1603.02012 [astro-ph.SR].

Marschall, L. A., G. B. Karshner, and N. F. Comins (1990). 'Photometry of the young open cluster Trumpler 37'. In: *Astron. J.* 99, pp. 1536–1547. DOI: 10.1086/115437.

Marschall, L. A. and W. F. van Altena (1987). 'Membership in the young cluster Trumpler 37'. In: *Astron. J.* 94, pp. 71–83. DOI: 10.1086/114448.

Martig, M., M. Fouesneau, H.-W. Rix, M. Ness, S. Mészáros, D. A. García-Hernández, M. Pinsonneault, A. Serenelli, V. Silva Aguirre, and O. Zamora (2016). 'Red giant masses and ages derived from carbon and nitrogen abundances'. In: *MNRAS* 456, pp. 3655–3670. DOI: 10.1093/mnras/stv2830. arXiv: 1511.08203 [astro-ph.SR].

Martin, A. J., M. J. Stift, L. Fossati, S. Bagnulo, C. Scalia, F. Leone, and B. Smalley (2017). 'A spectroscopic study of the open cluster NGC 6250'. In: *MNRAS* 466, pp. 613–627. DOI: `10.1093/mnras/stw3052`. arXiv: `1612.05739 [astro-ph.SR]`.

Masseron, T. and G. Gilmore (2015). 'Carbon, nitrogen and α-element abundances determine the formation sequence of the Galactic thick and thin discs'. In: *MNRAS* 453, pp. 1855–1866. DOI: `10.1093/mnras/stv1731`. arXiv: `1503.00537 [astro-ph.SR]`.

Mathieu, R. D. and A. M. Geller (2009). 'A binary star fraction of 76 per cent and unusual orbit parameters for the blue stragglers of NGC 188'. In: *Nature* 462, pp. 1032–1035. DOI: `10.1038/nature08568`.

Mathieu, R. D., D. W. Latham, and R. F. Griffin (1990). 'Orbits of 22 spectroscopic binaries in the open cluster M67'. In: *Astron. J.* 100, pp. 1859–1881. DOI: `10.1086/115643`.

Mathieu, R. D., D. W. Latham, R. F. Griffin, and J. E. Gunn (1986). 'Precise radial velocities of late-type stars in the open clusters M11 and M67'. In: *Astron. J.* 92, pp. 1100–1117. DOI: `10.1086/114240`.

Mathieu, R. D., M. van den Berg, G. Torres, D. Latham, F. Verbunt, and K. Stassun (2003). 'Sub-Subgiants in the Old Open Cluster M67?' In: *Astron. J.* 125, pp. 246–259. DOI: `10.1086/344944`. eprint: `astro-ph/0209568`.

Mathys, G. (1991). 'The blue stragglers of M67'. In: *A&A* 245, pp. 467–484.

McCrea, W. H. (1964). 'Extended main-sequence of some stellar clusters'. In: *MNRAS* 128, p. 147. DOI: `10.1093/mnras/128.2.147`.

Mdzinarishvili, T. G. and K. B. Chargeishvili (2005). 'New runaway OB stars with HIPPARCOS'. In: *A&A* 431, pp. L1–L4. DOI: `10.1051/0004-6361:200400134`.

Melo, C. H. F., L. Pasquini, and J. R. De Medeiros (2001). 'Accurate Vsin i measurements in M 67: The angular momentum evolution of 1.2 M_{sun} stars'. In: *A&A* 375, pp. 851–862. DOI: `10.1051/0004-6361:20010897`.

Mercer, E. P., J. M. Miller, N. Calvet, L. Hartmann, J. Hernandez, A. Sicilia-Aguilar, and R. Gutermuth (2009). 'Chandra and Spitzer Observations Reveal New YSOs in the Heart of Trumpler 37'. In: *Astron. J.* 138, pp. 7–18. DOI: `10.1088/0004-6256/138/1/7`.

Michalik, D., L. Lindegren, and D. Hobbs (2015). 'The Tycho-Gaia astrometric solution . How to get 2.5 million parallaxes with less than one year of Gaia data'. In: *A&A* 574, A115, A115. DOI: `10.1051/0004-6361/201425310`. arXiv: `1412.8770 [astro-ph.IM]`.

Michaud, G., G. Alecian, and J. Richer (2015). *Atomic Diffusion in Stars*. Springer International Publishing, Switzerland. DOI: `10.1007/978-3-319-19854-5`.

Michaud, G., O. Richard, J. Richer, and D. A. VandenBerg (2004). 'Models for Solar Abundance Stars with Gravitational Settling and Radiative Accelerations: Application to M67 and NGC 188'. In: *ApJ* 606, pp. 452–465. DOI: `10.1086/383001`. eprint: `astro-ph/0402544`.

Mooley, K. P. and K. P. Singh (2015). 'Study of X-ray emission from the old open cluster, M67'. In: *MNRAS* 452, pp. 3394–3407. DOI: `10.1093/mnras/stv1472`. arXiv: `1507.00759 [astro-ph.HE]`.

Morbidelli, L., P. Patriarchi, M. Perinotto, G. Barbaro, and A. di Bartolomeo (1997). 'Dust properties in the direction of Trumpler 37.' In: *A&A* 327, pp. 125–129.

Mucciarelli, A., L. Lovisi, F. R. Ferraro, E. Dalessandro, B. Lanzoni, and L. Monaco (2014). 'Spinning Like a Blue Straggler: The Population of Fast Rotating Blue Straggler Stars in ω Centauri'. In: *ApJ* 797, 43, p. 43. DOI: 10.1088/0004-637X/797/1/43. arXiv: 1410.2275 [astro-ph.SR].

Münch, L. and W. W. Morgan (1953). 'Notes: A Probable Clustering of Blue Giants in Cygnus.' In: *ApJ* 118, pp. 161–162. DOI: 10.1086/145737.

Murakami, H. et al. (2007). 'The Infrared Astronomical Mission AKARI*'. In: *PASJ* 59, S369–S376. DOI: 10.1093/pasj/59.sp2.S369. arXiv: 0708.1796.

Nakano, M., K. Sugitani, M. Watanabe, N. Fukuda, D. Ishihara, and M. Ueno (2012). 'Wide-field Survey of Emission-line Stars in IC 1396'. In: *Astron. J.* 143, 61, p. 61. DOI: 10.1088/0004-6256/143/3/61. arXiv: 1201.2761 [astro-ph.SR].

Naoz, S. and D. C. Fabrycky (2014). 'Mergers and Obliquities in Stellar Triples'. In: *ApJ* 793, 137, p. 137. DOI: 10.1088/0004-637X/793/2/137. arXiv: 1405.5223 [astro-ph.SR].

Nardiello, D., M. Libralato, L. R. Bedin, G. Piotto, L. Borsato, V. Granata, L. Malavolta, and V. Nascimbeni (2016a). 'A PSF-based approach to Kepler/K2 data - III. Search for exoplanets and variable stars within the open cluster M 67 (NGC 2682)'. In: *MNRAS* 463, pp. 1831–1843. DOI: 10.1093/mnras/stw2169. arXiv: 1608.08539 [astro-ph.SR].

Nardiello, D., M. Libralato, L. R. Bedin, G. Piotto, P. Ochner, A. Cunial, L. Borsato, and V. Granata (2016b). 'Variable stars in one open cluster within the Kepler/K2-Campaign-5 field: M 67 (NGC 2682)'. In: *MNRAS* 455, pp. 2337–2344. DOI: 10.1093/mnras/stv2439. arXiv: 1510.05693 [astro-ph.SR].

Nault, K. A. and C. A. Pilachowski (2013). 'The Abundance of Fluorine in the Hyades, NGC 752, and M67'. In: *Astron. J.* 146, 153, p. 153. DOI: 10.1088/0004-6256/146/6/153.

Ness, M. et al. (2017). 'Galactic Doppelganger: The chemical similarity among field stars and among stars with a common birth origin'. In: *ArXiv e-prints*. arXiv: 1701.07829 [astro-ph.SR].

Nordlander, T. and K. Lind (2017). 'Non-LTE aluminium abundances in late-type stars'. In: *ArXiv e-prints*. arXiv: 1708.01949 [astro-ph.SR].

Nordlander, T., A. J. Korn, O. Richard, and K. Lind (2012). 'Atomic Diffusion and Mixing in Old Stars. III. Analysis of NGC 6397 Stars under New Constraints'. In: *ApJ* 753, 48, p. 48. DOI: 10.1088/0004-637X/753/1/48. arXiv: 1204.5600 [astro-ph.SR].

Olano, C. A., P. I. Meschin, and V. S. Niemela (2006). 'The interstellar medium in the Upper Cepheus-Cassiopeia region'. In: *MNRAS* 369, pp. 867–874. DOI: 10.1111/j.1365-2966.2006.10343.x.

Önehag, A., B. Gustafsson, and A. Korn (2014). 'Abundances and possible diffusion of elements in M 67 stars'. In: *A&A* 562, A102, A102. DOI: 10.1051/0004-6361/201322663. arXiv: 1310.6297 [astro-ph.SR].

Önehag, A., A. Korn, B. Gustafsson, E. Stempels, and D. A. Vandenberg (2011). 'M67-1194, an unusually Sun-like solar twin in M67'. In: *A&A* 528, A85, A85. DOI: 10.1051/0004-6361/201015138. arXiv: 1009.4579 [astro-ph.SR].

Pace, G., L. Pasquini, and P. François (2008). 'Abundances of four open clusters from solar stars'. In: *A&A* 489, pp. 403–412. DOI: 10.1051/0004-6361:200809969. arXiv: 0806.2280.

Pace, G., M. Castro, J. Meléndez, S. Théado, and J.-D. do Nascimento Jr. (2012). 'Lithium in M 67: From the main sequence to the red giant branch'. In: *A&A* 541, A150, A150. DOI: `10.1051/0004-6361/201117704`. arXiv: `1203.4440 [astro-ph.SR]`.

Pasquali, A. and M. Perinotto (1993). 'Chemical behavior of planetary nebulae and galactic abundance gradients'. In: *A&A* 280, pp. 581–591.

Pasquini, L. and T. Belloni (1998). 'Optical identification of ROSAT sources in M 67: activity in an old cluster'. In: *A&A* 336, pp. 902–910. eprint: `astro-ph/9805364`.

Pasquini, L., T. Belloni, and T. M. C. Abbott (1994). 'Optical identification of two soft ROSAT sources in the old open cluster M67'. In: *A&A* 290.

Pasquini, L., S. Randich, and R. Pallavicini (1997). 'Lithium in M 67: evidence for spread in a solar age cluster.' In: *A&A* 325, pp. 535–541.

— (2001). 'Lithium in the intermediate age cluster <ASTROBJ>NGC 3680</ASTROBJ>: Following Li evolution along the C-M diagram'. In: *A&A* 374, pp. 1017–1029. DOI: `10.1051/0004-6361:20010822`.

Pasquini, L. et al. (2002). 'Installation and commissioning of FLAMES, the VLT Multifibre Facility'. In: *The Messenger* 110, pp. 1–9.

Pasquini, L., K. Biazzo, P. Bonifacio, S. Randich, and L. R. Bedin (2008). 'Solar twins in M 67'. In: *A&A* 489, pp. 677–684. DOI: `10.1051/0004-6361:200809714`. arXiv: `0807.0092`.

Pasquini, L., A. Brucalassi, M. T. Ruiz, P. Bonifacio, C. Lovis, R. Saglia, C. Melo, K. Biazzo, S. Randich, and L. R. Bedin (2012). 'Search for giant planets in M 67. I. Overview'. In: *A&A* 545, A139, A139. DOI: `10.1051/0004-6361/201219169`. arXiv: `1206.5820 [astro-ph.EP]`.

Patel, N. A., P. F. Goldsmith, M. H. Heyer, R. L. Snell, and P. Pratap (1998). 'Origin and Evolution of the Cepheus Bubble'. In: *ApJ* 507, pp. 241–253. DOI: `10.1086/306305`.

Perets, H. B. and D. C. Fabrycky (2009). 'On the Triple Origin of Blue Stragglers'. In: *ApJ* 697, pp. 1048–1056. DOI: `10.1088/0004-637X/697/2/1048`. arXiv: `0901.4328 [astro-ph.SR]`.

Pichardo, B., E. Moreno, C. Allen, L. R. Bedin, A. Bellini, and L. Pasquini (2012). 'The Sun was Not Born in M67'. In: *Astron. J.* 143, 73, p. 73. DOI: `10.1088/0004-6256/143/3/73`. arXiv: `1201.0987`.

Pietrinferni, A., S. Cassisi, M. Salaris, and F. Castelli (2004). 'A Large Stellar Evolution Database for Population Synthesis Studies. I. Scaled Solar Models and Isochrones'. In: *ApJ* 612, pp. 168–190. DOI: `10.1086/422498`. eprint: `astro-ph/0405193`.

Pribulla, T. et al. (2008). 'MOST satellite photometry of stars in the M67 field: eclipsing binaries, blue stragglers and δ Scuti variables'. In: *MNRAS* 391, pp. 343–353. DOI: `10.1111/j.1365-2966.2008.13889.x`. arXiv: `0809.0503`.

Qian, S.-B., L. Liu, B. Soonthornthum, L.-Y. Zhu, and J.-J. He (2006). 'Deep, Low Mass Ratio Overcontact Binary Systems. VI. AH Cancri in the Old Open Cluster M67'. In: *Astron. J.* 131, pp. 3028–3039. DOI: `10.1086/503561`.

Randich, S., G. Gilmore, and Gaia-ESO Consortium (2013). 'The Gaia-ESO Large Public Spectroscopic Survey'. In: *The Messenger* 154, pp. 47–49.

Randich, S., P. Sestito, F. Primas, R. Pallavicini, and L. Pasquini (2006). 'Element abundances of unevolved stars in the open cluster M 67'. In: *A&A* 450, pp. 557–567. DOI: 10.1051/0004-6361:20054291. eprint: astro-ph/0601239.

Randich, S., F. Primas, L. Pasquini, P. Sestito, and R. Pallavicini (2007). 'Tracing mixing in stars: new beryllium observations of the open clusters NGC 2516, Hyades, and M 67'. In: *A&A* 469, pp. 163–172. DOI: 10.1051/0004-6361:20066218. arXiv: 0705.2330.

Reddish, V. C., L. C. Lawrence, and N. M. Pratt (1966). 'The Cygnus II association 2. The Distribution of Stars and Interstellar Matter'. In: *Publications of the Royal Observatory of Edinburgh* 5, pp. 111–180.

Reiners, A. and M. S. Giampapa (2009). 'The Origin of Enhanced Activity in the Suns of M67'. In: *ApJ* 707, pp. 852–857. DOI: 10.1088/0004-637X/707/1/852. arXiv: 0911.0424 [astro-ph.SR].

Reipurth, B. and N. Schneider (2008). 'Star Formation and Young Clusters in Cygnus'. In: *Handbook of Star Forming Regions, Volume I*. Ed. by B. Reipurth, p. 36.

Richard, O., G. Michaud, and J. Richer (2001). 'Iron Convection Zones in B, A, and F Stars'. In: *ApJ* 558, pp. 377–391. DOI: 10.1086/322264.

Richard, O., G. Michaud, J. Richer, S. Turcotte, S. Turck-Chièze, and D. A. Vanden-Berg (2002). 'Models of Metal-poor Stars with Gravitational Settling and Radiative Accelerations. I. Evolution and Abundance Anomalies'. In: *ApJ* 568, pp. 979–997. DOI: 10.1086/338952.

Richer, H. B., G. G. Fahlman, J. Rosvick, and R. Ibata (1998). 'The White Dwarf Cooling Age of M67'. In: *ApJL* 504, pp. L91–L94. DOI: 10.1086/311586. eprint: astro-ph/9806172.

Roeser, S., M. Demleitner, and E. Schilbach (2010). 'The PPMXL Catalog of Positions and Proper Motions on the ICRS. Combining USNO-B1.0 and the Two Micron All Sky Survey (2MASS)'. In: *Astron. J.* 139, pp. 2440–2447. DOI: 10.1088/0004-6256/139/6/2440. arXiv: 1003.5852.

Rygl, K. L. J., A. Brunthaler, A. Sanna, K. M. Menten, M. J. Reid, H. J. van Langevelde, M. Honma, K. J. E. Torstensson, and K. Fujisawa (2012). 'Parallaxes and proper motions of interstellar masers toward the Cygnus X star-forming complex. I. Membership of the Cygnus X region'. In: *A&A* 539, A79, A79. DOI: 10.1051/0004-6361/201118211. arXiv: 1111.7023.

SDSS Collaboration et al. (2016). 'The Thirteenth Data Release of the Sloan Digital Sky Survey: First Spectroscopic Data from the SDSS-IV Survey MApping Nearby Galaxies at Apache Point Observatory'. In: *ArXiv e-prints*. arXiv: 1608.02013.

Sacco, G. G. et al. (2014). 'The Gaia-ESO Survey: processing FLAMES-UVES spectra'. In: *A&A* 565, A113, A113. DOI: 10.1051/0004-6361/201423619. arXiv: 1403.4865 [astro-ph.IM].

Salaris, M. and S. Cassisi (2005). *Evolution of Stars and Stellar Populations*, p. 400.

Salaris, M. and A. Weiss (2001). 'Atomic Diffusion in Stellar Interiors and Field Halo Subdwarfs Ages'. In: *Astrophysical Ages and Times Scales*. Ed. by T. von Hippel, C. Simpson, and N. Manset. Vol. 245. Astronomical Society of the Pacific Conference Series, p. 367.

Salaris, M., A. Weiss, and S. M. Percival (2004). 'The age of the oldest Open Clusters'. In: *A&A* 414, pp. 163–174. DOI: 10.1051/0004-6361:20031578. eprint: astro-ph/0310363.

Salaris, M., A. Pietrinferni, A. M. Piersimoni, and S. Cassisi (2015). 'Post first dredge-up [C/N] ratio as age indicator. Theoretical calibration'. In: *A&A* 583, A87, A87. DOI: 10.1051/0004-6361/201526951. arXiv: 1509.06904 [astro-ph.SR].

Sandage, A. R. (1953). 'The color-magnitude diagram for the globular cluster M 3.' In: *Astron. J.* 58, pp. 61–75. DOI: 10.1086/106822.

Sandage, A. (1962). 'Photometric Data for the Old Galactic Cluster NGC 188.' In: *ApJ* 135, p. 333. DOI: 10.1086/147274.

Sanders, W. L. (1977). 'Membership of the open cluster M67.' In: *A&AS* 27, pp. 89–116.

Sandquist, E. L. (2006). 'New Eclipsing Variables in the Field of M67'. In: *Information Bulletin on Variable Stars* 5679.

Sandquist, E. L. and M. D. Shetrone (2003). 'Time Series Photometry of M67: W Ursae Majoris Systems, Blue Stragglers, and Related Systems'. In: *Astron. J.* 125, pp. 2173–2187. DOI: 10.1086/368139. eprint: astro-ph/0301278.

Sandquist, E. L., D. W. Latham, M. D. Shetrone, and A. A. E. Milone (2003). 'The Blue Straggler RS Canum Venaticorum Star S1082 in M67: A Detailed Light Curve and the Possibility of a Triple'. In: *Astron. J.* 125, pp. 810–824. DOI: 10.1086/346087. eprint: astro-ph/0211313.

Sarajedini, A., A. Dotter, and A. Kirkpatrick (2009). 'Deep 2MASS Photometry of M67 and Calibration of the Main-Sequence J - K_S Color Difference as an Age Indicator'. In: *ApJ* 698, pp. 1872–1878. DOI: 10.1088/0004-637X/698/2/1872. arXiv: 0904.2907 [astro-ph.SR].

Sarajedini, A. et al. (2007). 'The ACS Survey of Galactic Globular Clusters. I. Overview and Clusters without Previous Hubble Space Telescope Photometry'. In: *Astron. J.* 133, pp. 1658–1672. DOI: 10.1086/511979. eprint: astro-ph/0612598.

Sargent, A. I. (1977). 'Molecular clouds and star formation. I - Observations of the Cepheus OB3 molecular cloud'. In: *ApJ* 218, pp. 736–748. DOI: 10.1086/155729.

— (1979). 'Molecular clouds and star formation. II - Star formation in the Cepheus OB3 and Perseus OB2 molecular clouds'. In: *ApJ* 233, pp. 163–181. DOI: 10.1086/157378.

Sarna, M. J. and J.-P. De Greve (1996). 'Chemical Evolution of Algols'. In: *QJRAS* 37, p. 11.

Saurin, T. A., E. Bica, and C. Bonatto (2012). 'The embedded cluster or association Trumpler 37 in IC 1396: a search for evolutionary constraints'. In: *MNRAS* 421, pp. 3206–3216. DOI: 10.1111/j.1365-2966.2012.20541.x. arXiv: 1201.2704.

Sbordone, L., E. Caffau, P. Bonifacio, and S. Duffau (2014). 'MyGIsFOS: an automated code for parameter determination and detailed abundance analysis in cool stars'. In: *A&A* 564, A109, A109. DOI: 10.1051/0004-6361/201322430. arXiv: 1311.5566 [astro-ph.IM].

Schmeja, S., N. V. Kharchenko, A. E. Piskunov, S. Röser, E. Schilbach, D. Froebrich, and R.-D. Scholz (2014). 'Global survey of star clusters in the Milky Way. III. 139 new open clusters at high Galactic latitudes'. In: *A&A* 568, A51, A51. DOI: 10.1051/0004-6361/201322720. arXiv: 1406.6267.

Scholz, R.-D., N. V. Kharchenko, A. E. Piskunov, S. Röser, and E. Schilbach (2015). 'Global survey of star clusters in the Milky Way. IV. 63 new open clusters detected by proper motions'. In: *A&A* 581, A39, A39. DOI: 10.1051/0004-6361/201526312. arXiv: 1507.02125 [astro-ph.SR].

Schulz, N. S., T. W. Berghoefer, and H. Zinnecker (1997). 'The X-ray view of the central part of IC 1396.' In: *A&A* 325, pp. 1001–1012.

Sestito, P., S. Randich, and A. Bragaglia (2007). 'Element abundances in the metal-rich open cluster NGC 6253'. In: *A&A* 465, pp. 185–196. DOI: 10.1051/0004-6361:20066643. eprint: astro-ph/0701182.

Shetrone, M. D. and E. L. Sandquist (2000). 'Spectroscopy of Blue Stragglers and Turnoff Stars in M67 (NGC 2682)'. In: *Astron. J.* 120, pp. 1913–1924. DOI: 10.1086/301569. eprint: astro-ph/0006399.

Sicilia-Aguilar, A., T. Henning, and L. W. Hartmann (2010). 'Accretion in Evolved and Transitional Disks in CEP OB2: Looking for the Origin of the Inner Holes'. In: *ApJ* 710, pp. 597–612. DOI: 10.1088/0004-637X/710/1/597. arXiv: 1001.3026 [astro-ph.SR].

Sicilia-Aguilar, A., L. W. Hartmann, C. Briceño, J. Muzerolle, and N. Calvet (2004). 'Low-Mass Stars and Accretion at the Ages of Planet Formation in the Cepheus OB2 Region'. In: *Astron. J.* 128, pp. 805–821. DOI: 10.1086/422432.

Sicilia-Aguilar, A., L. W. Hartmann, J. Hernández, C. Briceño, and N. Calvet (2005). 'Cepheus OB2: Disk Evolution and Accretion at 3-10 Myr'. In: *Astron. J.* 130, pp. 188–209. DOI: 10.1086/430748.

Sicilia-Aguilar, A. et al. (2006). 'Disk Evolution in Cep OB2: Results from the Spitzer Space Telescope'. In: *ApJ* 638, pp. 897–919. DOI: 10.1086/498085.

Sicilia-Aguilar, A., T. Henning, C. P. Dullemond, N. Patel, A. Juhász, J. Bouwman, and B. Sturm (2011). 'Dust Properties and Disk Structure of Evolved Protoplanetary Disks in Cep OB2: Grain Growth, Settling, Gas and Dust Mass, and Inside-out Evolution'. In: *ApJ* 742, 39, p. 39. DOI: 10.1088/0004-637X/742/1/39. arXiv: 1108.5258 [astro-ph.SR].

Sicilia-Aguilar, A., V. Roccatagliata, K. Getman, T. Henning, B. Merín, C. Eiroa, P. Rivière-Marichalar, and T. Currie (2014). 'A Herschel view of IC 1396 A: Unveiling the different sequences of star formation'. In: *A&A* 562, A131, A131. DOI: 10.1051/0004-6361/201322609. arXiv: 1312.3867 [astro-ph.SR].

Sicilia-Aguilar, A., V. Roccatagliata, K. Getman, P. Rivière-Marichalar, T. Birnstiel, B. Merín, M. Fang, T. Henning, C. Eiroa, and T. Currie (2015). 'The Herschel/PACS view of the Cep OB2 region: Global protoplanetary disk evolution and clumpy star formation'. In: *A&A* 573, A19, A19. DOI: 10.1051/0004-6361/201424669. arXiv: 1410.2713 [astro-ph.SR].

Sills, A., T. Adams, and M. B. Davies (2005). 'Blue stragglers as stellar collision products: the angular momentum question'. In: *MNRAS* 358, pp. 716–725. DOI: 10.1111/j.1365-2966.2005.08809.x. eprint: astro-ph/0501142.

Simonson III, S. C. and H. W. van Someren Greve (1976). 'Neutral hydrogen in a region of Cepheus - Nearby galactic structure'. In: *A&A* 49, pp. 343–356.

Skrutskie, M. F. et al. (2006). 'The Two Micron All Sky Survey (2MASS)'. In: *Astron. J.* 131, pp. 1163–1183. DOI: 10.1086/498708.

Smiljanic, R. et al. (2014). 'The Gaia-ESO Survey: The analysis of high-resolution UVES spectra of FGK-type stars'. In: *A&A* 570, A122, A122. DOI: 10.1051/0004-6361/201423937. arXiv: 1409.0568 [astro-ph.SR].

Smiljanic, R. et al. (2016). 'The Gaia-ESO Survey: Sodium and aluminium abundances in giants and dwarfs. Implications for stellar and Galactic chemical evolution'. In: *A&A* 589, A115, A115. DOI: 10.1051/0004-6361/201528014. arXiv: 1602.03289 [astro-ph.SR].

Souto, D. et al. (2016). 'Chemical Abundances in a Sample of Red Giants in the Open Cluster NGC 2420 from APOGEE'. In: *ArXiv e-prints*. arXiv: 1607.06102 [astro-ph.SR].

Spite, F., M. Spite, R. C. Peterson, and F. H. Chaffee Jr. (1987). 'Measurement of lithium abundance in dwarf stars of M67'. In: *A&A* 171, p. L8.

Stassun, K. G., M. van den Berg, R. D. Mathieu, and F. Verbunt (2002). 'Photometric variability in the old open cluster M 67. II. General survey'. In: *A&A* 382, pp. 899–909. DOI: 10.1051/0004-6361:20011737. eprint: astro-ph/0112189.

Stello, D., A. Vanderburg, L. Casagrande, R. Gilliland, V. Silva Aguirre, E. Sandquist, E. Leiner, R. Mathieu, and D. R. Soderblom (2016). 'The K2 M67 Study: Revisiting Old Friends with K2 Reveals Oscillating Red Giants in the Open Cluster M67'. In: *ApJ* 832, 133, p. 133. DOI: 10.3847/0004-637X/832/2/133. arXiv: 1610.03060 [astro-ph.SR].

Strom, K. M. and S. E. Strom (1970). 'A Study of the Blue Stragglers in the Open Cluster NGC 7789'. In: *ApJ* 162, p. 523. DOI: 10.1086/150685.

Takeda, Y. and S. Honda (2015). 'On the oxygen abundances of M 67 stars from the turn-off point through the red giant branch$^{\text{Ď}}$'. In: *PASJ* 67, 25, p. 25. DOI: 10.1093/pasj/psu157. arXiv: 1412.7230 [astro-ph.SR].

Tautvaišiene, G., B. Edvardsson, I. Tuominen, and I. Ilyin (2000). 'Chemical composition of evolved stars in the open cluster M 67'. In: *A&A* 360, pp. 499–508. eprint: astro-ph/0006001.

Taylor, B. J. (2007). 'The Benchmark Cluster Reddening Project. II. A Reddening Value for M67'. In: *Astron. J.* 133, pp. 370–386. DOI: 10.1086/509781.

Tian, B., L. Deng, Z. Han, and X. B. Zhang (2006). 'The blue stragglers formed via mass transfer in old open clusters'. In: *A&A* 455, pp. 247–254. DOI: 10.1051/0004-6361:20064879. eprint: astro-ph/0604290.

Tripicco, M. J., B. Dorman, and R. A. Bell (1993). 'Mass loss in M67 giants - Evidence from isochrone fitting'. In: *Astron. J.* 106, pp. 618–626. DOI: 10.1086/116666. eprint: astro-ph/9304011.

Turcotte, S., J. Richer, G. Michaud, C. A. Iglesias, and F. J. Rogers (1998). 'Consistent Solar Evolution Model Including Diffusion and Radiative Acceleration Effects'. In: *ApJ* 504, pp. 539–558. DOI: 10.1086/306055.

VandenBerg, D. A., B. Edvardsson, K. Eriksson, and B. Gustafsson (2008). 'On the Use of Blanketed Atmospheres as Boundary Conditions for Stellar Evolutionary Models'. In: *ApJ* 675, 746-763, pp. 746–763. DOI: 10.1086/521600. arXiv: 0708.1188.

Vickers, J. J., S. Röser, and E. K. Grebel (2016). 'A Global Correction to PPMXL Proper Motions'. In: *Astron. J.* 151, 99, p. 99. DOI: 10.3847/0004-6256/151/4/99. arXiv: 1602.08868.

Webbink, R. F. (1976). 'The evolution of low-mass close binary systems. I - The evolutionary fate of contact binaries'. In: *ApJ* 209, pp. 829–845. DOI: `10.1086/154781`.

Williams, K. A., S. B. Howell, J. Liebert, P. S. Smith, A. Bellini, K. H. R. Rubin, and M. Bolte (2013). 'Time-resolved Spectroscopy of the Polar EU Cancri in the Open Cluster Messier 67'. In: *Astron. J.* 145, 129, p. 129. DOI: `10.1088/0004-6256/145/5/129`. arXiv: `1301.5936 [astro-ph.SR]`.

Wright, N. J., J. E. Drew, and M. Mohr-Smith (2015). 'The massive star population of Cygnus OB2'. In: *MNRAS* 449, pp. 741–760. DOI: `10.1093/mnras/stv323`. arXiv: `1502.05718 [astro-ph.SR]`.

Yadav, R. K. S., L. R. Bedin, G. Piotto, J. Anderson, S. Cassisi, S. Villanova, I. Platais, L. Pasquini, Y. Momany, and R. Sagar (2008). 'Ground-based CCD astrometry with wide-field imagers. II. A star catalog for M 67: WFI@2.2 m MPG/ESO astrometry, FLAMES@VLT radial velocities'. In: *A&A* 484, pp. 609–620. DOI: `10.1051/0004-6361:20079245`. arXiv: `0803.0004`.

Yakut, K. et al. (2009). 'Close binary and other variable stars in the solar-age Galactic open cluster M 67'. In: *A&A* 503, pp. 165–176. DOI: `10.1051/0004-6361/200911918`. arXiv: `0906.4908 [astro-ph.SR]`.

Yong, D., B. W. Carney, and M. L. Teixera de Almeida (2005). 'Elemental Abundance Ratios in Stars of the Outer Galactic Disk. I. Open Clusters'. In: *Astron. J.* 130, pp. 597–625. DOI: `10.1086/430934`. eprint: `astro-ph/0504193`.

Zhang, J., J. Shi, K. Pan, C. Allende Prieto, and C. Liu (2016). 'NLTE Analysis of High-Resolution H-band Spectra. I. Neutral Silicon'. In: *ApJ* 833, 137, p. 137. DOI: `10.3847/1538-4357/833/2/137`.

— (2017). 'NLTE Analysis of High-resolution H-band Spectra. II. Neutral Magnesium'. In: *ApJ* 835, 90, p. 90. DOI: `10.3847/1538-4357/835/1/90`. arXiv: `1610.05893 [astro-ph.SR]`.

Zhang, X. B., R. X. Zhang, and L. Deng (2005). 'Photometric Study of AH Cancri, a W UMa-Type System in M67'. In: *Astron. J.* 129, pp. 979–984. DOI: `10.1086/426914`.

Zhao, J. L., K. P. Tian, and C. G. Su (1996). 'Discussions of the Internal Motions and Mass Segregation of M67 on the Basis of Accurate Proper Motions'. In: *Ap&SS* 235, pp. 93–108. DOI: `10.1007/BF00643593`.

de Zeeuw, P. T., R. Hoogerwerf, J. H. J. de Bruijne, A. G. A. Brown, and A. Blaauw (1999). 'A HIPPARCOS Census of the Nearby OB Associations'. In: *Astron. J.* 117, pp. 354–399. DOI: `10.1086/300682`. eprint: `astro-ph/9809227`.

van den Berg, M., J. Orosz, F. Verbunt, and K. Stassun (2001). 'The blue straggler S 1082: A triple system in the old open cluster M 67'. In: *A&A* 375, pp. 375–386. DOI: `10.1051/0004-6361:20010589`. eprint: `astro-ph/0104322`.

van den Berg, M., K. G. Stassun, F. Verbunt, and R. D. Mathieu (2002). 'Photometric variability in the open cluster M 67. I. Cluster members detected in X-rays'. In: *A&A* 382, pp. 888–898. DOI: `10.1051/0004-6361:20011521`. eprint: `astro-ph/0112186`.

van den Berg, M., G. Tagliaferri, T. Belloni, and F. Verbunt (2004). 'A Chandra observation of the old open cluster M 67'. In: *A&A* 418, pp. 509–523. DOI: `10.1051/0004-6361:20031642`. eprint: `astro-ph/0311138`.

ACKNOWLEDGEMENTS

The years of my PhD have been exciting and eventful and I would like to thank all the people that were part of this experience, although it will be impossible to cite them all by name.

I would like to thank my supervisor, Prof. E. K. Grebel, for welcoming me in her research group at ARI and for supporting me throughout the PhD.

I am also thankful to PD Sabine Reffert for kindly agreeing to be the second referee of this thesis, and to Prof. Joachim Wambsganß and Prof. Mario Trieloff for agreeing to be part of the examination committee.

All my gratitude goes to Dr. Anna Pasquali, who offered me to work with her on this project and supported me through each step of the way. I cannot even begin to explain how much I have learnt from her and how precious her presence has been for me.

During the years of my PhD I also started several collaborations that have been very enriching and fruitful. I therefore thank Prof. Maurizio Salaris, Dr. Angela Bragaglia, Dr. Elisabetta Caffau, Prof. Georges Michaud, Dr. Jacques Richer, Dr. Sofia Randich, and Dr. Laura Magrini for their work and the numerous helpful discussions.

All of the ARI staff has contributed to a very nice and positive work environment and I would like to thank in particular Martina Buchhaupt, Besma Klinger-Araifa, Eleonora Grauer, Saskia Mayer, Helga Ballmann, Hildrun Pisch, and Diana Schwalbe for their help in all administrative issues, Dr. Peter Schwekendiek and Sven Weimann for the help in sorting out IT problems, and Dr. Robert Schmidt and Dr. Guido Thimm for always being available to answer any of my questions.

I would also like to thank the other PhD students with whom I shared this experience and a lot of cheerful moments. Especially my officemates, Frederik, Bekdaulet, and Gergely were always available for helpful discussions and chats.

A special thank goes to my parents and my family, who always supported me making it seem with endless phone calls as if I was not so far away from home. I would also like to thank the friends of a lifetime, Martina and Valentina, who are always there for jokes and serious conversations, no matter how far away, and the new friends who accompanied me through the past years in Heidelberg: Federica, Marco, Tobias, Reza, Marcelo, Giulio, Emanuela, and especially Roxana.